Title
Investigating Hemoglobin Capture and Heme Acquisition by the Pathogen Staphylococcus aureus

Author
Sjodt, Megan Marie

Publication Date
2016

Peer reviewed|Thesis/dissertation

UNIVERSITY OF CALIFORNIA

Los Angeles

Investigating Hemoglobin Capture and Heme Acquisition by the Pathogen *Staphylococcus aureus*

A dissertation submitted in partial satisfaction of the requirements for the degree

Doctor of Philosophy in Biochemistry and Molecular Biology

by

Megan Marie Sjodt

2016

ABSTRACT OF THE DISSERTATION

Investigating Hemoglobin Capture and Heme Acquisition by the Pathogen *Staphylococcus aureus*

by

Megan Marie Sjodt

Doctor of Philosophy in Biochemistry and Molecular Biology

University of California, Los Angeles, 2016

Professor Robert Thompson Clubb, Chair

Staphylococcus aureus is a medically important Gram-positive bacterial pathogen that actively procures heme from human hemoglobin (Hb) using the iron-regulated surface determinant (Isd) system. Research described in this dissertation investigated how the Isd system uses the IsdH receptor protein to capture Hb and extract its hemin (the oxidized form of heme). To rapidly extract Hb's hemin, IsdH employs a conserved tri-domain unit that contains two NEAr iron Transporter (NEAT) domains that are connected by a helical linker domain. The work described in chapter 2 used UV-Vis spectroscopy, nuclear magnetic resonance (NMR) spectroscopy, and electrospray ionization mass spectrometry (ESI-MS) methods to define the importance of the conserved linker domain in hemin extraction and revealed that this domain

enables the NEAT domains within the tri-domain unit to work together to synergistically extract hemin. Chapter 3 of this thesis describes the structure and dynamics of the tri-domain unit ($IsdH^{N2N3}$). The solution structure of the apo-receptor was defined using small angle X-ray scattering, and advanced NMR methods such as paramagnetic relaxation enhancement (PRE), residual dipolar coupling (RDC), and selective methyl labeling approaches. The structure and inter-domain dynamics of $IsdH^{N2N3}$ in the absence of Hb were further defined using ensemble modeling calculations. The results of these studies illustrated that the receptor adaptively recognizes Hb using a combination of conformational selection and induced fit mechanisms, and suggests that the linker domain may facilitate hemin transfer by destabilizing the iron-coordinating F-helix in Hb. Chapter 4 describes studies that investigated the kinetic and thermodynamic basis of hemin transfer using stopped-flow UV-Vis spectroscopy, analytical ultracentrifugation sedimentation equilibrium, and isothermal titration methods. The results of this work provide insight into the kinetic and thermodynamic determinants that facilitate receptor-mediated hemin release from Hb. Lastly, Chapter 5 describes the methods that were used to site-specifically label proteins with nitroxide spin-label probes and the subsequent derivation of paramagnetic NMR distance restraints. Altogether, the results of the work described in this dissertation have advanced our knowledge of Hb recognition and hemin acquisition by the pathogen *S. aureus*.

The dissertation of Megan Marie Sjodt is approved.

Feng Guo

Todd O. Yeates

Robert Thompson Clubb, Committee Chair

University of California, Los Angeles

2016

DEDICATION

To my parents, who've always believed in me and taught me the value of hard work. To my brother, Kevin, for motivating me to excel in school and to my brother, Brian, who always shared and encouraged my love of science. I'm truly lucky to have all their love and support.

TABLE OF CONTENTS

LIST OF FIGURES

LIST OF TABLES

ACKNOWLEDGEMENTS

First and foremost, I would like to thank my advisor, Dr. Robert Clubb, for his guidance, support, and encouragement to pursue opportunities that I sometimes didn't believe I deserved. My collaborators, Dr. John Olson and Dr. David Gell for all of the indispensable advice in the design and execution of various experiments throughout the years, Dr. Robert Peterson for all the help with setting up NMR experiments, Dr. Martin Phillips for all the help in the instrumentation room, and Dr. Duilio Cascio for always believing in me and being a great shoulder to cry on. I also thank my rotation mentors, Dr. Steven Clarke and Dr. Joseph Loo for their advice in and out of the lab, and my committee members, Dr. Pascal Egea, Dr. Feng Guo, Dr. Joseph Loo, and Dr. Todd Yeates for their thoughts and willingness to help. Help from my undergraduate, Joanna Marshall, and my rotation student, Ramsay Macdonald, has been invaluable in advancing my projects. Moral support and friendship from members of the Clubb lab are the reasons I've succeeded in graduate school. They include Dr. Thomas Spirig, Dr. Ethan Weiner, Dr. Reza Malmirchegini, Dr. Albert Chan, Dr. Alex Jacobitz, Brendan Amer, Grace Huang, Michele Kattke, Ramsay Macdonald, Jason Gosschalk, and Scott McConnell, as well as Dr. Sara Weitz and Andrea Hadjikyriacou. I thank my dearest friends, Brianne Worley, Samantha Humphries, and Meagan Blome for all the fun, love, and support throughout these past 15 years. Lastly, I would like to thank the Chemistry and Biochemistry Department for not only making my dream of becoming a UCLA Bruin true but also providing me the opportunity to meet the love of my life, Austin Gable.

The work in this dissertation was supported by the Ruth L. Kirschstein National Research Service Award (NRSA) Pre-Doctoral Fellowship (F31 GM 101931), and the Cellular and Molecular Biology Training Grant (GM 007185).

Chapter Two of this dissertation is a version of the manuscript: Spirig, T., Malmirchegini, G. R., Zhang, J., Robson, S. A., Sjodt, M., Liu, M., Krishna Kumar, K., Dickson, C. F., Gell, D. A., Lei, B., Loo, J. A., & Clubb, R. T. *Staphylococcus aureus* uses a novel multidomain receptor to break apart human hemoglobin and steal its heme. *J. Biol. Chem*., 2013; 288(2):1065-78. doi: 10.1074/jbc.M112.419119. Reproduced with permission. Copyright 2013, American Society of Biochemistry and Molecular Biology, Inc. This work was supported, in whole or in part, by National Institutes of Health Grants AI52217 (to R. T. C.), RR020004 (now reassigned as GM103479) (to J. A. L.), and S10RR028893 from the National Center for Research Resources for purchase of the Fourier transform ion cyclotron resonance mass spectrometer. This work was also supported by Swiss National Science Foundation Fellowship PBEZP3–124281 (to T. S.). TS, GRM, JZ, RTC, JAL, and DAG designed the experiments. TS, GRM, JZ, SR, MS, ML, KKK, CFD performed the experiments. TS, GRM, and RTC wrote the manuscript.

Chapter Three of this dissertation is a version of the manuscript: Sjodt, M., Macdonald, R., Spirig, T., Chan, A. H., Dickson, C. F., Fabian, M., Olson, J. S., Gell, D. A., & Clubb, R. T. The PRE-Derived NMR Model of the 38.8 kDa Tri-Domain IsdH Protein from *Staphylococcus aureus* Suggests that it Adaptively Recognizes Human Hemoglobin. *J. Mol Biol*., 2016; 428(6):1107-29. doi: 10.1016/j.jmb.2015.02.008 (Accepted February 7, 2015). Reproduced with permission. Copyright 2015, Elsevier Ltd. This work was supported, in whole or in part, by National Institutes of Health Grants AI52217 (to R.T.C.), P01-HL110900 (to J.S.O.), the Robert A. Welch Foundation Grant C-0612 (to J.S.O.), and the National Institutes of Health Award

F31GM101931 (to M.S.). The chemical shift assignments, residual dipolar couplings, and relaxation data have been deposited at the BioMagResBank (http://www.bmrb.wisc.edu) under accession number 25113. MS, DAG, JSO, and RTC designed the experiments. MS, RM, TS, CFD, and MF performed the experiments. MS and RTC wrote the manuscript. AHC, DAG, and JSO edited the manuscript.

Chapter Four of this dissertation is a version of the manuscript in preparation for publication: Sjodt, M., Macdonald, R., Marshall, J.D., Phillips, M., Olson, J.S., & Clubb, R.T. The *S. aureus* IsdH Protein Accelerates Hemin Release from the α-Subunit of the Hemoglobin Tetramer by at least 10,000-fold. 2016. This work was supported, in whole or in part, by National Institutes of Health Grants AI52217 (to R.T.C.), and the National Institutes of Health Award F31GM101931 (to M.S.). MS, JSO, and R.T.C designed the experiments. MS, RM, JDM, and MP performed the experiments. MS and RTC wrote the manuscript.

Chapter Five of this dissertation is a version of the manuscript in preparation for publication: Sjodt, M., & Clubb, R.T. Nitroxide Labeling and Derivation of Paramagnetic NMR Distance Restraints for Protein Structure Determination, 2016. This work was supported, in whole or in part, by National Institutes of Health Grants AI52217 (to R.T.C.), and the National Institutes of Health Award F31GM101931 (to M.S.). MS and R.T.C designed the experiments. MS performed all the experiments. MS and RTC wrote the manuscript.

VITA

2005-2010	Bachelor of Science, Chemistry California State Polytechnic University, Pomona
2011	Teaching Assistant, Department of Chemistry and Biochemistry University of California, Los Angeles
2011	Hanson-Dow Award for Excellence in Teaching, Department of Chemistry and Biochemistry University of California, Los Angeles
2011-2012	Cellular and Molecular Biology Training Grant University of California, Los Angeles
2012	Candidate in Philosophy, Department of Chemistry and Biochemistry University of California, Los Angeles
2012-2016	Ruth L. Kirschstein National Research Service Award (NRSA) Predoctoral Fellowship to Promote Diversity in Health-Related Research National Institute of Heath
2015	Dissertation Year Fellowship (respectfully declined), Graduate Division University of California, Los Angeles
2015	John M. Jordan Memorial Award for Research in Biochemistry University of California, Los Angeles
2016	Daniel E. Atkinson and Charles A. West Dissertation Award University of California, Los Angeles

PUBLICATIONS

Sjodt, M., Macdonald, R., Spirig, T., Chan, A. H., Dickson, C. F., Fabian, M., Olson, J. S., Gell, D. A., & Clubb, R. T. The PRE-Derived NMR Model of the 38.8 kDa Tri-Domain IsdH Protein from *Staphylococcus aureus* Suggests that it Adaptively Recognizes Human Hemoglobin. *J. Mol. Biol.*, 2016; 428(6):1107-29. doi: 10.1016/j.jmb.2015.02.008 (Accepted February 7, 2015)

Zilbermintz L., Leonardi W., Jeong S. Y., **Sjodt, M.**, McComb R., Ho C. L., Retterer C., Gharaibeh D., Zamani R., Soloveva V., Bavari S., Levitin A., West J., Bradley K. A., Clubb R. T., Cohen S. N., Gupta V., & Martchenko M. Identification of agents effective against multiple toxins and viruses by host-oriented cell targeting. *Sci. Rep.*, 2015; 5:13476. doi:10.1038/srep13476

Malmirchegini, G. R., **Sjodt, M**., Shnitkind, S., Sawaya, M. R., Rosinski, J., Newton, S. M., Klebba, P. E., & Clubb, R. T. Novel mechanism of hemin capture by Hbp2, the hemoglobin-binding hemophore from *Listeria monocytogenes*. *J. Biol. Chem.,* 2014; 289(50):34886-99. doi: 10.1074/jbc.M114.583013

Spirig, T., Malmirchegini, G. R., Zhang, J., Robson, S. A., **Sjodt, M.**, Liu, M., Krishna Kumar, K., Dickson, C. F., Gell, D. A., Lei, B., Loo, J. A., & Clubb, R. T. Staphylococcus aureus uses a novel multidomain receptor to break apart human hemoglobin and steal its heme. *J. Biol. Chem*., 2013; 288(2):1065-78. doi: 10.1074/jbc.M112.419119

SELECTED PRESENTATIONS

Sjodt, M., Macdonald, R., Spirig, T., Gell, D. A., & Clubb, R. T. The NMR Model of the 39-kDa Tri-Domain IsdH Protein from *Staphylococcus aureus* Suggests That It Uses Inter-Domain Motions to Recognize Human Hemoglobin and Promote Heme Release. Poster presentation at the Annual American Society for Biochemistry and Molecular Biology Meeting, San Diego, CA. April 1-6, 2016

Sjodt, M., Macdonald, R., Gell, D. A., & Clubb, R. T. The PRE-Derived NMR Model of the Tri-Domain IsdH Protein from *Staphylococcus aureus* Reveals that it Adaptively Recognizes Human Hemoglobin. Poster presentation at the 60th Annual Biophysical Society Meeting, Los Angeles, CA. February 27-March 2, 2016

Sjodt, M., Macdonald, R., Spirig, T., Gell, D. A., & Clubb, R. T. NMR model of a 38.8 kDa hemoglobin receptor from *Staphylococcus aureus*. Poster presentation at EMBO|EMBL Symposium, Molecular Machines: Lessons from Integrating Structure, Biophysics, and Chemistry, Heidelberg, Germany. May 18-22, 2014

Chapter 1

Heme Acquisition Systems in *Staphylococcus aureus* and other Gram-Positive Bacteria

1.1 Overview

Staphylococcus aureus is Gram-positive pathogen capable of causing a wide range of life-threatening illnesses such as septicemia, meningitis, endocarditis, pneumonia, and toxic shock syndrome [1]. The pervasiveness of antibiotic resistant *S. aureus* strains has made it a major health threat and imperative to understand the molecular mechanisms used by this microbe to establish an infection. *S. aureus* and other bacterial pathogens require iron to survive as this element is a key biocatalyst involved in the synthesis of DNA, RNA, and amino acids, microbial electron transport, and peroxide reduction [2–4]. In the human body, free iron isn't readily available and is therefore actively procured by *S. aureus* during infections. Heme-iron (protoporphyrin IX + iron) bound to the oxygen carrying protein, hemoglobin, accounts for 75-80% of the total iron in the human body and is a preferred iron-source for *S. aureus* [5,6]. As a result, studying the mechanisms of heme acquisition could lead to the development of novel anti-infective therapeutics that prevent access to this essential nutrient. The scope of this introduction is to review what is currently known about the mechanisms through which *S. aureus* and other medically important Gram-positive pathogens acquire heme from the human host. Additionally, Gram-negative bacterial iron acquisition systems do exist and have been extensively characterized; however, they have been reviewed elsewhere [7–9] and are therefore outside the scope of this introductory chapter.

1.2 *Staphylococcus aureus*

S. aureus is a Gram-positive bacterium that colonizes the anterior nares of approximately 30% of people in the United States asymptomatically [10]. Since the beginning of the modern antibiotic era in the 1940's, *S. aureus* and other pathogenic bacteria have evolved resistance mechanisms to nearly all antibiotics that have been deployed resulting in a worldwide problem [11,12]. In particular, methicillin-resistant *Staphylococcus aureus* (MRSA) is one of the leading causes of hospital-acquired infections and accounts for up to 50% of infectious *S. aureus* isolates [13]. Moreover, community-associated MRSA strains have become commonplace with some regions reporting that up to 75% of *S. aureus* infections were MRSA [14]. The widespread colonization by this microbe has been implicated as a risk factor for subsequent infections as 2% of the population carry methicillin-resistant *Staphylococcus aureus* (MRSA) strains and as high as 7% of hospital patients are MRSA carriers [10,15]. In 2013, the Centers for Disease Control (CDC) estimated that MRSA infections are responsible for 11,285 deaths with other reports attributing that these infections impose an economic burden of approximately $14 billion annually [12,16]. Moreover, last resort antibiotics traditionally used to treat MRSA infections such as vancomycin, linezolid, daptomycin, and ceftaroline have decreasing efficacy as strains of *S. aureus* resistant to those treatments are on the rise [17]. While staphylococcal infections are most commonly found in skin and soft tissues and are usually not serious, the bacterium can cause lethal infections when it breaches the body's defense mechanisms [18].

The success of *S. aureus* as a human pathogen can be attributed to its vast array of virulence factors that circumvent the host's defense mechanisms (**Figure 1.1**). Several noteworthy features that promote *S. aureus* survival within its human host include, but are not limited to, surface proteins called microbial surface components recognizing adhesive matrix

molecules (MSCRAMMs) that promote adherence to host tissues, such as fibronectin-binding protein and collagen-binding protein [19], as well as proteins involved in immune evasion such as protein A binding to the Fc region of IgG preventing phagocytosis [20,21], the chemotaxis inhibitory protein of staphylococci (CHIPS) that prevents neutrophil chemotaxis [22], and lastly secreted cytolytic toxins such as enterotoxins, leukocidins, hemolysins, and phenol soluble modulins (PSMs), which commonly form pores in the cytoplasmic membranes of host cells resulting in cell lysis [23–26]. In particular, these lytic agents such as α-toxin and δ-hemolysin can lyse erythrocytes releasing large amounts of the iron-rich protein, hemoglobin (Hb), which provides *S. aureus* access to this essential element that is necessary to sustain its growth within its host [27].

1.3 Nutritional Necessity of Iron

1.3.1 The Role of Iron in Biology

Iron is an essential nutrient for nearly all forms of life because this element is required for several critical cellular processes. The utility of iron in biology lies within its ability to cycle between two different oxidation states, ferrous (Fe^{2+}) and ferric (Fe^{3+}), rendering it capable of accepting and donating electrons. Therefore, iron serves as a redox active molecule used by many enzymes that mediate basic biochemical processes required to support life [28,29]. However, the iron levels within cells must be tightly regulated as high levels of iron can be toxic to cells. The deleterious effects of iron are due to its participation in the Fenton reaction that forms hydroxyl and superoxide free radicals (Equations 1 & 2) [29–31].

$$H_2O_2 + Fe^{2+} \longrightarrow Fe^{3+} + OH^- + OH^{\cdot} \quad (1)$$

$$Fe^{3+} + O_2^{\cdot -} \longrightarrow Fe^{2+} + O_2 \quad (2)$$

These reactive oxygen species are highly toxic since they react readily with nearly every biomolecule found in cells. As a result, DNA is damaged, synthesis of proteins, carbohydrates and lipids is impaired, expression of proteases is increased, and cell proliferation is altered [29]. Furthermore, iron-induced oxidative stress has been implicated in the various processes of carcinogenesis, atherosclerosis, diabetes, as well as neurodegenerative disorders such as Parkinson's, Alzheimer's, and Huntington's disease [32–34]. Consequently, the human body has evolved elaborate mechanisms to sequester free iron for its own protection and to prevent its access to potential pathogens.

1.3.1 Nutritional Immunity

Humans and other vertebrates exhibit nutritional immunity; a process in which they sequester iron and other essential nutrients to restrict pathogens from establishing infections (**Figure 1.b**) [35]. The majority of iron in the human body is complexed to protoporphyrin-IX, which is called heme. This cofactor is bound tightly to an array of proteins, including the oxygen carrying protein, hemoglobin (Hb). Hb is present in erythrocytes and is a tetrameric protein consisting of two heterodimers of α- and β-globin chains, with each subunit capable of binding one heme molecule [35]. Each erythrocyte contains approximately 280 million Hb molecules, each of which is capable of binding four iron atoms resulting in an overall iron capacity of greater than 1 billion atoms per erythrocyte cell [6,28]. If heme or hemoglobin is released from erythrocytes by spontaneous lysis or the action of a pathogen, they are rapidly cleared from the

bloodstream by binding to hemopexin (HPX) and haptoglobin (Hp), respectively. Heme-bound HPX is then targeted to liver parenchymal cells to be catabolized, allowing for the iron to be recycled [36], whereas the Hp:Hb complex is eliminated from the bloodstream via macrophage uptake by CD163 receptor mediated endocytosis [37].

Iron is also bound to other proteins in the human body. Within cells is it is bound to ferritin, a 24 subunit protein complex that binds over 4000 ferric iron atoms [28]. However, less iron is stored in ferritin as it accounts for less than 30% of the total body's iron content compared to 70-80% found in heme [5,38]. Humans also restrict access to extracellular iron to prevent infections. Extracellular iron primarily exists in its ferric state and is insoluble at physiological pH. Outside the cell it is chelated by the protein transferrin in blood serum, and by the glycoprotein, lactoferrin in tears, breast milk, seminal fluid, and saliva [28,35,39,40]. Beyond sequestration by binding to proteins, the host exhibits nutritional immunity against intracellular pathogens that reside within phagosomes using the natural resistance-associated macrophage protein 1, NRAMP1. It pumps ferrous iron and manganese out of the phagosomal compartment, starving the microbe of these nutrients [41]. Overall these mechanisms limit iron bioavailability, lowering the concentration of free iron to 10^{-24} M [42], far below what is needed for *S. aureus* growth (~10^{-6} M).

1.4 Iron-Acquisition During Staphylococcal Infections

To overcome human nutritional immunity, pathogens like *S. aureus* actively acquire iron. Discussed below are the two main strategies *S. aureus* employs to obtain iron from its human host: siderophores and heme acquisition systems.

1.4.1 Iron Procurement by Siderophores

S. aureus steals iron from host proteins like transferrin and lactoferrin by secreting iron-chelating molecules called siderophores. These small molecules are usually < 1 kDa, and outcompete host proteins for ferric iron by binding this metal with extremely high affinity; they exhibit ferric iron binding constants (K_a) on the order of 10^{30} to 10^{52} M^{-1} [43,44]. *S. aureus* produces two main carboxylate-type siderophores, staphyloferrin A (SA) and staphyloferrin B (SB) (**Figure 1.3**) [27]. They outcompete host proteins for iron, and then bind to cognate receptors on the surface of *S. aureus* that import them into the cytoplasm where the iron is released from the siderophore. Both of the genes involved in the biosynthesis and import of SA and SB are upregulated during iron-deplete conditions by the ferric uptake regulator, Fur [45]. Import of SB is mediated by the staphylococcal iron regulated transporter complex (SirABC), while import of SA occurs via the heme transport system (HtsABC). The system was originally misnamed as a heme importer, but subsequently shown only to import SA [6,46]. The role of the HtsA lipoprotein receptor component in HtsABC was verified by determining crystal structures of it bound to SA [47]. Interestingly, both SA and SB siderophore operons lack the ATPase gene whose product provides the energy needed to transport them into the cytoplasm. Instead, the FhuC ATPase expressed from the ferric hydroxymate uptake (*fhuCBG)* operon drives both SA and SB import [46,48]. Once the siderophore is imported into the cell, the mechanism to release iron remains unknown. The most widely accepted method is thought to involve iron reduction of the ferric-siderophore complex into a ferrous-siderophore state that is both thermodynamically and kinetically less stable [49]. To support this notion, a very recent study showed that the nitroreductase, NrtA, is necessary for SA-iron utilization. However, it was not necessary for iron release from SB [50].

Humans have also evolved mechanisms to prevent iron-laden siderophores from reaching potential pathogens. The host secretes proteins called siderocalins (also known as lipocalins), which bind siderophores with high affinity, disrupting the access of pathogens to extracellular iron [51]. However, some bacteria are capable of secreting stealth siderophores that are chemically modified to prevent siderocalin binding, thus enabling the pathogen to overcome this defense mechanism.

1.4.2 Heme Acquisition by *S. aureus*

The vast majority of iron in the human body is found in heme (protoporphyrin-IX bound to ferrous iron), which has been shown to be preferentially used by *S. aureus* as an iron source [6]. Most heme is bound to Hb, but it is also present in hemoproteins such as: myoglobin (Mb), hemopexin (HPX), and cytochromes (CYPs). Only Hb and Mb appear to be important sources of iron during infections, as CYPs are localized to the mitochondria and are not thought to be easily accessible to extracellular pathogens, and studies have shown HPX does not support *S. aureus* growth in cell culture [52]. While it's unclear if Mb's heme-iron is used by *S. aureus* during infection, *S. aureus* colonization can damage cardiac myocytes, which contain large amounts of Mb [40,53]. In contrast, it is well established that Hb is an important iron source for *S. aureus*, and intact erythrocytes have been reported to be used by *S. aureus* as the sole source of iron *in vitro* [52]. Utilization of heme-iron from Hb has also been shown to play an important role in *S. aureus* virulence, as microbes lacking their Hb receptors show reduced abscess formation [52] and are impaired in their ability to establish systemic infections in murine models [54]. Other bacterial pathogens also use Hb as an iron source, including *Pseudomonas aeruginosa* [55], *Bacillus anthracis* [56], *Bacillus cereus* [57], *Streptococcus pyogenes* [58,59], *Streptococcus*

pneumoniae [60], *Staphylococcus lugdunensis* [61], *Staphylococcus simulans* [62], and *Corynebacterium diphtheriae* [63]. Interestingly, similar to *S. aureus*, several of these microbes preferentially use the human variant of Hb as a nutrient source [62], suggesting that these pathogens are optimized to infect humans.

1.5 Heme Acquisition Systems in Gram-Positive Bacteria

1.5.1 The Iron Regulated Surface Determinant (Isd) System in *S. aureus*

S. aureus captures heme using the iron-regulated surface determinant (Isd) system. Since the system's discovery in 2002, extensive work has shown that the Isd system is comprised of nine proteins that form a heme relay system. In this process, the Isd-system captures Hb on the cell surface, extracts its heme molecule, shuttles heme across the bacterial cell wall, and transports it into the cytoplasm where it is degraded to release free iron [2,64–75] (**Figure 1.4**, **left panel**). The Isd system is believed to capture heme from lysed erythrocytes. Heme procurement is initiated when *S. aureus* secretes cytolytic agents such as α-toxin and δ-hemolysin in response to iron insufficiency in human blood [43,76]. These toxins lyse erythrocytes, thereby releasing significant amounts of iron-rich Hb into the bloodstream, which is then harvested by the microbe's Isd system. Like siderophores, the genes encoding proteins within the Isd system are regulated by the ferric uptake regulator (Fur) protein and are maximally expressed during iron-deplete conditions [66,77]. Four Isd proteins (IsdA, IsdB, IsdC, and IsdH/HarA) are covalently tethered by their C-termini to the cell wall by sortase transpeptidases [66,78,79]. While the exact architectural arrangement of these cell wall anchored proteins isn't known, protease sensitivity experiments suggest that they form a heme funnel within the cell

wall with proteins that have increasing affinity for heme situated closer to the membrane. The IsdB and IsdH proteins are positioned on the cell surface, while IsdA and IsdC proteins are partially and fully buried within the cell wall, respectively. The funnel terminates at the cell membrane, where the ABC transporter complex, IsdDEF, is located and has the highest affinity for heme [64]. Biochemical, kinetic, and thermodynamic studies indicate that heme transfer across the cell wall occurs in a unidirectional fashion via protein-protein heme transfer complexes, with the heme flowing from Hb → IsdB/H → IsdA → IsdC → IsdE [67,72–74,80,81]. Heme is then transported into the bacterial cytoplasm through the IsdDEF transporter complex and is thereafter degraded by IsdG (or its paralog IsdI), releasing free iron to be used by the microbe.

The cell wall anchored Isd proteins (IsdA, IsdB, IsdC, and IsdH) bind to the oxidized form of heme (hereafter referred to as hemin) and Hb using NEAr iron Transporter (NEAT) domains. These domains were initially named because they were found in genes that are proximal to putative Fe^{3+} siderophore transporter genes [82]. NEAT domains are ~125 residues in length and adopt a conserved immunoglobulin fold consisting of 8 β-strands [83]. Numerous structural studies of both the apo- and holo- forms of NEAT domains have elucidated the molecular determinants of hemin and Hb binding [81,84–90]. NEAT domains bind hemin via a pocket formed by residues in strands β7 and β8 (the β7-β8 sheet), which contains the iron-coordinating tyrosine residue. The hemin moiety is further stabilized by a 3_{10}-helical "lip" that is situated above the β7-β8 sheet. Residues forming the β7-β8 sheet contain a YxxxY sequence motif; the side chain of the first tyrosine coordinates the hemin-iron atom, while the second tyrosine residue stabilizes the iron-coordinating tyrosine through hydrogen bonding, and participates in favorable π-stacking interactions with the porphyrin ring [83,91]. Intriguingly, the

same region used to bind hemin is also used by NEAT domains that interact with Hb in the IsdH and IsdB proteins. However, these domains lack the conserved YxxxY motif and are incapable of binding hemin. Instead the 3_{10}-helical lip portion contains a conserved aromatic-rich region that has been shown to interact the A- and E-helices of Hb [89,92–95].

The first step in hemin-acquisition by the Isd system is the capture of Hb by the receptors, IsdB and IsdH. Upon hemolysis, these surface receptors bind liberated Hb molecules and extract their hemin. IsdB and IsdH are the only Isd system proteins that contain multiple NEAT domains, with two and three domains, respectively. The domains in the protein have distinct functions; their N-terminal domain(s) ($IsdB^{N1}$, $IsdH^{N1}$, and $IsdH^{N2}$) only bind Hb, while their C-terminal NEAT domain ($IsdB^{N2}$ and $IsdH^{N3}$) binds hemin [95–97]. Interestingly, $IsdH^{N1}$ and $IsdH^{N2}$ also bind haptoglobin (Hp) through an unknown mechanism [84,95,96]. A considerable body of work demonstrates that IsdB and IsdH use a conserved tri-domain unit to synergistically extract hemin from Hb [69,98,99]. Studies of the IsdH protein are presented in this thesis. Its tri-domain unit consists of the second (N2, $IsdH^{N2}$) and third (N3, $IsdH^{N3}$) NEAT domains and a conserved helical linker domain that connects the NEAT domains (the tri-domain receptor is denoted $IsdH^{N2N3}$, residues A326-D660). A detailed and complete description of the molecular basis through which IsdH captures Hb and extracts its hemin is presented in chapters 2-4.

After the IsdB/IsdH surface receptors capture hemin from Hb, hemin is transferred to the IsdA protein. In vitro studies have shown that it has higher affinity than IsdB, and that holo-IsdB passes hemin to apo-IsdA at a rate that is ~87,000 times faster than the rate of spontaneous hemin release from IsdB. Therefore, hemin transfer is believed to occur via a protein-protein hemin transfer complex [73,100]. Like other Isd NEAT domains, the single NEAT domain in

IsdA binds hemin-iron in the high-spin penta-coordinate ferric (Fe(III)) state using the conserved YxxxY motif [80,88,100]. However, IsdA is unique as it is also capable of binding the low-spin hexa-coordinate ferrous (Fe(II)) state in which the iron atom is no longer coordinated by the tyrosine in the β7/β8 loop, but instead by a histidine residue in the 3_{10}-helical lip region [88,101]. IsdA is also unusual since unlike other Isd proteins it binds to host proteins such as fibronectin, fibrinogen, transferrin, fetuin, and asialofetuin, and possibly hemoglobin [64,102,103]. Adherence to these host proteins may facilitate infections, as IsdA has been shown to be necessary for adhesion of *S. aureus* to human desquamated epithelial cells [104,105].

In the third stage of the acquisition process hemin is transferred from IsdA to the IsdC protein. Of the NEAT-domain containing Isd proteins, IsdC has the highest affinity for hemin [100]. The structure of apo-IsdC is not known, but NMR experiments demonstrate that there is a flexible to rigid transition of the 3_{10}-helical lip upon binding hemin [85]. The structural plasticity of this region presumably promotes rapid hemin transfer from holo-IsdA to apo-IsdC, which occurs a rate that is > 70,000 times faster than the rate of simple hemin dissociation from IsdA [106]. As in the IsdH/B → IsdA hemin transfer step, IsdA → IsdC is believed to occur via an activated protein-protein hemin transfer complex. Paramagnetic NMR relaxation experiments have demonstrated that IsdA and IsdC associate via a transient ultra-weak "handclasp" complex, which juxtaposes their respective β7/β8 loops and 3_{10}-helical lip regions. This handclasp model has been further probed by molecular dynamics (MD) and quantum mechanics/molecular mechanics (QM/MM) simulations, which illustrated that NEAT domains orient themselves such that they there is two-fold symmetry about the hemin axis. From these studies it is thought that hemin transfer most likely proceeds through the simultaneous coordination of the iron atom by the conserved tyrosine residues in both the donor (IsdA) and acceptor (IsdC) proteins [72].

Interestingly, the ability of NEAT domains to transfer hemin to the IsdE protein is dependent upon stereospecific interactions. This is substantiated by the documented inability of holo-IsdA to transfer hemin to apo-IsdE, despite IsdE's higher affinity for hemin [74]. Photo-crosslinking experiments were able to localize the source of this specificity to a six-amino acid region that extends the β7/β8 loop of IsdC enabling hemin transfer to IsdE, whereas this section is absent in IsdA [107]. Interestingly, a chimera of IsdA that includes this extended region was indeed capable of rapidly transferring hemin to apo-IsdE. In addition to heterotypic hemin transfer between different types of proteins, homotypic transfer is also thought to mediate transfer across the cell wall between multiple copies of IsdA and/or IsdC [108]. In support of this notion, homotypic, self-transfer between either IsdA and IsdC proteins has been reported *in vitro* [107].

The fourth stage of hemin procurement is the passage of hemin from holo-IsdC to the IsdDEF ABC transporter, which imports hemin into the bacterial cytoplasm. Typical ABC transporters contain three main parts: a substrate binding component, a membrane permease, and an ATP hydrolase [109]. The substrate binding component, IsdE, is externally anchored to the cell membrane via a covalently attached lipid anchor. IsdE has the highest affinity for hemin of all the Isd proteins, but does not contain a NEAT domain. Instead, a crystal structure of IsdE revealed that it contains two domains bridged by a long helical backbone that provides a hemin binding grove at the domain-domain interface [110]. Unlike NEAT domains, the hemin moiety is completely buried and the hemin-iron is six-coordinate with protein axial ligands that originate from each domain, M78 and H229 [110–112]. It is unclear how hemin is passed through the membrane, but it has been suggested that interactions between IsdE and the membrane permease, IsdF, may facilitate this process. The energy needed to transport nutrients across the membrane usually involves the hydrolysis of ATP [113], but the ATP hydrolase that drives hemin import

has not been identified. IsdD is a putative membrane protein thought to act in conjunction with IsdE and IsdF, but its role in the hemin acquisition pathway has not been established and there are no known IsdD homologs in other Gram-positive bacteria. Interestingly, other *S.aureus* ABC transporters, like the siderophore transporters HtsABC and SiaABC, lack a dedicated ATP hydrolase and instead utilize FhuC to provide the power necessary to transport their cognate siderophores. Therefore, it is possible that FhuC could interact with the IsdEF complex to pump hemin into the cytoplasm [46,48]. Additionally, *S. aureus* strains lacking *isdDEF* are not growth impaired when hemin is the sole source of iron, further supporting the notion that alternative systems may exist that transport hemin across the cell membrane [6,64].

Upon reaching the bacterial cytoplasm, the hemin molecule is degraded by hemin oxygenases, IsdG or IsdI. While many bacterial hemin oxygenases (HO), such as HmuO in *C. diphtheriae*, share structurally similarity with known eukaryotic HOs, IsdG and IsdI are novel [114]. In particular, canonical HOs adopt structures that are predominantly formed by α-helices, whereas members of the IsdG family adopt ferrodoxin-like homodimeric structures [115]. Another unique feature of members of the IsdG family of HOs is that their bound hemin porphyrin rings are distorted or "ruffled" by a conserved tryptophan residue within their NWH catalytic triad [116]. Hemin-ruffling is thought to enhance the reactivity of IsdG and IsdI by eliminating the need for a catalytic hydrogen-bonding network that is usually present in canonical HOs. Unlike canonical HOs that break hemin down into biliverdin and carbon monoxide via cleavage at the α-meso carbon position, hemin ruffling by IsdG-like HOs facilitates cleavage at either the β- or δ-meso carbons, resulting in the release of two distinct staphylobilins (5-oxo-δ-bilirubin and 15-oxo-β-bilirubin) as well as formaldehyde. [114,117]. Since their discovery by Skaar and coworkers [75], IsdG homologs have been also been

characterized in *Bacillus anthracis* [118] and *Staphylococcus lugdunensis* [119], suggesting that Gram-positive pathogens use a conserved mechanism of hemin degradation.

The Isd hemin acquisition system is required by *S. aureus* to successfully establish infections [94,97,120]. Notably, work reported in two papers have suggested that the IsdA, IsdB, IsdH, and IsdE proteins are dispensable for *S. aureus* hemin-iron utilization from Hb [121,122]. However, the results of these studies are likely erroneous as they employed a lyophilized version of Hb that is structurally compromised [94,123]. This presumably led to supraphysiological concentrations of free hemin in these studies, which would mask the utility of the Isd system. Evidence that the Isd-system is important includes the results of numerous studies that have shown that even single deletions in *isdA, isdB, isdC, isdG, isdH,* or *isdI* are sufficient to significantly reduce *S. aureus* infectivity [52,94,124,125]. Furthermore, IsdA and IsdB have been shown to be required for the formation of staphylococcal abscesses, which are known to help prolong and disseminate infections [126,127].

1.5.2 Hemin Acquisition Systems in Other Gram-Positive Pathogens

Similar to *Staphylococcus aureus*, several other Gram-positive bacterial pathogens employ surface displayed proteins to capture hemin from human hemoglobin during infections. These hemin acquisition systems also employ proteins that contain NEAT domains, which are capable of either binding to hemin or hemoglobin. Below I briefly summarize what is known about these hemin acquisition systems and their relationship to the *S. aureus* Isd system.

1.5.3 *Streptococcus pyogenes*

Streptococcus pyogenes, commonly known as group A streptococcus (GAS), *S. pyogenes* is a β-hemolytic extracellular pathogen that causes disease directly (e.g. pharyngitis, sepsis, and impetigo) and indirectly (e.g. immune-mediated rheumatic fever, or toxin-mediated scarlet fever and toxic shock syndrome) [128–130]. GAS utilize host hemin-iron sources but there is no precedence for them to obtain iron from transferrin or lactoferrin, which is supported by their apparent lack of endogenous siderophore production [59]. GAS acquire hemin-iron using a 10-gene iron-regulated operon called the streptococcal iron acquisition (Sia) system that contains proteins that function similar to the Isd system (**Figure 1.4, panel second from the left**) [58]. In particular, the streptococcal hemoprotein receptor, Shr, is a large 145 kDa muti-domain protein that is functionally analogous to the Hb receptors, IsdB and IsdH. However, Shr lacks the overall sequence homology and domain architecture of these proteins. Shr is therefore a novel Hb receptor that consists of an N-terminal domain (NTD), an EF-hand motif and leucine rich repeat (LRR) sequences that are flanked by two NEAT domains (N1 and N2) [131]. Shr localizes to the cell membrane and spans the entire cell wall, exposing it to the extracellular environment and allowing it to also act as a bacterial adhesion to host proteins fibronectin and laminin [132]. Interestingly, it was shown that only the NTD was sufficient to mediate binding to Hb and there was no significant contribution to Hb binding by the two NEAT domains. This is consistent with both domains lacking the conserved aromatic-rich 3_{10}-helix found in IsdB and IsdH in *S. aureus* [83,93,131]. Within the NTD are two domains of unknown function (DUF1533), and future work characterizing these domains will shed light on the novel method GAS utilizes for Hb recognition. While the two NEAT domains bind hemin, they also lack the conserved iron-coordinating tyrosine found in many other NEAT domains suggesting a novel axial-ligand

mechanism by Shr. Furthermore, the C-terminal NEAT domain, N2, was shown to bind both ferrous and ferric heme-iron states, which has only been seen elsewhere in the *S. aureus* IsdA protein [101,131]. The function of the LRR region in Shr is also unknown. This architectural element is known to form horseshoe like structures [133], so it could position the N1 and N2 domains in close proximity to facilitate inter-domain hemin transfer. In support of this notion, isolated N1 and N2 domains rapidly transfer hemin to one another *in vitro* [134]. Furthermore, hemoproteins Hal and IlsA in *B. anthracis* [135] and *B. cereus* [57], respectively, also contain LRRs, suggesting a conserved function for these regions in hemin-iron acquisition.

Shr can rapidly remove hemin from Hb and transfer it to the streptococcal hemin-associated cell-surface protein, Shp [134,136]. Evidence suggests that Shp is a cell wall associated hemoprotein like acts similarly to IsdC in *S. aureus* [133]. It is the central conduit of the system, accepting hemin from Shr and passing it to the lipoprotein component of the ABC transporter complex, HtsABC (also known as SiaABC) [137]. The structure of Shp bound to hemin has been solved revealing a novel bis-methionyl hemin-iron ligation with an otherwise similar NEAT domain fold [138]. Holo-Shp rapidly transfers hemin to HtsA, which binds hemin vis a Met/His bis-ligation similar to IsdE [139,140]. Like the Isd system, hemin transfer is unidirectional with hemin flowing from Hb → Shr → Shp → HtsA [136,141,142]. After HtsA receives the hemin from Shp, it is translocated into the bacterial cytoplasm by the membrane permease, HtsB, which is powered by the ATP hydrolase, HtsC. However, once the hemin reaches the cytoplasm, the mechanisms by which it is degraded remain unclear, as no genes with homology to known hemin oxygenases have been discovered.

1.5.4 *Bacillus anthracis*

Bacillus anthracis is an endospore-forming anaerobe that is the causative agent of anthrax, which is a rare, but deadly disease that has a mortality rate as high as 90% [143]. The resilience of *B. anthracis* spores and its high lethality rate make this microbe a potential bioweapon [144]. *B. anthracis*' life cycle is complex and dynamic [145]. Initially, infectious spores enter the host via inhalation, ingestion, or a breach in the host's cutaneous layer. The spores are then rapidly phagocytosed by macrophages, where they subsequently germinate within the phagosome and proliferate in a vegetative state to cause macrophage lysis. Once liberated from the macrophages, bacteria disseminate throughout the host via the bloodstream. Siderophore production is essential for the intracellular survival of *B. anthracis* in locations where hemin isn't readily available [146]. However, the bacterium also employs hemin acquisition systems to access iron from host proteins to rapidly propagate within its host.

B. anthracis acquires hemin using proteins that are similar to those found in the *S. aureus'* Isd system, as well as other proteins that have unique localization and ligand binding characteristics (**Figure 1.4, middle panel**). Similar to the Isd system in *S. aureus, B. anthracis* encodes a cog-wheel for hemin transport, IsdC, as well as an ABC hemin transporter complex, IsdEF, and a hemin oxygenase, IsdG. However, it is distinct from *S. aureus*, as it secretes two hemophores, IsdX1 and IsdX2. It also displays a surface associated BslK protein that is non-covalently attached to the bacterium's protein rich crystalline S-layer, as well as the cell wall attached Hal protein [145]. The IsdX1 and IsdX2 hemophores contain one and five NEAT domains, respectively. [56,147]. Unlike characterized hemophores described in Gram-negative bacteria that scavenge hemin from various host proteins [9], the IsdX1 and IsdX2 proteins have limited specificity as they only appear to procure hemin from hemoglobin, and not from

myoglobin or the haptoglobin/hemoglobin complex [56,147]. Interestingly, biochemical studies indicate that the NEAT domains within these hemophores have distinct functionalities [56,148,149]. IsdX1, and IsdX2's N1, N3, N4, and N5 domains bind hemin using a canonical YxxxY motif, with N5 displaying the highest affinity for hemin. With the exception of the N5 domain in IsdX2 that is believed to function as a "hemin sponge", all of these domains are capable of rapidly transferring hemin to apo-IsdC. Intriguingly, IsdX2^{N2} does not bind hemin, but has been reported to bind Hb through a modified hemin-binding YxxxY motif in which the second tyrosine is replaced with a histidine residue [149]. Furthermore, it has also been reported that IsdX1, IsdX2^{N2}, IsdX2^{N5}, are capable of acquiring hemin from Hb. Notably, all of the NEAT domains in IsdX1 and IsdX2 lack the canonical aromatic-rich Hb-binding motif that is present in the *S. aureus'* IsdB^{N1}, IsdH^{N1}, and IsdH^{N2} Hb domains. This suggests that these domains will bind Hb via a novel mechanism. The mechanism of hemin extraction from Hb is not known, but recent studies have implicated residues within the 3_{10}-helix of IsdX1, IsdX2^{N2}, and IsdX2^{N5} proteins to be involved in Hb recognition [86,150]. Binding and transport of hemin at the cell surface is further facilitated by the *B. anthracis* S-layer homology protein K (BlsK) protein, which is localized to the bacterium's S-layer by its SLH (S-layer homology) domains. BlsK has been shown to rapidly transfer hemin to apo-IsdC, but the biological relevance of this event remains to be determined [151]. The fate of the hemin after reaching IsdC is believed to be similar to *S. aureus*, in which IsdC passes hemin to the IsdEF complex that transports hemin across the cell membrane into the cytoplasm where it is degraded by the IsdG hemin oxygenase [118].

Interestingly, the virulence of *B. anthracis* is not attenuated when the *isdC, isdX1,* and *isdX2* genes are the deleted, and utilization of hemin from Hb is not completely abolished in *isdC*

and BslK deletion strains [135,147,152]. This finding led to the discovery of the last protein implicated in *B. anthracis* hemin-iron acquisition, Hal (hemin-acquisition leucine-rich repeat protein). Hal contributes to *B. anthracis* virulence in a murine model of inhalational anthrax [153] and contains one NEAT domain and a LRR region that are capable of directly acquiring hemin from Hb [135]. However, how hemin is procured by Hal and imported into the cytoplasm remains a mystery.

1.5.5 *Listeria monocytogenes*

Listeria monocytogenes is a facultative intracellular pathogen that is the causative agent of listeriosis, a rare food-borne illness that has a mortality rate as high as 30% [154]. *L. monocytogenes* proliferates within its host using an array of virulence factors, including some that can promote its internalization into non-phagocytic cells [155]. *L. monocytogenes* contains an iron-regulated operon that contains nine protein encoding genes. Two of the genes encode for proteins that contain NEAT domains: Hbp1 and Hbp2 (for hemin binding protein, formally known as Lmo2186/SvpB and Lmo2185/SvpA, respectively) (**Figure 1.4, panel second from the right**). [156]. Previous immuno-labeling studies of Hbp1 and Hbp2 have shown that they are surface-exposed, whereas a western blot analysis has illustrated that most of the Hbp2 protein is secreted. Hbp1 and Hbp2 contain one and three NEAT domains, respectively [157–159]. Biochemical studies have shown that all of the domains bind to hemin, and have provided evidence that Hbp1 and the first (N1) and third (N3) NEAT domains in Hbp2 bind Hb. Although Hbp1 and Hbp2 are capable of binding Hb and hemin [160], there is no evidence that these proteins actively extract hemin from hemoglobin similar to the IsdB and IsdH proteins in *S. aureus* [68,69,99]. However, the hemophore characteristics of acquiring hemin from Hb and

inter-domain hemin transfer are analogous to *B. anthracis* proteins IsdX1 and IsdX2 [56,149]. While the hemin transfer mechanism is not known, it most likely occurs via a transient handclasp complex proposed for staphylococcal Isd proteins, as the individual NEAT domains in listerial proteins can transfer hemin rapidly between NEAT domains [160]. Interestingly, the second NEAT domain (N2) within Hbp2 that binds hemin lacks the second conserved tyrosine residue in the YxxxY hemin-binding motif. A recent structural study of the hemin-free and –bound states of $Hbp2^{N2}$ elucidated the molecular basis of hemin recognition, revealing an unusual mode of binding in which a tyrosine in the β7 strand (Y280) coordinates the hemin-iron atom instead of the canonical tyrosine located in the β8 strand [160]. Furthermore, a comparison of the structures of apo- and holo-$Hbp2^{N2}$ revealed unusually large hemin independent conformational changes. Cellular studies have suggested that Hbp1 and Hbp2 are required to scavenge hemin when it is at low concentrations (< 50 nM), [161] but that they are not needed when hemin is abundant. At these conditions hemin is thought to be transported into the cytoplasm by the HupDGC ABC transporter complex, which is required for growth on Hb or hemin as the sole source of iron [161,162]. The other protein products in the iron regulated operon of the *L. monocytogenes*' hemin acquisition locus have not been characterized. However, that locus contains a putative ABC transporter (Lmo2184, Lmo2183, and Lmo2182) that has been proposed to function similarly to the IsdDEF complex in *S. aureus* [156]. *L. monocytogenes* also encodes for proteins that are homologous to the IsdG hemin oxygenase in *S. aureus* [75,163], but they have not been characterized.

1.5.6 *Corynebacterium diphtheriae*

C. diphtheriae is a non-motile, non-spore forming anaerobe that is the causative agent of diphtheria, a severe respiratory disease that can lead to death [164]. The *C. diphtheriae* diphtheria toxin, DT, is a primary contributor to virulence as it inhibits protein synthesis. DT dissemination is believed to cause systemic toxic effects, particularly in the nervous system [165]. A hemin uptake system (Hmu) system is encoded by the *hmu* locus (**Figure 1.4, right panel**) [9]. It encodes for three proteins, a membrane-associated hemin/hemoglobin-binding protein (HmuT), a permease (HumU), and an ATPase (HmuV) [166]. HmuT is a lipoprotein and is thought to function similarly to *S. aureus* IsdE. However, unlike IsdE, HmuT has been reported *in vitro* to bind Hb [166]. Moreover, a recent study revealed that HmuT uses a conserved Tyr-His pair as axial ligands for hemin, which differs from the bis-Met-His ligands employed by IsdE [111,139,140,167,168]. Subsequent studies found additional genes located upstream of the hmu locus that are involved in hemin capture. Three genes are located in the *htaABC* operon positioned upstream [169]. These genes encode for HtaA and HtaB proteins, with the latter localizing to the cell membrane. This is in contrast to the HtaA protein, which is secreted into the extracellular environment when cells are grown in nutrient rich media, but associated with the cell membrane when they are grown in minimal media [169]. The role of the HtaC protein is unknown. Hemin and hemoprotein binding by HtaA and HtaB is facilitated by conserved regions, termed CR domains, that are ~150 amino acids in length and are believed to be structurally distinct from NEAT domains found in the aforementioned systems [170]. Hemin binding by CR domains is mediated by two conserved tyrosine residues and a conserved histidine residue, but the molecular basis of hemin binding has not been characterized. HtaB and HtaA contain one and two CR domains, respectively. HtaB has only been shown to bind hemin,

suggesting that it plays a intermediator role in hemin transport, whereas both CR domains in HtaA bind hemin, Hb, the Hp:Hb complex, Mb, and serum albumin [63]. HtaA can acquire hemin from host hemoproteins and transfer it to HtaB and/or HmuT, which is then transported into *C. diphtheriae*'s cytoplasm by HmuTUV to be degraded by a canonical hemin oxygenase, HmuO. This suggests a generally similar hemin uptake pathway as the Isd system in *S. aureus* despite the absence of NEAT domains [170,171].

The *Hmu-Hta* locus seems to be required for maximal growth during low concentrations of hemin and host proteins. However, deletion of the *Hmu-Hta* locus does not completely abolish growth when hemin is the sole source of iron [166,169,170]. This finding led to the discovery of the second and third corynebacterial hemin transport loci called *chtAB* and *cirA-chtC* [172]. Ongoing work has shed light on a complex yet redundant interplay between ChtA/ChtB, CirA/ChtC, and HtaA/HtaB systems in hemin acquisition by *C. diphtheriae.* ChtA, ChtB, and ChrC are membrane associated and surface exposed with each containing a single CR domain that mediates binding to hemin and Hb. In contrast, CirA lacks a CR domain and apparently does not bind hemin and/or Hb. Therefore, its role in hemin acquisition remains unclear. Recently it was shown that, like IsdH in *S. aureus*, HtaA, ChtA, and ChtC are able to bind the haptoglobin/hemoglobin complex and are required for utilization of Hp:Hb as an iron source [63,95,97]. ChtB was shown to not bind Hb, suggesting a similar functional role as HtaB. The fate of hemin procured by ChtA and ChtC is not known, but it has been suggested that these proteins could interact with HtaA, which could then transfer the hemin to HtaB (or ChtB), and then transport the hemin into the cytoplasm via HmuTUV [173]. However, future studies are necessary to test this hypothesis. Finally, isolates of *C. diphtheriae* that lack *htaA*, *chtA*, and *chtC*

are still capable of exploiting host hemoproteins as sources of iron [173], suggesting the presence of yet another unidentified hemin acquisition system.

1.6 Scope of the Dissertation

During infections the pathogen *Staphylococcus aureus* actively procures hemin-iron from human hemoglobin (Hb) using the iron-regulated surface determinant (Isd) system. Related systems are also used by other Gram-positive pathogens to acquire hemin from hemoglobin. Research described in this dissertation investigated how the Isd system uses the IsdH protein to extract hemin from Hb. IsdH uses NEAr iron Transporter (NEAT) domains with a conserved tri-domain unit to rapidly extract Hb's hemin. Research described in Chapter 2 used UV-Vis spectroscopy, nuclear magnetic resonance (NMR) spectroscopy, and electrospray ionization mass spectrometry (ESI-MS) methods to illustrate that the components of the tri-domain unit work together to synergistically extract hemin. Among other findings, the results highlighted the importance of the conserved linker domain. The work described in Chapter 3 defined the structure and dynamics of the tri-domain unit, hereafter referred to as $IsdH^{N2N3}$. The structure of the apo-receptor in solution was defined using small angle X-ray scattering, and advanced NMR methods such as paramagnetic relaxation enhancement (PRE), residual dipolar coupling (RDC), and selective methyl labeling approaches. Using ensemble modeling calculations, the structure and inter-domain dynamics of $IsdH^{N2N3}$ were defined. The results of these studies indicate that the receptor binds to Hb using a combination of conformational selection and induced fit mechanisms, and suggest that the linker domain may facilitate hemin transfer by destabilizing the F-helix in Hb. In chapter 4, the kinetic and thermodynamic basis of hemin transfer were investigated using stopped-flow UV-Vis spectroscopy, analytical ultracentrifugation

sedimentation equilibrium and isothermal titration experiments. The results of this work shed light on the kinetic and thermodynamic determinants that facilitate receptor-mediated hemin release from Hb. Lastly, Chapter 5 describes the methods that were used to site-specifically label proteins with nitroxide probes and to derive paramagnetic distance restraints. Combined, the results of the work described in this dissertation have advanced our knowledge of Hb recognition and hemin acquisition by the medically important pathogen, *S. aureus*.

1.7 Figures

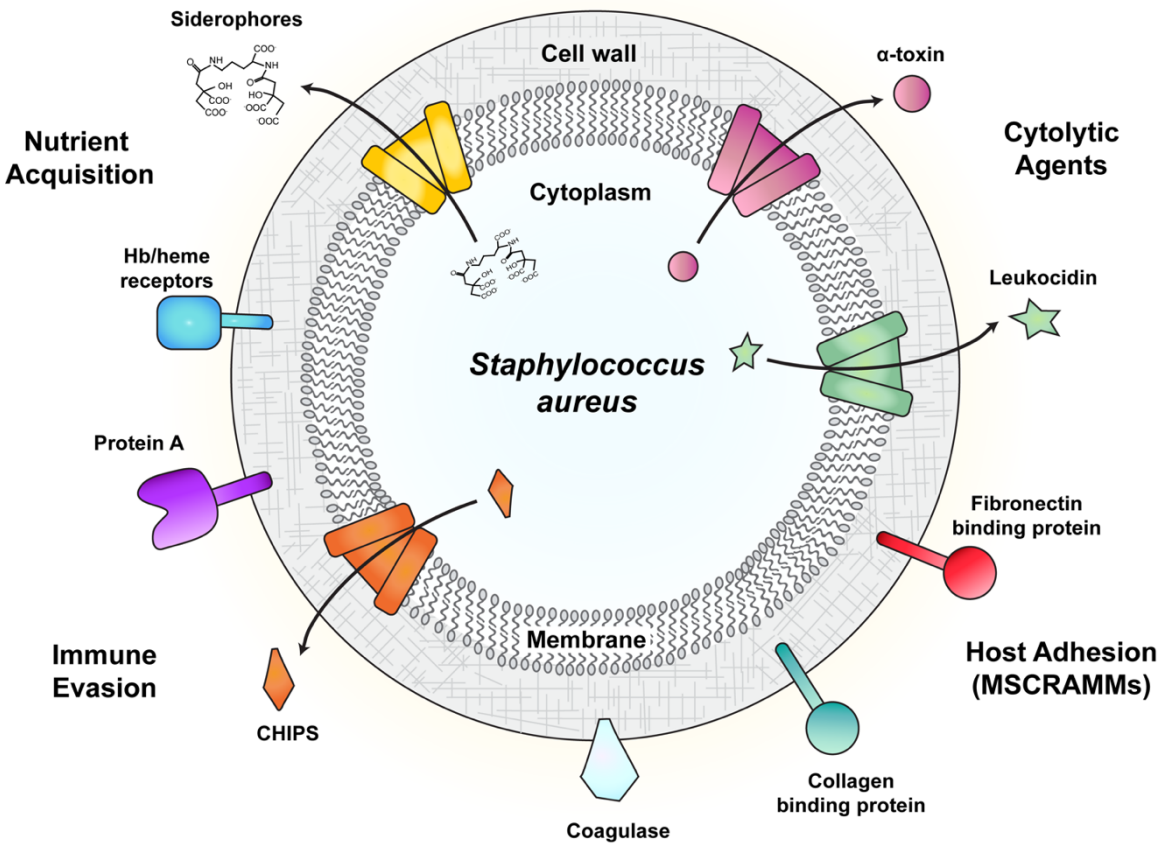

Figure 1.1 Virulence factors of *Staphylococcus aureus*

Both structural and secreted virulence factors play a direct role in *S. aureus* infectivity. Clockwise from the top right, secreted cytolytic agents such as α-toxin and leukocidin are pore-forming proteins that lyse host cells to gain access to their nutrients or to neutralize the innate host immune defense. Adhesion to the host is mediated by MSCRAMMs (microbial surface components recognizing adhesive matrix molecules) which is a large family of proteins that contain two subdomains with IgG-like folds. Generally, these factors facilitate binding to extracellular matrix molecules such as fibronectin and collagen. Coagulase interacts with

prothrombin that catalyzes the conversion of fibrinogen to fibrin leading to blood clotting. Immune evasion is carried out by structural proteins such as protein A that binds the Fc region of IgG inhibiting phagocytic engulfment, while secreted CHIPS (chemotaxis inhibitory protein of *S. aureus*) inhibit neutrophil and monocyte chemotaxis. Nutrient acquisition allows the microbe to proliferate within its host. In particular, iron acquisition is mediated by surface proteins that capture iron-laden hemin (oxidized form of heme) and hemoglobin (Hb) from lysed erythrocytes as well as small siderophore molecules that bind extracellular iron with high affinity. This image was adapted from [24].

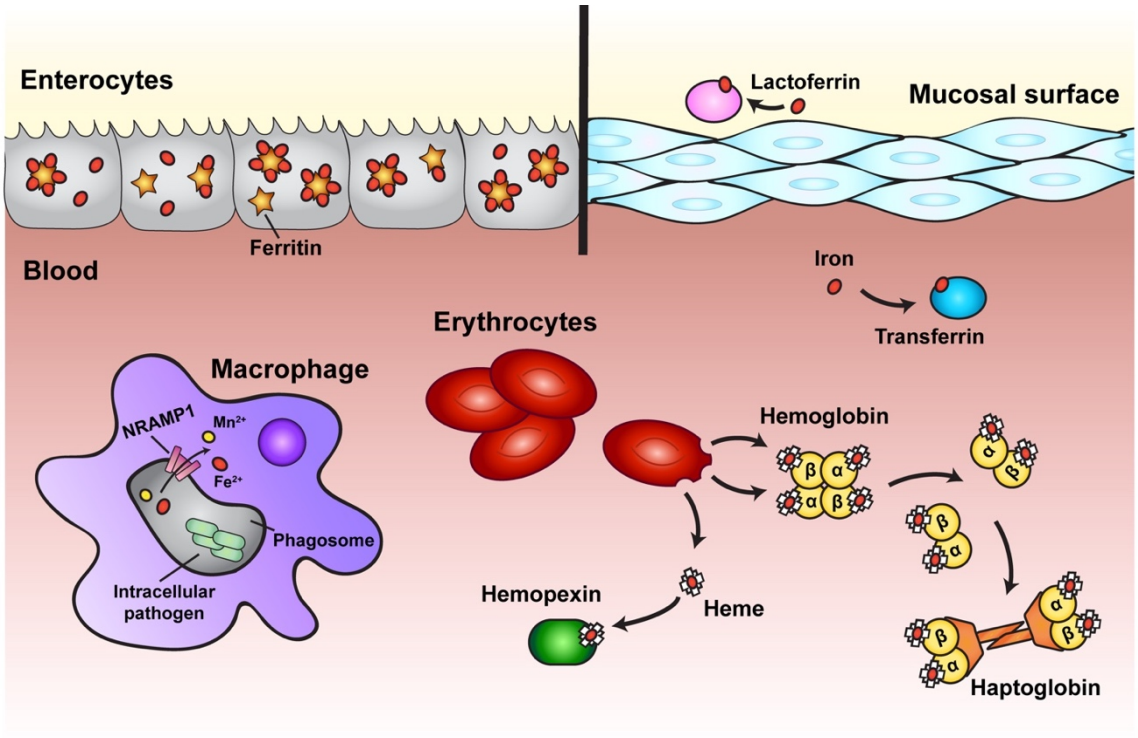

Figure 1.2 Overview of human nutritional immunity strategies

Iron is stored intracellularly by complexing with ferritin, or bound extracellularly by binding to transferrin in serum or lactoferrin at mucosal surfaces. In blood, iron is complexed with heme, which is bound by hemoglobin found in erythrocytes. Upon erythrocyte lysis, hemoglobin is released and dissociates into its respective dimeric units, which is bound by haptoglobin. Any free heme is scavenged by hemopexin. In addition, any intracellular pathogens are limited in their access to metal ions, as the natural resistance-associated macrophage protein 1 (NRAMP1) found in the phagosomal membrane, pumps Fe^{2+} and Mn^{2+}out of the phagosomal compartment. This image was adapted from [35].

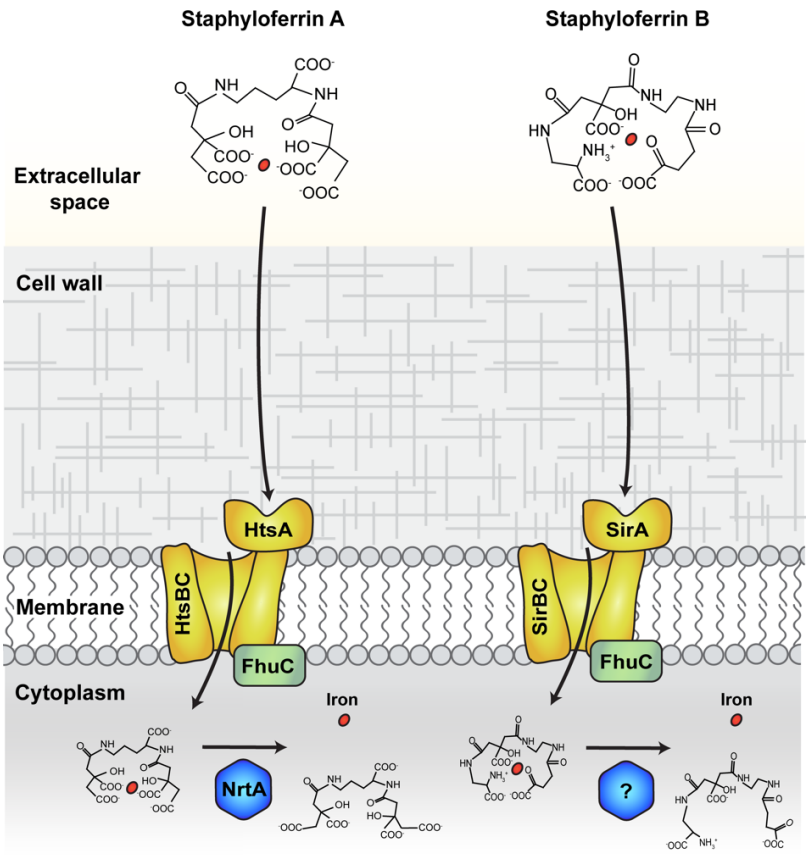

Figure 1.3 Siderophore transport in *S. aureus*

Secreted siderophores, Staphyloferrin A and B, bind ferric iron extracellularly and are transported into the bacterium by their respective ABC transporters. Staphyloferrin A import is facilitated by the HtsA lipoprotein and HtsBC permease, whereas the liprotein, SirA, is the receptor for staphyloferrin B and translocation across the membrane is mediated by the SirBC permease. The FhuC ATPase provides the energy necessary to drive translocation for both siderophores' import. Once in the cytoplasm, iron release from siderophores is facilitated by reductases that reduce the ferric-siderophore complex to the less stable ferrous state, releasing free iron for the microbe to use. For staphyloferrin A, the reductase is an iron-regulated nitroreductase, NrtA, while the reductase for staphyloferrin B remains unknown.

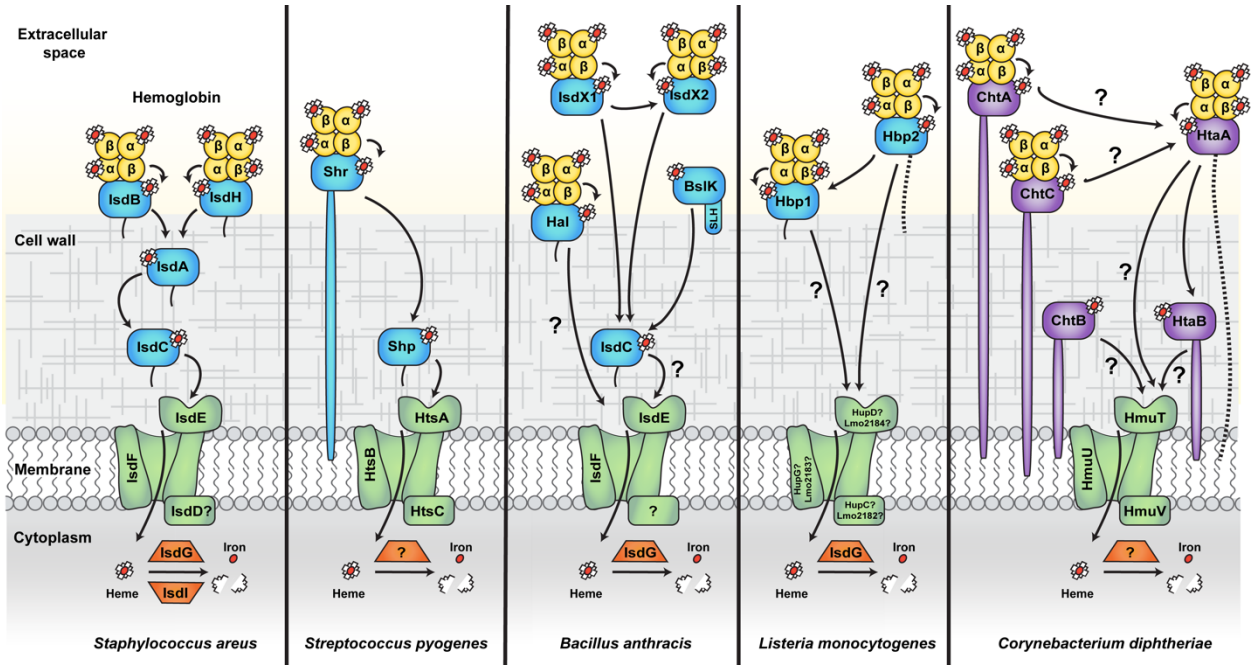

Figure 1.4 Heme acquisition systems in Gram-positive bacteria

Iron import varies greatly among various Gram-positive microbes. In general, hemoglobin is captured by surface receptors that acquire its hemin which is then transferred through the cell wall by other hemoproteins (colored blue and purple). The hemin is then translocated through the cell membrane by bacterial ABC transporters (colored in green). Once in the cytoplasm, the hemin is degraded by hemin oxygenases (colored in orange) that release free iron for the bacterium to use. Proteins that bind hemin and/or Hb using NEAT and CR domains are colored in blue and purple, respectively. Proteins known to have different localizations have dotted lines, whereas solid lines represent covalent attachment to the cell wall. A ‘‘?’’ denotes uncharacterized proteins or stages in hemin transport.

1.8 References

[1] R.M. Klevens, M.A. Morrison, J. Nadle, S. Petit, K. Gershman, S. Ray, L.H. Harrison, R. Lynfield, G. Dumyati, J.M. Townes, A.S. Craig, E.R. Zell, G.E. Fosheim, L.K. McDougal, R.B. Carey, S.K. Fridkin, Active Bacterial Core surveillance (ABCs) MRSA Investigators, Invasive methicillin-resistant Staphylococcus aureus infections in the United States., J. Am. Med. Assoc., 298 (2007) 1763–71. doi:10.1001/jama.298.15.1763.

[2] A.W. Maresso, O. Schneewind, Iron acquisition and transport in Staphylococcus aureus., Biometals. 19 (2006) 193–203. doi:10.1007/s10534-005-4863-7.

[3] U.E. Schaible, S.H.E. Kaufmann, Iron and microbial infection., Nat. Rev. Microbiol. 2 (2004) 946–53. doi:10.1038/nrmicro1046.

[4] P. Cornelis, S.C. Andrews, eds. Iron Uptake and Homeostasis in Microorganisms, Caister Academic Press, Norfolk, UK, pp 302 (2010).

[5] A.J. Farrand, M.L. Reniere, H. Ingmer, D. Frees, E.P. Skaar, Regulation of Host Hemoglobin Binding by the Staphylococcus aureus Clp Proteolytic System, J. Bacteriol. 195 (2013) 5041–5050. doi:10.1128/JB.00505-13.

[6] E.P. Skaar, M. Humayun, T. Bae, K.L. DeBord, O. Schneewind, Iron-source preference of Staphylococcus aureus infections., Science. 305 (2004) 1626–8. doi:10.1126/science.1099930.

[7] C. Ratledge, L.G. Dover, Iron metabolism in pathogenic bacteria., Annu. Rev. Microbiol. 54 (2000) 881–941. doi:10.1146/annurev.micro.54.1.881.

[8] C. Wandersman, P. Delepelaire, Bacterial Iron Sources: From Siderophores to Hemophores. (2004).

[9] L.J. Runyen-Janecky, Role and regulation of heme iron acquisition in gram-negative pathogens., Front. Cell. Infect. Microbiol. 3 (2013) 55. doi:10.3389/fcimb.2013.00055.

[10] R.J. Gorwitz, D. Kruszon-Moran, S.K. McAllister, G. McQuillan, L.K. McDougal, G.E. Fosheim, B.J. Jensen, G. Killgore, F.C. Tenover, M.J. Kuehnert, Changes in the prevalence of nasal colonization with Staphylococcus aureus in the United States, 2001-2004., J. Infect. Dis. 197 (2008) 1226–34. doi:10.1086/533494.

[11] C.L. Ventola, The antibiotic resistance crisis: part 1: causes and threats., Pharmacy & Therapeutics. 40 (2015) 277–83.

[12] CDC, Antibiotic resistance threats in the United States, 2013. (2013) 114. doi:CS239559-B.

[13] M. Otto, MRSA virulence and spread., Cell. Microbiol. 14 (2012) 1513–21. doi:10.1111/j.1462-5822.2012.01832.x.

[14] M.Z. David, R.S. Daum, Community-associated methicillin-resistant Staphylococcus aureus: epidemiology and clinical consequences of an emerging epidemic., Clin. Microbiol. Rev. 23 (2010) 616–87. doi:10.1128/CMR.00081-09.

[15] A.I. Hidron, E. V Kourbatova, J.S. Halvosa, B.J. Terrell, L.K. McDougal, F.C. Tenover, H.M. Blumberg, M.D. King, Risk factors for colonization with methicillin-resistant

Staphylococcus aureus (MRSA) in patients admitted to an urban hospital: emergence of community-associated MRSA nasal carriage., Clin. Infect. Dis. 41 (2005) 159–66. doi:10.1086/430910.

[16] B. Lee, A. Singh, M. David, S.M. Bartsch, R.B. Slayton, S.S. Huang, S.M. Zimmer, M.A. Potter, C.M. Macal, D.S. Lauderdale, L. Miller, R. Daum, The economic burden of community-associated methicillin-resistant Staphylococcus aureus (CA-MRSA), Clin. Microbiol. Infect. 19 (2013) 528–536. doi:10.1111/j.1469-0691.2012.03914.x.

[17] N.E. Holmes, B.P. Howden, What's new in the treatment of serious MRSA infection?, Curr. Opin. Infect. Dis. 27 (2014) 471–8. doi:10.1097/QCO.0000000000000101.

[18] I.A. Myles, S.K. Datta, Staphylococcus aureus: an introduction, Semin. Immunopathol. 34 (2012) 181–184. doi:10.1007/s00281-011-0301-9.

[19] T.J. Foster, J.A. Geoghegan, V.K. Ganesh, M. Höök, Adhesion, invasion and evasion: the many functions of the surface proteins of Staphylococcus aureus, Nat. Rev. Microbiol. 12 (2014) 49–62. doi:10.1038/nrmicro3161.

[20] M. Graille, E.A. Stura, a L. Corper, B.J. Sutton, M.J. Taussig, J.B. Charbonnier, G.J. Silverman, Crystal structure of a Staphylococcus aureus protein A domain complexed with the Fab fragment of a human IgM antibody: structural basis for recognition of B-cell receptors and superantigen activity., Proc. Natl. Acad. Sci. U. S. A. 97 (2000) 5399–5404. doi:10.1073/pnas.97.10.5399.

[21] P.K. Peterson, J. Verhoef, L.D. Sabath, P.G. Quie, Effect of protein A on staphylococcal opsonization., Infect. Immun. 15 (1977) 760–4.

[22] C.J.C. de Haas, K.E. Veldkamp, A. Peschel, F. Weerkamp, W.J.B. Van Wamel, E.C.J.M. Heezius, M.J.J.G. Poppelier, K.P.M. Van Kessel, J.A.G. van Strijp, Chemotaxis Inhibitory Protein of *Staphylococcus aureus*, a Bacterial Antiinflammatory Agent, J. Exp. Med. 199 (2004) 687–695. doi:10.1084/jem.20031636.

[23] R.J. Gordon, F.D. Lowy, Pathogenesis of Methicillin-Resistant *Staphylococcus aureus* Infection, Clin. Infect. Dis. 46 (2008) S350–S359. doi:10.1086/533591.

[24] F.D. Lowy, Staphylococcus aureus infections., N. Engl. J. Med. 339 (1998) 520–32. doi:10.1056/NEJM199808203390806.

[25] A. Peschel, M. Otto, Phenol-soluble modulins and staphylococcal infection, Nat. Rev. Microbiol. 11 (2013) 667–673. doi:10.1038/nrmicro3110.

[26] M. Otto, Staphylococcus aureus toxins, Curr. Opin. Microbiol. 17 (2014) 32–37. doi:10.1016/j.mib.2013.11.004.

[27] N.D. Hammer, E.P. Skaar, Molecular Mechanisms of Staphylococcus aureus Iron Acquisition., Annu. Rev. Microbiol. 65 (2011) 129–47. doi:10.1146/annurev-micro-090110-102851.

[28] J.E. Cassat, E.P. Skaar, Iron in Infection and Immunity, Cell Host Microbe. 13 (2013) 509–519. doi:10.1016/j.chom.2013.04.010.

[29] P.T. Lieu, M. Heiskala, P.A. Peterson, Y. Yang, The roles of iron in health and disease, Mol. Aspects Med. 22 (2001) 1–87. doi:10.1016/S0098-2997(00)00006-6.

[30] D. Touati, Iron and oxidative stress in bacteria., Arch. Biochem. Biophys. 373 (2000) 1–6. doi:10.1006/abbi.1999.1518.
[31] M. Wessling-Resnick, Biochemistry of iron uptake., Crit. Rev. Biochem. Mol. Biol. 34 (1999) 285–314. doi:10.1080/10409239991209318.
[32] N.A. Sirnonian, J.T. Coyle, Oxidative Stress in Neurodegenerative Diseases, Annu Rev. Pharmacol. Toxicol. 36 (1996) 83–106. doi:10.1007/s12035-015-9337-5.
[33] B. Halliwell, J.M.C. Gutteridge, Lipid Peroxidation in Brain Homogenates: The Role of Iron and Hydroxyl Radicals, J. Neurochem. 69 (2002) 1330–1330. doi:10.1046/j.1471-4159.1997.69031330.x.
[34] J.A. Simcox, D.A. McClain, Iron and Diabetes Risk, Cell Metab. 17 (2013) 329–341. doi:10.1016/j.cmet.2013.02.007.
[35] M.I. Hood, E.P. Skaar, Nutritional immunity: transition metals at the pathogen-host interface., Nat. Rev. Microbiol. 10 (2012) 525–37. doi:10.1038/nrmicro2836.
[36] A. Smith, R.J. McCulloh, Hemopexin and haptoglobin: allies against heme toxicity from hemoglobin not contenders., Front. Physiol. 6 (2015) 187. doi:10.3389/fphys.2015.00187.
[37] M. Kristiansen, J.H. Graversen, C. Jacobsen, O. Sonne, H.J. Hoffman, S.K. Law, S.K. Moestrup, Identification of the haemoglobin scavenger receptor., Nature. 409 (2001) 198–201. doi:10.1038/35051594.
[38] P.L.M. Schmaier A.H., Hematology for Medical Students, Lippincott Williams & Wilkins, Philadelphia, PA, 2003.
[39] E.P. Skaar, The Battle for Iron between Bacterial Pathogens and Their Vertebrate Hosts, PLoS Pathog. 6 (2010) e1000949. doi:10.1371/journal.ppat.1000949.
[40] K.P. Haley, E.P. Skaar, A battle for iron: host sequestration and Staphylococcus aureus acquisition., Microbes Infect. 14 (2012) 217–27. doi:10.1016/j.micinf.2011.11.001.
[41] N. Jabado, A. Jankowski, S. Dougaparsad, V. Picard, S. Grinstein, P. Gros, Natural resistance to intracellular infections: natural resistance-associated macrophage protein 1 (Nramp1) functions as a pH-dependent manganese transporter at the phagosomal membrane., J. Exp. Med. 192 (2000) 1237–48.
[42] K.N. Raymond, E.A. Dertz, S.S. Kim, Enterobactin: an archetype for microbial iron transport., Proc. Natl. Acad. Sci. U. S. A. 100 (2003) 3584–8. doi:10.1073/pnas.0630018100.
[43] J.R. Sheldon, D.E. Heinrichs, Recent developments in understanding the iron acquisition strategies of gram positive pathogens., FEMS Microbiol. Rev. 39 (2015) 592–630. doi:10.1093/femsre/fuv009.
[44] T. Zheng, E.M. Nolan, Siderophore-based detection of Fe(iii) and microbial pathogens, Metallomics. 4 (2012) 866. doi:10.1039/c2mt20082a.
[45] D.B. Friedman, D.L. Stauff, G. Pishchany, C.W. Whitwell, V.J. Torres, E.P. Skaar, Staphylococcus aureus Redirects Central Metabolism to Increase Iron Availability, PLoS Pathog. 2 (2006) e87. doi:10.1371/journal.ppat.0020087.
[46] F.C. Beasley, E.D. Vinés, J.C. Grigg, Q. Zheng, S. Liu, G.A. Lajoie, M.E.P. Murphy, D.E.

Heinrichs, Characterization of staphyloferrin A biosynthetic and transport mutants in *Staphylococcus aureus*, Mol. Microbiol. 72 (2009) 947–963. doi:10.1111/j.1365-2958.2009.06698.x.

[47] J.C. Grigg, J.D. Cooper, J. Cheung, D.E. Heinrichs, M.E.P. Murphy, The Staphylococcus aureus Siderophore Receptor HtsA Undergoes Localized Conformational Changes to Enclose Staphyloferrin A in an Arginine-rich Binding Pocket, J. Biol. Chem. 285 (2010) 11162–11171. doi:10.1074/jbc.M109.097865.

[48] C.D. Speziali, S.E. Dale, J.A. Henderson, E.D. Vines, D.E. Heinrichs, Requirement of Staphylococcus aureus ATP-Binding Cassette-ATPase FhuC for Iron-Restricted Growth and Evidence that It Functions with More than One Iron Transporter, J. Bacteriol. 188 (2006) 2048–2055. doi:10.1128/JB.188.6.2048-2055.2006.

[49] R.C. Hider, X. Kong, Chemistry and biology of siderophores, Nat. Prod. Rep. 27 (2010) 637. doi:10.1039/b906679a.

[50] M. Hannauer, A.J. Arifin, D.E. Heinrichs, Involvement of reductases IruO and NtrA in iron acquisition by *S taphylococcus aureus*, Mol. Microbiol. 96 (2015) 1192–1210. doi:10.1111/mmi.13000.

[51] A.K. Sia, B.E. Allred, K.N. Raymond, Siderocalins: Siderophore binding proteins evolved for primary pathogen host defense, Curr. Opin. Chem. Biol. 17 (2013) 150–157. doi:10.1016/j.cbpa.2012.11.014.

[52] V.J. Torres, G. Pishchany, M. Humayun, O. Schneewind, E.P. Skaar, Staphylococcus aureus IsdB is a hemoglobin receptor required for heme iron utilization., J. Bacteriol. 188 (2006) 8421–9. doi:10.1128/JB.01335-06.

[53] T.A. Patel, E. Belcher, T.D. Warner, S.E. Harding, J.A. Mitchell, Identification and characterization of a dysfunctional cardiac myocyte phenotype: role of bacteria, Toll-like receptors, and endothelin., Shock. 28 (2007) 434–440. doi:10.1097/shk.0b013e31804a55a7.

[54] G. Pishchany, S.E. Dickey, E.P. Skaar, Subcellular localization of the Staphylococcus aureus heme iron transport components IsdA and IsdB., Infect. Immun. 77 (2009) 2624–34. doi:10.1128/IAI.01531-08.

[55] R.L. Marvig, S. Damkiær, S.M.H. Khademi, T.M. Markussen, S. Molin, L. Jelsbak, Within-host evolution of Pseudomonas aeruginosa reveals adaptation toward iron acquisition from hemoglobin., MBio. 5 (2014) e00966–14. doi:10.1128/mBio.00966-14.

[56] A.W. Maresso, G. Garufi, O. Schneewind, Bacillus anthracis secretes proteins that mediate heme acquisition from hemoglobin., PLoS Pathog. 4 (2008) e1000132. doi:10.1371/journal.ppat.1000132.

[57] N. Daou, C. Buisson, M. Gohar, J. Vidic, H. Bierne, M. Kallassy, D. Lereclus, C. Nielsen-LeRoux, IlsA, a unique surface protein of Bacillus cereus required for iron acquisition from heme, hemoglobin and ferritin., PLoS Pathog. 5 (2009) e1000675. doi:10.1371/journal.ppat.1000675.

[58] C.S. Bates, G.E. Montañez, C.R. Woods, R.M. Vincent, Z. Eichenbaum, Identification

and characterization of a Streptococcus pyogenes operon involved in binding of hemoproteins and acquisition of iron., Infect. Immun. 71 (2003) 1042–55.
[59] Z. Eichenbaum, E. Muller, S.A. Morse, J.R. Scott, Acquisition of iron from host proteins by the group A streptococcus., Infect. Immun. 64 (1996) 5428–9.
[60] S.S. Tai, C.J. Lee, R.E. Winter, Hemin utilization is related to virulence of Streptococcus pneumoniae., Infect. Immun. 61 (1993) 5401–5.
[61] J.R. Brozyna, J.R. Sheldon, D.E. Heinrichs, Growth promotion of the opportunistic human pathogen, Staphylococcus lugdunensis, by heme, hemoglobin, and coculture with Staphylococcus aureus., Microbiologyopen. 3 (2014) 182–95. doi:10.1002/mbo3.162.
[62] G. Pishchany, A.L. McCoy, V.J. Torres, J.C. Krause, J.E. Crowe, M.E. Fabry, E.P. Skaar, Specificity for human hemoglobin enhances Staphylococcus aureus infection., Cell Host Microbe. 8 (2010) 544–50. doi:10.1016/j.chom.2010.11.002.
[63] C.E. Allen, M.P. Schmitt, Utilization of Host Iron Sources by Corynebacterium diphtheriae: Multiple Hemoglobin-Binding Proteins Are Essential for the Use of Iron from the Hemoglobin-Haptoglobin Complex, J. Bacteriol. 197 (2015) 553–562. doi:10.1128/JB.02413-14.
[64] S.K. Mazmanian, E.P. Skaar, A.H. Gaspar, M. Humayun, P. Gornicki, J. Jelenska, A. Joachmiak, D.M. Missiakas, O. Schneewind, Passage of heme-iron across the envelope of Staphylococcus aureus., Science. 299 (2003) 906–9ma. doi:10.1126/science.1081147.
[65] M.L. Reniere, V.J. Torres, E.P. Skaar, Intracellular metalloporphyrin metabolism in Staphylococcus aureus., Biometals. 20 (2007) 333–45. doi:10.1007/s10534-006-9032-0.
[66] S.K. Mazmanian, H. Ton-That, K. Su, O. Schneewind, An iron-regulated sortase anchors a class of surface protein during Staphylococcus aureus pathogenesis., Proc. Natl. Acad. Sci. U. S. A. 99 (2002) 2293–8. doi:10.1073/pnas.032523999.
[67] N. Muryoi, M.T. Tiedemann, M. Pluym, J. Cheung, D.E. Heinrichs, M.J. Stillman, Demonstration of the Iron-regulated Surface Determinant (Isd) Heme Transfer Pathway in Staphylococcus aureus, J. Biol. Chem. 283 (2008) 28125–28136. doi:10.1074/jbc.M802171200.
[68] C.F. Bowden, M.M. Verstraete, L.D. Eltis, M.E.P. Murphy, Hemoglobin binding and catalytic heme extraction by IsdB NEAT domains., Biochemistry. (2014). doi:10.1021/bi500230f.
[69] T. Spirig, G.R. Malmirchegini, J. Zhang, S.A. Robson, M. Sjodt, M. Liu, K. Krishna Kumar, C.F. Dickson, D.A. Gell, B. Lei, J. A. Loo, R.T. Clubb, Staphylococcus aureus uses a novel multidomain receptor to break apart human hemoglobin and steal its heme., J. Biol. Chem. 288 (2013) 1065–78. doi:10.1074/jbc.M112.419119.
[70] M. Sjodt, R. Macdonald, T. Spirig, A.H. Chan, C.F. Dickson, M. Fabian, J.S. Olson, D.A. Gell, R.T. Clubb, The PRE-Derived NMR Model of the 38.8kDa Tri-Domain IsdH Protein from Staphylococcus aureus Suggests that it Adaptively Recognizes Human Hemoglobin., J. Mol. Biol. (2015). doi:10.1016/j.jmb.2015.02.008.
[71] V.A. Villareal, T. Spirig, S.A. Robson, M. Liu, B. Lei, R.T. Clubb, Transient weak

protein-protein complexes transfer heme across the cell wall of Staphylococcus aureus., J. Am. Chem. Soc. 133 (2011) 14176–9. doi:10.1021/ja203805b.

[72] Y. Moriwaki, T. Terada, K. Tsumoto, K. Shimizu, Rapid Heme Transfer Reactions between NEAr Transporter Domains of Staphylococcus aureus: A Theoretical Study Using QM/MM and MD Simulations, PLoS One. 10 (2015) e0145125. doi:10.1371/journal.pone.0145125.

[73] H. Zhu, G. Xie, M. Liu, J.S. Olson, M. Fabian, D.M. Dooley, B. Lei, Pathway for heme uptake from human methemoglobin by the iron-regulated surface determinants system of Staphylococcus aureus., J. Biol. Chem. 283 (2008) 18450–60. doi:10.1074/jbc.M801466200.

[74] M.T. Tiedemann, M.J. Stillman, Heme binding to the IsdE(M78A; H229A) double mutant: challenging unidirectional heme transfer in the iron-regulated surface determinant protein heme transfer pathway of Staphylococcus aureus., J. Biol. Inorg. Chem. 17 (2012) 995–1007. doi:10.1007/s00775-012-0914-z.

[75] E.P. Skaar, A.H. Gaspar, O. Schneewind, IsdG and IsdI, heme-degrading enzymes in the cytoplasm of Staphylococcus aureus., J. Biol. Chem. 279 (2004) 436–43. doi:10.1074/jbc.M307952200.

[76] F. Vandenesch, G. Lina, T. Henry, Staphylococcus aureus hemolysins, bi-component leukocidins, and cytolytic peptides: a redundant arsenal of membrane-damaging virulence factors?, Front. Cell. Infect. Microbiol. 2 (2012) 12. doi:10.3389/fcimb.2012.00012.

[77] E.P. Skaar, O. Schneewind, Iron-regulated surface determinants (Isd) of Staphylococcus aureus: stealing iron from heme., Microbes Infect. 6 (2004) 390–7.

[78] H. Ton-That, L.A. Marraffini, O. Schneewind, Protein sorting to the cell wall envelope of Gram-positive bacteria., Biochim. Biophys. Acta. 1694 (2004) 269–78. doi:10.1016/j.bbamcr.2004.04.014.

[79] T. Spirig, E.M. Weiner, R.T. Clubb, Sortase enzymes in Gram-positive bacteria, Mol. Microbiol. 82 (2011) 1044–59. doi:10.1111/j.1365-2958.2011.07887.x.

[80] J.C. Grigg, C.X. Mao, M.E.P.P. Murphy, Iron-coordinating tyrosine is a key determinant of NEAT domain heme transfer., J. Mol. Biol. 413 (2011) 684–98. doi:10.1016/j.jmb.2011.08.047.

[81] M. Watanabe, Y. Tanaka, A. Suenaga, M. Kuroda, M. Yao, N. Watanabe, F. Arisaka, T. Ohta, I. Tanaka, K. Tsumoto, Structural basis for multimeric heme complexation through a specific protein-heme interaction: the case of the third neat domain of IsdH from Staphylococcus aureus., J. Biol. Chem. 283 (2008) 28649–59. doi:10.1074/jbc.M803383200.

[82] M. Andrade, F. Ciccarelli, C. Perez-Iratxeta, P. Bork, NEAT: a domain duplicated in genes near the components of a putative Fe3+ siderophore transporter from Gram-positive pathogenic bacteria, Genome Biol. 3 (2002) research0047.1–research0047.5. doi:10.1186/gb-2002-3-9-research0047.

[83] J.C. Grigg, G. Ukpabi, C.F.M. Gaudin, M.E.P. Murphy, Structural biology of heme

binding in the Staphylococcus aureus Isd system., J. Inorg. Biochem. 104 (2010) 341–8. doi:10.1016/j.jinorgbio.2009.09.012.

[84] R.M. Pilpa, E.A. Fadeev, V.A. Villareal, M.L. Wong, M. Phillips, R.T. Clubb, Solution structure of the NEAT (NEAr Transporter) domain from IsdH/HarA: the human hemoglobin receptor in Staphylococcus aureus., J. Mol. Biol. 360 (2006) 435–47. doi:10.1016/j.jmb.2006.05.019.

[85] V.A. Villareal, R.M. Pilpa, S.A. Robson, E.A. Fadeev, R.T. Clubb, The IsdC protein from Staphylococcus aureus uses a flexible binding pocket to capture heme., J. Biol. Chem. 283 (2008) 31591–600. doi:10.1074/jbc.M801126200.

[86] M.T. Ekworomadu, C.B. Poor, C.P. Owens, M.A. Balderas, M. Fabian, J.S. Olson, F. Murphy, E. Bakkalbasi, E. Balkabasi, E.S. Honsa, C. He, C.W. Goulding, A.W. Maresso, Differential function of lip residues in the mechanism and biology of an anthrax hemophore., PLoS Pathog. 8 (2012) e1002559. doi:10.1371/journal.ppat.1002559.

[87] C.F.M. Gaudin, J.C. Grigg, A.L. Arrieta, M.E.P. Murphy, Unique heme-iron coordination by the hemoglobin receptor IsdB of Staphylococcus aureus., Biochemistry. 50 (2011) 5443–52. doi:10.1021/bi200369p.

[88] J.C. Grigg, C.L. Vermeiren, D.E. Heinrichs, M.E.P. Murphy, Haem recognition by a Staphylococcus aureus NEAT domain, Mol. Microbiol. 63 (2007) 139–149. doi:10.1111/j.1365-2958.2006.05502.x.

[89] K. Krishna Kumar, D.A. Jacques, G. Pishchany, T. Caradoc-Davies, T. Spirig, G.R. Malmirchegini, D.B. Langley, C.F. Dickson, J.P. Mackay, R.T. Clubb, E.P. Skaar, J.M. Guss, D.A. Gell, Structural basis for hemoglobin capture by Staphylococcus aureus cell-surface protein, IsdH., J. Biol. Chem. 286 (2011) 38439–47. doi:10.1074/jbc.M111.287300.

[90] K.H. Sharp, S. Schneider, A. Cockayne, M. Paoli, Crystal structure of the heme-IsdC complex, the central conduit of the Isd iron/heme uptake system in Staphylococcus aureus., J. Biol. Chem. 282 (2007) 10625–31. doi:10.1074/jbc.M700234200.

[91] E.S. Honsa, A.W. Maresso, S.K. Highlander, Molecular and evolutionary analysis of NEAr-iron Transporter (NEAT) domains., PLoS One. 9 (2014) e104794. doi:10.1371/journal.pone.0104794.

[92] C.F. Dickson, K. Krishna Kumar, D.A. Jacques, G.R. Malmirchegini, T. Spirig, J.P. Mackay, R.T. Clubb, J.M. Guss, D.A. Gell, Structure of the Hemoglobin-IsdH Complex Reveals the Molecular Basis of Iron Capture by Staphylococcus aureus., J. Biol. Chem. (2014). doi:10.1074/jbc.M113.545566.

[93] C.F. Dickson, D.A. Jacques, R.T. Clubb, J.M. Guss, D.A. Gell, The structure of haemoglobin bound to the haemoglobin receptor IsdH from Staphylococcus aureus shows disruption of the native α-globin haem pocket, Acta Crystallogr. Sect. D Biol. Crystallogr. 71 (2015). doi:10.1107/S1399004715005817.

[94] G. Pishchany, J.R. Sheldon, C.F. Dickson, M.T. Alam, T.D. Read, D.A. Gell, D.E. Heinrichs, E.P. Skaar, IsdB-dependent Hemoglobin Binding Is Required for Acquisition

of Heme by Staphylococcus aureus., J. Infect. Dis. (2014). doi:10.1093/infdis/jit817.

[95] R.M. Pilpa, S.A. Robson, V.A. Villareal, M.L. Wong, M. Phillips, R.T. Clubb, Functionally distinct NEAT (NEAr Transporter) domains within the Staphylococcus aureus IsdH/HarA protein extract heme from methemoglobin., J. Biol. Chem. 284 (2009) 1166–76. doi:10.1074/jbc.M806007200.

[96] A. Dryla, B. Hoffmann, D. Gelbmann, C. Giefing, M. Hanner, A. Meinke, A.S. Anderson, W. Koppensteiner, R. Konrat, A. von Gabain, E. Nagy, High-Affinity Binding of the Staphylococcal HarA Protein to Haptoglobin and Hemoglobin Involves a Domain with an Antiparallel Eight-Stranded-Barrel Fold, J. Bacteriol. 189 (2007) 254–264. doi:10.1128/JB.01366-06.

[97] A. Dryla, D. Gelbmann, A. Von Gabain, E. Nagy, Identification of a novel iron regulated staphylococcal surface protein with haptoglobin-haemoglobin binding activity, Mol. Microbiol. 49 (2003) 37–53. doi:10.1046/j.1365-2958.2003.03542.x.

[98] B.A. Fonner, B.P. Tripet, B. Eilers, J. Stanisich, R.K. Sullivan-Springhetti, R. Moore, M. Liu, B. Lei, V. Copie, Solution Structure and Molecular determinants of Hemoglobin Binding of the first NEAT Domain of IsdB in Staphylococcus aureus., Biochemistry. 53 (2014) 3922–3933. doi:10.1021/bi5005188.

[99] H. Zhu, D. Li, M. Liu, V. Copié, B. Lei, Non-Heme-Binding Domains and Segments of the Staphylococcus aureus IsdB Protein Critically Contribute to the Kinetics and Equilibrium of Heme Acquisition from Methemoglobin., PLoS One. 9 (2014) e100744. doi:10.1371/journal.pone.0100744.

[100] Y. Moriwaki, T. Terada, J.M.M. Caaveiro, Y. Takaoka, I. Hamachi, K. Tsumoto, K. Shimizu, Heme binding mechanism of structurally similar iron-regulated surface determinant near transporter domains of Staphylococcus aureus exhibiting different affinities for heme., Biochemistry. 52 (2013) 8866–77. doi:10.1021/bi4008325.

[101] M. Pluym, N. Muryoi, D.E. Heinrichs, M.J. Stillman, Heme binding in the NEAT domains of IsdA and IsdC of Staphylococcus aureus., J. Inorg. Biochem. 102 (2008) 480–8. doi:10.1016/j.jinorgbio.2007.11.011.

[102] J.M. Taylor, D.E. Heinrichs, Transferrin binding in Staphylococcus aureus: involvement of a cell wall-anchored protein, Mol. Microbiol. 43 (2002) 1603–1614. doi:10.1046/j.1365-2958.2002.02850.x.

[103] S.R. Clarke, M.D. Wiltshire, S.J. Foster, IsdA of Staphylococcus aureus is a broad spectrum, iron-regulated adhesin., Mol. Microbiol. 51 (2004) 1509–19. doi:10.1111/j.1365-2958.2003.03938.x.

[104] R.M. Corrigan, H. Miajlovic, T.J. Foster, Surface proteins that promote adherence of Staphylococcus aureus to human desquamated nasal epithelial cells., BMC Microbiol. 9 (2009) 22. doi:10.1186/1471-2180-9-22.

[105] S.R. Clarke, G. Andre, E.J. Walsh, Y.F. Dufrene, T.J. Foster, S.J. Foster, Iron-Regulated Surface Determinant Protein A Mediates Adhesion of Staphylococcus aureus to Human Corneocyte Envelope Proteins, Infect. Immun. 77 (2009) 2408–2416.

doi:10.1128/IAI.01304-08.
[106] M. Liu, W.N. Tanaka, H. Zhu, G. Xie, D.M. Dooley, B. Lei, Direct hemin transfer from IsdA to IsdC in the iron-regulated surface determinant (Isd) heme acquisition system of Staphylococcus aureus., J. Biol. Chem. 283 (2008) 6668–76. doi:10.1074/jbc.M708372200.
[107] R. Abe, J.M.M. Caaveiro, H. Kozuka-Hata, M. Oyama, K. Tsumoto, Mapping the ultra-weak protein-protein interactions between heme transporters of Staphylococcus aureus., J. Biol. Chem. 287 (2012) 16477–87. doi:10.1074/jbc.M112.346700.
[108] T.J. Silhavy, D. Kahne, S. Walker, The bacterial cell envelope., Cold Spring Harb. Perspect. Biol. 2 (2010) a000414. doi:10.1101/cshperspect.a000414.
[109] S. Wilkens, Structure and mechanism of ABC transporters, F1000Prime Rep. 7 (2015). doi:10.12703/P7-14.
[110] J.C. Grigg, C.L. Vermeiren, D.E. Heinrichs, M.E.P. Murphy, Heme Coordination by *Staphylococcus aureus* IsdE, J. Biol. Chem. 282 (2007) 28815–28822. doi:10.1074/jbc.M704602200.
[111] M. Pluym, C.L. Vermeiren, J. Mack, D.E. Heinrichs, M.J. Stillman, Heme binding properties of Staphylococcus aureus IsdE, Biochemistry. 46 (2007) 12777–12877.
[112] J. Mack, C. Vermeiren, D.E. Heinrichs, M.J. Stillman, In vivo heme scavenging by Staphylococcus aureus IsdC and IsdE proteins., Biochem. Biophys. Res. Commun. 320 (2004) 781–8. doi:10.1016/j.bbrc.2004.06.025.
[113] W. Köster, ABC transporter-mediated uptake of iron, siderophores, heme and vitamin B12., Res. Microbiol. 152 (n.d.) 291–301.
[114] M.L. Reniere, G.N. Ukpabi, S.R. Harry, D.F. Stec, R. Krull, D.W. Wright, B.O. Bachmann, M.E. Murphy, E.P. Skaar, The IsdG-family of haem oxygenases degrades haem to a novel chromophore., Mol. Microbiol. 75 (2010) 1529–38. doi:10.1111/j.1365-2958.2010.07076.x.
[115] R. Wu, E.P. Skaar, R. Zhang, G. Joachimiak, P. Gornicki, O. Schneewind, A. Joachimiak, Staphylococcus aureus IsdG and IsdI, Heme-degrading Enzymes with Structural Similarity to Monooxygenases, J. Biol. Chem. 280 (2005) 2840–2846. doi:10.1074/jbc.M409526200.
[116] W.C. Lee, M.L. Reniere, E.P. Skaar, M.E.P. Murphy, Ruffling of Metalloporphyrins Bound to IsdG and IsdI, Two Heme-degrading Enzymes in Staphylococcus aureus, J. Biol. Chem. 283 (2008) 30957–30963. doi:10.1074/jbc.M709486200.
[117] T. Matsui, S. Nambu, Y. Ono, C.W. Goulding, K. Tsumoto, M. Ikeda-Saito, Heme degradation by Staphylococcus aureus IsdG and IsdI liberates formaldehyde rather than carbon monoxide., Biochemistry. 52 (2013) 3025–7. doi:10.1021/bi400382p.
[118] E.P. Skaar, A.H. Gaspar, O. Schneewind, Bacillus anthracis IsdG, a Heme-Degrading Monooxygenase, J. Bacteriol. 188 (2006) 1071–1080. doi:10.1128/JB.188.3.1071-1080.2006.
[119] K.P. Haley, E.M. Janson, S. Heilbronner, T.J. Foster, E.P. Skaar, Staphylococcus

lugdunensis IsdG Liberates Iron from Host Heme, J. Bacteriol. 193 (2011) 4749–4757. doi:10.1128/JB.00436-11.

[120] S. Sassa, Why Heme Needs to Be Degraded to Iron, Biliverdin IXα, and Carbon Monoxide., Antioxid. Redox Signal. 6 (2004) 819-24.

[121] A.F. Hurd, J. Garcia-Lara, Y. Rauter, M. Cartron, R. Mohamed, S.J. Foster, The iron-regulated surface proteins IsdA, IsdB, and IsdH are not required for heme iron utilization in Staphylococcus aureus., FEMS Microbiol. Lett. 329 (2012) 93–100. doi:10.1111/j.1574-6968.2012.02502.x.

[122] J.A. Wright, S.P. Nair, The lipoprotein components of the Isd and Hts transport systems are dispensable for acquisition of heme by Staphylococcus aureus., FEMS Microbiol. Lett. 329 (2012) 177–85. doi:10.1111/j.1574-6968.2012.02519.x.

[123] Brian L. Boys, A. Mark C. Kuprowski, L. Konermann, Symmetric Behavior of Hemoglobin α- and β- Subunits during Acid-Induced Denaturation Observed by Electrospray Mass Spectrometry., Biochemistry. 46 (2007) 10675-10684.

[124] M.L. Reniere, E.P. Skaar, Staphylococcus aureus haem oxygenases are differentially regulated by iron and haem., Mol. Microbiol. 69 (2008) 1304–15. doi:10.1111/j.1365-2958.2008.06363.x.

[125] L. Visai, N. Yanagisawa, E. Josefsson, A. Tarkowski, I. Pezzali, S.H.M. Rooijakkers, T.J. Foster, P. Speziale, Immune evasion by Staphylococcus aureus conferred by iron-regulated surface determinant protein IsdH, Microbiology. 155 (2009) 667–679. doi:10.1099/mic.0.025684-0.

[126] H.K. Kim, A. DeDent, A.G. Cheng, M. McAdow, F. Bagnoli, D.M. Missiakas, O. Schneewind, IsdA and IsdB antibodies protect mice against Staphylococcus aureus abscess formation and lethal challenge., Vaccine. 28 (2010) 6382–92. doi:10.1016/j.vaccine.2010.02.097.

[127] A.G. Cheng, H.K. Kim, M.L. Burts, T. Krausz, O. Schneewind, D.M. Missiakas, Genetic requirements for Staphylococcus aureus abscess formation and persistence in host tissues, FASEB J. 23 (2009) 3393–3404. doi:10.1096/fj.09-135467.

[128] Y. Terao, The virulence factors and pathogenic mechanisms of Streptococcus pyogenes, J. Oral Biosci. 54 (2012) 96–100. doi:10.1016/j.job.2012.02.004.

[129] M.W. Cunningham, Pathogenesis of Group A Streptococcal Infections, Clin. Microbiol. Rev. 13 (2000) 470–511. doi:10.1128/CMR.13.3.470-511.2000.

[130] Y.K. Stranger-Jones, T. Bae, O. Schneewind, Vaccine assembly from surface proteins of Staphylococcus aureus, Proc. Natl. Acad. Sci. 103 (2006) 16942–16947. doi:10.1073/pnas.0606863103.

[131] M. Ouattara, E.B. Cunha, X. Li, Y.-S. Huang, D. Dixon, Z. Eichenbaum, Shr of group A streptococcus is a new type of composite NEAT protein involved in sequestering haem from methaemoglobin., Mol. Microbiol. 78 (2010) 739–56. doi:10.1111/j.1365-2958.2010.07367.x.

[132] M. Fisher, Y.-S. Huang, X. Li, K.S. McIver, C. Toukoki, Z. Eichenbaum, Shr is a broad-

spectrum surface receptor that contributes to adherence and virulence in group A streptococcus., Infect. Immun. 76 (2008) 5006–15. doi:10.1128/IAI.00300-08.

[133] J. Bella, K.L. Hindle, P.A. McEwan, S.C. Lovell, The leucine-rich repeat structure, Cell. Mol. Life Sci. 65 (2008) 2307–2333. doi:10.1007/s00018-008-8019-0.

[134] M. Ouattara, A. Pennati, D.J. Devlin, Y. Huang, G. Gadda, Z. Eichenbaum, Kinetics of heme transfer by the Shr NEAT domains of Group A Streptococcus., Arch. Biochem. Biophys. 538 (2013) 71–9. doi:10.1016/j.abb.2013.08.009.

[135] M.A. Balderas, C.L. Nobles, E.S. Honsa, E.R. Alicki, A.W. Maresso, Hal Is a Bacillus anthracis heme acquisition protein., J. Bacteriol. 194 (2012) 5513–21. doi:10.1128/JB.00685-12.

[136] H. Zhu, M. Liu, B. Lei, The surface protein Shr of Streptococcus pyogenes binds heme and transfers it to the streptococcal heme-binding protein Shp., BMC Microbiol. 8 (2008) 15. doi:10.1186/1471-2180-8-15.

[137] M. Liu, B. Lei, Heme transfer from streptococcal cell surface protein Shp to HtsA of transporter HtsABC., Infect. Immun. 73 (2005) 5086–92. doi:10.1128/IAI.73.8.5086-5092.2005.

[138] R. Aranda, C.E. Worley, M. Liu, E. Bitto, M.S. Cates, J.S. Olson, B. Lei, G.N. Phillips, Bis-methionyl coordination in the crystal structure of the heme-binding domain of the streptococcal cell surface protein Shp., J. Mol. Biol. 374 (2007) 374–83. doi:10.1016/j.jmb.2007.08.058.

[139] Y. Ran, M. Liu, H. Zhu, T.K. Nygaard, D.E. Brown, M. Fabian, D.M. Dooley, B. Lei, Spectroscopic identification of heme axial ligands in HtsA that are involved in heme acquisition by Streptococcus pyogenes., Biochemistry. 49 (2010) 2834–42. doi:10.1021/bi901987h.

[140] Y. Ran, H. Zhu, M. Liu, M. Fabian, J.S. Olson, R. Aranda, G.N. Phillips, D.M. Dooley, B. Lei, Bis-methionine ligation to heme iron in the streptococcal cell surface protein Shp facilitates rapid hemin transfer to HtsA of the HtsABC transporter., J. Biol. Chem. 282 (2007) 31380–8. doi:10.1074/jbc.M705967200.

[141] T.K. Nygaard, G.C. Blouin, M. Liu, M. Fukumura, J.S. Olson, M. Fabian, D.M. Dooley, B. Lei, The mechanism of direct heme transfer from the streptococcal cell surface protein Shp to HtsA of the HtsABC transporter., J. Biol. Chem. 281 (2006) 20761–71. doi:10.1074/jbc.M601832200.

[142] C. Lu, G. Xie, M. Liu, H. Zhu, B. Lei, Direct heme transfer reactions in the Group A Streptococcus heme acquisition pathway., PLoS One. 7 (2012) e37556. doi:10.1371/journal.pone.0037556.

[143] A.W. Artenstein, S.M. Opal, Novel approaches to the treatment of systemic anthrax., Clin. Infect. Dis. 54 (2012) 1148–61. doi:10.1093/cid/cis017.

[144] M.E. Ivarsson, J.-C. Leroux, B. Castagner, Targeting Bacterial Toxins, Angew. Chemie Int. Ed. 51 (2012) 4024–4045. doi:10.1002/anie.201104384.

[145] E.S. Honsa, A.W. Maresso, Mechanisms of iron import in anthrax., Biometals. 24 (2011)

533–45. doi:10.1007/s10534-011-9413-x.
[146] S. Cendrowski, W. MacArthur, P. Hanna, Bacillus anthracis requires siderophore biosynthesis for growth in macrophages and mouse virulence, Mol. Microbiol. 51 (2004) 407–417. doi:10.1046/j.1365-2958.2003.03861.x.
[147] O. Gat, G. Zaide, I. Inbar, H. Grosfeld, T. Chitlaru, H. Levy, A. Shafferman, Characterization of *Bacillus anthracis* iron-regulated surface determinant (Isd) proteins containing NEAT domains, Mol. Microbiol. 70 (2008) 983–999. doi:10.1111/j.1365-2958.2008.06460.x.
[148] M. Fabian, E. Solomaha, J.S. Olson, A.W. Maresso, Heme transfer to the bacterial cell envelope occurs via a secreted hemophore in the Gram-positive pathogen Bacillus anthracis., J. Biol. Chem. 284 (2009) 32138–46. doi:10.1074/jbc.M109.040915.
[149] E.S. Honsa, M. Fabian, A.M. Cardenas, J.S. Olson, A.W. Maresso, The five near-iron transporter (NEAT) domain anthrax hemophore, IsdX2, scavenges heme from hemoglobin and transfers heme to the surface protein IsdC., J. Biol. Chem. 286 (2011) 33652–60. doi:10.1074/jbc.M111.241687.
[150] E.S. Honsa, C.P. Owens, C.W. Goulding, A.W. Maresso, The Near-iron Transporter (NEAT) Domains of the Anthrax Hemophore IsdX2 Require a Critical Glutamine to Extract Heme from Methemoglobin, J. Biol. Chem. 288 (2013) 8479–8490. doi:10.1074/jbc.M112.430009.
[151] Y. Tarlovsky, M. Fabian, E. Solomaha, E. Honsa, J.S. Olson, A.W. Maresso, A Bacillus anthracis S-Layer Homology Protein That Binds Heme and Mediates Heme Delivery to IsdC, J. Bacteriol. 192 (2010) 3503–3511. doi:10.1128/JB.00054-10.
[152] A.W. Maresso, T.J. Chapa, O. Schneewind, Surface Protein IsdC and Sortase B Are Required for Heme-Iron Scavenging of Bacillus anthracis, J. Bacteriol. 188 (2006) 8145–8152. doi:10.1128/JB.01011-06.
[153] P.E. Carlson, K.A. Carr, B.K. Janes, E.C. Anderson, P.C. Hanna, Transcriptional Profiling of Bacillus anthracis Sterne (34F2) during Iron Starvation, PLoS One. 4 (2009) e6988. doi:10.1371/journal.pone.0006988.
[154] B. Swaminathan, P. Gerner-Smidt, The epidemiology of human listeriosis, Microbes Infect. 9 (2007) 1236–1243. doi:10.1016/j.micinf.2007.05.011.
[155] A. Camejo, F. Carvalho, O. Reis, E. Leitão, S. Sousa, D. Cabanes, The arsenal of virulence factors deployed by Listeria monocytogenes to promote its cell infection cycle.,Virulence. 2 (2011) 379-94. doi:104161/viru.2.5.17703
[156] P.E. Klebba, A. Charbit, Q. Xiao, X. Jiang, S.M. Newton, Mechanisms of iron and haem transport by Listeria monocytogenes, Mol. Membr. Biol. 29 69–86. doi:10.3109/09687688.2012.694485.
[157] S. Bruck, N. Personnic, M.-C. Prevost, P. Cossart, H. Bierne, Regulated Shift from Helical to Polar Localization of Listeria monocytogenes Cell Wall-Anchored Proteins, J. Bacteriol. 193 (2011) 4425–4437. doi:10.1128/JB.01154-10.
[158] E. Borezee, T. Msadek, L. Durant, P. Berche, Identification in Listeria monocytogenes of

MecA, a Homologue of the Bacillus subtilis Competence Regulatory Protein, J. Bacteriol. 182 (2000) 5931–5934. doi:10.1128/JB.182.20.5931-5934.2000.

[159] E. Borezée, E. Pellegrini, J.-L. Beretti, P. Berche, SvpA, a novel surface virulence-associated protein required for intracellular survival of Listeria monocytogenes, Microbiology. 147 (2001) 2913–2923. doi:10.1099/00221287-147-11-2913.

[160] G.R. Malmirchegini, M. Sjodt, S. Shnitkind, M.R. Sawaya, J. Rosinski, S.M. Newton, P.E. Klebba, R.T. Clubb, Novel Mechanism of Hemin Capture by Hbp2, the Hemoglobin-binding Hemophore from Listeria monocytogenes., J. Biol. Chem. 289 (2014) 34886–99. doi:10.1074/jbc.M114.583013.

[161] Q. Xiao, X. Jiang, K.J. Moore, Y. Shao, H. Pi, I. Dubail, A. Charbit, S.M. Newton, P.E. Klebba, Sortase independent and dependent systems for acquisition of haem and haemoglobin in Listeria monocytogenes., Mol. Microbiol. 80 (2011) 1581–97. doi:10.1111/j.1365-2958.2011.07667.x.

[162] B. Jin, S.M.C. Newton, Y. Shao, X. Jiang, A. Charbit, P.E. Klebba, Iron acquisition systems for ferric hydroxamates, haemin and haemoglobin in Listeria monocytogenes, Mol. Microbiol. 59 (2006) 1185–1198. doi:10.1111/j.1365-2958.2005.05015.x.

[163] S.A. Loutet, M.J. Kobylarz, C.H.T. Chau, M.E.P. Murphy, IruO Is a Reductase for Heme Degradation by IsdI and IsdG Proteins in Staphylococcus aureus, J. Biol. Chem. 288 (2013) 25749–25759. doi:10.1074/jbc.M113.470518.

[164] T.L. Hadfield, P. McEvoy, Y. Polotsky, V.A. Tzinserling, A.A. Yakovlev, The Pathology of Diphtheria, J. Infect. Dis. 181 (2000) S116–S120. doi:10.1086/315551.

[165] R.K. Holmes, Biology and Molecular Epidemiology of Diphtheria Toxin and the *tox* Gene, J. Infect. Dis. 181 (2000) S156–S167. doi:10.1086/315554.

[166] E.S. Drazek, C.A. Hammack, M.P. Schmitt, Corynebacterium diphtheriae genes required for acquisition of iron from haemin and haemoglobin are homologous to ABC haemin transporters, Mol. Microbiol. 36 (2000) 68–84. doi:10.1046/j.1365-2958.2000.01818.x.

[167] E.B. Draganova, N. Akbas, S.A. Adrian, G.S. Lukat-Rodgers, D.P. Collins, J.H. Dawson, C.E. Allen, M.P. Schmitt, K.R. Rodgers, D.W. Dixon, Heme Binding by Corynebacterium diphtheriae HmuT: Function and Heme Environment, (2015).

[168] J.C. Grigg, C.L. Vermeiren, D.E. Heinrichs, M.E.P. Murphy, Heme coordination by Staphylococcus aureus IsdE., J. Biol. Chem. 282 (2007) 28815–22. doi:10.1074/jbc.M704602200.

[169] C.E. Allen, M.P. Schmitt, HtaA Is an Iron-Regulated Hemin Binding Protein Involved in the Utilization of Heme Iron in Corynebacterium diphtheriae, J. Bacteriol. 191 (2009) 2638–2648. doi:10.1128/JB.01784-08.

[170] C.E. Allen, M.P. Schmitt, Novel Hemin Binding Domains in the Corynebacterium diphtheriae HtaA Protein Interact with Hemoglobin and Are Critical for Heme Iron Utilization by HtaA, J. Bacteriol. 193 (2011) 5374–5385. doi:10.1128/JB.05508-11.

[171] M.P. Schmitt, Utilization of host iron sources by Corynebacterium diphtheriae: identification of a gene whose product is homologous to eukaryotic heme oxygenases and

is required for acquisition of iron from heme and hemoglobin., J. Bacteriol. 179 (1997) 838–45.

[172] C.E. Allen, J.M. Burgos, M.P. Schmitt, Analysis of Novel Iron-Regulated, Surface-Anchored Hemin-Binding Proteins in Corynebacterium diphtheriae, J. Bacteriol. 195 (2013) 2852–2863. doi:10.1128/JB.00244-13.

[173] M.P. Schmitt, Iron Acquisition and Iron-Dependent Gene Expression in Corynebacterium diphtheriae, in: Corynebacterium Diphtheriae Relat. Toxigenic Species, Springer Netherlands, Dordrecht, 2014: pp. 95–121. doi:10.1007/978-94-007-7624-1_6.

Chapter 2

Staphylococcus aureus Uses a Novel Multidomain Receptor to Break Apart Human Hemoglobin and Steal its Heme

The work described in this chapter has been reproduced with permission from:

Spirig, T., Malmirchegini, G. R., Zhang, J., Robson, S. A., Sjodt, M., Liu, M., Krishna Kumar, K., Dickson, C. F., Gell, D. A., Lei, B., Loo, J. A., & Clubb, R. T. *Staphylococcus aureus* uses a novel multidomain receptor to break apart human hemoglobin and steal its heme. *J. Biol. Chem*., 2013; 288(2):1065-78. doi: 10.1074/jbc.M112.419119.

I contributed residual dipolar coupling NMR experiments and analyzed data.

2.1 Overview

Staphylococcus aureus is a leading cause of life-threatening infections in the United States. It requires iron to grow, which must be actively procured from its host to successfully mount an infection. Heme-iron within hemoglobin (Hb) is the most abundant source of iron in the human body and is captured by *S. aureus* using two closely related receptors, IsdH and IsdB. Here we demonstrate that each receptor captures heme using two conserved near iron transporter (NEAT) domains that function synergistically. NMR studies of the 39-kDa conserved unit from IsdH ($IsdH^{N2N3}$, Ala^{326}–Asp^{660}) reveals that it adopts an elongated dumbbell-shaped structure in which its NEAT domains are properly positioned by a helical linker domain, whose three-dimensional structure is determined here in detail. Electrospray ionization mass spectrometry and heme transfer measurements indicate that $IsdH^{N2N3}$ extracts heme from Hb via an ordered process in which the receptor promotes heme release by inducing steric strain that dissociates the Hb tetramer. Other clinically significant Gram-positive pathogens capture Hb using receptors that contain multiple NEAT domains, suggesting that they use a conserved mechanism.

2.2 Introduction

Staphylococcus aureus is a leading cause of lethal hospital- and community-acquired infections in the United States. These infections result in a range of life-threatening diseases, such as pneumonia, meningitis, osteomyelitis, endocarditis, toxic shock syndrome, bacteremia, and sepsis. Highly virulent methicillin-resistant strains of *S. aureus* are now common, which annually cause more deaths in the United States (over 18,500) than any other single infectious agent [1). Iron is an essential nutrient required for *S. aureus* growth and is actively procured from its host during infections. As an innate defense mechanism, humans and other vertebrates exploit this dependence by sequestering the majority of the body's total iron within cells and by binding extracellular iron to transferrin and lactoferrin glycoproteins [2, 3]. Iron-protoporphyrin IX (heme), found in the oxygen transport protein hemoglobin (Hb), contains 75% of the body's total iron. As a result, *S. aureus* and other microbial pathogens have developed elaborate heme acquisition systems to exploit this rich nutrient source.

S. aureus captures heme-iron from human Hb using nine iron-regulated surface determinant (Isd) proteins [4–7]. Four Isd proteins are attached to the cell wall and capture Hb, extract its heme, and pass it across the peptidoglycan to the membrane. These proteins include IsdA, IsdB, and IsdH (also known as HarA), which are attached to the cell wall by the SrtA sortase enzyme [8 –11), and IsdC, which is attached to the cell wall by the SrtB sortase [12]. Biochemical and cellular localization studies indicate that heme capture is mediated by an ordered set of heme transfer reactions. This process is initiated when the IsdH and IsdB proteins exposed on the cell surface bind Hb and remove its heme [8, 11]. Heme is then transferred to IsdA, which, in turn, relays it to the IsdC protein buried within the cell wall [11, 13, 14]. Holo-IsdC then passes heme to the IsdE-IsdF complex, a transporter that pumps heme across the

membrane into the cytoplasm. In the cytoplasm, the heme oxygenase IsdG or its paralog, IsdI, degrades the tetrapyrrole ring to release free iron for use by the bacterium [15]. A molecular level under- standing of the Isd system could facilitate the development of new anti-infective agents that work by disrupting heme uptake, because several studies have shown that its components are required for *S. aureus* virulence [12, 16 –19), and related systems are present in a number of other important pathogens, including *Listeria monocytogenes* [20, 21), *Bacillus anthracis* [22), and *Streptococcus pyogenes* [23–25].

In the Isd system, both Hb and heme are captured by near iron transporter (NEAT) domains that are located within the IsdA, IsdB, IsdC, and IsdH proteins. These conserved binding modules are 125 residues in length and are named for the location of their genes, which are proximal to putative Fe^{3+} siderophore transporter genes [26]. Biochemical studies of isolated NEAT domains indicate that they have distinct binding specificities that enable interactions with one or more distinct ligands, including heme, Hb, haptoglobin, and other host proteins. The atomic structures of several isolated NEAT domains have now been determined, revealing the mechanism of heme and Hb binding [27–29]. In addition, recent studies have shown that heme transfer from IsdA to IsdC occurs when their NEAT domains transiently associate via an ultra-low affinity hand clasp complex [30, 31].

The first step in heme acquisition is the capture of Hb and the extraction of its heme molecules by IsdH and IsdB. Both receptors are potential targets for the development of novel antibiotics because *isdH* and *isdB* mutant strains of *S. aureus* are reduced in their ability to infect mice [16, 19, 32, 33), and purified antibodies against IsdH and IsdB confer protection from staphylococcal infections in animal models [33]. IsdH and IsdB share a significant degree of primary sequence homology, and, unlike other components of the Isd system, they contain

multiple NEAT domains. IsdB has been shown to bind Hb and capture its heme at least 150 times faster than the rate at which Hb spontaneously releases heme into the solvent, suggesting that the receptors capture heme via an activated receptor-Hb complex [14, 34]. Here we demonstrate that heme capture by IsdB and IsdH is mediated by a conserved structured unit that contains two NEAT domains that are connected by an -helical linker domain. We show, based on absorbance spectroscopy and electrospray ionization mass spectrometry (ESI-MS) measurements, that the linker domain in IsdH forms a three-helix bundle structure that is essential for efficient heme capture. NMR studies of a 39-kDa polypeptide containing the conserved unit from IsdH indicate that it adopts an extended but ordered structure. A model of the heme extraction process is presented in which IsdH dissociates the Hb tetramer to promote heme release.

2.3 Results

2.3.1 A Conserved Unit in IsdB and IsdH Containing Two NEAT Domains Rapidly Captures Heme from Hb

The *S. aureus* Hb receptors IsdB and IsdH contain two and three NEAT domains, respectively (**Figure 2.1*A***). Isolated domains from these receptors have been characterized *in vitro* and bind to either Hb or heme; the $IsdH^{N1}$, $IsdH^{N2}$, and $IsdB^{N1}$ NEAT domains bind to Hb, whereas the C-terminal NEAT domains in both proteins interact with heme ($IsdH^{N3}$ and $IsdB^{N2}$) [32, 38, 50–54]. Interestingly, a sequence alignment reveals that IsdB and IsdH share 64% primary sequence identity with one another over a region that encodes two NEAT domains (**Figs. 1*A* and 2**). This conserved unit contains two NEAT domains that are joined by a 70-amino acid segment, hereafter referred to as the "linker." In IsdH, the unit corresponds to the N2 and N3 domains, which are homologous to the N1 and N2 domains in IsdB, respectively (**Figure 2.1*A*, *enclosed* in a *dashed box***). *In vitro*, full-length IsdB rapidly captures heme from Hb [14]. To determine if the con- served unit within IsdB and IsdH is responsible for efficient heme capture, UV-visible absorption spectroscopy was used to measure the rate of heme transfer from heme-loaded methemoglobin (MetHb) to either $IsdB^{N1N2}$ (residues Thr^{121}–Asn^{458}, containing the N1 and N2 domains in IsdB) or $IsdH^{N2N3}$ (Ala^{326}–Asp^{660}, containing the N2 and N3 domains in IsdH). All studies were performed under oxidizing conditions, in which heme is in its ferric form. Upon mixing of MetHb with apo-$IsdH^{N2N3}$, a rapid shift of the UV absorbance spectrum of Hb to the heme bound spectrum of $IsdH^{N2N3}$ is observed (**Figure 2.1*B***). This spectral change is indicative of heme transfer to IsdH and is most pronounced at 371 and 406 nm where the absorbance increases and decreases, respectively. A kinetic analysis of the heme transfer data indicates that $IsdB^{N1N2}$ and $IsdH^{N2N3}$ capture heme from Hb at similar rates, 0.055 0.001 and

0.048 0.001 s^{-1}, respectively (**Figure 2.1*C***). These rates are similar to those measured for intact IsdB and are up to 580 times faster than the rate at which tetrameric Hb spontaneously releases heme into the solvent, suggesting that heme transfer to IsdB and IsdH occurs via a MetHb-receptor complex [14, 34].

To determine if the NEAT domains within IsdH need to be part of the same polypeptide to rapidly extract heme, we measured the rate of heme transfer from MetHb to the isolated N3 domain in the presence and absence of the Hb binding N2 domain (**Figure 2.3, *A* and *B***). Compared with $IsdH^{N2N3}$, the isolated heme binding domain $IsdH^{N3}$ (Leu^{544}–Asp^{660}) acquires heme from MetHb very slowly, which is consistent with an indirect transfer mechanism in which heme is first released from MetHb into the solvent before it is acquired by $IsdH^{N3}$ (**Figure 2.3*B***). The addition of the MetHb binding $IsdH^{N2}$ protein (Ala^{326}– Pro^{466}) in *trans* to this transfer reaction fails to increase the rate of heme transfer from MetHb to $IsdH^{N3}$ (**Figure 2.3*B*, *N2* + *N3***). This indicates that $IsdH^{N2}$ binding to MetHb itself does not perturb its structure so as to promote heme release and subsequent capture by the isolated N3 domain. The presence of the N2 domain also does not significantly alter the heme binding affinity of the N3 domain within $IsdH^{N2N3}$, because $IsdH^{N2N3}$ and $IsdH^{N3}$ bind heme with similar affinities, K_D values of 3.2 ± 0.7 and 3.4 ± 0.6 μM, respectively (**Figure 2.4**). Combined, these data strongly suggest that the N2 and N3 domains of IsdH need to reside within the same polypeptide to efficiently capture heme from Hb. Because IsdB contains this conserved unit, its NEAT domains also presumably synergistically extract heme (**Figure 2.2**).

2.3.2 The NEAT Domains within IsdH and IsdB Are Connected by a Functionally Important Helical Linker

The 70-amino acid linker segments that connect the NEAT domains in IsdB and IsdH share 70% sequence identity (**Figure 2.2**). To investigate their structure, we purified polypeptides containing this segment from IsdB ($IsdB^{linker}$, Ser^{263}–Ser^{361}) and IsdH ($IsdH^{linker}$, Pro^{466}–Val^{564}). Their circular dichroism (CD) spectra indicate that $IsdB^{linker}$ and $IsdH^{linker}$ adopt a helical conformation, which is evident by negative bands in their CD spectra at 222 and 208 nm and a positive band at 193 nm (**Figure 2.5*A***). This is consistent with secondary structure predictions, which propose that amino acids in this region form several -helices. To explore the functional role of the linker domain in IsdH, UV-visible absorbance spectroscopy was used to follow heme cap- ture from MetHb. $IsdH^{linker}$ was unable to acquire heme from MetHb (**Figure 2.3*B***). Moreover, the presence of $IsdH^{linker}$ and $IsdH^{N2}$ did not accelerate the rate at which $IsdH^{N3}$ captures heme from MetHb (**Figure 2.3*C*, *N2* + *linker* + *N3***). This indicates that the isolated components of the conserved unit in IsdH are unable to associate with one another via non-covalent interactions to form a fully functioning receptor. To further investigate the function of the linker, polypeptides in which the linker was fused to either the N2 ($IsdH^{N2\text{-}linker}$, Ala^{326}–Gln^{543}) or N3 ($IsdH^{linker\text{-}N3}$, Leu-544–Asp^{660}) domains were studied. Slow transfer from MetHb to the isolated N3 domain was observed when $IsdH^{N2\text{-}linker}$ was added in *trans*, indicating that MetHb binding by $IsdH^{N2\text{-}lnker}$ did not significantly promote heme release and subsequent capture by $IsdH^{N3}$. Similarly, $IsdH^{linker\text{-}N3}$ captures heme slowly from MetHb in either the presence or absence of $IsdH^{N2}$, indicating that the presence of the helical linker does not influence the N3 domain's ability to scavenge heme (**Figure 2.3*C***). To determine if the structure of the linker is important for function, we studied $IsdH^{N2\text{-}GS\text{-}N3}$, which replaces the linker with a nine-residue

glycine- and serine-rich polypeptide (GSGSGSGSG). Spectroscopic measurements reveal that $IsdH^{N2\text{-}GS\text{-}N3}$ captures heme slowly from MetHb at a rate that is similar to that of the isolated N3 domain (**Figure 2.3, compare *B* and *C***). Combined, these data indicate that the NEAT domains in IsdB and IsdH are connected by a helical linker, whose primary function is to properly position the domains so as to specifically facilitate heme transfer from MetHb to the N3 domain.

2.3.3 IsdH Destabilizes Hb to Promote Heme Release

We used ESI-mass spectrometry to investigate the mechanism through which IsdH accelerates heme release from Hb. ESI-MS allows the quantification of different Hb oligomers in the presence and absence of IsdH [55]. Hb consists of α- and β-globin chains each bound to a heme. The globins assemble into a noncovalently bound $(\alpha\beta)_2$ tetramer that dissociates into $(\alpha\beta)$ dimers with a dissociation constant (K_D) of 2 μM [56]. This is evident from the ESI-MS spectrum of a 10 μM solution of Hb; from the ratio of the signal from the dimer and tetramer ions, the dimer/ tetramer ratio is 1:1.4. This is consistent with previously reported studies [57, 58) and validates the use of ESI-MS to estimate the relative abundances of Hb species. ESI-MS spectra of Hb were acquired in the presence or absence of either wildtype $IsdH^{N2N3}$, $IsdH^{N2\text{-}GS\text{-}N3}$, or $IsdH^{N2N3(Y642A)}$, which contains a Y642A mutation in the N3 domain that disrupts heme binding (**Figure 2.6, *A–D***). In all of the experiments, the receptors were present at a 2-fold molar excess relative to Hb (expressed in tetrameric units). The ESI-MS data are summarized in **Figure 2.6*E***, which shows a histogram plot of the relative abundances of the various forms of Hb (the sum of the monomeric α- or β-globins (*M*); $(\alpha\beta)$ dimer (*D*); and $(\alpha\beta)_2$ tetramer (*T*)), as well as receptor-bound forms of the $(\alpha\beta)_2$ tetramer (*T*:*R*), and $(\alpha\beta)$ dimer (*D*:*R*). Incubation of $IsdH^{N2N3}$

with Hb substantially reduces the amount of dimeric and tetrameric Hb, which is converted into monomeric globins. This is consistent with previous studies that have shown that Hb dissociates into its component globins upon heme removal [58, 59]. Because substoichiometric amounts of the receptor were used, Hb dissociation is not complete, leaving mostly a mixture of dimeric Hb and the ($\alpha\beta$) dimer-receptor complex. Importantly, after the IsdH^{N2N3} addition, most of the Hb tetramer disappears, and very little $(\alpha\beta)_2$ tetramer-receptor complex is formed. This indicates that receptor binding and/or heme removal significantly destabilizes the tetramer.

To gain insight into the role of the linker and heme binding in the acquisition process, ESI-MS spectra of Hb in the presence of IsdH$^{N2\text{-}GS\text{-}N3}$ or IsdH$^{N2N3(Y642A)}$ were acquired. Unlike the wild-type receptor, when the IsdH$^{N2\text{-}GS\text{-}N3}$ linker mutant is incubated with Hb, the majority of the receptor binds to the $(\alpha\beta)_2$ tetramer to form a $(\alpha\beta)_2$-IsdH$^{N2\text{-}GS\text{-}N3}$ complex, and a significant fraction of the tetramer remains intact (**Figure 2.6*E***). Moreover, smaller amounts of Hb are converted to its monomeric globins, whereas roughly similar amounts of ($\alpha\beta$) dimer and ($\alpha\beta$) dimer-receptor complex are present. The absence of monomeric globins is compatible with the kinetic data that showed that IsdH$^{N2\text{-}GS\text{-}N3}$ extracted heme from Hb inefficiently. The fact that the linker mutant does not disrupt the tetramer suggests that it adopts a unique structure as compared with the wildtype protein, such that the mutant receptor can no longer impart sufficient structural strain to rupture the tetramer. To determine if the receptor needs to bind heme in order to dissociate the Hb tetramer, we studied IsdH$^{N2N3(Y642A)}$ which contains a Y642A mutation in the N3 domain that disrupts heme binding. When Hb is incubated with IsdH$^{N2N3(Y642A)}$, the amount of tetrameric Hb is significantly reduced as a result of its conversion into the ($\alpha\beta$)-IsdH$^{N2N3(Y642A)}$ complex. However, only small amounts of monomeric globin are produced. This suggests that heme removal from the tetramer by the receptor is not required to dissociate it into

its dimeric state. However, heme removal appears to be required to convert Hb into its monomeric units. A working model of the extraction process is presented under "Discussion."

2.3.4 Structure of the Linker Domain

To gain a better under- standing of the molecular basis of heme capture, we determined the NMR solution structure of $IsdH^{linker}$ (Protein Data Bank accession code 2LHR). The NMR spectra of $IsdH^{linker}$ are well resolved, enabling nearly complete ^{1}H, ^{13}C, and ^{15}N resonance assignments (**Figure 2.5*B***). A total of 1793 experimentally derived restraints were used to determine the structure, including 1469 interproton distance restraints, 118 dihedral angle restraints, 54 $^{3}J_{HN\alpha}$ restraints, and 152 ^{13}C secondary shift restraints. An ensemble of 20 conformers representing the structure of $IsdH^{linker}$ is displayed in **Figure 2.7*A***. The structure is well defined by the NMR data; the backbone and heavy atom coordinates of the structured residues Val^{470}–Val^{531} can be superimposed with a root mean square deviation of 0.42 ± 0.10 and 0.87 ± 0.07 Å, respectively (experimental and structural parameters are presented in **Table 2.1**).

The linker forms a three-helix bundle that is composed of helices α1 (Asp^{471}–Lys^{486}), α2 (Leu^{490}–Lys^{503}), and α3 (Glu^{506}–Ala^{530}) (**Figure 2.7*B***). In the bundle, the long axes of the helices are co-linear and are connected by short reverse turns. The structure is stabilized by a hydrophobic core that is formed by nine leucine and tyrosine residues (Leu^{477}, Leu^{480}, Leu^{481}, Tyr^{484}, Leu^{497}, Leu^{500}, Leu^{504}, Tyr^{508}, and Tyr^{512}; **Figure 2.7*C***). Although each helix contributes residues to the hydrophobic core, helix α3 is longer than the other helices, such that its C terminus projects from the bundle. This region and residues immediately following it presumably facilitate interactions with the N3 domain in the intact receptor (see below). $\{^{1}H\}^{15}N$-

heteronuclear NOE measurements are compatible with the structure because residues Val^{470}–Val^{531}, whose coordinates are precisely defined in the ensemble, exhibit large magnitude NOE values, indicating that they are immobile on the picosecond time scale (**Figure 2.5*C***).

2.3.5 $IsdH^{N2N3}$ Adopts an Extended but Ordered Multidomain Structure

We used NMR to investigate the structure and dynamics of $IsdH^{N2N3(Y642A)}$. It is structurally identical to the wild-type protein based on its HSQC spectrum but is reduced in its ability to bind heme. Previously, we sequence-specifically assigned the chemical shifts of its backbone atoms [36]. To learn whether the domains form a rigid unit within $IsdH^{N2N3(Y642A)}$, we measured $\{^1H\}^{15}N$-heteronuclear NOE relaxation parameters. As shown in **Figure 2.8*A***, residues spanning the N2, linker, and N3 domains exhibit positive and mostly uniform $\{^1H\}^{15}N$-heteronuclear NOEs, which indicates that they are structurally ordered. Notably, residues that connect the domains also exhibit positive NOEs. Because some of these residues are unstructured in the isolated linker polypeptide (**Figure 2.5*C***), this suggests that in the context of $IsdH^{N2N3(Y642A)}$, they form stabilizing interactions with residues located in the N2 and/or N3 domains and that the domains form a single structured unit. Although the structure of the full receptor is unknown, the structures of the isolated linker and N3 domains are known, and the structure of the N2 domain can be accurately modeled using the previously determined NMR and crystal structures of $IsdH^{N1}$, which shares 54% sequence identity with N2 [50, 51, 53]. To determine whether the domains undergo major structural changes upon incorporation into $IsdH^{N2N3}$, we measured ^{15}N-^1H residual dipolar couplings ($^1D_{NH}$ RDCs) in a sample of $IsdH^{N2N3}$ partially aligned in pentaethylene glycol monododecyl ether ($C_{12}E_5$ PEG)/hexanol. The $^1D_{NH}$ data provide information about the angle of each backbone N–H bond relative to an alignment

tensor. The compatibility of the individual domain structures with the RDC data was evaluated by plotting the back-calculated *versus* experimental $^{1}D_{NH}$ values (**Figure 2.9**). There is good agreement between the experimental data and the individual structures of the N2, linker, and N3 domains, which have calculated *Q*-factors of 0.28, 0.10, and 0.23, respectively. This indicates that incorporation of the domains into IsdH^{N2N3} does not significantly alter their structure and is consistent with our previously reported C_α and C_β backbone secondary chemical shifts of IsdH^{N2N3}, which suggested that the domains have similar secondary structures in isolation and when incorporated into IsdH^{N2N3} [36].

The chemical shifts of IsdH$^{N2N3(Y642A)}$ and polypeptides containing its isolated domains were compared with the aim of learning if the domains interact with one another in the context of IsdH$^{N2N3(Y642A)}$. **Figure 2.8*B*** shows an overlay of the secondary chemical shifts of IsdH$^{N2N3(Y642A)}$ and IsdH^{linker}. Similar secondary chemical shifts were observed for the structured part of the linker, suggesting that its conformation is preserved in IsdH$^{N2N3(Y642A)}$. Average chemical shift differences of the backbone amide signals of isolated linker and the corresponding residues in IsdH^{N2N3} are displayed in **Figure 2.8*C***. In general, small chemical shift differences were observed for residues in the core helices of the linker, indicating that they do not form a molecular surface that interacts with the N2 or the N3 domains. However, significant chemical shift differences in the linker occur for residues located at the beginning of helix α2 (Leu^{490}–Arg^{492}) and at its N terminus (Asp^{468}-Glu^{472}, Thr^{474}–Tyr^{475}) and C terminus (Gln^{526}–Ser^{529}, Val^{531}–Thr^{538}, Thr^{540}– Gln^{543}). Mapping these changes onto the NMR structure of the linker reveals that they reside at distinct ends of the domain (**Figure 2.8*D***). This is consistent with residues at the beginning of helix α2 and the N terminus of the linker contacting the N2 domain, while residues at the C-terminal end interact with the N3 domain. Interestingly, comparison of

the secondary chemical shifts suggests that helix α3 in the linker domain is lengthened at its C terminus when it is incorporated into $IsdH^{N2N3}$ (**Figure 2.8*B***). Moreover, residues immediately following this segment, based on their secondary chemical shifts, do not participate in regular secondary structure when located in $IsdH^{N2N3}$ but are nevertheless highly ordered, based on the heteronuclear NOE data (**Figure 2.8*A***). To further ascertain whether the domains in $IsdH^{N2N3}$ might be significantly interacting with one another in $IsdH^{N2N3}$, we produced ^{15}N samples of $IsdH^{N2}$ and $IsdH^{N3}$. The ^{1}H-^{15}N HSQC spectrum of $IsdH^{N2}$ is well resolved and, when overlaid with the spectrum of $IsdH^{N2N3}$, reveals very similar chemical shifts (data not shown). This suggests that, in the context of $IsdH^{N2N3}$, the N2 domain does not contain a large contact surface that interacts with the remainder of the protein. A similar analysis using ^{15}N-labeled $IsdH^{N3}$ was also attempted but did not prove fruitful because the cross-peaks in its spectrum are partially broadened, presumably because of protein aggregation. Combined, the absence of extensive interaction surfaces in the linker and N2 domains suggests that, while ordered, $IsdH^{N2N3}$ does not adopt a compact structure.

2.4 Discussion

To successfully mount an infection, *S. aureus* and other pathogens acquire the essential nutrient iron from human Hb. Two surface-displayed *S. aureus* receptors capture Hb on the cell surface, IsdB and IsdH. The receptors share a high degree of sequence homology over a region that contains two NEAT domains that are separated by a 70-amino acid "linker" segment (**Figs. 1*A* and 2**). The NEAT domains in the conserved units have distinct functions; in each protein, the N-terminal domain binds to Hb, and the C-terminal domain interacts with heme [8, 38]. Interestingly, the NEAT domains in IsdB appear to function synergistically, because Lei and

colleagues [14) have shown that IsdB captures heme from Hb ~28–250 times faster than proteins that contain only a single NEAT domain. To gain insight into the molecular basis of this synergy, we studied the conserved bi-NEAT domain unit located within IsdH ($IsdH^{N2N3}$). UV-visible spectroscopy measurements of heme transfer from Hb indicate that $IsdH^{N2N3}$ rapidly acquires the heme of Hb at a rate that is 110–580 times faster than the rate at which Hb spontaneously releases heme into the solvent ($IsdH^{N2N3}$acquires heme at a rate of $0.048 \pm 0.001 s^{-1}$,whereas the and subunits in tetrameric Hb release heme into the solvent at a rate of 0.000083 and 0.00042 $s^{-1,}$ respectively) [34]. IsdB and $IsdH^{N2N3}$capture heme from Hb at a similar rate, compatible with both proteins forming a receptor-Hb complex in which heme is actively removed. These transfer rates may be slower if the heme iron in Hb is in its reduced state, because $IsdH^{N3}$ has been shown to bind ferric heme more tightly than ferrous heme [60]. Systematic dissection of $IsdH^{N2N3}$ into its components indicates that its NEAT domains need to be part of the same polypeptide chain in order to rapidly acquire heme from Hb. Moreover, a linker with a *specific* structure and size that connects the domains is required for efficient heme capture; an $IsdH^{N2\text{-}GS\text{-}N3}$ mutant in which the linker is replaced with a glycine-serine nonapeptide acquires heme slowly from Hb.

$IsdH^{N2N3}$ adopts an ordered elongated dumbbell-shaped structure in which its NEAT domains are separated by a helical linker domain. The NMR structure of the linker domain (called $IsdH^{linker}$) reveals that it adopts a three-helix bundle. First observed in the IgG-binding domain of *S. aureus*, three-helix bundles serve as robust scaffolds for molecular recognition and are ubiquitously found in structural proteins, enzymes, and DNA-binding proteins [61, 62]. Because the N and C termini in $IsdH^{linker}$ are positioned at opposite ends of the bundle, in the context of the $IsdH^{N2N3}$ receptor, the linker domain presumably acts as a spacer that holds the N2 and N3 domains apart from another by 40 Å. This is compatible with the assigned NMR spectra

of the intact 39-kDa IsdH^{N2N3} receptor, because a comparison with the NMR spectra of IsdH^{linker} reveals that only residues located at the ends of the helical bundle near the connection points to the N2 and N3 domains exhibit large chemical shift differences. Moreover, the NMR chemical shifts of residues in the isolated IsdH^{N2} domain and IsdH^{N2N3} are similar, suggesting that N2 is not involved in extensive interdomain interactions in the structure of IsdH^{N2N3}. Interestingly, although IsdH^{N2N3} adopts an elongated structure, the domains do not appear to be connected by flexible loops. Inspection of the heteronuclear NOE data of IsdH^{N2N3} reveals nearly uniform values over the length of the polypeptide, including amino acids that connect the domains. Notably, several residues at the N and C termini of the linker domain that are unstructured in the isolated IsdH^{linker} become ordered when they are located in IsdH^{N2N3} (in IsdH^{N2N3}, 2 and 11 residues preceding and following the linker domain, respectively, exhibit elevated NOE values in IsdH^{N2N3} as compared with IsdH^{linker}). Thus, the three domains within IsdH^{N2N3} adopt an extended conformation in which their positioning is fixed with respect to one another. IsdB can be assumed to adopt a similar structure because it shares significant sequence homology with IsdH^{N2N3}, and we have shown that its linker region also adopts a helical conformation.

From the ESI-MS data, IsdH extracts heme from Hb via the ordered process shown in **Figure10*A***. On the cell surface, IsdB and IsdH can be expected to encounter Hb in its $(\alpha\beta)_2$ tetrameric and dimeric forms, whose relative abundance depends on protein concentration. When IsdH^{N2N3} binds to the $(\alpha\beta)_2$ tetramer, it promotes its dissociation into dimers, which is presumably caused by receptor-induced steric strain that ruptures the weaker $\alpha_1\beta_2$ interface of the tetrameric Hb [63]. Dimer formation is expected to facilitate heme transfer to IsdH^{N2N3} because dimeric Hb releases heme more readily than the $(\alpha\beta)_2$ tetramer; compared with the tetramer, the

rate of heme loss from the and chains in the isolated (αβ) dimer is 2 and 10 times faster, respectively [34]. In the second step, heme is transferred from the (αβ) dimer to the N3 domain within the $IsdH^{N2N3}$ receptor. Our data do not reveal which globin chain, if any, serves as the preferred heme donor for $IsdH^{N2N3}$. It is possible that heme is first removed from the subunit because it has intrinsically weaker affinity for heme as compared with the subunit [34]. Alternatively, structural distortions induced in the dimer by the receptor may trigger heme transfer from the chain, creating semi- Hb from which heme is known to be rapidly released [34]. In the final step, after the loss of one of its heme molecules, the (αβ) dimer dissociates completely. Formation of monomeric species is probably driven by the greater tendency of Hb dimers to dissociate [59]. As the monomeric and chains quickly lose their heme to the environment, both globins could be expected to readily release their ligand to IsdH [34]. A similar transfer reaction is expected to occur when IsdH encounters an (αβ) Hb dimer, but it would bypass the need for tetramer dissociation. An alternative heme transfer pathway is also possible. In it, the receptor would remove heme directly from the tetramer or concurrently with tetramer dissociation. Heme removal from the tetramer could be advantageous because it would produce semi-Hb tetramers that are prone to dissociate [64]. However, as described immediately below, heme capture from the Hb tetramer is not an obligate step in the transfer reaction.

Several lines of evidence indicate that binding of the $IsdH^{N2N3}$ receptor to tetrameric Hb induces steric strain in Hb that causes it to dissociate into dimers and that this process does not require heme transfer to $IsdH^{N2N3}$ (**Figure 2.10*A***). The most compelling evidence comes from the ESI-MS data of $IsdH^{N2N3}$ and $IsdH^{N2N3(Y642A)}$, which indicate that both proteins readily disrupt the tetramer. Because $IsdH^{N2N3(Y642A)}$ binds heme with lower affinity, this indicates that structural perturbations in Hb induced by receptor binding are sufficient to cause it to dissociate.

This process requires two NEAT domains that are connected by a structured linker because the Hb tetramer does not dissociate when it is bound to an $IsdH^{N2\text{-}GS\text{-}N3}$ mutant in which the linker domain is replaced with a flexible glycine-serine peptide. The idea that an intact bi-NEAT domain receptor is required to dissociate the tetramer is also consistent with a recent crystal structure of the $IsdH^{N1}$-Hb complex, which revealed that binding of the isolated N1 NEAT domain to Hb induced only modest structural changes in Hb [50]. As we have shown, $IsdH^{N2N3}$ adopts a rigid structure in its apo state; this suggests that binding of $IsdH^{N2N3}$ to Hb results in atomic overlap between the proteins that causes the tetramer to dissociate. A model of the structure of the $IsdH^{N2N3}$-Hb complex illustrates a possible orientation of the receptor protein on Hb (**Figure 2.10*B***). The orientation of the sub-domains (N1, linker, and N2) within $IsdH^{N2N3}$ has not been experimentally determined, and only one possible orientation is shown. The model was constructed using the NMR structure of $IsdH^{linker}$, the crystal structure of the isolated N3 domain, and a homology model of the N2 domain based on the structure of $IsdH^{N1}$. Based on the recently reported crystal structure of the isolated N1 domain bound to Hb, the N2 domain in $IsdH^{N2N3}$ can be expected to engage the subunit of Hb via its A-helix [50]. Contacts from N2 presumably originate from residues located within surface loops positioned at one end of its β-barrel structure because these residues are conserved in N1 and N2. The relative positioning of the remainder of the $IsdH^{N2N3}$ protein and its contacts to Hb cannot be predicted from our NMR data. However, assuming that $IsdH^{N2N3}$ adopts an extended structure, the N3 domain could, in principle, be positioned adjacent to the heme pockets of either the α or β subunits. Unlike IsdB, the IsdH protein contains an N-terminal NEAT domain (N1) that binds to the subunit of Hb (**Figure 2.1*A***) [50]. It is possible that the N1 and N2 domains in IsdH simultaneously engage the Hb tetramer via its two subunits. Alternatively, N1 and N2 may not simultaneously engage the

same tetramer. In this scenario, Hb binding by N1 may function to increase the efficiency of heme capture by increasing the local concentration of Hb that is proximal to $IsdH^{N2N3}$. A more detailed understanding of the mechanism of extraction and the origin of molecular strain induced by the receptor on Hb will require studies of the full-length IsdH protein and the structure determination of $IsdH^{N2N3}$ in both its free- and Hb-bound states.

We have demonstrated that the NEAT domains within IsdH function synergistically to capture heme from Hb. Interestingly, several other pathogenic species of Gram-positive bacteria display surface proteins implicated in heme capture that contain more than one NEAT domain [26]. At present, only a few of these proteins have been characterized biochemically. *S. pyogenes* encodes the membrane-anchored Shr protein, which has two NEAT domains, and, similar to IsdB and IsdH, it has been proposed to acquire heme via a receptor-Hb complex [65, 66]. *B. anthracis* produces a Hb hemophore called IsdX2 that contains five NEAT domains [67, 68]. All of its domains bind Hb, and some are multifunctional because they can also bind heme. It will be interesting to see if subsets of these domains are also connected by structured linker segments that enable their NEAT domains to function synergistically. Despite the prevalence and importance of multi-NEAT domain proteins in Gram-positive bacteria, this present study is the first to address in detail the possible interactions between NEAT domains, the role of the linker segments, and functional synergy between these regions. Further research will be required to reveal if the mechanism of extraction described here can be generalized to other NEAT-containing Hb receptors. This work could lead to small molecule antibiotics that work by limiting microbial access to heme-iron.

2.5 Materials and Methods

2.5.1 Cloning, Protein Expression, and Purification

Plasmids were generated encoding IsdH and IsdB receptor constructs as small hexahistidine-ubiquitin-like modifier (SUMO)-tagged proteins under control of an inducible promoter: pRM208 coding for amino acids 326–660 in IsdH ($IsdH^{N2N3}$), pRM213 coding for amino acids 326–466 in IsdH ($IsdH^{N2}$), pRM214 coding for amino acids 466–660 in IsdH ($IsdH^{linker\text{-}N3}$), pRM234 coding for amino acids 326–543 in IsdH ($IsdH^{N2\text{-}linker}$), pRM219 coding for amino acids 467–543 in IsdH ($IsdH^{linker}$), and pRM221 coding for amino acids 544–600 in IsdH ($IsdH^{N3}$). Briefly, the DNA was amplified from the *S. aureus* RN4220 genome by polymerase chain reaction (PCR) and cloned into the vector pHis-SUMO using BamHI and XhoI restriction enzymes [35]. pRM233 coding for amino acids 326–660 ($IsdH^{N2\text{-}GS\text{-}N3}$) was generated from pRM208 using two-step PCR, such that the linker was replaced with a nine-amino acid artificial linker (GSGSGSGSG). The sequence of all plasmids was verified by DNA sequencing. Generation of the plasmid pRM216 coding for amino acids 326–660 in IsdH with an alanine substitution of Tyr^{642} ($Isd^{N2N3(Y642A)}$) has been described earlier [36]. Protein expression in *Escherichia coli* BL21(DE3) cells (New England BioLabs) transformed with the overexpression plasmids in LB/kanamycin (50 g/ml) was induced with 1 mM isopropyl-β-D-thiogalactoside for 4 h at 37 °C. For production of isotopically labeled [^{13}C,^{15}N]protein, the cells were grown in M9 minimal medium containing $^{15}NH_4Cl$ and [^{13}C]glucose (Cambridge Isotope Laboratories). The bacterial cells were harvested by centrifugation, resuspended in 50 mM NaH_2PO_4, 300 mM NaCl, pH 7.0, and ruptured by sonication. The cell debris was removed by centrifugation, and the supernatant containing the SUMO-tagged proteins was purified using a Co^2-chelating

column (Thermo Scientific). After cleavage of the fusion proteins with ULP1 protease for 2 h at 4 °C, they were reapplied to the Co^{2} chelating column to remove the protease and cleaved SUMO-affinity tag. The receptor proteins were further purified by gel filtration on a Superdex 75 column (GE Healthcare) equilibrated with 20 mM NaH_2PO_4, 50 mM NaCl, pH 6.0. Heme contents of holo- and apoproteins were determined with the pyridine hemochrome assay, and homogeneous apo forms of the heme-binding proteins were generated by extraction with methyl ethyl ketone [37]. Expression and purification of [U-^{2}H,^{13}C,^{15}N]$Isd^{N2N3(Y642A)}$ was performed according to a previously published protocol [36].

2.5.2 Preparation of Human Hemoglobin

Human blood (30–40 ml) was collected with heparin anticoagulant by a health practitioner following appropriate institutional protocols. Red blood cells were collected by centrifugation at 700 *g* for 10 min at 4 °C. The cells were washed three times with 0.9% NaCl and bubbled with carbon monoxide (CO) for 5 min. The cells were then collected by centrifugation and lysed by resuspension in five volumes of water, followed by incubation on ice for 30 min. NaCl was added to a final concentration of 0.9%, resulting in aggregation of the membrane fractions into a gelatinous phase, which was removed by centrifugation for 15 min at 9500 *g*. The supernatant containing Hb was supplemented with 1 mM EDTA and bubbled with CO for 5 min. After adjusting the pH to 6.9, the hemolysate was applied to an SP Sepharose Fast Flow column (GE Healthcare) equilibrated with 10 mM NaH_2PO_4, 1 mM DTT, pH 6.9, and Hb was eluted with 10 mM Tris-HCl, pH 8.5. The fractions containing Hb were pooled, supplemented with 1 mM EDTA, and bubbled with CO for 5 min. Subsequently, the sample was applied to a Q Sepharose Fast Flow column (GE Healthcare) equilibrated with 10 mM Tris-HCl,

pH 8.5. Pure Hb was eluted with 30 mM NaH_2PO_4, pH 6.9, with a yield of 100 mg of protein/ml of blood. Hb concentrations were determined using Drabkin's reagent (Sigma).

2.5.3 Electrospray Ionization Mass Spectrometry and Circular Dichroism Spectroscopy

Purified human Hb and IsdH proteins were prepared in 10 mM ammonium acetate buffer at pH 6.9, subsequently mixed to concentrations of 10 and 20 μM, respectively, and incubated at 25 °C for 1 h. MS measurements of protein samples were performed on a Waters Synapt G1 QTOF mass spectrometer (Waters Corp., Milford, MA) [35]. The protein solutions were electrosprayed using Proxeon glass capillary nanoelectrospray emitters at flow rates between 30 and 50 nl/min. Quantification of Hb and Hb-receptor complexes was performed based on the Waters Synapt data by comparing summed peak heights. Higher resolution mass spectrometry experiments were performed using a 15-tesla Fourier transform ion cyclotron resonance instrument (SolariX hybrid Qq-FTMS, Bruker Daltonics, Billerica, MA). Circular dichroism spectra of 0.2 mg/ml $IsdB^{linker}$ and $IsdH^{linker}$ in 10 mM NaH_2PO_4, 50 mM NaF, pH 6.8, were recorded on a JASCO J-715 spectropolarimeter (JASCO Corp.) at 25 °C with a scan rate of 20 nm/min.

2.5.4 Heme Transfer Kinetics and Affinity Measurements

Heme transfer reactions from Hb to $IsdB^{N1N2}$ and various IsdH protein constructs were monitored by following absorbance changes using a conventional spectrophotometer (Shimadzu UV-1700 PharmaSpec), as described previously [14]. Human hemoglobin was purchased from Sigma and dissolved in 20 mM $NaPO_4$, pH 7.5, 150 mM NaCl. Briefly, 1 μM holo-Hb (expressed

in tetrameric units) was mixed with 10 μM apo-receptor protein in 20 mM $NaPO_4$, pH 7.5, 150 mM NaCl. Entire absorbance spectra were recorded for hemin transfer from holo-Hb to apo-$IsdH^{N2N3}$overtime. To compare the heme transfer rates from Hb to the various acceptor proteins, changes in absorbance at 371 and 406 nm were recorded over time at 25 °C for up to 2 h. Apparent rate constants for the heme transfer reactions were obtained by fitting the time courses of the absorbance changes $A_{406-371}$ to single or double exponential curves with Sigma-Plot (Systat Software Inc.). Affinities of $IsdH^{N3}$ and $IsdH^{N2N3}$ for heme were determined by fluorescence spectroscopy as described [38].

2.5.5 NMR Spectroscopy and Solution Structure Determination

NMR spectra of $IsdH^{linker}$ were acquired at 25 °C on cryoprobe-equipped Bruker Avance 500-, 600-, and 800-MHz spectrometers. Backbone and side-chain chemical shift assignments were obtained by analyzing the following experiments: ^{1}H,^{15}N HSQC, HNCO, HN(CA)CO, HNCACB, HNCA, CBCA- (CO)NH, ^{15}N-edited TOCSY, HNCA, HNHA, HNHB, HBHA-(CO)NH, CC(CO)NH, HCCH-TOCSY, HCCH-COSY, ^{15}N- edited NOESY, and ^{13}C-edited NOESY [reviewed in Ref. 39]. TALOS was used to obtain a majority of the and dihedral angle restraints [40]. Additional dihedral angle restraints were obtained by analyzing HNHA spectra [41]. Stereo-specific assignments of methylene protons were obtained by analyzing HNHB and ^{15}N-edited TOCSY spectra. Distance constraints were identified in three-dimensional ^{15}N- and ^{13}C-edited NOESY spectra with mixing times of 125 and 130 ms, respectively. NMR spectra were processed using NMRPipe and analyzed using the CARA and PIPP software packages [42, 43]. The program UNIO was used for automated NOE assignments and structure determination of $IsdH^{linker}$ [44]. The NOESY data were manually inspected to verify all NOE assignments and

identify additional NOE restraints. The structures were improved by iterative rounds of structure calculations in which hydrogen bond restraints, backbone torsion angle restraints obtained from the program TALOS, and side-chain torsion angle restraints were added [45]. A final set of 100 conformers was generated with a standard simulated annealing protocol, as implemented in the program NIH-XPLOR, of which 51 had no NOE, dihedral angle, or scalar coupling violations greater than 0.5 Å, 5°, or 2 Hz, respectively [46]. Of these, the 20 conformers with lowest overall energy were chosen to represent the structure of $IsdH^{linker}$. The quality of the structural ensemble was evaluated with PROCHECK and visualized with PyMOL [47, 48]. Statistics for the linker structure are presented in **Table 2.1**. Details on the NMR experiments used to obtain the backbone chemical shifts of $IsdH^{N2N3(Y642A)}$ have been described [36]. $^{1}D_{NH}$ residual dipolar couplings were measured using protein samples partially aligned in PEG C12E5/hexanol using two-dimensional ^{15}N-coupled IPAP ^{1}H-^{15}N HSQC experiments. Steady-state ^{15}N heteronuclear NOE values for the $IsdH^{linker}$ and $IsdH^{N2N3(Y642A)}$ were acquired on cryoprobe-equipped Bruker Avance 600- and 800-MHz spectrometers, respectively. The heteronuclear NOE experiments were carried out in an interleaved manner, with and without proton saturation, and analyzed using the program SPARKY [49].

2.6 Tables and Figures

TABLE 1

Structural statistics for the solution structure of IsdH linker domain

The notation of the NMR structures is as follows. ⟨SA⟩ are the final 20 simulated annealing structures; (SA) is the average energy-minimized structure. The number of terms for each restraint is given in parentheses.

	⟨SA⟩[a]	(SA)
Root mean square. deviations		
NOE interproton distance restraints (Å) (1469)	0.046 ± 0.002	0.051
Dihedral angle restraints (degrees)[b] (118)	0.072 ± 0.099	0.306
$^{3}J_{HN}$[a] coupling constants (Hz) (54)	0.532 ± 0.018	0.543
Secondary ^{13}C shifts (ppm)		
$13C_{\alpha}$ (76)	1.212 ± 0.206	1.267
$^{13}C_{\beta}$ (76)	0.816 ± 0.206	0.791
Deviations from idealized covalent geometry		
Bonds (Å)	0.0044 ± 0.0002	0.0174
Angles (degrees)	0.623 ± 0.028	1.538
Impropers (degrees)	0.492 ± 0.031	1.181
PROCHECK results (%)[c]		
Most favorable region	96.7 ± 2.8	96.7
Additionally allowed region	3.3 ± 2.8	3.3
Generously allowed region	0.0 ± 0.0	0.0
Disallowed region	0.0 ± 0.0	0.0
Coordinate precision (Å)[d]		
Protein backbone	0.42 ± 0.10	
Protein heavy atoms	0.87 ± 0.07	

[a] None of the structures exhibits distance violations greater than 0.5 Å, dihedral angle violations greater than 5°, or coupling constant violations greater than 2 Hz.

[b] Experimental dihedral angle restraints comprised 48 φ, 48 ψ, and 16 χ_1 angles.

[c] PROCHECK-NMR data include residues Val^{470}–Val^{531} of the linker domain.

[d] The coordinate precision is defined as the average atomic root mean square deviation of the 20 individual simulated annealing structures and their mean coordinates. The reported values are for residues Val^{470}–Val^{531} of the linker domain.

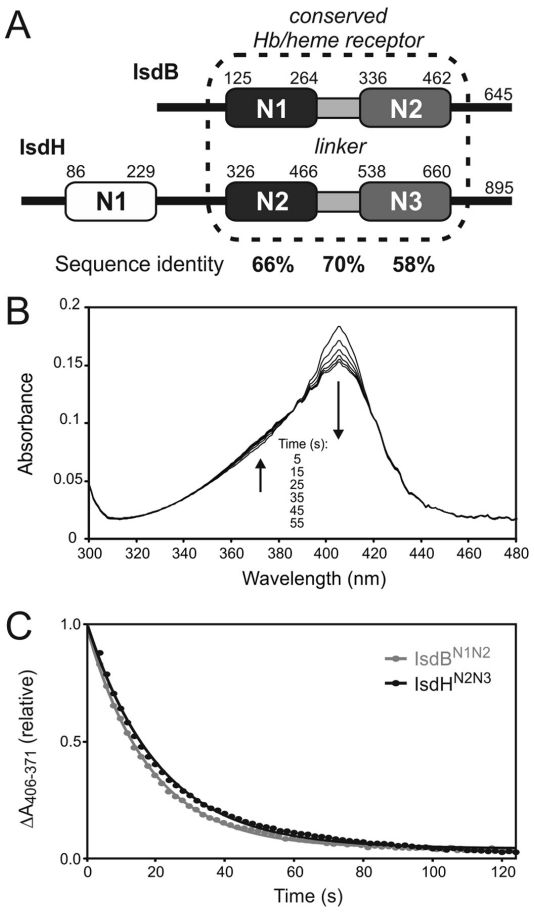

Figure 2.1 A homolog bidomain unit for heme capture in IsdH and IsdB

(A) Schematic of the NEAT domains present in *S. aureus* IsdH and IsdB. NEAT domains binding to Hb or heme are colored in black/white or gray, respectively. Sequence identities of functionally homologous NEAT domains as well as the linker connecting them are indicated. (B) Spectral shifts as a function of time after mixing for the reaction of 1 μM holo-Hb with 10 μM apo-IsdH^{N2N3}. Arrows indicate the increase and decrease in absorbance over time at 371and 406 nm, respectively. (C) Time courses of $\Delta A_{406-371}$ for the heme transfer reaction from Hb to IsdH^{N2N3} or IsdB^{N1N2}. The symbols and curves represent the observed data and the single-exponential fitting curves, respectively, yielding heme transfer rates of 0.048 ± 0.001 s^{-1} and 0.055 ± 0.001 s-1 for IsdH^{N2N3} and IsdB^{N1N2}, respectively.

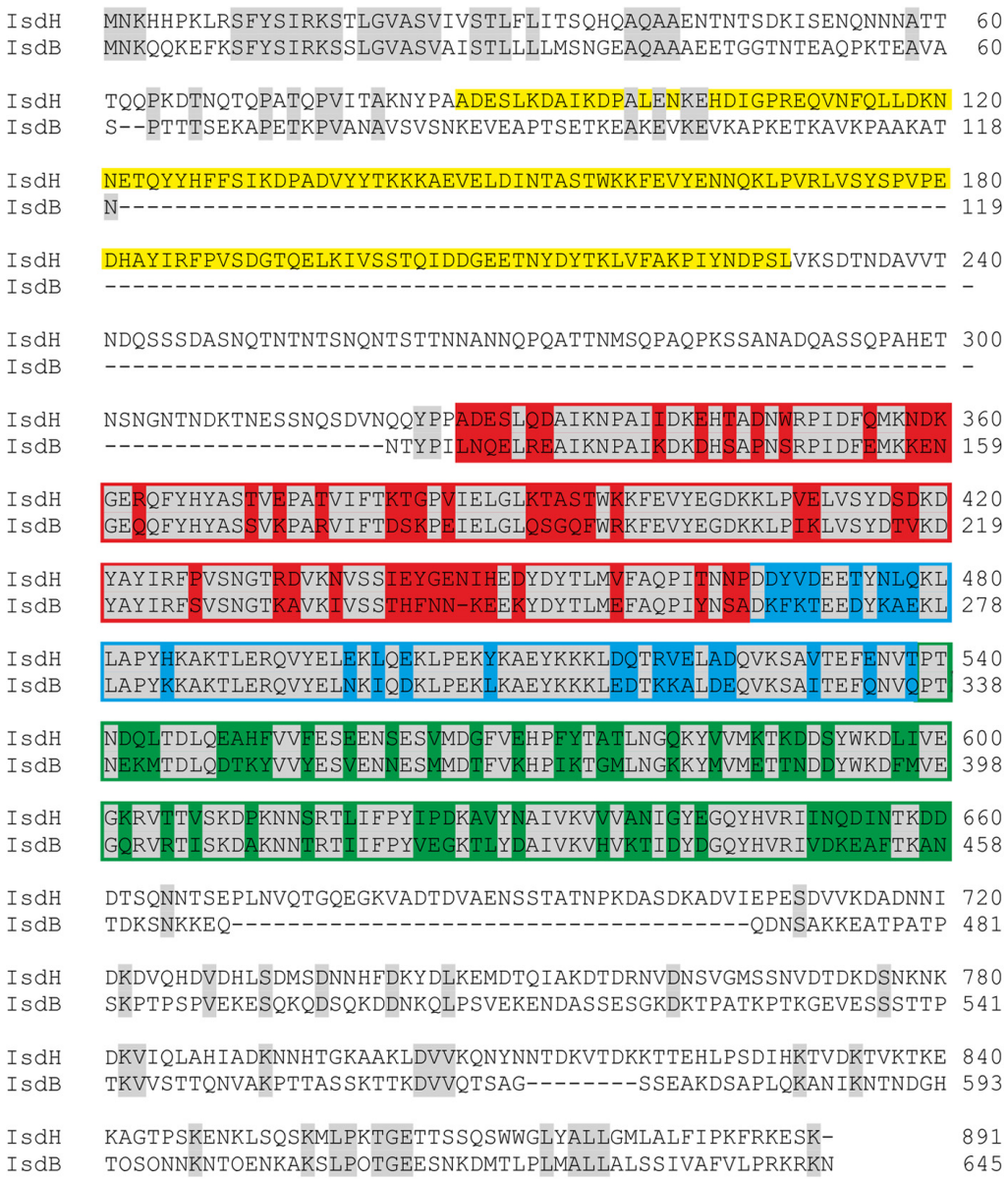

Figure 2.2 Alignment of IsdH and IsdB

A primary sequence alignment of IsdH (Q99TD3) and IsdB (Q7A656) was generated using ClustalW (69). Conserved residues are indicated by gray boxes. The predicted NEAT domains $IsdH^{N1}$, $IsdH^{N2}$/$IsdB^{N1}$, and $IsdH^{N3}$/$IsdB^{N2}$ are highlighted by yellow, red, and green boxes, respectively. The IsdH and IsdB linker domains are indicated by blue boxes.

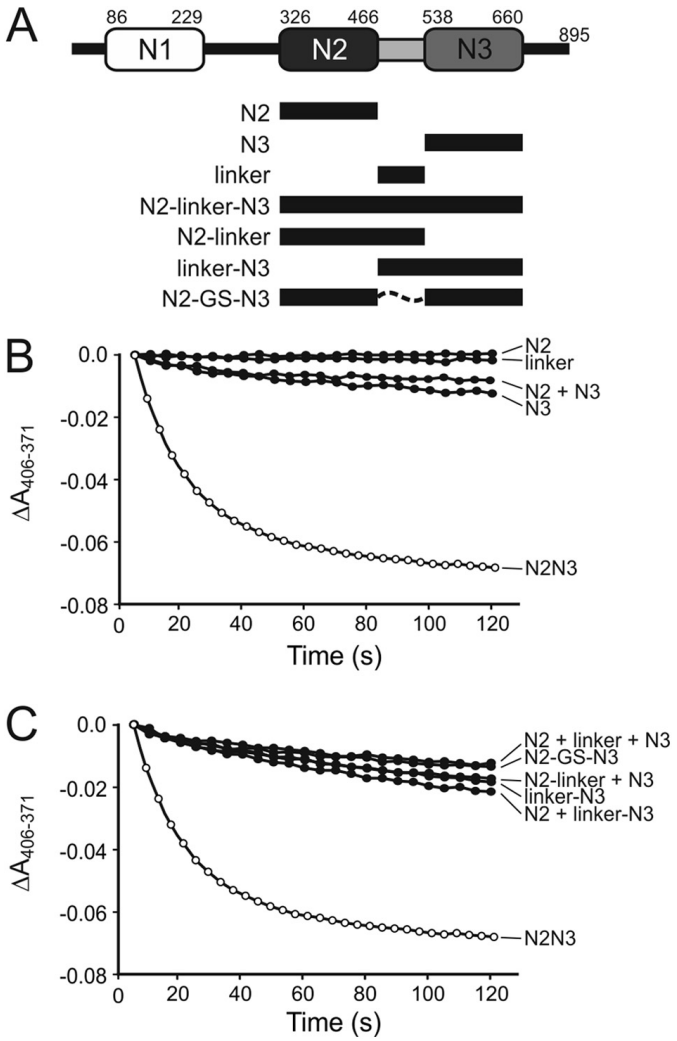

Figure 2.3 Heme transfer by various fragments of IsdH

(A) A schematic of the different fragments of IsdH used for heme transfer experiments. (B) and (C) Time courses for the heme transfer reaction from 1 μM holo-Hb to 10 μM apo-IsdHN2N3. Various IsdH receptor fragments as well as combinations thereof and the linker deletion construct $IsdH^{N2\text{-}GS\text{-}N3}$ are displayed. Heme transfer is followed by monitoring $\Delta A_{406–371}$ over 2 min.

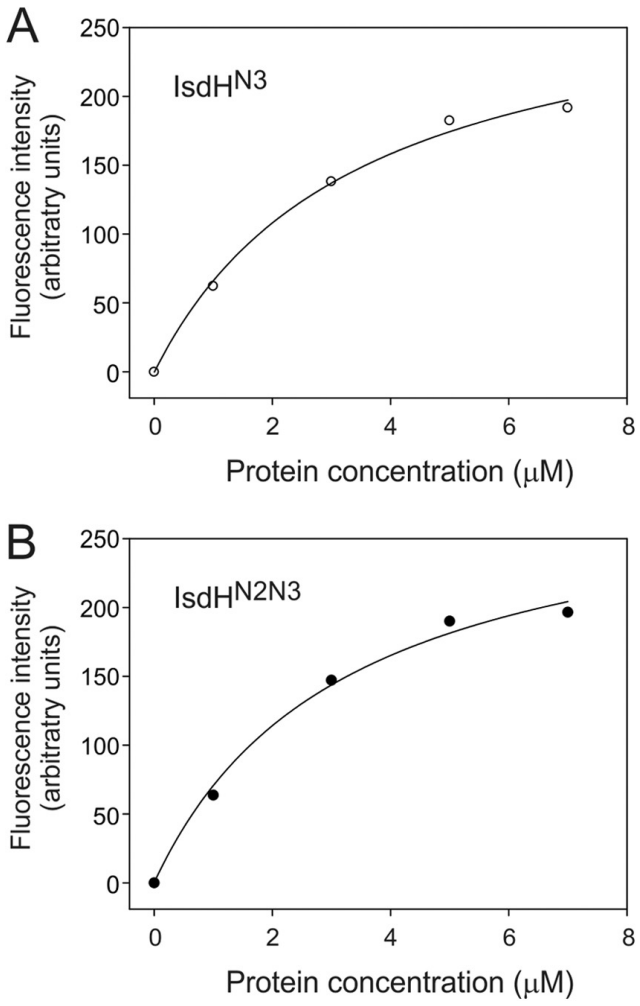

Figure 2.4 Heme binding properties of IsdH^{N3} and IsdH^{N2N3}

Protoporphyrin binding of IsdH^{N3} (A) or IsdH^{N2N3} (B) was measured following zinc-protoporphyrin IX fluorescence as a function of protein concentration (38). The solid lines represent best fits of the data yielding dissociation constants (KD) of 3.4 ± 0.6 μM and 3.2 ± 0.7 μM for IsdH^{N3} and IsdH^{N2N3}, respectively.

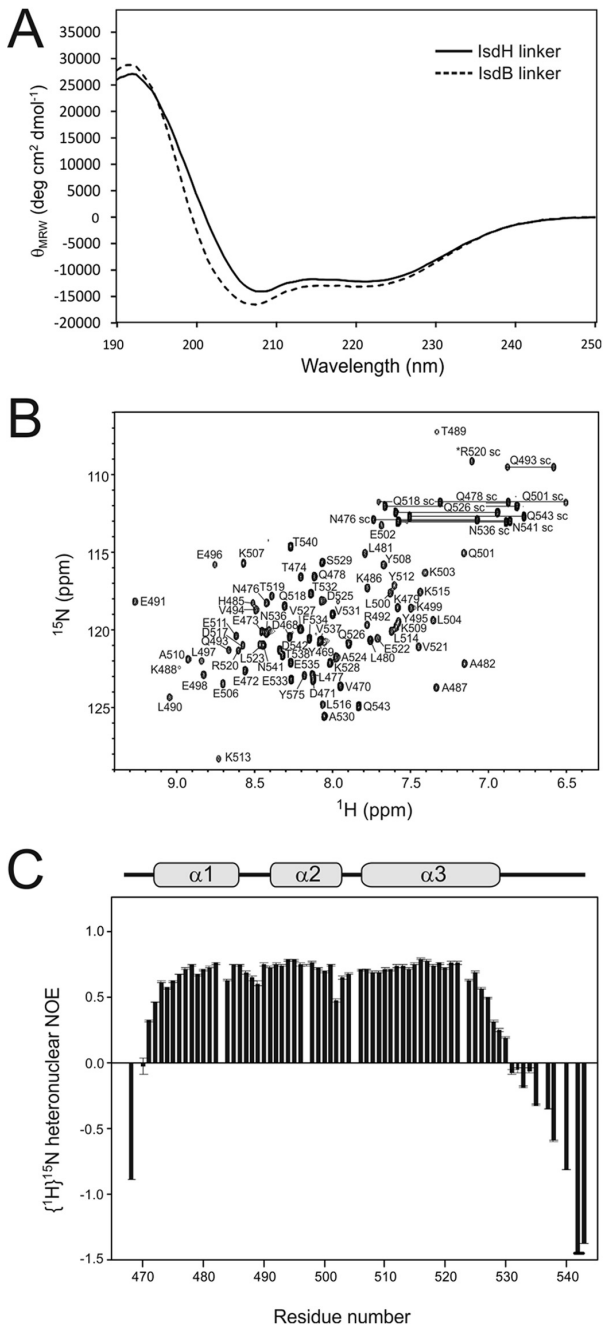

Figure 2.5 The IsdH and IsdB linkers fold into soluble α-helical domains

(A) Far UV-CD spectra of the linker domains of IsdH (solid) and IsdB (dashed).The strongly negative CD signals with minima around 208 and 222 nm are indicative of α-helical proteins. (B) ^{1}H-^{15}N HSQC spectrum of 1.1 mM ^{15}N-labeled $IsdH^{linker}$ acquired at 800 MHz. The amino

acid assignment for each cross-peak is indicated with one-letter code and residue number. Amide $^{\delta}$NH2 of Asn and $^{\gamma}$NH2 of Gln are connected by lines and denoted as sc for side chain. An asterisk indicates the cross-peak from the $^{\varepsilon}$NH of Arg520, which was folded in the ^{15}N dimension. (C) $\{^{1}H\}$-^{15}N heteronuclear NOE data of the IsdHl^{inker}. The peak intensity ratio between spectra with and without ^{1}H saturation as a function of the residue number is shown. The average heteronuclear NOE values and S.D. values of two experiments are displayed, and the location of the three α-helices is indicated at the top.

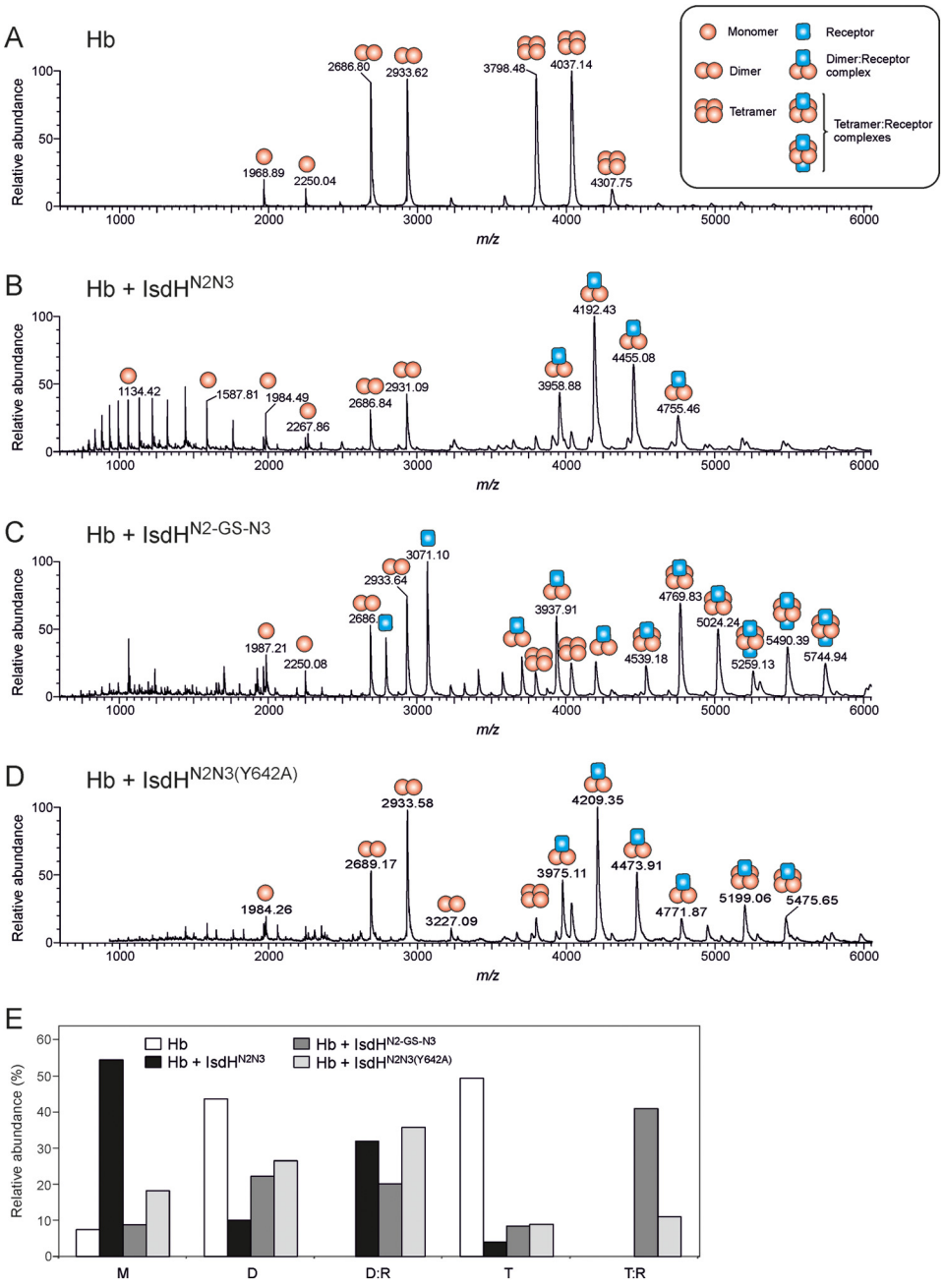

Figure 2.6 The IsdH and IsdB linkers fold into soluble α-helical domains

ESI-MS analysis of Hb dissociation by the IsdH receptor. Positive MS spectra are shown for 10 μM Hb (A) and 10 μM Hb in the presence of either 20 μM $IsdH^{N2N3}$ (B), $IsdH^{N2-GS-N3}$ (C), or $IsdH^{N2N3(Y642A)}$ (D). The most prominent peaks corresponding to monomeric, dimeric, or

tetrameric Hb as well as their complexes with the receptor proteins are labeled by the indicated symbols. (E) relative amounts of the different Hb oligomeric states, IsdH receptor proteins, and complexes thereof were quantified from ESI-MS spectra when10μM Hb was added to either 20 μM apo-IsdH^{N2N3} (black), 20 μM apo-IsdH$^{N2\text{-}GS\text{-}N3}$ (dark gray), or 20 μM apo-IsdH$^{N2N3(Y642A)}$ (light gray). 10 μM Hb was run as a control (white). M, monomer; D, dimer; DR, dimer-receptor complex; T, tetramer; TR, tetramer-receptor complex.

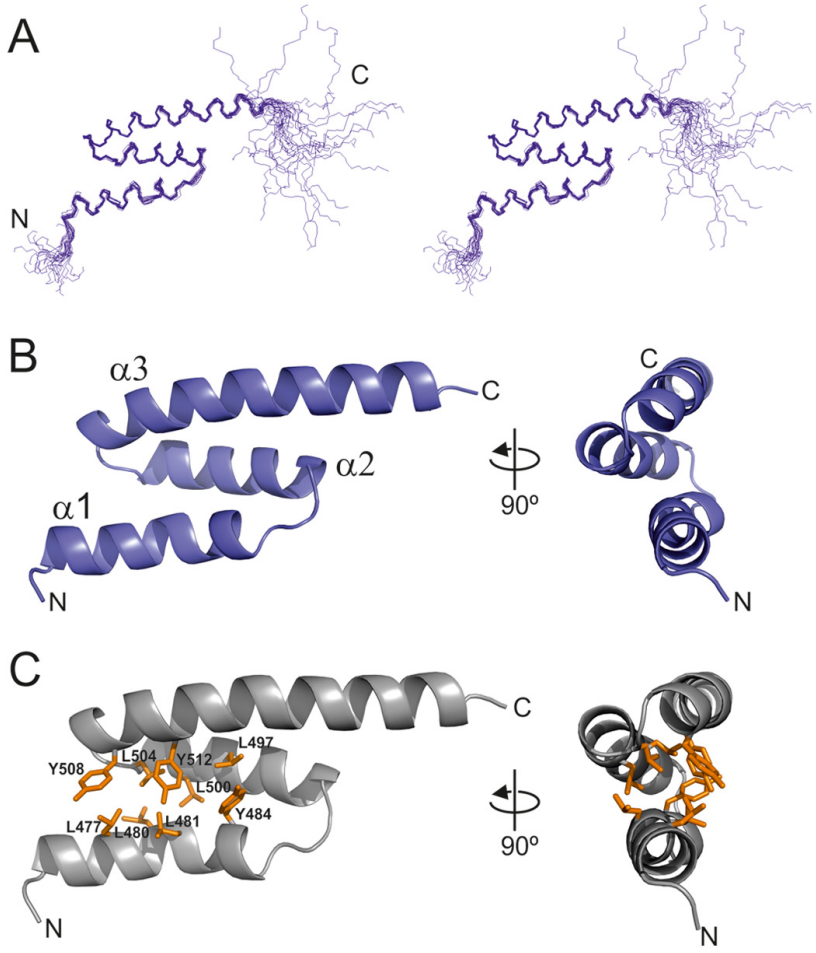

Figure 2.7 NMR structure of IsdH^{Linker}

(A) cross-eyed stereo view representation of the ensemble of 20 lowest energy structures. The coordinates were superimposed by aligning the backbone N, C_α, and C' atoms of residues Val470–Asp531. (B) ribbon diagram of the structured part encompassing residues Val470–Asp531 of the lowest energy conformer of IsdH^{linker}. The view on the left is in a similar orientation as shown in B, whereas the structure on the right has been rotated by 90°. The α-helices are labeled α1– α3. (C) Location of the residues of the hydrophobic core of IsdH^{linker}. A ribbon diagram of the structured part encompassing residues Val470–Asp531 of the linker structure is shown. The nine residues that form the hydrophobic core are indicated, and heavy atoms of their side chains are shown in stick representation.

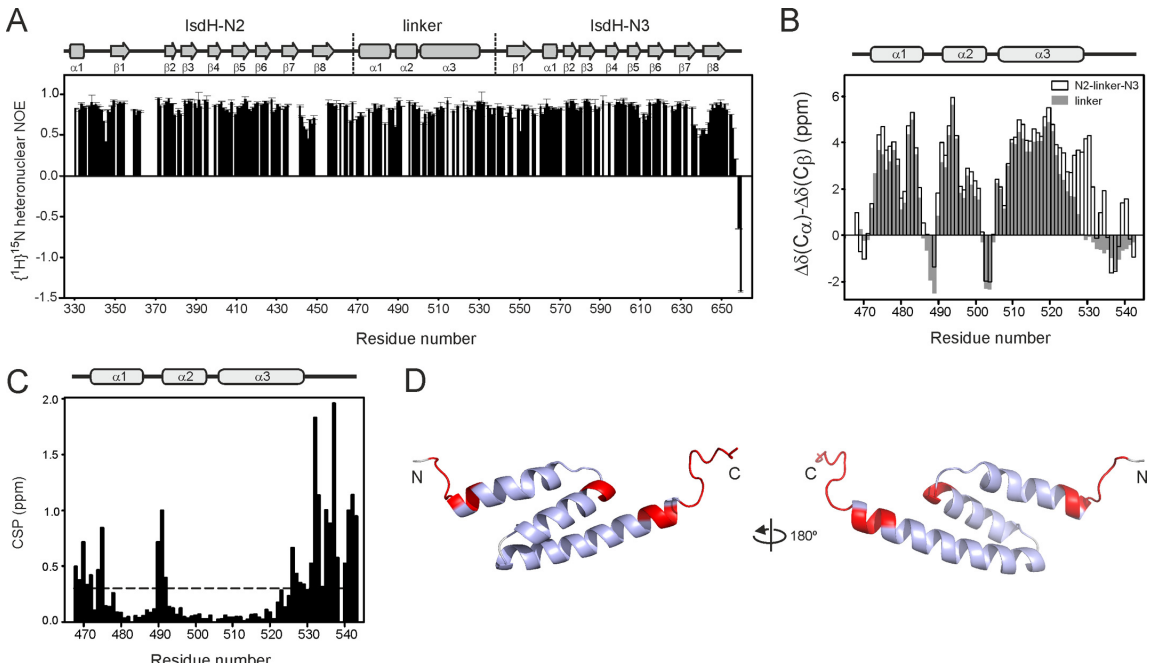

Figure 2.8 Interactions of IsdH linker with NEAT domains N2 and N3

(A) {^{1}H}-^{15}N heteronuclear NOE data of IsdH^{N2N3}. The peak intensity ratio between spectra with and without 1Hsaturation as a function of the residue number is shown. The average heteronuclear NOE values and S.D. values of two experiments are displayed. The domain boundaries of IsdH^{N2N3} and the location of predicted secondary structure elements are indicated at the top. (B) Comparison of the backbone conformations of the isolated IsdH linker region and the corresponding residues in IsdH^{N2N3}. Chemical shift deviations of the linker (gray bars) and IsdHN2N3 (open bars) with respect to the corresponding random coil values are plotted versus amino acid residue number, after multiplication with a 1:2:1 weighing function for residues i–1/i/i +1 (70). Positive values for the chemical shift deviations $\Delta\delta(C_\alpha) - \Delta\delta(C_\beta)$ are indicative of a helical conformation. (C) Average chemical shift differences of the backbone amide signals $(CSP = \Delta\delta_H^2 + (\Delta\delta_N/6.49)^2)^{1/2}$ of isolated IsdH^{linker} and the linker in the context of the functional receptor IsdH^{N2N3}. (D) Mapping of the perturbed residues on ribbon diagrams of the linker. The residues with CSP > 0.3 ppm are highlighted in red.

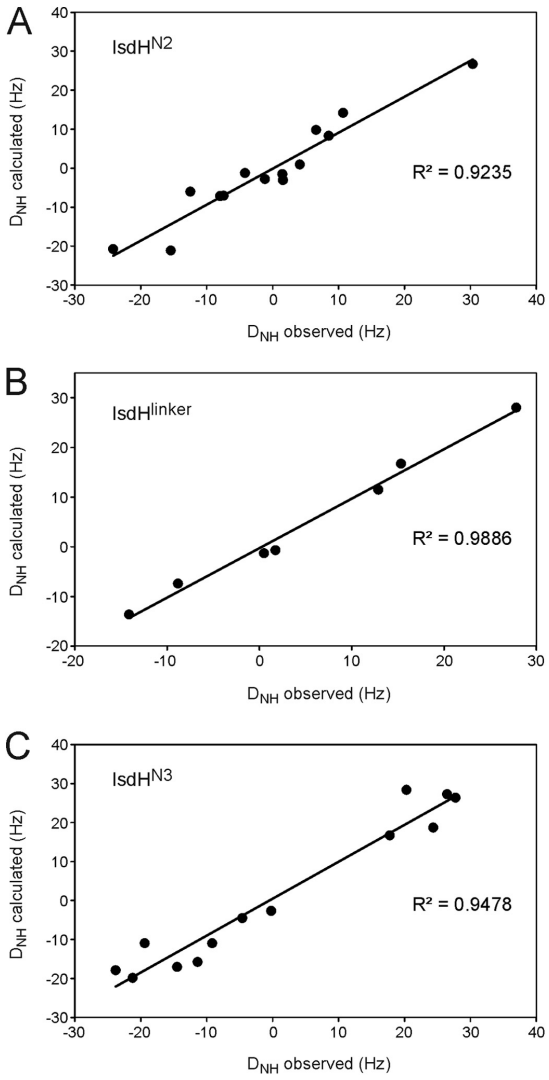

Figure 2.9 Comparison of experimental and back-calculated RDC values of backbone amide protons in IsdH$^{N2N3(Y642A)}$

(A) Observed $^{1}D_{NH}$ RDCs for the N2 domain were plotted versus back-calculated RDCs from a homology model of IsdH^{N2}. (B) Experimentally measured $^{1}D_{NH}$ RDCs for the linker domain were plotted versus back-calculated RDCs from the solution structure of the isolated linker. (C) observed $^{1}D_{NH}$ RDCs for the N3 domain were plotted versus back-calculated RDCs from the crystal structure of IsdH^{N3} (Protein Data Bank entry 2Z6F). The correlation factors, R^2, are indicated in the plots.

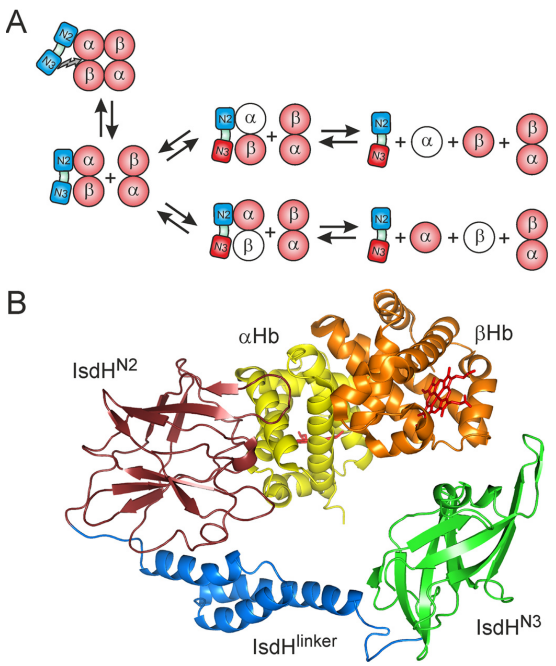

Figure 2.10 Model of heme extraction by IsdH

(A) A model for the mechanism of heme acquisition by the surface receptor IsdH^{N2N3}. A schematic diagram shows the binding equilibria involved in the extraction process. Wild- type IsdH^{N2N3} binds to the α-chain of Hb promoting its dissociation into (αβ) dimers. Heme acquisition by the receptor protein results in further dissociation of Hb into its monomeric subunits. See "Discussion" for details. (B) A model of IsdH^{N2N3} in complex with Hb. IsdH^{N2} (red) was modeled based on the solution structure of IsdH^{N1} (Protein Data Bank entry 2H3K). The complex model with Hb was generated by superposition over the crystal structure of the IsdH^{N1}-Hb complex (Protein Data Bank entry 3SZK). A possible orientation of the linker (blue) and IsdH^{N3} (green; Protein Data Bank entry 2Z6F) allowing productive heme transfer from a Hb (αβ) dimer (yellow-orange) to IsdH is indicated. The orientation of the subdomains (N1, linker, and N2) within IsdH^{N2N3} has not been experimentally determined, and only one possible orientation is shown. The protein backbones are shown as schematics. The heme groups in Hb are shown in stick representation.

2.7 References

[1] Klevens R. M., Morrison M. A., Nadle J., Petit S., Gershman K., Ray S., Harrison L. H., Lynfield R., Dumyati G., Townes J. M., Craig A. S., Zell E. R., Fosheim G. E., McDougal L. K., Carey R. B., Fridkin S. K., and Active Bacterial Core surveillance (ABCs) MRSA Investigators (2007) Invasive methicillin-resistant*Staphylococcus aureus* infections in the United States. J. Am. Med. Assoc. 298, 1763–1771 [PubMed: 17940231]

[2] Papanikolaou G., Pantopoulos K. (2005) Iron metabolism and toxicity. Toxicol. Appl. Pharmacol. 202, 199–211 [PubMed: 15629195]

[3] Ward P. P., Conneely O. M. (2004) Lactoferrin. Role in iron homeostasis and host defense against microbial infection. Biometals 17, 203–208 [PubMed: 15222466]

[4] Grigg J. C., Ukpabi G., Gaudin C. F., Murphy M. E. (2010) Structural biology of heme binding in the *Staphylococcus aureus* Isd system. J. Inorg. Biochem. 104, 341–348 [PubMed: 19853304]

[5] Reniere M. L., Torres V. J., Skaar E. P. (2007) Intracellular metalloporphyrin metabolism in *Staphylococcus aureus*. Biometals 20, 333–345 [PubMed: 17387580]

[6] Skaar E. P., Schneewind O. (2004) Iron-regulated surface determinants (Isd) of *Staphylococcus aureus*. Stealing iron from heme. Microbes Infect. 6, 390–397

[7] Ton-That H., Marraffini L. A., Schneewind O. (2004) Protein sorting to the cell wall envelope of Gram-positive bacteria. Biochim. Biophys. Acta 1694, 269–278[PubMed: 15546671]

[8] Dryla A., Gelbmann D., von Gabain A., Nagy E. (2003) Identification of a novel iron regulated staphylococcal surface protein with haptoglobin-haemoglobin binding activity. Mol. Microbiol. 49, 37–53 [PubMed: 12823809]

[9] Taylor J. M., Heinrichs D. E. (2002) Transferrin binding in *Staphylococcus aureus*. Involvement of a cell wall-anchored protein. Mol. Microbiol. 43, 1603–1614[PubMed: 11952908]

[10] Clarke S. R., Wiltshire M. D., Foster S. J. (2004) IsdA of *Staphylococcus aureus* is a broad spectrum, iron-regulated adhesin. Mol. Microbiol. 51, 1509–1519[PubMed: 14982642]

[11] Mazmanian S. K., Skaar E. P., Gaspar A. H., Humayun M., Gornicki P., Jelenska J., Joachmiak A., Missiakas D. M., Schneewind O. (2003) Passage of heme-iron across the envelope of *Staphylococcus aureus*. Science 299, 906–909 [PubMed: 12574635]

[12] Mazmanian S. K., Ton-That H., Su K., Schneewind O. (2002) An iron-regulated sortase anchors a class of surface protein during *Staphylococcus aureus*pathogenesis. Proc. Natl. Acad. Sci. U.S.A. 99, 2293–2298 [PMCID: PMC122358] [PubMed: 11830639]

[13] Muryoi N., Tiedemann M. T., Pluym M., Cheung J., Heinrichs D. E., Stillman M. J. (2008) Demonstration of the iron-regulated surface determinant (Isd) heme transfer

pathway in *Staphylococcus aureus*. J. Biol. Chem. 283, 28125–28136 [PMCID: PMC2661384] [PubMed: 18676371]

[14] Zhu H., Xie G., Liu M., Olson J. S., Fabian M., Dooley D. M., Lei B. (2008) Pathway for heme uptake from human methemoglobin by the iron-regulated surface determinants system of *Staphylococcus aureus*. J. Biol. Chem. 283, 18450–18460 [PMCID: PMC2440603] [PubMed: 18467329]

[15] Skaar E. P., Gaspar A. H., Schneewind O. (2004) IsdG and IsdI, heme-degrading enzymes in the cytoplasm of *Staphylococcus aureus*. J. Biol. Chem. 279, 436–443[PubMed: 14570922]

[16] Pishchany G., Dickey S. E., Skaar E. P. (2009) Subcellular localization of the *Staphylococcus aureus* heme iron transport components IsdA and IsdB. Infect. Immun.77, 2624–2634 [PMCID: PMC2708553] [PubMed: 19398548]

[17] Pishchany G., McCoy A. L., Torres V. J., Krause J. C., Crowe J. E., Jr., Fabry M. E., Skaar E. P. (2010) Specificity for human hemoglobin enhances *Staphylococcus aureus* infection. Cell Host Microbe 8, 544–550 [PMCID: PMC3032424] [PubMed: 21147468]

[18] Grigg J. C., Vermeiren C. L., Heinrichs D. E., Murphy M. E. (2007) Heme coordination by *Staphylococcus aureus* IsdE. J. Biol. Chem. 282, 28815–28822[PubMed: 17666394]

[19] Visai L., Yanagisawa N., Josefsson E., Tarkowski A., Pezzali I., Rooijakkers S. H., Foster T. J., Speziale P. (2009) Immune evasion by *Staphylococcus aureus*conferred by iron-regulated surface determinant protein IsdH. Microbiology 155, 667–679 [PubMed: 19246738]

[20] Newton S. M., Klebba P. E., Raynaud C., Shao Y., Jiang X., Dubail I., Archer C., Frehel C., Charbit A. (2005) The *svpA-srtB* locus of *Listeria monocytogenes*. Fur-mediated iron regulation and effect on virulence. Mol. Microbiol. 55, 927–940 [PubMed: 15661014]

[21] Xiao Q., Jiang X., Moore K. J., Shao Y., Pi H., Dubail I., Charbit A., Newton S. M., Klebba P. E. (2011) Sortase independent and dependent systems for acquisition of haem and haemoglobin in *Listeria monocytogenes*. Mol. Microbiol. 80, 1581–1597 [PMCID: PMC3115469] [PubMed: 21545655]

[22] Honsa E. S., Maresso A. W. (2011) Mechanisms of iron import in anthrax. Biometals 24, 533–545 [PubMed: 21258843]

[23] Liu M., Lei B. (2005) Heme transfer from streptococcal cell surface protein Shp to HtsA of transporter HtsABC. Infect. Immun. 73, 5086–5092 [PMCID: PMC1201258] [PubMed: 16041024]

[24] Nygaard T. K., Blouin G. C., Liu M., Fukumura M., Olson J. S., Fabian M., Dooley D. M., Lei B. (2006) The mechanism of direct heme transfer from the streptococcal cell surface protein Shp to HtsA of the HtsABC transporter. J. Biol. Chem. 281, 20761–20771 [PMCID: PMC2423311] [PubMed: 16717094]

[25] Zhu H., Liu M., Lei B. (2008) The surface protein Shr of *Streptococcus pyogenes* binds heme and transfers it to the streptococcal heme-binding protein Shp. BMC Microbiol. 8, 15. [PMCID: PMC2266757] [PubMed: 18215300]

[26] Andrade M. A., Ciccarelli F. D., Perez-Iratxeta C., Bork P. (2002) NEAT: a domain duplicated in genes near the components of a putative Fe^{3+} siderophore transporter from Gram-positive pathogenic bacteria. Genome Biol. 3, RESEARCH0047 [PMCID: PMC126872]

[27] Grigg J. C., Vermeiren C. L., Heinrichs D. E., Murphy M. E. (2007) Haem recognition by a *Staphylococcus aureus* NEAT domain. Mol. Microbiol. 63, 139–149[PubMed: 17229211]

[28] Villareal V. A., Pilpa R. M., Robson S. A., Fadeev E. A., Clubb R. T. (2008) The IsdC protein from *Staphylococcus aureus* uses a flexible binding pocket to capture heme. J. Biol. Chem. 283, 31591–31600 [PMCID: PMC2581589] [PubMed: 18715872]

[29] Sharp K. H., Schneider S., Cockayne A., Paoli M. (2007) Crystal structure of the heme-IsdC complex, the central conduit of the Isd iron/heme uptake system in *Staphylococcus aureus*. J. Biol. Chem. 282, 10625–10631 [PubMed: 17287214]

[30] Villareal V. A., Spirig T., Robson S. A., Liu M., Lei B., Clubb R. T. (2011) Transient weak protein-protein complexes transfer heme across the cell wall of *Staphylococcus aureus*. J. Am. Chem. Soc. 133, 14176–14179 [PMCID: PMC3174093] [PubMed: 21834592]

[31] Abe R., Caaveiro J. M., Kozuka-Hata H., Oyama M., Tsumoto K. (2012) Mapping ultra-weak protein-protein interactions between heme transporters of *Staphylococcus aureus*. J. Biol. Chem. 287, 16477–16487 [PMCID: PMC3351326] [PubMed: 22427659]

[32] Torres V. J., Pishchany G., Humayun M., Schneewind O., Skaar E. P. (2006) *Staphylococcus aureus* IsdB is a hemoglobin receptor required for heme iron utilization. J. Bacteriol. 188, 8421–8429 [PMCID: PMC1698231] [PubMed: 17041042]

[33] Kim H. K., DeDent A., Cheng A. G., McAdow M., Bagnoli F., Missiakas D. M., Schneewind O. (2010) IsdA and IsdB antibodies protect mice against *Staphylococcus aureus* abscess formation and lethal challenge. Vaccine 28, 6382–6392 [PMCID: PMC3095377] [PubMed: 20226248]

[34] Hargrove M. S., Whitaker T., Olson J. S., Vali R. J., Mathews A. J. (1997) Quaternary structure regulates hemin dissociation from human hemoglobin. J. Biol. Chem. 272, 17385–17389 [PubMed: 9211878]

[35] Senturia R., Faller M., Yin S., Loo J. A., Cascio D., Sawaya M. R., Hwang D., Clubb R. T., Guo F. (2010) Structure of the dimerization domain of DiGeorge critical region 8. Protein Sci. 19, 1354–1365 [PMCID: PMC2974827] [PubMed: 20506313]

[36] Spirig T., Clubb R. T. (2012) Backbone ^{1}H, ^{13}C, and ^{15}N resonance assignments of the 39 kDa staphylococcal hemoglobin receptor IsdH. Biomol. NMR Assign. 6, 169–172 [PMCID: PMC3590065] [PubMed: 22101872]

[37] Ascoli F., Fanelli M. R., Antonini E. (1981) Preparation and properties of apohemoglobin and reconstituted hemoglobins. Methods Enzymol. 76, 72–87[PubMed: 7329287]

[38] Pilpa R. M., Robson S. A., Villareal V. A., Wong M. L., Phillips M., Clubb R. T. (2009) Functionally distinct NEAT (NEAr Transporter) domains within the*Staphylococcus aureus* IsdH/HarA protein extract heme from methemoglobin. J. Biol. Chem. 284, 1166–1176 [PMCID: PMC2613621] [PubMed: 18984582]

[39] Cavanagh J., Fairbrother W. J., Palmer A. G., Skelton N. J. (1996) Protein NMR Spectroscopy: Principles and Practice. Academic Press, San Diego, CA

[40] Shen Y., Delaglio F., Cornilescu G., Bax A. (2009) TALOS+. A hybrid method for predicting protein backbone torsion angles from NMR chemical shifts. J. Biomol. NMR 44, 213–223 [PMCID: PMC2726990] [PubMed: 19548092]

[41] Vuister G. W., Bax A. (1993) Quantitative J correlation. A new approach for measuring homonuclear three-bond *J*(HNH.α.) coupling constants in ^{15}N-enriched proteins. J. Am. Chem. Soc. 115, 7772–7777

[42] Delaglio F., Grzesiek S., Vuister G. W., Zhu G., Pfeifer J., Bax A. (1995) NMRPipe. A multidimensional spectral processing system based on UNIX pipes. J. Biomol. NMR 6, 277–293 [PubMed: 8520220]

[43] Garrett D. S., Powers R., Gronenborn A. M., Clore G. M. (2011) A common sense approach to peak picking in two-, three-, and four-dimensional spectra using automatic computer analysis of contour diagrams. J. Magn. Reson. 213, 357–363 [PubMed: 22152355]

[44] Herrmann T., Güntert P., Wüthrich K. (2002) Protein NMR structure determination with automated NOE-identification in the NOESY spectra using the new software ATNOS. J. Biomol. NMR 24, 171–189 [PubMed: 12522306]

[45] Cornilescu G., Delaglio F., Bax A. (1999) Protein backbone angle restraints from searching a database for chemical shift and sequence homology. J. Biomol. NMR13, 289–302 [PubMed: 10212987]

[46] Brünger A. T., Clore G. M., Gronenborn A. M., Saffrich R., Nilges M. (1993) Assessing the quality of solution nuclear magnetic resonance structures by complete cross-validation. Science 261, 328–331 [PubMed: 8332897]

[47] Laskowski R. A., Rullmannn J. A., MacArthur M. W., Kaptein R., Thornton J. M. (1996) AQUA and PROCHECK-NMR. Programs for checking the quality of protein structures solved by NMR. J. Biomol. NMR 8, 477–486 [PubMed: 9008363]

[48] DeLano W. L. (2006) The PyMOL Molecular Graphics System, version 0.99, DeLano Scientific, South San Francisco, CA

[49] Goddard T. D., Kneller D. G. (2001) Sparky NMR Analysis Software, University of California, San Francisco

[50] Krishna Kumar K., Jacques D. A., Pishchany G., Caradoc-Davies T., Spirig T., Malmirchegini G. R., Langley D. B., Dickson C. F., Mackay J. P., Clubb R. T., Skaar E. P., Guss J. M., Gell D. A. (2011) Structural basis for hemoglobin capture

by *Staphylococcus aureus* cell-surface protein, IsdH. J. Biol. Chem. 286, 38439–38447[PMCID: PMC3207429] [PubMed: 21917915]

[51] Pilpa R. M., Fadeev E. A., Villareal V. A., Wong M. L., Phillips M., Clubb R. T. (2006) Solution structure of the NEAT (NEAr Transporter) domain from IsdH/HarA. The human hemoglobin receptor in *Staphylococcus aureus*. J. Mol. Biol. 360, 435–447 [PubMed: 16762363]

[52] Dryla A., Hoffmann B., Gelbmann D., Giefing C., Hanner M., Meinke A., Anderson A. S., Koppensteiner W., Konrat R., von Gabain A., Nagy E. (2007) High-affinity binding of the staphylococcal HarA protein to haptoglobin and hemoglobin involves a domain with an antiparallel eight-stranded β-barrel fold. J. Bacteriol. 189, 254–264 [PMCID: PMC1797202] [PubMed: 17041047]

[53] Watanabe M., Tanaka Y., Suenaga A., Kuroda M., Yao M., Watanabe N., Arisaka F., Ohta T., Tanaka I., Tsumoto K. (2008) Structural basis for multimeric heme complexation through a specific protein-heme interaction. The case of the third neat domain of IsdH from *Staphylococcus aureus*. J. Biol. Chem. 283, 28649–28659[PMCID: PMC2661414] [PubMed: 18667422]

[54] Gaudin C. F., Grigg J. C., Arrieta A. L., Murphy M. E. (2011) Unique heme-iron coordination by the hemoglobin receptor IsdB of *Staphylococcus aureus*. Biochemistry 50, 5443–5452 [PMCID: PMC3114464] [PubMed: 21574663]

[55] Loo J. A. (2000) Electrospray ionization mass spectrometry. A technology for studying noncovalent macromolecular complexes. Int. J. Mass Spectrom. 200, 175–186

[56] Sugita Y. (1975) Differences in spectra of α and β chains of hemoglobin between isolated state and in tetramer. J. Biol. Chem. 250, 1251–1256 [PubMed: 1112803]

[57] Liu J., Konermann L. (2011) Protein-protein binding affinities in solution determined by electrospray mass spectrometry. J. Am. Soc. Mass Spectrom. 22, 408–417[PubMed: 21472560]

[58] Griffith W. P., Kaltashov I. A. (2003) Highly asymmetric interactions between globin chains during hemoglobin assembly revealed by electrospray ionization mass spectrometry. Biochemistry 42, 10024–10033 [PubMed: 12924951]

[59] Benesch R. E., Kwong S. (1995) Coupled reactions in hemoglobin. Heme-globin and dimer-dimer association. J. Biol. Chem. 270, 13785–13786[PubMed: 7775434]

[60] Moriwaki Y., Caaveiro J. M., Tanaka Y., Tsutsumi H., Hamachi I., Tsumoto K. (2011) Molecular basis of recognition of antibacterial porphyrins by heme-transporter IsdH-NEAT3 of *Staphylococcus aureus*. Biochemistry 50, 7311–7320 [PubMed: 21797259]

[61] Gouda H., Torigoe H., Saito A., Sato M., Arata Y., Shimada I. (1992) Three-dimensional solution structure of the B domain of staphylococcal protein A. Comparisons of the solution and crystal structures. Biochemistry 31, 9665–9672 [PubMed: 1390743]

[62] Schneider J. P., Lombardi A., DeGrado W. F. (1998) Analysis and design of three-stranded coiled coils and three-helix bundles. Fold. Des. 3, R29–R40[PubMed: 9565750]

[63] Bunn F. H., Forger B. G. (1986) Hemoglobin: Molecular, Genetic, and Clinical Aspects, pg. 21–27, W. B. Saunders Co., Philadelphia

[64] Waks M., Yip Y. K., Beychok S. (1973) Influence of prosthetic groups on protein folding and subunit assembly. Recombination of separated human α- and β-globin chains with heme and alloplex interactions of globin chains with heme-containing subunits. J. Biol. Chem. 248, 6462–6470 [PubMed: 4730328]

[65] Lu C., Xie G., Liu M., Zhu H., Lei B. (2012) Direct heme transfer reactions in the group a streptococcus heme acquisition pathway. PLoS One 7, e37556.[PMCID: PMC3359286] [PubMed: 22649539]

[66] Ouattara M., Cunha E. B., Li X., Huang Y. S., Dixon D., Eichenbaum Z. (2010) Shr of group A streptococcus is a new type of composite NEAT protein involved in sequestering haem from methaemoglobin. Mol. Microbiol. 78, 739–756 [PMCID: PMC2963705] [PubMed: 20807204]

[67] Honsa E. S., Fabian M., Cardenas A. M., Olson J. S., Maresso A. W. (2011) The five near-iron transporter (NEAT) domain anthrax hemophore, IsdX2, scavenges heme from hemoglobin and transfers heme to the surface protein IsdC. J. Biol. Chem. 286, 33652–33660 [PMCID: PMC3190864] [PubMed: 21808055]

[68] Maresso A. W., Garufi G., Schneewind O. (2008) *Bacillus anthracis* secretes proteins that mediate heme acquisition from hemoglobin. PLoS Pathog. 4, e1000132.[PMCID: PMC2515342] [PubMed: 18725935]

[69] Thompson J. D., Gibson T. J., Higgins D. G. (2002) Multiple sequence alignment using ClustalW and ClustalX. Curr. Protoc. Bioinformatics, Chapter 2, Unit 2.3

[70] Wishart D. S., Bigam C. G., Holm A., Hodges R. S., Sykes B. D. (1995) ^{1}H, ^{13}C, and ^{15}N random coil NMR chemical shifts of the common amino acids. I. Investigations of nearest-neighbor effects. J. Biomol. NMR 5, 67–81 [PubMed: 7881273]

Chapter 3

The PRE-Derived NMR Model of the 38.8 kDa Tri-Domain IsdH Protein from *Staphylococcus aureus* Suggests that it Adaptively Recognizes Human Hemoglobin

The work described in this chapter has been reproduced with permission from:

Sjodt, M., Macdonald, R., Spirig, T., Chan, A. H., Dickson, C. F., Fabian, M., Olson, J. S., Gell, D. A., & Clubb, R. T. The PRE-Derived NMR Model of the 38.8 kDa Tri-Domain IsdH Protein from *Staphylococcus aureus* Suggests that it Adaptively Recognizes Human Hemoglobin. *J. Mol Biol*., 2016; 428(6):1107-29. doi: 10.1016/j.jmb.2015.02.008

I was the primary author of this work. I designed the experiments, performed the biochemical assays, NMR experiments, structure calculations, computational modelling, and analyzed data.

3.1 Overview

Staphylococcus aureus is a medically important bacterial pathogen that during infections acquires iron from human hemoglobin (Hb). It uses two closely related iron regulated surface determinant (Isd) proteins to capture and extract the oxidized form of heme (hemin) from Hb, IsdH and IsdB. Both receptors rapidly extract hemin using a conserved tri-domain unit consisting of two NEAr iron Transporter (NEAT) domains connected by a helical linker domain. To gain insight into the mechanism of extraction we used NMR to investigate the structure and dynamics of the 38.8 kDa tri-domain IsdH protein ($IsdH^{N2N3}$, A326-D660 with a Y642A mutation that prevents hemin binding). The structure was modeled using long-range paramagnetic relaxation enhancement (PRE) distance restraints, dihedral angle, small angle x-ray scattering, residual dipolar coupling and inter-domain NOE data. The receptor adopts an extended conformation wherein the linker and N3 domains pack against each other via a hydrophobic interface. In contrast, the N2 domain contacts the linker domain via a hydrophilic interface, and based on NMR relaxation data undergoes inter-domain motions enabling it to reorient with respect to the body of the protein. Ensemble calculations were used to estimate the range of N2 domain positions compatible with the PRE data. A comparison of the Hb-free and -bound forms reveals that Hb binding alters the positioning of the N2 domain. We propose that binding occurs through a combination of conformational selection and induced fit mechanisms that may promote hemin release from Hb by altering the position of its F-helix.

3.2 Introduction

Staphylococcus aureus causes a range of illnesses from minor skin infections, to life-threatening diseases such as meningitis, pneumonia, osteomyelitis, endocarditis, toxic shock syndrome and septicemia [1]. In the United States *S. aureus* is a leading cause of life-threatening hospital and community acquired infections [2]. There is a growing need to understand the mechanism through which it causes disease as many strains of *S. aureus* have become resistant to conventional antibiotics, such as highly virulent methicillin-resistant strains of *S. aureus* (MRSA). *S. aureus'* ability to replicate within its host is critically dependent on access to iron, since this metal functions as a key biocatalyst and/or electron carrier in microbial enzymes that mediate metabolism [3]. Free iron is scarce in the human body and must therefore be actively procured during infections [4]. Heme (protoporphyrin IX + iron) bound to human hemoglobin (Hb) contains ~75-80% of the body's total iron content and is preferentially utilized by *S. aureus* [5]. An understanding of how *S. aureus* captures Hb and extracts its heme is therefore of fundamental importance and could potentiate the development of novel antimicrobial agents that work by disrupting heme acquisition.

S. aureus acquires heme-iron from human Hb using nine iron-regulated surface determinant (Isd) proteins [6–8]. Four Isd proteins (IsdA, IsdB, IsdC, and IsdH/HarA) bind heme and are covalently linked to the peptidoglycan cell wall by sortase transpeptidases [9–11]. Biochemical and cellular localization studies suggest that heme capture and transfer across the cell wall is mediated by an ordered set of heme transfer reactions. In this process, IsdB and IsdH first bind Hb and extract its heme [10,12]. Heme is then passed from IsdB/IsdH to IsdA, which is partially buried within the cell wall. Next, IsdA passes heme to the IsdC protein, which has recently been shown to occur via a transient ultra-weak IsdA-IsdC heme transfer complex

[10,13–16]. Holo-IsdC then delivers the heme to the IsdDEF complex, a bacterial ABC transporter that pumps heme into the cytoplasm. Free iron is then obtained when the heme oxidase, IsdG (or its paralog IsdI), degrades heme [17,18]. Hb and heme binding by the IsdA, IsdB, IsdC, and IsdH proteins is mediated by NEAr iron Transporter (NEAT) domains. These conserved binding modules are ~125 residues in length and were originally named based on the location of their parent genes, which are typically proximal to genes encoding putative Fe^{3+} siderophore transporter genes [19]. NEAT domains adopt a conserved β-sandwich fold and depending upon the domain, can bind to distinct ligands, including heme, Hb, haptoglobin, and other host proteins [20–23]. Additionally, these domains are also found in other Gram-positive bacteria containing systems similar to the Isd system [19,24,25].

The IsdB and IsdH surface receptors each contain a highly conserved tri-domain unit that rapidly extracts heme from Hb [26]. In IsdH, the tri-domain unit consists of the second (N2) and third (N3) NEAT domains that are connected by a helical linker domain (**Figure 3.1a**). The NEAT domains have distinct functions, N2 binds Hb, while the N3 domain binds to heme [20,22,27]. Heme extraction by the tri-domain occurs up to ~270 times faster than the rate at which Hb spontaneously releases heme into the solvent [26,28] (**Figure 3.1b-d**). All three domains are required for rapid heme extraction from Hb and must be located within the same polypeptide chain to function synergistically. IsdB likely operates through a similar mechanism as IsdH, since based on primary sequence homology it also contains the tri-domain unit that rapidly captures heme from Hb [14].

To gain insight into the mechanism of heme extraction, Gell and colleagues recently reported a 4.2 Å crystal structure of oxidized Hb in complex with the tri-domain unit from IsdH ($IsdH^{N2N3}$, residues A326-D660) [29]. In the crystal four $IsdH^{N2N3}$ proteins bind to Hb, each

interacting with one of the globin chains. Each $IsdH^{N2N3}$ protein adopts an extended conformation in which its N2 domain engages the A and E helices of the globin, while the linker domain positions the N3 domain near the heme molecule that is bound to the same globin chain. Because the structure was determined at low resolution, the mechanism through which $IsdH^{N2N3}$ triggers heme release is not well understood, and the structure of the intact receptor remains unknown because the structure of the peptide segments that join the three domains could not be determined. Moreover, the structure and dynamics of the receptor in its Hb-free state have yet to be determined, so it is not known if the receptor adopts a rigid, preformed binding surface for Hb, or if its domains flexibly reorient with respect to one another prior to engaging Hb. To address these issues we used solution state NMR and small angle x-ray scattering (SAXS) data to characterize the structure and dynamics of the 38.8 kDa tri-domain $IsdH^{N2N3}$ protein in its Hb-free state, providing insight into the mechanism of heme extraction.

3.3 Results

3.3.1 Rate of heme transfer from Hb to $IsdH^{N2N3}$

Previous studies have shown that $IsdH^{N2N3}$ containing the N2 and N3 NEAT domains (38.8 kDa, residues A326 to D660 of IsdH) rapidly removes the oxidized form of heme (hereafter referred to as hemin) from Hb through a process that requires protein complex formation [26]. However, the rate constant describing the transfer reaction was not accurately defined because the kinetics were measured using a conventional UV-Vis instrument that failed to capture the early steps in the transfer process. To overcome this limitation, we re-measured the transfer kinetics using a stopped-flow UV-Vis spectrophotometer that has a significantly shorter dead time (dead time ~3 ms versus 5 s). Upon mixing methemoglobin (metHb) with excess apo-

$IsdH^{N2N3}$, a rapid shift in the UV absorbance spectrum of metHb is observed as hemin is transferred to apo-$IsdH^{N2N3}$ (**Figure 3.1b**). Curve fitting of the time-dependent spectral changes reveals biphasic behavior with fast and slow rate constants of 0.85 ± 0.11 and 0.099 ± 0.14 s^{-1}, respectively (**Figure 3.1c**). As a negative control similar experiments were performed using a mutant in which the linker domain is replaced with a glycine-serine nonapeptide, $IsdH^{N2\text{-}GS\text{-}N3}$. As expected, it does not acquire hemin from metHb over the timeframe of the experiment indicating the linker domain plays a critical role in hemin capture [26]. When metHb is mixed with an excess of H64Y/V68F apo-Mb as a hemin scavenging agent, the rates of simple hemin release are much slower [30] (**Figure 3.1d**). As shown, simple thermal dissociation from metHb also shows a biphasic time course with a beta chain rate of ~ 0.003 s^{-1} and an alpha chain rate of ~0.0002 s^{-1} [28]. The fast and slow phases of hemin transfer to apo-$IsdH^{N2N3}$ may therefore correspond to hemin removal from the beta and alpha chains of metHb, respectively. Regardless of the exact interpretation, it is clear that the receptor dramatically accelerates the rate of hemin release from the beta and alpha subunits of metHb by ~250-500 fold.

3.3.2 NMR relaxation measurements reveal the presence of motions between the N2 and linker domains

To investigate the mobility of the receptor we quantitatively measured ^{15}N relaxation parameters of $IsdH^{N2N3}$ containing a Y642A mutation in the N3 domain that disrupts hemin binding. The ^{1}H-^{15}N HSQC spectrum of this protein is well resolved (**Figure 3.2a**) and the mutation does not significantly alter the structure of the protein (not shown) [31]. Unless otherwise indicated, all NMR and SAXS studies made use of this Y642A mutant of $IsdH^{N2N3}$. For this protein ^{15}N spin-spin (R_2), ^{15}N spin-lattice (R_1) and $\{^{1}H\}$-^{15}N heteronuclear NOE

relaxation parameters were measured for 155, 142, and 238 backbone amides, respectively (**Figure 3.S1**). The NMR relaxation data indicate that the domains within $IsdH^{N2N3}$ predominantly tumble as a single unit in solution. Measured R_1 and R_2 relaxation rate constants indicate that $IsdH^{N2N3}$ has a molecular correlation time (τ_c) of 16.3 ± 0.1 ns, which is very similar to the predicted τ_c value for a spherical protein of similar molecular mass (**Table 3.1**). Moreover, each of the three component domains within $IsdH^{N2N3}$ have τ_c values that are substantially larger than values predicted for the domains if they were to tumble independently of one-another. Specifically, the N2 and N3 domains within $IsdH^{N2N3}$ have experimental τ_c values of 13.9 ± 0.1 and 15.5 ± 0.1 ns, respectively. This indicates that they tumble as part of a larger unit, since significantly smaller τ_c values are predicted if they tumbled freely in solution. The NMR data also indicate that the intervening linker domain is part of the ordered unit that contains the N2 and N3 domains. While its τ_c value could not be reliably determined from the relaxation data because the majority of its amide bond vectors are co-linear in the structure of this module, its ^{15}N R_2 values have similar magnitudes as residues located in the surrounding N2 and N3 domains, compatible with it being part of this ordered unit.

Although the domains within $IsdH^{N2N3}$ primarily tumble as a single unit, inter-domain motions enable the N2 domain to reorient with respect to the body of the protein. This is apparent from the experimentally determined τ_c value of the N2 domain, which is slightly smaller than the N3 domain's τ_c. The N2 domain's elevated mobility is further substantiated by the data shown in **Figure 3.S1**, which reveals that on average its residues have R_2 and R_1 values that are, respectively, slightly smaller and larger than residues located in the linker and N3 domains. The ability of the N2 domain to reorient is also compatible with the structure of $IsdH^{N2N3}$ as a hydrophilic interface connects it to the linker domain (*vida infra*). Several residues

connecting the domains (N465-E472 and V531-Q543) that were not determined in the crystal structure are ordered based on their relaxation data. Data for three residues located within the N2-linker connector are available for analysis (N465, D467, and V470) and are structured as they have R_2 and NOE values of 21-37 s^{-1} and 0.67-0.90, respectively. Residues within the segment connecting the linker and N3 domains are similarly structured, as a total of 9 residues in this segment have R_2 and NOE values of 22-43 s^{-1} and 0.73-0.90, respectively.

The relaxation data also provided insight into the dynamics of the ligand binding surfaces within the N2 and N3 domains, which bind Hb and hemin, respectively. Both proteins use residues in the β7/β8 hairpin and a proximal 3_{10} helix to bind their respective ligands. Interestingly, the Hb binding surface in N2 is disordered, while the hemin binding surface in N3 is well-ordered. For example, after significant attempts were made, resonances for residues N358-D359, Q364-T370, K397-F399, A422, S439-S440, and Y451-T454 in N2 could not be assigned in the NMR spectra. These residues form the aromatic α-helix (H2) and portions of the β4, β6, β7, and β8 sheets in the Hb binding pocket, and presumably their absence in the NMR data is caused by fluctuations in their magnetic environment that occur on the micro- to milli-second time scale. In contrast, the hemin binding pocket in N3 adopts an ordered conformation in its apo-state as the backbone amide resonances of its residues could be assigned, do not exhibit significant line-broadening, and nearly all have heteronuclear NOE values greater than 0.8.

3.3.3 Experimental restraints used to model the structure of apo-IsdH^{N2N3}

Resonance overlap caused by the large number of residues in IsdH^{N2N3} (335 amino acids) makes it difficult to determine its structure using conventional NOE-based NMR methods. We

therefore modeled the structure of the receptor using paramagnetic relaxation enhancement (PRE) derived distance restraints obtained from six single cysteine mutants of $IsdH^{N2N3}$ that each contained a disulfide linked nitroxide spin label (R1, methanesulfonothioate) [32]. The samples have probes attached to each of the three domains: R363C (N2), E400C (N2), K499C (linker), E511C (linker), K528C (linker) and E559C (N3) (**Figure 3.3**). Probes were attached to residues whose side chains project into the solvent in the NMR and crystal structures of the isolated domains. The backbone atoms of these residues are also structured based on their NMR relaxation data and the attached probes do not significantly alter the NMR spectra of the receptor indicating that they do not perturb the structure of the receptor. The backbone assignments of unmodified $IsdH^{N2N3}$ have been reported previously and were used to assign the ^{1}H-^{15}N HSQC spectra of each nitroxide labeled sample recorded in its paramagnetic (oxidized) and diamagnetic (reduced) states (**Figure 3.2b**). A comparison of the paramagnetic (I_{ox}) and diamagnetic (I_{red},) signal intensities reveal distance-dependent line-broadening of proximal amide protons. **Figure 3.3a** summarizes the PRE data for each probe showing an extended representation of $IsdH^{N2N3}$. Residues near each probe ($I_{ox}/I_{red} < 0.8$) are colored green, while residues separated by more than 20 Å ($I_{ox}/I_{red} \geq 0.80$) are colored red. All probes cause line-broadening in signals originating from proximal amide atoms located within the same domain. PRE-derived distance restraints were obtained as described in detail by Sattler and colleagues using an apparent molecular correlation time of 16 ns for the electron-nucleus vector [33–35]. Use of this correlation time provides good agreement with the probe-amide distances present in the known structures of the isolated domains (**Figure 3.S2**). As described by Clore and colleagues, in all calculations three conformers were used to represent the positioning of the probe to account for probe flexibility [36–38].

The PRE-derived distance restraints were supplemented with several other types of experimental data. TALOS+ was used to obtain phi and psi dihedral angle restraints for residues within the polypeptide segments that connect the domains. Two sets of $^{1}D_{HN}$ residual dipolar couplings were used as domain orientational restraints and were measured for proteins aligned in either PEG/Hexanol or *pf1* phage media. The rhombicity and magnitude of the alignment tensors were determined using the program by MODULE by best-fitting the RDC data to the known structures of the isolated N2 and N3 domains (the linker domain was not used to estimate the tensor values as its amide vectors are primarily co-linear) [39]. Several short-range NOE distance restraints were also used to define the linker-N3 domain interface and were identified by analyzing 3D ^{15}N- and ^{13}C-edited NOESY spectra recorded using a methyl selective protonated sample (U-[^{2}H], Ile-[$^{13}CH_3$ δ1], Leu, Val [$^{13}CH_3$,$^{12}CD_3$]IsdH^{N2N3}) (**Figure 3.2C**). Finally, small angle x-ray scattering (SAXS) data was used to define the size and shape of the receptor [40].

The final model of IsdH^{N2N3} was determined using a total of 807 experimental restraints: 108 $^{1}D_{NH}$ restraints obtained using two alignment media, 629 attractive and repulsive PRE restraints, 19 NOE distance restraints, SAXS data collected in the range of $q \leq 0.3$ Å^{-1}, and 50 backbone torsion angle restraints for residues locating in the polypeptide segments that connect the domains (26 and 24 restraints for the N2-Linker and N3-linker connectors, respectively).

3.3.4 Structure Calculation

A conjoined rigid body/torsion angle simulated annealing protocol was used to model the structure of the receptor [41,42]. In the calculation, the coordinates of the individual domains were treated as rigid bodies and are derived from the 4.2 Å crystal structure of the IsdH^{N2N3}:Hb complex (PDB code: 4IJ2). The domains were allowed to reorient with respect to one another to

best-fit the experimental data by enabling the residues connecting the domains to move freely (I462-Y475 connecting the N2 and linker domains and V531-Q543 connecting the linker and N3 domains).

A multi-step calculation procedure was employed in which the N2-linker and linker-N3 inter-domain interfaces were treated separately (**Figure 3.4**). Initially, only the structure of the interface between the linker and N3 domains was determined as it is better defined by the NOE data (a total of 1 and 7 inter-domain NOEs define the N2-linker and linker-N3 interfaces, respectively). In this calculation, residues connecting the linker and N3 domains were allowed to move freely (V531-Q543) so as to satisfy the appropriate linker-N3 inter-domain PRE, NOE, dihedral angle and RDC restraints. In addition, side chains located at this interface were allowed to move during the calculation (K488-E491, Q526-V527, S529-A530, L544, A576, Y583, K595-D596, R603, T605-S608, I619, N630, I632, K634, and Q645-H647). The SAXS data was not used in this initial calculation as it is sensitive to the global structure of the intact receptor, which is not modeled in this calculation as N2 is not considered. This calculation led to an ensemble of 20 conformers that define the relative positioning of the linker and N3 domains (**step 1 in Figure 3.4**). The structures are compatible with the experimental data and are described in greater detail later in the text (**Table 3.2**). Next, the position of the N2 domain was determined by allowing amino acids connecting the N2 and linker domains to move freely (I462-Y475), while residues in the remainder of the protein were held rigid (atoms in the N2 domain and residues spanning the linker and N3 domains were treated as rigid bodies) (step 2 in **Figure 3.4**). The side chains of residues at the N2-linker domain interface were also allowed to move during the calculation (N348-D353, V372-P374, T376, and N476-Q478). Conformers generated from the first set of calculations were used as input, thus the positioning of the linker and N3 domains is *a priori* well

defined (**Figure 3.5A**). These calculations generated a 'standard' single conformer depiction of the structure of the intact receptor shown in **Figure 3.5B** (structural statistics are presented in **Table 3.3**).

The NMR structure generated from the two step procedure agrees well with the experimental PRE and SAXS data. **Figure 3.5D** shows a summary of the attractive and repulsive PRE restraints demonstrating a high level of redundancy. These restraints agree well with the structure based on a violation analysis of the PRE-derived distance restraints for all of the probes versus the corresponding distance in the NMR structure (**Figure 3.S3**). When the experimental error is considered, all of the PRE-derived distance restraints are satisfied to within 2.7 Å, with 98.7% of them agreeing to within 0.5 Å. **Figure 3.6A** shows a more detailed analysis of the PRE data as a function of residue number. The plots show for each probe the distance between the receptor backbone amide protons to the average position of the nitrogen atom in the spin label. There is a very good correspondence for the attractive restraints, while as expected, the repulsive restraints exhibit weaker correlation to the structure as they have no upper bound. Interestingly, a total of eight PRE-derived distance restraints are systematically violated by 0.5-2.7 Å in all conformers of the NMR ensemble. All of these restraints involve interactions with the N2 domain and suggest that this domain may undergo inter-domain rearrangements (addressed below). As expected, the NMR-derived model of apo-IsdH^{N2N3} is compatible with small angle x-ray scattering (SAXS) information as the structures were directly refined against this data (**Figure 3.6b**). Theoretical scattering curves were generated for each member of the NMR ensemble using the program CRYSOL [43]. Individual members of the NMR ensemble fit extremely well to the solution scattering data of apo-IsdH^{N2N3} with χ values of 0.96 for the lowest energy structure. Combined, the good agreement with the PRE and SAXS data indicates that the

NMR structure shown in **Figure 3.5b** represents the predominating conformer of the receptor that exists in solution.

3.3.5 Model of Apo-IsdH^{N2N3}

IsdH^{N2N3} adopts an extended dumb-bell shaped structure in which the helical linker domain forms a handle that separates the N2 and N3 domains by ~23 Å (**Figure 3.5b**). The interface between the linker and N3 domains is primarily formed by hydrophobic residues and buries ~690 Å^2 of solvent accessible surface area (**Figure 3.5c**). At this interface, residues located at the C-terminal end of helix H3 in the linker domain pack against residues in strands β4, β5, and β7 in the N3 domain. Additional domain-domain packing interactions occur between the turn that connects the H1 and H2 helices (H1/H2 turn), and residues within strands β7 and β8 in the N3 domain. The structure of this portion of the interface is supported by inter-domain NOEs between the backbone amides of T489 and L490 located in the H1/H2 turn and the methyl group of I632 located in strand β7 (**Figure 3.2c**). Interestingly, all of the thirteen residues that connect the linker and N3 domains (V531-Q543) are well ordered in the NMR ensemble, whereas they were not modeled in the crystal structure of the bound protein because of the low resolution of the diffraction data. In apo-IsdH^{N2N3} they wrap around the face of the N3 domain packing against residues located in strands β2, β3, β5, and β6 in the N3 domain. While the side chain positioning for these residues is not well-defined, evidence for this interaction is provided by the NOESY data, as methyl-amide NOEs are observed between the N3 and linker domains (e.g. V537-methyl to T606-HN, V607-methyl to N541-HN and V607-methyl to D542-HN) (**Figure 3.2c**).

In contrast to the linker-N3 interface, the contact surface between the N2 and linker domains primarily contains hydrophilic residues that bury ~550 Å^2 of solvent accessible surface

area (**Figure 3.5c**). In the IsdH^{N2N3}:Hb complex electron density for residues N465-E472 connecting the N2 and linker domains is missing. In apo-IsdH^{N2N3} these residues pack against the N-terminal end of the H1 helix within the linker domain, as well as residues located proximal to, and within, the β1a and β2 strands of the N2 domain. This connector segment is not well defined by the NOE data as the majority of its residues contain polar side chains whose proton resonances are significantly overlapped in the NOESY spectra (the N2-linker interface has only a single methyl-containing residue (V470) that exhibits an NOE to the backbone amide of Y475 located in helix H1 (**Fig 3.2c**)). Even so, the overall orientation of the domains and intervening connector are reasonably well defined by the long-range PRE data and in 75% of the conformers, interactions are observed between the ε-amino group of K391 located in the N2 domain and the hydroxyl group of Y475 located in the H1 helix of the linker domain. Additional polar interactions between the guanidino group of R350 located in the N2 domain and the side chains of N464, N465, or D468 located in the connector segment were observed in 40% of conformers.

3.3.6 Ensemble modeling to account for N2 domain motions

While the structure described above shown in **Figure 3.5b** is the predominate form of the receptor in solution, it seems likely that additional, less frequently populated conformers exist in which the N2 domain adopts distinct positions relative to the linker and N3 domains. This conclusion is supported by the smaller molecular correlation time of the N2 domain compared to the remainder of the protein suggesting that it undergoes additional motions, and the fact that the single depiction of the structure results in systematic, albeit small PRE-derived distance restraint violations to the N2 domain. This notion is substantiated by an analysis of the eight violated PRE restraints. An inspection of the structure of IsdH^{N2N3} reveals that no single orientation of the N2

domain can simultaneously satisfy all of the violated restraints. This is demonstrated in **Figure 3.7a**, which shows six consistently violated PRE-derived distance restraints that originate from the E511R1, R363R1 and E559R1 probes. Violated restraints involving the R363R1 and E559R1 probes can only be satisfied by moving the N2 and N3 domains closer to together, whereas an opposing movement of the N2 domain is required to satisfy violated restraints originating from the E511R1 probe. Thus, both the NMR relaxation and PRE data suggest that the N2 domain undergoes motions that alter its poisoning relative to the remainder of the receptor resulting in a minor set of conformers that are distinct from the average conformation shown in **Figure 3.5b**.

To gain insight into the range of conformations that are accessible to the N2 domain, a third set of calculations were performed in which the receptor was modeled as an ensemble of four molecular structures (**Figure 3.4, step 3**). Since all of the systematically violated restraints originate from the N2 domain only the polypeptide segment that connects it to the linker domain was allowed to move, whereas residues spanning the linker and N3 domains were held rigid during the calculation. As described previously, all of the probes were modeled using three conformers and the full suite of NMR experimental data was employed. However, in the ensemble calculation four conformers were used to model the structure of the receptor and the terms of the energy potential were ensemble averaged [36]. In particular, each member of the ensemble was required to have good covalently geometries and minimal atomic overlap, whereas the entire ensemble of four molecular structures were allowed to collectively satisfy the distance, RDC and SAXS data. An ensemble size of four (Ne = 4) was used because test calculations revealed that it provided good agreement with the experimental data, whereas calculations using larger ensemble sizes resulted in minimal improvement (**Figure 3.7b**).

The results of the Ne = 4 ensemble calculation indicate that the N2 domain can sample a range of positions relative to the linker and N3 domains that enable it to completely satisfy the PRE data. **Figure 3.7c** shows a plot of the reweighted atomic probability density map for the members of the ensemble (contoured at 10% (grey) and 50% (green) of the maximum value) [44]. Superimposed onto this map is the NMR structure of the receptor calculated assuming only a single position for the N2 domain. The density plot reveals that the N2 domain predominantly samples a narrow region of conformational space that closely matches its position in the single conformer depiction of the receptor (shaded green). In contrast, to more completely satisfy the PRE data, less frequently populated conformers exist in which the N2 adopts positions that are both closer or father away from the N3 domain.

3.4 Discussion

The bacterial pathogen *S. aureus* employs two surface receptors to capture the oxidized form of heme (hemin) from human hemoglobin (Hb), IsdB and IsdH. The receptors share extensive sequence homology over a region that contains two NEAT domains that are separated by a conserved helical "linker" domain (**Figure 3.1a**). The N-terminal NEAT domain in each receptor binds Hb, while the C-terminal NEAT domain interacts with hemin. In IsdH, this tri-domain unit is comprised of the N2, linker, and N3 domains ($IsdH^{N2N3}$). Based on our stopped-flow hemin transfer experiments the domains in $IsdH^{N2N3}$ function synergistically, extracting hemin from Hb ~250-500 times more rapidly than the rate at which Hb spontaneously releases hemin into the solvent (**Figure 3.1**) [26]. Previously we determined a 4.2 Å structure of the receptor bound to Hb revealing that the receptor adopts an extended structure in which the N2 domain engages the A and E helices of each globin chain enabling the linker domain to properly

position the N3 domain near the hemin molecule in the same globin chain [29]. The crystal structure of the complex revealed the overall mode of binding, but it did not define the structure and dynamics of the tri-domain receptor prior to engaging Hb. We therefore used NMR spectroscopy and conjoined rigid body/torsion angle dynamics to model the solution structure of $IsdH^{N2N3}$. The NMR data indicate that in the absence of Hb, the receptor adopts an elongated dumbbell shaped structure in which the N2 and N3 domains pack against opposite ends of the central linker domain (**Figure 3.5**). Residues located within polypeptide segments that connect the domains that were not modeled in the low resolution structure of the $IsdH^{N2N3}$:Hb complex (PDB code: 4IJ2) are defined in the NMR model of the apo-form of the receptor and are conformationally ordered based on NMR relaxation data (**Figures. 5 and S1**).

In $IsdH^{N2N3}$ the N2 domain appears to undergo motions that alter its positioning relative to the linker domain, whereas the N3 domain is immobilized relative to the linker domain. These structural changes are substantiated by NMR relaxation data and the presence of two physiochemically distinct domain-domain interfaces. The linker-N3 interface is extensive and primarily hydrophobic in character with residues in the H1/H2 turn and H3 helix of the linker domain contacting residues within the β4 strand and β7/β8 hemin-binding pocket of the N3 domain. This interface is further stabilized by the polypeptide segment connecting the domains, which wraps around the body of the N3 domain making contacts to residues in strands β2, β3, β5, and β6. On the contrary, the N2-linker interface is less extensive and largely hydrophilic with only the N-terminal portion of the linker domain packing against the N2 domain. Compatible with these distinct interfaces, the NMR relaxation data indicate that the N2 domain has elevated mobility relative to the rest of the protein as it tumbles more rapidly and has shorter R2 values (**Table 3.1 and Figure 3.S1**). A more thorough analysis of the relaxation data is necessary to

rigorously define the mobility of the N2 domain. In our analysis, fitting of R1 and R2 data yielded a slightly smaller τ_c value for N2. However, it is possible it undergoes more substantial motions. This would be the case if our R2 values were overestimated as a result of chemical exchange processes. Regardless of the degree of flexibility at the N2-linker interface, the relaxation data strongly supports the notion that the N2 domain undergoes rearrangements that move it relative to the body of the protein. Movement of the N2 domain is probably facilitated by the presence of a polar interface between it and the linker domain, whereas a hydrophobic interface between the linker and N3 domains presumably restricts inter-domain motions. N2 domain rearrangements may originate at a hinge point near residues N465-D468 that connect the N2 and linker domains, as ^{15}N relaxation analysis suggests that this is the location at which the R_1 and R_2 rates switch from N2's longer and shorter times, respectively, to the times seen throughout the linker and N3 domains.

We estimated the range of positions that are accessible to the N2 domain by performing ensemble calculations in which four molecular structures of the receptor were allowed to collectively satisfy the experimental data [36]. These calculations were performed because single conformer depictions of the receptor exhibited small, but persistent PRE-derived distance restraint violations to the more mobile N2 domain (**Figure 3.7a**). The ensemble calculation reveals that in order to completely satisfy the PRE-derived distance restraint data the N2 domain can adopt positions that differ by as much as ~10 Å from its average position (**Figure 3.7c**). These small excursions are compatible with our finding that the N2 domain has a smaller τ_c than the remainder of the protein and its hydrophilic interface with the linker domain. However, they presumably occur infrequently as a single depiction of the structure shown in **Figure 3.5b** satisfies nearly all of the NMR and SAXs data. The time scale of N2 domain motions has not

been defined by our analysis, but likely occurs in the nanosecond range, since residues in the polypeptide that connect the N2 domain to the body of the protein do not exhibit substantial line-broadening and are ordered on the picosecond time scale based on their heteronuclear NOE data. Intriguingly, a proline (P466) is located at the center of this potential hinge suggesting it may be a focal point for conformational changes that reorient the domains.

The NMR data provides insight into the mobility of the hemin and Hb ligand binding pockets in the receptor. In the crystal structure of the $IsdH^{N2N3}$:Hb complex, residues in the H2 and H3 helices and strands β3, β6, and β7 in the N2 domain contact the A and E helices in Hb. This binding surface is unstructured and flexible in the absence of Hb, as resonances for many residues in this region are absent in the NMR spectra, presumably because they undergo micro- to milli-second motions that cause line-broadening. Specifically, resonances in the H2 helix of the N2 domain could not be assigned (Q364-T370), as well as several residues in the underlying stands β4, β6, β7, and β8 (K397-F399, A422, S439-S440, and Y451-T454). Interestingly, similar resonance line-broadening has been observed in the N1 domains from IsdB [45] and IsdH [46], which also bind Hb and like the N2 domain in $IsdH^{N2N3}$ contain a conserved aromatic motif within the H2-helix that interacts with Hb. This suggests that like $IsdH^{N2N3}$, these NEAT domains also undergo a disordered to ordered transition upon binding Hb.

In contrast to the Hb binding pocket in the N2 domain, the backbone atoms of residues in the hemin binding pocket in the N3 domain are generally inflexible in the absence of hemin based on the observation that their backbone amide atoms could be assigned in the NMR spectra and their heteronuclear NOE values and R_2 relaxation parameters. Notably, the relaxation data indicate that residues connecting strands β7 and β8 that form one face of the hemin pocket are semi-ordered in the absence of hemin (V637-E645). In particular, the amide cross-peaks of

residues A638 and I640-E645 are not significantly broadened in the NMR data, have R_2 values near the average for the core of the N3 domain, and have heteronuclear NOE values > 0.5. Interestingly, many of these residues are absent in the electron density for two out of three N3 domains in the 4IJ2 crystal structure. Their absence may be caused by static disorder in the crystal as hemin derived from denatured Hb in the crystallization drop was proposed to partially occupy the binding site in N3. This notion is compatible with structural studies of the isolated N3 domain which show that hemin binding causes a small shift in the conformation of this hairpin which is otherwise conformationally ordered [47].

A comparison of the NMR model of the average structure of $IsdH^{N2N3}$ with the structure of the receptor in the $IsdH^{N2N3}$:Hb complex reveals that Hb binding repositions the N2 domain (**Figure 3.8**). As compared to the NMR structure of the apo-form of the protein, the receptor in the crystal structure of the complex is more compact as a result of a ~30° rotation that moves it ~7 Å towards the N3 domain. This structural difference is substantiated by PRE-derived distance restraints obtained from the R363R1 and E511R1 samples, which are incompatible with the conformation of the bound receptor observed in the crystal structure (**Figure 3.3b**). For example, the PRE data indicate that the E511R1 probe located in the N-terminal portion of helix H3 in the linker domain is within ~15-20 Å of the backbone amide hydrogen atoms of several residues located within the N2-linker interface (H344, N348, V372, T376, I379-F379, E387) as their resonances are substantially broadened by the probe (I_{ox}/I_{red} ratios ~0.3-0.7) (**Figure 3.3b**). In contrast, modeling studies using the crystal structure indicate that the E511R1 probe would be separated from these residues by at least 27 Å. Data derived from the R363R1 probe attached to the N2 are also incompatible with the crystal structure; the probe is at least 20 Å away from the backbone amides of F555, E562, S563, V628-N630, and V648-N652 located in the N3 domain

of apo-IsdH^{N2N3} as supported by I_{ox}/I_{red} values greater than 0.9, but in the crystal structure they are closer than this distance. While the positioning of the N2 domain is different between the bound and unbound states of IsdH^{N2N3}, not surprisingly the relative domain orientation at the extensive hydrophobic linker-N3 interface is largely unaffected by Hb binding, suggesting that this portion of the receptor moves as a rigid unit in solution. The incompatibility of the PRE data with the crystal structure of the receptor is solely due to differences in domain positioning as only these types of long-range distance restraints were used in our calculations. Interestingly, the structural differences in the N2 domain supported by the PRE data are not distinguished by the SAXS data. This result is demonstrated in **Figure 3.6a and 6b**, which shows excellent agreement between the SAXS data and the coordinates of the free and bound forms of IsdH^{N2N3}, respectively (the χ values of the NMR and crystal structures are 0.96 and 0.92, respectively).

It seems likely that receptor binding to Hb occurs through a combination of 'induced fit' and 'conformational selection' mechanisms. The results of the Ne = 4 ensemble calculation provide strong evidence that Hb binding in part occurs through 'conformational selection' in which Hb selects from among different forms of the receptor a binding competent conformer. This idea is evident in **Figure 3.7d**, which displays the reweighted atomic probability density map of apo-IsdH^{N2N3} superimposed onto the crystal structure of the receptor in the IsdH^{N2N3}:Hb complex. The plot reveals that in the absence of Hb, the receptor may infrequently sample conformers that resemble its Hb-bound form in which the N2 and N3 domains are more closely positioned (**Figure 3.8**). However, as described above, the predominating form of the receptor in solution adopts a more open state in which the N2 domain is displaced from the N3 domain as a significant portion of the crystal structure resides outside the highly populated region of the density map (shaded green).

Receptor binding to Hb presumably must also occur through an induced fit mechanism in order to explain how the receptor captures hemin from Hb ~250-500 times faster than the rate at which Hb spontaneously releases hemin into the solvent (**Figs. 3.1c versus 3.1d**). To promote hemin release, the receptor must destabilize Hb-hemin interactions. Our single conformer model of the receptor (**Figure 3.5b**), in combination with the crystal structure of the complex, suggests how the receptor might transiently induce structural changes in Hb that promote hemin release. A model of Hb bound to the structure of $IsdH^{N2N3}$ determined by NMR (called $^{NMR}IsdH^{N2N3}$:Hb) was generated by superimposing the coordinates of the N2 domain in the NMR model of $IsdH^{N2N3}$ onto the corresponding coordinates in the crystal structure of the $IsdH^{N2N3}$:Hb complex (**Figure 3.9**). The modeled structure of $^{NMR}IsdH^{N2N3}$:Hb may represent the initial binding of Hb to the receptor prior to it rearranging through N2 domain motions into the more stable structure visualized by x-ray crystallography. As seen in the $^{NMR}IsdH^{N2N3}$:Hb model, initial binding of the apo-receptor to Hb results in atomic overlap between residues in the F-helix and C-terminus of αHb (A79, N78, S81, D85, and Y140) and residues in the H1 and H2 helices of the linker domain (K479, K486, R492, E496, K499, and K503). Similar atomic overlap is seen when the apo-receptor is docked to Hb's beta subunit (model not shown). We speculate that these receptor-Hb interactions may promote hemin release by altering the positioning of the F-helix which houses the proximal histidine that coordinates the iron in hemin (H87 in the alpha subunits and H92 in the beta subunits, which is conventionally referred to as HisF8). Although details of this process are not known, this transient distortion in Hb may increase fluctuations in the proximal pocket area that facilitate water penetration needed to break the Fe-HisF8 bonds in both subunits. The receptor would then undergo a structural transition about the N2-linker interface so as to adopt the more stable conformation observed in the 4.2 Å crystal structure of the

IsdH^{N2N3}:Hb complex (**Figure 3.8**) [29].

Receptor mediated transient distortion of Hb may also explain recent mass spectrometry results, which demonstrated that a hemin-binding impaired receptor can nevertheless promote Hb tetramer dissociation [26]. In principle, receptor binding to Hb could also accelerate hemin transfer by increasing the effective concentration of the N3 domain near Hb's bound hemin molecule. However, this effect is expected to be small as the rate of hemin transfer exhibits a hyperbolic dependence on the concentration of the receptor (data not shown), compatible with the rate limiting step in the transfer reaction being breakage of the Fe-HisF8 bond in Hb. Based on the ensemble calculations Hb may also bind to other, more sparsely populated conformers of the receptor ('conformational selection') that could also induce transient structural changes in the F-helix to promote hemin release. This idea is intriguing, as it suggests that the plasticity of the N2-linker interface is critical for function. If the interface is too flexible, binding would occur solely through the conformational selection process and would presumably not alter Hb-hemin interactions needed to promote hemin release. In contrast, if the N2-linker interface was stabilized by extensive inter-domain interactions and therefore too structurally rigid, binding to Hb would be impaired as a result of sustained atomic overlap with the F-helix.

The *S. aureus* IsdB protein presumably extracts hemin from Hb through a similar mechanism as described here for IsdH^{N2N3} because the proteins share 48% primary sequence identity, and similar to IsdH^{N2N3}, the IsdB protein extracts hemin using functionally and structurally homologous NEAT domains that are separated by a helical linker segment. Recent results reported independently by the Lei and Murphy groups further support mechanistic similarity between the two Hb receptors as they imply that the linker domain in IsdB plays an important role in Hb binding and hemin capture [45,48,49]. This is consistent with our proposal

that the related region in $IsdH^{N2N3}$ may transiently interact with Hb to destabilize the F-helix that interacts with hemin. It will be interesting to discover if similar to $IsdH^{N2N3}$, the Hb binding NEAT domain in IsdB also undergoes domain rearrangements upon binding Hb. This would appear to be the case as recently reported NMR studies of the Hb binding NEAT domain in IsdB suggest that it does not significantly interact with the linker domain in the absence of Hb [45].

It is also possible that IsdB and IsdH may not use identical mechanisms to extract hemin from Hb. The Lei group showed that a ~85 residue segment preceding the Hb-binding domain (called the NS in their study) is important for the rapid kinetics observed in the hemin transfer reaction between metHb and IsdB. It is unclear if residues preceding IsdH's Hb-binding N1 and N2 domains share a similar function as the NS in IsdB. Furthermore, recent reports [48,49] have independently shown that IsdB constructs containing the Hb binding N1 domain and the analogous linker domain could bind Hb and promote hemin transfer to the isolated hemin binding N2 domain when provided *in trans*. This finding is in contrast to IsdH, where all three domains must be within the same polypeptide for rapid hemin transfer from metHb [26]. The origin of this difference needs to be resolved, but could be caused by non-covalent interactions between Hb and the hemin-binding domain and/or the linker domain, which are not present in $IsdH^{N2N3}$. In order to elucidate mechanistic differences between IsdB and IsdH, the structure of the IsdB in its Hb-free and -bound state will need to be determined.

In summary, our NMR results in combination with the recently determined crystal structure of the Isd^{N2N3}:Hb complex suggest that the receptor may accelerate hemin release from Hb by transiently contacting Hb's F-helix. A generally similar mechanism may also be used by IsdB based on primary sequence homology and recent biochemical studies. Many other Gram-positive microbes use NEAT containing proteins to acquire heme from Hb [24]. How these

proteins operate to capture heme is only beginning to be elucidated, and is important, as it could lead to development of broad-spectrum anti-infective agents that target nutrient acquisition.

3.5 Material and Methods

3.5.1 Protein production for NMR studies

Two IsdH polypeptides were characterized by NMR: (1) $IsdH^{N2N3(Y642A)}$, which contains N2, linker and N3 domains (residues A326-D660) and a Y642A mutation in the hemin pocket of $IsdH^{N3}$ domain that disrupts hemin binding and (2) $IsdH^{N2\text{-}Linker}$, which contains the N2 and linker domains (residues A326-Q543). As described previously, both polypeptides were produced from pET-28b-based expression plasmids and initially contained a removable N-terminal hexahistidine-small-ubiquitin-like modifier (SUMO) tag to facilitate purification [50,51]. Several uniformly isotopically labeled samples were produced for NMR studies using *Escherichia coli* BL21 (DE3) cells (New England BioLabs, Beverly, MA). Uniformly isotopically labeled proteins were expressed from cells grown in M9 minimal media containing 2 g/L [^{13}C]-glucose and/or 1 g/L $^{15}NH_4Cl$ as the sole source of carbon and nitrogen, respectively (Cambridge Isotope Laboratories, Andover, MA). The methods to overexpress the proteins have been described previously [26,31]. Briefly, expression proceeded overnight at 25°C by adding 1 mM isopropyl-*β*-D-thiogalactoside to cell cultures. The bacterial cells were then harvested by centrifugation, lysed by sonication, and the protein was purified using a Co^{2+}-chelating column (Thermo Scientific, Waltham, MA). The amino terminal 6x-His-SUMO tag was then cleaved using ULP1 protease and reapplied to the Co^{2+}-chelating column to remove the protease and cleaved SUMO tag. The final protein yield for U-[^{13}C,^{15}N]$IsdH^{N2N3(Y642A)}$ and U-

[^{13}C,^{15}N]IsdH$^{N2\text{-}Linker}$ was 21 mg/L and 14 mg/L, respectively. Methods used to produce the U-[^{2}H,^{13}C,^{15}N]IsdH$^{N2N3(Y642A)}$ NMR sample have been described previously [31]. The protocol used to produce the methyl protonated U-[^{2}H], Ile-[$^{13}CH_3$ δ1], Leu, Val-[$^{13}CH_3$,$^{12}CD_3$] IsdH$^{N2N3(Y642A)}$ sample is similar to the protocol used to produce the U-[^{2}H,^{13}C,^{15}N]IsdH$^{N2N3(Y642A)}$ sample. However, 3 g/L of U-[^{13}C, ^{2}H]-glucose (Isotec, Miamisburg, OH) was used as the carbon source, as well as one hour prior to induction 60 mg/L of [U-$^{13}C_4$, 3,3-$^{2}H_2$]-α-ketobutyrate (Cambridge Isotope Laboratories, Andover, MA) and 100 mg/L of [1,2,3,4-$^{13}C_4$, 3,4',4',4'-$^{2}H_4$]-α-ketoisovalerate (Cambridge Isotope Laboratories, Andover, MA) were added to the growth medium to yield 33 mg/L culture. All NMR samples were dissolved in NMR buffer containing 20 mM NaH_2PO_4, 50 mM NaCl, 0.01% NaN_3, pH 6.0 supplemented with ~8% D_2O. The following samples were used for NMR studies: 1.1 mM U-[^{2}H, ^{13}C,^{15}N]IsdH$^{N2N3(Y642A)}$, 1.0 mM U-[^{13}C,^{15}N]IsdH$^{N2N3(Y642A)}$, 0.8 mM U-[^{2}H], Ile-[$^{13}CH_3$ δ1], Leu, Val-[$^{13}CH_3$,$^{12}CD_3$]IsdH$^{N2N3(Y642A)}$, 0.675 mM U-[^{13}C,^{15}N]IsdH$^{N2\text{-}Linker}$, and two additional samples of 1.2 mM U-[^{13}C,^{15}N]IsdH$^{N2N3(Y642A)}$ and 1.2 mM U-[^{13}C,^{15}N]IsdH$^{N2\text{-}Linker}$, both lyophilized in NMR buffer and resolublized with an equal volume of 99.999% D_2O (Isotec, Miamisburg, OH).

PRE measurements were made using four double mutants of IsdH^{N2N3}. Each mutant contained the Y642A mutation that disrupts hemin binding as well as a single cysteine mutation at the following residues: R363C, E400C, K499C, E511C, K528C, and E559C. Expression plasmids producing the mutant proteins were obtained by site directed mutagenesis of plasmid pRM216 that produces IsdH$^{N2N3(Y642A)}$ with a N-terminal hexahistidine-small-ubiquitin-like modifier (SUMO) tag (QuikChange Site-Directed Mutagenesis Kit, Stratagene, La Jolla, CA). For NMR studies uniformly ^{15}N labeled samples of each protein were produced in an identical

manner as describe above, with the exception that 2.5 mM dithiothreitol (DTT) was added to all buffers used during the purification procedure. After purification and protein concentration, the sampled was dialyzed against labeling buffer (50 mM Tris, 50 mM NaCl, 2.5 mM DTT, pH 7.8). The DTT was then removed using a desalting column (Zeba Spin Desalting Column, Thermo Scientific, Waltham, MA). Probes were attached to each sample by immediately incubating them with a ten-fold molar excess of methanesulfonothioate (MTSL; Toronto Research Chemicals, North York, ON, CAN) for 15 minutes, after which an additional ten-fold molar excess of MTSL was added followed by incubation overnight at room temperature. Disulfide bond formation between MTSL and the sulfhydryl group of the cysteine was confirmed via MALDI-TOF and any unreacted MTSL was removed by buffer exchange (Amicon centrifugation filtration device, Millipore, Billerica, MA) with NMR buffer. For PRE measurements, each U-[^{15}N]-labeled cysteine mutant (IsdH$^{R363C(Y642A)}$, IsdH$^{E400C(Y642A)}$, IsdH$^{K499C(Y642A)}$, IsdH$^{E511C(Y642A)}$, IsdH$^{K528C(Y642A)}$, and IsdH$^{E559C(Y642A)}$) was concentrated to ~0.3 mM to prevent non-specific intermolecular effects.

3.7.2 Hemin transfer experiments

Purified unlabeled IsdH^{N2N3} and IsdH$^{N2\text{-}GS\text{-}N3}$ in which the linker was replaced with a nine-amino acid artificial linker (GSGSGSGSG) was produced as previously described [26]. The apo-form of IsdH^{N2N3} was generated by hemin extraction with methyl ethyl ketone [52] followed by buffer exchange into phosphate buffered saline solution, pH 7.4. Native human hemoglobin (Hb) was prepared in a complex with CO, as previously described [53]. Replacement of the bound CO by O_2 was accomplished by equilibrating the HbCO solution with 1 atm O_2, on ice, under light in a rotary evaporator. Methemoglobin (metHb) was produced by incubating the

oxyhemoglobin complex with excess potassium ferricyanide and loading the sample onto a G-25 sepharose column to remove excess ferricyanide [14]. metHb was then buffer exchanged into phosphate buffered saline solution, pH 7.4. The concentration of hemin within metHb was determined using the extinction coefficient of 179 $mM^{-1}cm^{-1}$ [54]. The rates of hemin transfer from metHb (hemin donor) to the hemin acceptors were measured using an OLIS RSM1000 stopped-flow spectrophotometer (OLIS, Bolgart, GA) at Rice University as previously described [55,56]. Holo-protein (HbA) in one syringe was mixed with apo-acceptor at ~4x molar excess in another syringe. The entire spectrum was recorded over 300 seconds with a dead time of ~3ms. The absorbance changes at 370 and 404 nm ($\Delta A_{404-370}$) [26] were fitted to a double phase exponential expression to obtain the apparent rate constants for the transfer reaction using GraphPad Prism version 5.01 for Windows (GraphPad Software, La Jolla, CA). The rates of hemin transfer from metHb to H64Y/V68F apo-Mb [30] in ~16x molar excess was measured using a conventional UV-vis spectrophotometer (Cary50, Varian, Inc., Palo Alto, CA) also at Rice University. The entire spectrum was recorded over 790 min and the absorbance change at 409 nm was fitted to a double phase exponential equation.

3.5.3 NMR data acquisition

NMR spectra were acquired at 310 K for $IsdH^{N2N3(Y642A)}$ and 323 K for $IsdH^{N2\text{-}Linker}$ on Bruker Avance 500-, 600-, and 800-MHz spectrometers equipped with triple resonance cryogenic probes. All NMR spectra were processed using NMRPipe [57] and analyzed using CARA (version 1.8.4) [58] and/or SPARKY [59] software packages. Chemical shift assignments (^{1}H, ^{13}C, ^{15}N) for the backbone of $IsdH^{N2N3(Y642A)}$ have been described earlier [31]. Backbone assignments for the U-[^{13}C,^{15}N]$IsdH^{N2\text{-}Linker}$ protein were obtained by analyzing the following

experiments: HNCACB, CBCA(CO)NH, HNCO, HN(CA)CO, and CC(CO)NH [60]. Side chain assignments were obtained by analyzing HNHA, HNHB, HBHA(CO)NH, (h)CCH-TOCSY, HCCH-TOCSY, and HCCH-COSY spectra acquired using U-[^{13}C,^{15}N]IsdH$^{N2N3(Y642A)}$ and U-[^{13}C,^{15}N]IsdH$^{N2\text{-}Linker}$ samples. The majority of methyl resonance assignments were obtained by analyzing the following NMR spectra acquired using the methyl protonated sample: (1) ^{15}N-edited TROSY-NOESY (200 ms mixing time; collected with 2048, 64, and 160 complex points for the direct ^{1}H, ^{15}N, and indirect ^{1}H dimensions, respectively, and processed to a digital resolution of 0.09 ppm, 0.11 Hz, and 0.03 ppm for direct ^{1}H, ^{15}N, and indirect ^{1}H dimensions, respectively), (2) ^{13}C-edited NOESY in H_2O (200 ms mixing time; acquired with 2048, 76, and 244 complex points for the direct ^{1}H, ^{13}C, and indirect ^{1}H dimensions, respectively, and processed to a digital resolution of 0.14 ppm, 0.08 ppm, and 0.04 ppm for direct ^{1}H, ^{13}C, and indirect ^{1}H dimensions, respectively), (3) (h)CCH-TOCSY, and (4) CC(CO)NH experiments [60].

$^{1}D_{NH}$ residual dipolar couplings were measured on protein samples partially aligned in either 5% PEG $C_{12}E_5$/hexanol [61] or 9 mg/mL *pf1* phages [62] (ASLA Biotech, Latvia). Two-dimensional ^{15}N-coupled IPAP ^{1}H-^{15}N HSQC [63] spectra were collected for both aligned and unaligned samples (collected with 2048, and 1200 complex points for the ^{1}H, and ^{15}N dimensions, respectively, and processed to a digital resolution of ~0.21 ppm for the ^{1}H and ~0.90 ppm for the ^{15}N dimensions). ^{15}N–^{1}H 2D TROSY-HSQC spectra were recorded for each PRE spin-labeled mutant (collected with 2048 and 256 complex points for the ^{1}H, and ^{15}N dimensions, respectively, and processed to a digital resolution of ~0.25 ppm for both ^{1}H and ^{15}N dimensions). After data acquisition for the paramagnetic samples was completed, ascorbic acid (5-fold molar excess relative to MTSL concentration) was added to the NMR tube to generate the diamagnetic

sample, followed by a three-hour incubation period in the spectrometer before to acquiring the diamagnetic spectra.

^{15}N relaxation data (T1 and T2) and heteronuclear {^{1}H}-^{15}N NOE data was collected on Bruker Avance 800-MHz spectrometer equipped with a triple resonance cryogenic probe at protein concentrations of 1.9 mM for T1 and T2 relaxation experiments and 1.1 mM for heteronuclear NOE experiments. Delays used for T1 experiments were 41, 165, 393, 662, 848, and 1219 ms. For T2 experiments the delays were 17, 34, 51, 68, 85, and 118 ms. The heteronuclear NOE experiments were collected in duplicate with a relaxation delay of 5 s. Data was analyzed in SPARKY [59] to generate raw relaxation and NOE parameters.

3.5.4 RDC, dihedral angle, SAXS and NOE distance restraints

$^{1}D_{NH}$ couplings for 40 and 68 residues were obtained for the protein aligned in 5 % PEG/Hexanol and 9 mg/mL *pf1* phages, respectively. Data were analyzed using the program MODULE [39] to determine magnitude of the alignment tensor (D_a) and rhombicity (η). For the PEG/Hexanol data D_a and η values of 16.9 Hz and 0.21 were obtained, respectively. For the phage data D_a and η values of 10.9 Hz and 0.24 were obtained, respectively. Couplings were obtained by analyzing IPAP experiment data of unaligned and aligned samples using the published backbone chemical shifts of IsdH [31]. For both media, couplings were obtained for each of the three domains. An analysis of the euler angles of the alignment tensors revealed that they were not co-linear and aligned the protein to differing extents. The program TALOS+ [64] was used to obtain phi and psi dihedral angle restraints from backbone chemical shift assignments for the loop regions between N2-Linker (residues I462-Y475) and Linker-N3 (residues A530-L544) as well as residues Y629-I650 in the hemin binding pocket of N3. Methyl

side chain resonances were assigned by analyzing ^{15}N-NOESY, ^{13}C-NOESY (in H_2O), and CC(CO)NH spectra of this sample. In addition, limited side chain assignments for non-methyl side chains were obtained using a ^{13}C, ^{15}N labeled sample of IsdH$^{N2N3(Y642A)}$ and data from HCCH-COSY, HCCH-TOCSY, and (h)CCH-TOCSY spectra obtained using a ^{13}C, ^{15}N labeled sample of IsdH$^{N2N3(Y642A)}$. An analysis of the 3D-^{15}N-edited and ^{13}C-edited NOESY spectra of the selectively protonated samples identified a total of 1 and 8 inter-domain proton-proton NOEs that define the N2-linker and linker-N3 interfaces, respectively. A total of 8 hydrogen bond distance restraints for residues Y475-K479 and V531-E535 were included in the calculations and were based on alpha-helical NOE patterns observed in the ^{15}N-edited NOESY spectrum and TALOS+ calculated dihedral angles. Small angle x-ray scattering (SAXS) data for IsdH$^{N2N3(Y642A)}$ was collected using an Anton Paar SAXSess instrument with a sealed tube source. *I*(0) values and *P(r)* curves were calculated using GIFT (Anton Paar, Graz, Austria) and PRIMUS [29,65].

3.5.5 PRE-derived distance restraints

PRE-derived distance restraints were made for each cysteine mutant of U-[^{15}N] IsdH$^{N2N3(Y642A)}$ which contained an attached MTSL nitroxide spin label: IsdH$^{R363C(Y642A)}$, IsdH$^{E400C(Y642A)}$ IsdH$^{K499C(Y642A)}$, IsdH$^{E511C(Y642A)}$, IsdH$^{K528C(Y642A)}$, and IsdH$^{E559C(Y642A)}$. The procedure used to analyze the PRE data is similar to the method described Sattler and colleagues [33,34,37,66–71]. The PRE effect on the transverse relaxation rate of the amide proton, R_2^{sp}, was back calculated from the ratio of peak intensities for the paramagnetic (I_{ox}) and reduced diamagnetic (I_{red}) using equation 1

$$\frac{I_{ox}}{I_{red}} = \frac{R_2 \, e^{-R_2^{sp} t}}{R_2 + R_2^{sp}} \quad (1)$$

where R_2 is intrinsic amide proton transverse relaxation rate, and t is the total INEPT evolution time recorded (11 ms). The fitted PRE rate enhancements (R_2^{sp}) were converted into distances, *r*, using a modified version of the Solomon-Bloembergen in equation 2 [66,72]

$$r = \left[\frac{K}{R_2^{sp}}\left(4\tau_C + \frac{3\tau_C}{1+\omega_h^2\tau_C^2}\right)\right]^{1/6} \quad (2)$$

where *K* is a constant (1.23 x 10^{-32} cm^6 s^{-2}) that describes the spin properties of the MTSL spin label [66], ω_h is the Larmor frequency of the proton spin, and τ_C is the apparent PRE correlation time [33]. The value for τ_C was estimated by comparing the agreement between distances calculated from the PRE data with known intra-domain distances present in the structures of the isolated domains (**Figure 3.S2**) (PDB code: 4IJ2). To prevent over estimation of PREs, only residues with {^{1}H}-^{15}N NOE values > 0.6 and isolated ^{1}H-^{15}N cross-peaks in the spectra were used to obtain PRE-derived restraints. Intensity ratios were normalized from the average ratios of intra-domain backbone amides known to be ≥ 28 Å away from the probe based on the NMR and crystal structures of the isolated domains. In the structure calculations, two types of distance restraints were employed: (1) attractive restraints between the nitrogen atom of the MTSL ring and affected amide proton if I_{ox}/I_{red} was < 0.80. The distance restraint for these interactions was determined using equation 2 assuming an error of ± 5 Å (2) repulsive restraints were used if I_{ox}/I_{red} ≥ 0.80. For these amide-probe interactions a lower bound distance of 20 Å was employed and contained no upper bound [66,69,73]. Notably, all six probes caused modest line-broadening

in residues within the ligand binding pockets of the N2 and N3 NEAT domains. These interactions were deemed to be non-specific because both binding pockets contain a large number of aromatic residues that are expected to non-specifically interact with MTSL [66,74]. In addition, the interactions are incompatible with all of the other PRE-derived distance restraints and SAXS data. Moreover, many of the effected residues have $\{^1H\}$-^{15}N NOE values < 0.6. It should be noted that the probe located in the N3 domain, E559R1, also displayed non-specific effects to a portion of N2 domain near the N-terminus. Those residues were also omitted from the calculations for the aforementioned reasons, and because data collected on an additional probe near the N-terminus, E343R1, did not display the reciprocal effect.

3.5.6 Relaxation data analysis

NMR relaxation data for individual residues were interpreted as described previously [75,76]. Briefly, the program Pdbinertia was used to calculate the principal moments of inertia for the NMR model of $IsdHN^{2N3}$ yielding relative moments of inertia of 1.0:0.94:0.25. The program R2R1_tm was used to calculate an approximate correlation times (τ_m) on a per residue basis using R_2 /R_1 ratios. Only R_2 /R_1 ratios that met the following criteria were used in this analysis: (1) they were from isolated ^1H-^{15}N cross-peaks in each spectrum 2) they were within two standard deviations of the average and (3) the residue had a $\{^1H\}$-^{15}N NOE value > 0.6. The data was then inputted into the program Quadric_Diffusion [77,78], which indicated that the axially symmetric model statistically is preferred over the isotropic and anisotropic models of tumbling for the intact receptor and for every subdomain with the exception of the linker that favored isotropic model. NMR relaxation data were also interpreted to obtain the diffusion tensors and molecular correlation times of the individual subdomains. For this analysis NMR

data for 52, 10, and 29 residues in the N2, linker and N3 domains were used, respectively. These residues, in addition to meeting the R_2/R_1 criteria described above, were present in the electron density map of the crystal structure. Relaxation data were collecting using a 1.9 mM U-[^{15}N]IsdH$^{N2N3(Y642A)}$ dissolved in NMR buffer containing 20 mM NaH_2PO_4, 50 mM NaCl, 0.01% NaN_3, pH 6.0 supplemented with ~8% D_2O. The protein is monomeric based on size exclusion chromatography combined with multi angle light scattering (SEC-MALS).

3.5.7 Structure calculations

Structures were calculated using XPLOR-NIH (version 2.37) [79]. The coordinates of the N2, linker and N3 domains are derived from the 4.2 Å crystal structure of the IsdH^{N2N3}:Hb complex (PDB code: 4IJ2, chain G). Polypeptide segments connecting these subdomains (N465-E472 and V531-Q543) were added using the program COOT [80]. Because they are absent in the crystal structure of the IsdH^{N2N3}:Hb complex, the coordinates for residues in the hemin-binding region of the receptor (V635-Q645) were modeled using the previously reported structure of the isolated N3 domain [47] (PDB code: 2Z6F), except that an alanine was substituted at position Y642. Protons were then added to the starting model using http://spin.niddk.nih.gov/bax/nmrserver/pdbutil and the coordinates were energy minimized. Three conformers of each MTSL probe were then added to each of the six aforementioned probe attachment sites. The coordinates of each sub-domain in the MTSL-conjugated starting structure were energy minimized against the appropriate RDC data to optimize their agreement, and to improve covalent geometry and atomic overlap. Three distinct conjoined rigid body/torsion angle simulated annealing calculations were performed (summarized in **Figure 3.4**). In the first calculation, the coordinates of the linker and N3 domains were held rigid, but allowed to move

with respect to one another so as to satisfy the relevant RDC, dihedral angle, NOE, and PRE data. In this process the coordinates of residues connecting the domains (V531-Q543) were allowed to move freely as well as the coordinates of side chains that reside at the linker-N3 interface (K488-E491, Q526-V527, S529-A530, L544, A576, Y583, K595-D596, R603, T605-S608, I619, N630, I632, K634, Q645-H647). Both the NOE data and the results of initial structure calculations indicate that the packing between the H1/H2 turn in the linker domain and N3 domain are similar in the Hb-free and -bound forms of the receptor. The posDiffPotTool module in XPLOR-NIH was therefore employed to define this region. The statistics describing the results of the first calculation are presented in **Table 3.2**. The structures generated from the first calculation were used as input into a second set of calculations. In this calculation the coordinates the appropriate position of the N2 domain was determined. The coordinates of the N2 domain and residues spanning from the linker domain to end of the protein (N476-I655) were treated as rigid bodies. These segments were allowed to reorient with respect one another by allowing free movement of residues I462-Y475 that connect the N2 and linker domains. In addition, the coordinates for side chains of inter-facial residues (N348-D353, V372-P374, T376, and N476-Q478) were given full degrees of freedom. All of the experimental data was employed in this calculation, including SAXS data. The calculation resulted in single conformer representations of the structure that best satisfy the experimental data (statistics described in **Table 3.3**).

In the third set of calculations an ensemble approach was used to account for domain motions. This calculation is nearly identical to calculation #2, except that four conformers of the receptor (Ne = 4) were used to collectively satisfy the NMR data [36]. In particular, each member of the Ne = 4 ensemble was required to have good covalently geometries and minimal

atomic overlap, whereas the entire ensemble of four molecular structures were allowed to collectively satisfy the distance, RDC and SAXS data. The RAPPot potential in the posRMSDPotTools module in XPLOR-NIH was used to minimize the spread of the atomic coordinates [81]. A total of 100 four-member ensembles were calculated. The five lowest energy ensembles (20 structures total) were used to calculate a reweighted atomic probability density map using the program VMD-Xplor [44,82].

The following parameters were employed in each of the three calculations. Initially, a total of 5000 steps of higher energy dynamics at 3500K was performed, followed by 100 cooling cycles in which the bath temperature was decreased from 3500K to 25 K in 12.5 K increments. This was followed by 5 rounds of 500 steps of Cartesian coordinate energy minimization. The final force constants used during simulated annealing for RDC, NOE, and dihedral angle (CDIH) potentials were 1.5 kcal mol^{-1} Hz^{-2}, 30 kcal mol^{-1} $Å^{-2}$, and 400 kcal mol^{-1} rad^{-2}, respectively. The non-bonded interactions were described by a van der Waals repulsion term with a final force constant of 4 kcal mol^{-1} $Å^{-2}$ and a scale factor of 0.8. A multi-dimensional torsion angle database of mean force (RAMA) potential was applied with a final force constant of 1 kcal mol^{-1}. The bond length (BOND), bond angle (ANGL) and improper dihedral (IMPR) potentials employed force constants of 1 kcal $mol^{-1}Å^{-2}$, 1 kcal $mol^{-1}rad^{-2}$, and 1 kcal $mol^{-1}rad^{-2}$, respectively. All dynamics and minimization steps utilized the internal variable module (IVM) [81,83–86]. In the single conformer calculations (calculations #1 and #2), the D_a and rhombicity of the two alignment tensors for the RDC data were held fixed during the simulated annealing, and allowed to float during the Cartesian coordinate energy minimization. In the third calculation the alignment tensor parameters were fixed throughout the calculation as to not over-fit the RDC data [40,87]. Calculations that included the N2 domain (#2 and #3) used SAXS data collected in

the range of $q \leq 0.3$ Å^{-1}. The xray force constant was optimized such that the resulting χ^2 values were less than one, without causing violations of other restraints (final force constants of 200 and 40 kcal mol^{-1} for calculation #2 and #3, respectively [40]. Structural models were inspected and visualized using the programs MOLMOL [88] and PyMOL [89].

For the PRE data a quality factor, Q, was calculated using equation 3

$$Q = \sqrt{\frac{\Sigma(V_{backcalc} - V_{exp})^2}{\Sigma(V_{exp})^2}} \quad (3)$$

where $V_{backcalc}$ *and* V_{exp} are the back calculated and experimental I_{ox}/I_{red} ratios for a given spin label. This equation has been described previously [33,37] and is a modified version of the PRE Q-factor used in previous studies, which employs peak intensity ratios in place of enhanced relaxation rates [36,66]. The individual members within the final ensemble of back calculated scattering curves were fit to the experimental data using both the CalcSAXS helper program in the XPLOR-NIH structure determination package (v. 2.37) [40,79] as well as the program CYSOL [43].

Abbreviations: Hb, hemoglobin; Isd, iron-regulated surface determinant; NEAT, near iron transporter; NMR, nuclear magnetic resonance; PRE, paramagnetic relaxation enhancement; RDC, residual dipolar coupling; MTSL, methanesulfonothioate; HSQC, heteronuclear single quantum coherence; NOE, nuclear Overhauser effect; SAXS, small angle x-ray scattering; RMSD, root mean squared deviation; Mb, Myoglobin

3.6 Figures and Tables

Table 3.1 Predicted and experimental correlation times for the domains within IsdH^{N2N3}

τ_c (ns)	N2	N3	N2-linker-N3 (IsdH^{N2N3})
Experimental	13.9 ± 0.1	15.5 ± 0.1	16.3 ± 0.1
Predicted[†]	8.4[a] (7.1[b])	7.3[a] (6.0[b])	17.9[a](16.0[b])

[†]Predicted correlation times calculated from equations based on a spherical protein using either *a)* molecular weight [90] or *b)* temperature and number of amino acid residues [91].

Table 3.2 Structural statistics for linker and N3 domain-domain interface in $IsdH^{N2N3}$

PRE distance restraints	**R363R1**	**E400R1**	**K499R1**	**E511R1**	**K528R1**	**E559R1**
# of restraints	0	0	66	67	62	22
# of violations > 0.5 Å[a]	0	0	0	0	0	0
PRE *Q*-factor[b]	n/a	n/a	0.09	0.07	0.15	0.11

NOE distance restraints	**NOEs**
# of restraints[c]	13/7
# of violations > 0.5 Å[a]	0

Orientational restraints	
Total ^{1}H-^{15}N residual dipolar couplings	44
PEG C12E5/hexanol	20
pf1 phages	22
Dihedral Angles (Φ and ψ)	24

RDC *R-factor*	
PEG C12E5/hexanol	3.60 ± 0.03
pf1 phages	11.7 ± 0.05

PROCHECK-NMR results (%)[d]	
most favorable region	90.0 ± 0.6
additionally allowed region	10.0 ± 0.6
generously allowed region	0.0 ± 0.0
disallowed region	0.0 ± 0.0

Coordinate Precision (Å)[e]	
Protein back bone (N476-I655)	0.37 ± 0.11
Protein heavy atoms (N476-I655)	0.68 ± 0.11

[a] Average number of distance restraints violated in the 20 lowest energy structures.

[b] Quality factor of experimental I_{ox}/I_{red} vs. back-calculated I_{ox}/I_{red} of the ensemble. Only inter-domain restraints were included.

[c] Total number of restraints, with the number of inter-domain restraints indicated after the slash.

[d] PROCHECK-NMR [92] includes residues (N476-I655).

[e] The coordinate precision is defined as the average atomic root mean square deviation (RMSD) of the 20 individual simulated annealing structures and their mean coordinates. Backbone atoms are N, C^{α}, C′, and O. During the calculation the backbone coordinates of the linker (N476-A530) and N3 (L544-I655) were treated as rigid bodies.

Table 3.3 Structural statistics for intact IsdH^{N2N3}

PRE distance restraints	**R363R1**	**E400R1**	**K499R1**	**E511R1**	**K528R1**	**E559R1**
# of restraints[a]	87	83	133(67)	130(63)	130(68)	66(44)
# of violations > 0.5 Å[b]	4.2	0	0.8	2.9	0	2
Maximum violation (Å)	2.4	n/a	0.94	1.8	n/a	2.7
PRE *Q*-factor[c]	0.24	0.07	0.10	0.12	0.13	0.14

NOE distance restraints	**NOEs**
# of restraints[d]	19/8
N2-LN3[d]	6/1
L-N3[d]	13/7
# of violations > 0.5 Å[b]	0

Orientational restraints[a]	
Total ^{1}H-^{15}N residual dipolar couplings	108(64)
PEG C12E5/hexanol	40(20)
pf1 phages	68(46)
Dihedral Angles (Φ and ψ)	50(26)

RDC *R-factor*	
PEG C12E5/hexanol	9.9 ± 0.4
pf1 phages	16.9 ± 0.8

SAXS	
CRYSOL[e] χ	0.96

PROCHECK-NMR results (%)[e]	
most favorable region	87.9 ± 0.6
additionally allowed region	12.1 ± 0.6
generously allowed region	0.0 ± 0.0
disallowed region	0.0 ± 0.0

Molprobity (%)[e]	
Ramachandran outliers	0.0 ± 0.0
Ramachandran favored	91.13
Bad backbone (%)	0.13

Coordinate Precision (Å)[g]	
Protein back bone (A326-I655)	0.40 ± 0.11
Protein heavy atoms (A326-I655)	0.73 ± 0.09

[a] Total number of restraints, with the number of restraints to the N2 domain indicated in parentheses.

[b] Average number of distance restraints violated in the 20 lowest energy structures.

[c] Quality factor of experimental I_{ox}/I_{red} vs. back-calculated I_{ox}/I_{red} of the ensemble. Only inter-domain restraints were included.

[d] Total number of restraints, with the number of inter-domain restraints indicated after the slash.

[e] Fit to the experimental scattering curve for the lowest energy structure using CRYSOL [43]. The goodness of fit to the experimental scattering curve for each of the 20 individual simulated annealing structures was also measured using the CalcSAXS helper program in the XPLOR-NIH (v. 2.37) software package [40,79] and yielded values of $\chi^2 = 0.81 \pm 0.02$.

[e] PROCHECK-NMR [92] and Molprobity [93] results includes residues (A326-I655) and are of acceptable quality for an NMR structure.

[g] The coordinate precision is defined as the average atomic root mean square deviation (RMSD) of the 20 individual simulated annealing structures and their mean coordinates. Backbone atoms are N, C^{α}, C′, and O. During the calculation the backbone coordinates of the N2 domain (A326-P461) and residues spanning the linker and N3 domains (N476-I655) were treated as rigid bodies. The coordinates spanning the linker and N3 domains were derived from the calculation described in Table 3.2.

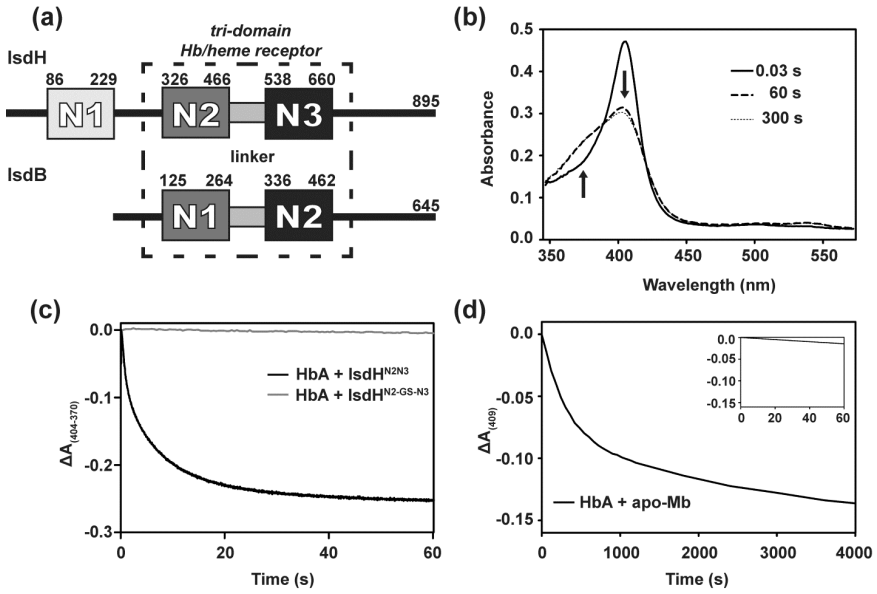

Figure 3.1 *S. aureus* uses conserved tri-domain receptors to rapidly capture hemin from Hb.

(*a*) Schematic of the conserved NEAT domains of *S. aureus* Hb receptors, IsdH and IsdB. NEAT domains that bind Hb and hemin (oxidized form of heme) are shown in gray and black, respectively. Residue numbers of the functionally homologous NEAT domains as well as the linker connecting them are indicated. (*b*) Rapid spectral changes in UV-Vis spectrum of the reaction of 1.5 μM metHb and 6.5 μM apo-IsdH^{N2N3}. Arrows indicate the increase and decrease over time for the absorbances at 370 and 404 nm, respectively. (c) Time course of the $\Delta A_{404-370}$ change after mixing 1.5 μM metHb and 6.5 μM apo-IsdH^{N2N3} (black line). The data was fit to a double-exponential equation and yielded hemin transfer rates of 0.85 ± 0.11 and 0.099 ± 0.14 s^{-1}. Similar hemin transfer data is shown for the reaction containing 1.5 μM metHb and 6.5 μM apo-IsdH$^{N2-GS-N3}$, a IsdH^{N2N3} mutant in which the linker is replaced with a glycine-serine nonapeptide (grey line). (d) Time course of the ΔA_{409} change after mixing 2.5 μM HbA and 40 μM H64Y/V68F apo-Mb. The first 60 seconds of the reaction is shown in the inset for comparison.

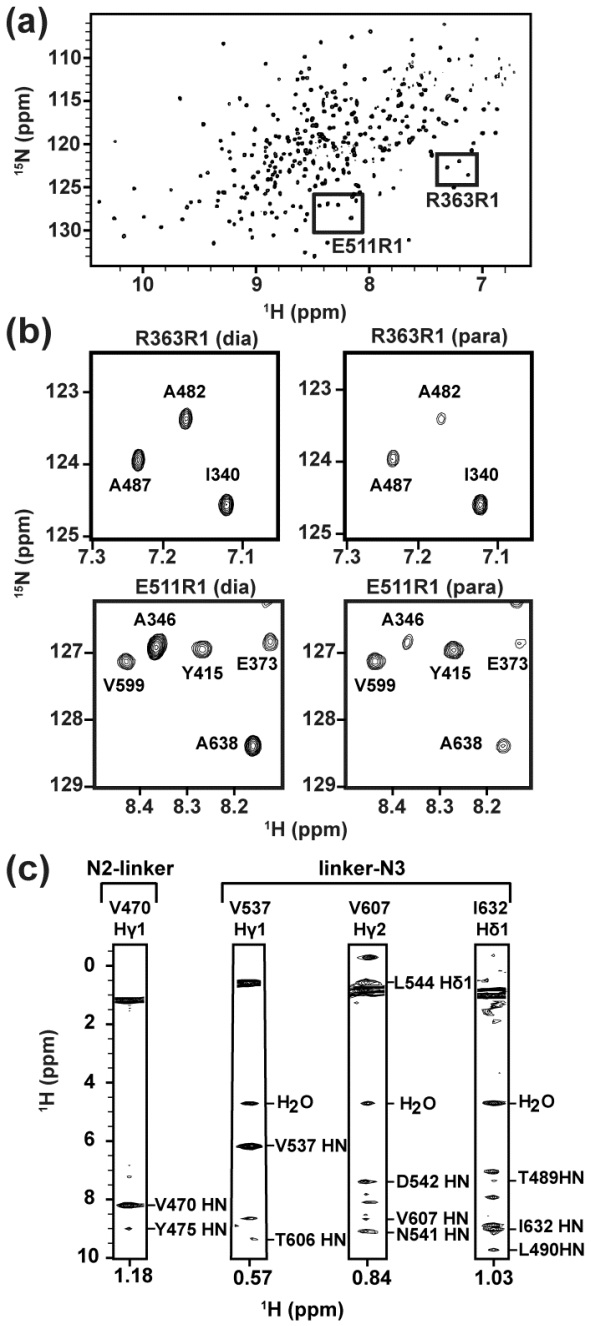

Figure 3.2 NMR spectra of IsdH^{N2N3}

(*a*) A representative ^{15}N-HSQC of IsdH^{N2N3}. Boxed regions indicate the representative sections of each PRE probe's spectra shown in (*b*) (E511R1 and R363R1 probes). (*b*) Magnified regions depicting selective distance dependent line-broadening for the E511R1 (bottom) and R363R1 (top) probes. For each probe selected diamagnetic and paramagnetic spectra are shown in the left

and right panels, respectively. (*c*) Representative NMR spectra of inter-domain methyl-edited NOEs in $IsdH^{N2N3}$. Panels show regions within the ^{13}C-edited NOESY. Methyl-amide NOEs were cross validated in the ^{15}N-edited NOESY spectra. The N2-linker interface is shown in the right panel and the linker-N3 interface in shown in the left panel. Inter-domain NOEs are labeled and any intra-domain NOEs or apodization effects were left unlabeled.

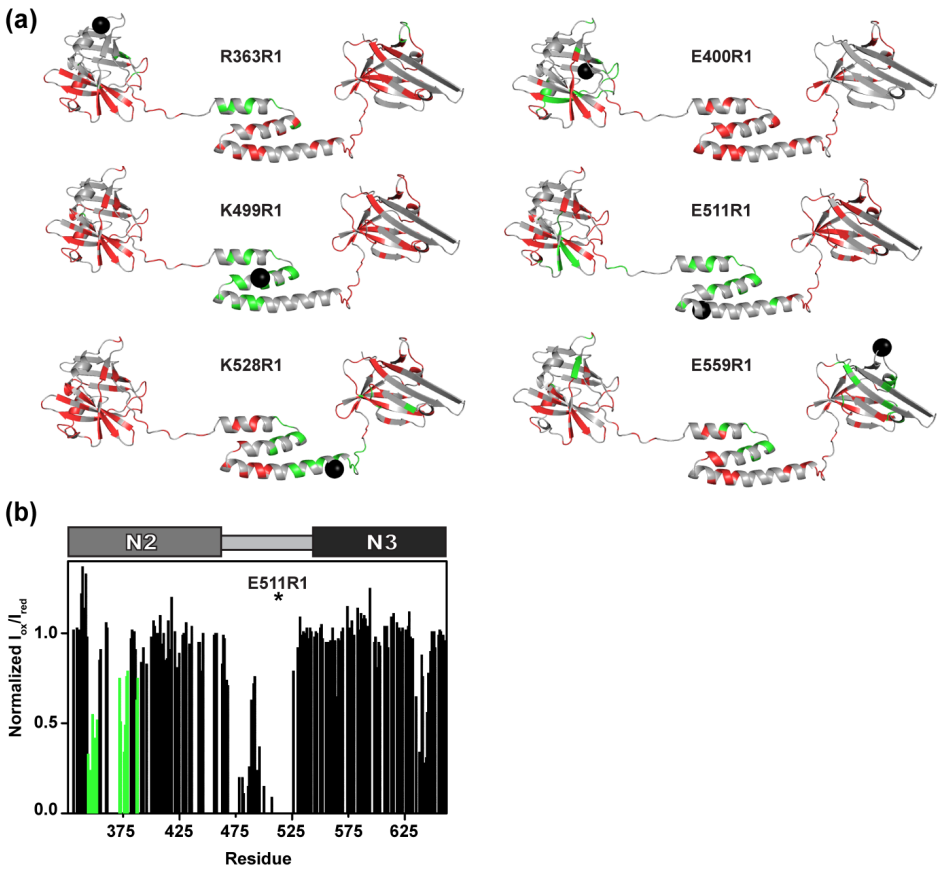

Figure 3.3 IsdH^{N2N3} PRE profile for each probe

(*a*) The distance-dependent line-broadening effect observed by each spin-label mutant is mapped to the extended starting structure of IsdH^{N2N3}. Attractive PRE effects ($I_{ox}/I_{red} < 0.80$) are shown in green and repulsive PRE effects ($I_{ox}/I_{red} \geq 0.80$) are shown in red. The alpha carbon of each residue where the probe is located is depicted as a black sphere. Residues to which no PRE information is available are shown in grey. Mapping data for the following probes is shown: R363R1, E400R1, K499R1, E511R1 K528R1, and E559R1. (*b*) representative PRE profile of the E511R1 probe data. Normalized PRE intensity ratios (I_{ox}/I_{red}) are shown as a function of residue number. The domain boundaries are shown in schematic above. The asterisk denotes the location of the probe. Green bars indicate the effect seen in the N2 domain that is not reflected in the

crystal structure. Errors in the ratio measurements are approximately 10-15% based on signal to noise of the NMR spectra, and thus can lead to values in excess of 1. Errors in the intensity ratio can also occur as a result of manipulating the sample (adding ascorbic acid to oxidize the probe) and instrument instability. These errors are partially accounted for by adding ± 5.0 Å to the distance restraints that are obtained from the ratio data.

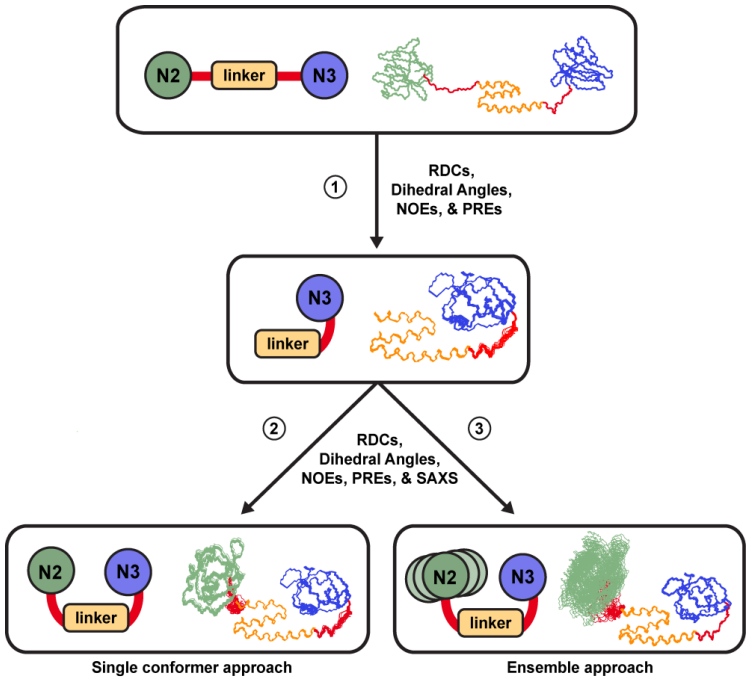

Figure 3.4 Schematic of the calculation strategy used to model the structure of IsdH^{N2N3}

In step (1), the structure of the linker-N3 inter-domain interface was determined using the appropriate NMR experimental restraints. In step (2), the coordinates from step (1) were used as input and only the structure of the N2-linker interface was refined against the NMR and SAXS data. The structure of the linker-N3 interface determined in step (1) is compatible with the experimental data, whereas the structure of the intact protein produced from step (2) exhibits slight, but systematic violations with the PRE distance data that originate from residues or probes located in the N2 domain (eight restraints have violations ranging from 0.5 to 2.7 Å). To account for this discrepancy, in step (3) ensemble calculations were performed in which the N2-linker interface calculations were using four molecular structures to represent the receptor. Color code: the N2, linker and N3 domains are colored green, yellow and blue, respectively, and the coordinates of residues that connect the domains are colored red (I462-Y475 connecting the N2 and linker domains and V531-Q543 connecting the linker and N3 domains).

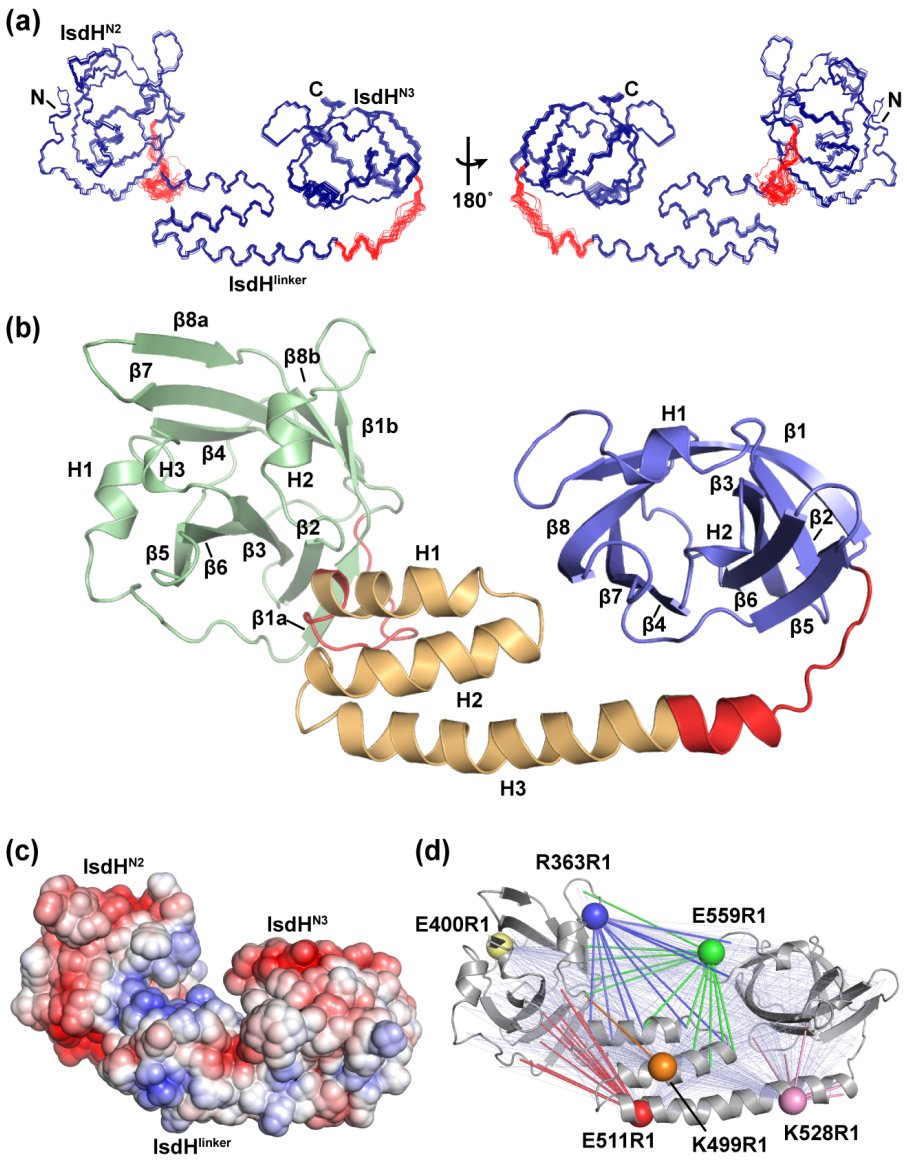

Figure 3.5 NMR structure model of a *S. aureus* tri-domain hemoglobin receptor, IsdH^{N2N3}

(*a*) The ensemble of the top 20 lowest energy structures for IsdH^{N2N3} calculated using the two step procedure outlined in Figure 4 (steps 1 and 2). The connector regions between each domain that were allowed to move during the conjoined rigid-body/torsion angle dynamics are colored in red. Two views are shown related by a 180°rotation. (*b*) Ribbon diagram of the lowest energy structure of IsdH^{N2N3}. The N2, linker, and N3 domains are colored in green, yellow, and blue,

respectively. The residues connecting the domains are colored in red. Secondary structure elements are labeled for each subdomain. (*c*) Electrostatic surface of $IsdH^{N2N3}$ showing positively and negatively charged residues colored in blue and red, respectively. (*d*) Graphical summary of the PRE-derived distance restraint data used to determine the structure showing its compatibility with the NMR structure. Data from probes providing attractive distance restraints are indicated by bold lines originating from spheres that correspond to the backbone position of each probe: R363R1 (dark blue), E400R1 (yellow), E511R1 (red), K528R1 (pink) and E559R1 (green). Repulsive restraints are shown as light blue lines. Only inter-domain attractive and repulsive restraints are shown. The structures shown in panels (*b* to *d*) are presented in the same orientation and were generated using the program PyMOL [89].

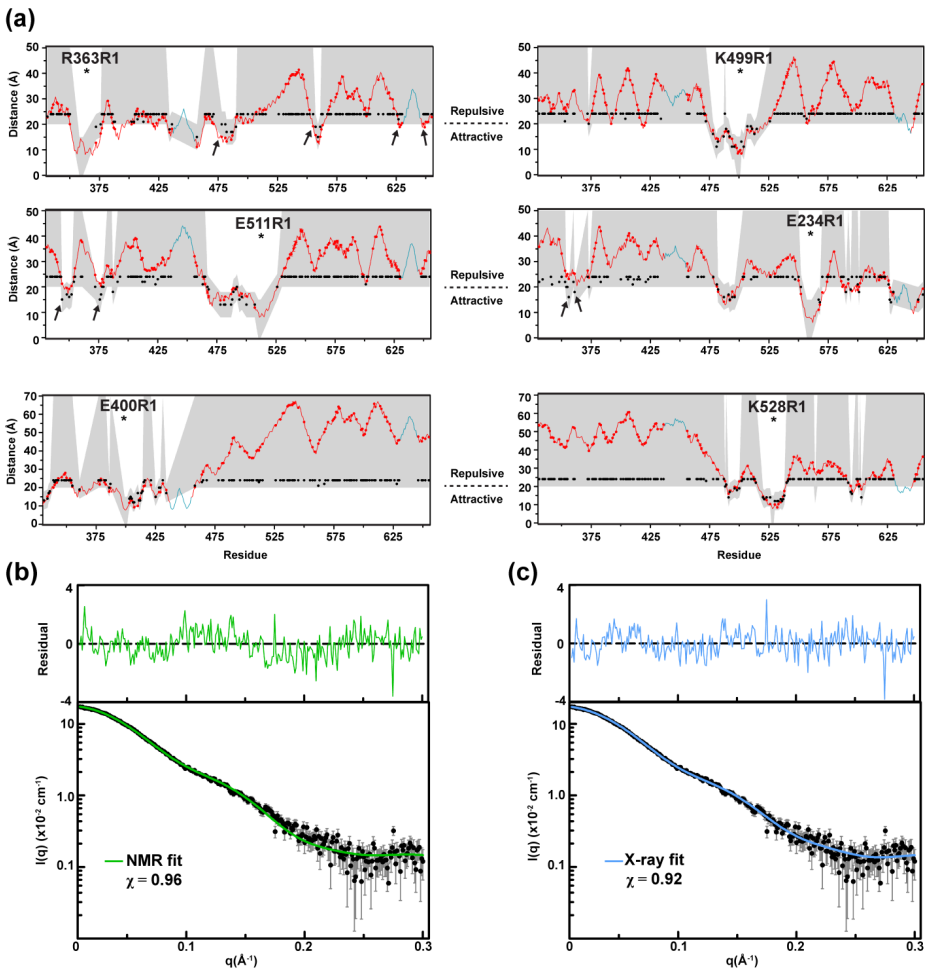

Figure 3.6 Compatibility of the structure of IsdH^{N2N3} with the PRE and SAXS data

(*a*) For each probe the panels as a function of residue number a graph of the distance between the backbone amide protons to each probe in the top 20 lowest energy NMR structures (red dots). Standard deviations are represented by error bars and in some cases are too small to be seen. The shaded regions indicate the range of the PRE-derived distance restraints used in the calculation between the probe and amide proton, while the PRE-derived distance is indicated by a black dot. Repulsive restraints span a wide range of distances (upper half of each figure); while attractive restraints are assigned narrower ranges of ± 5.0 Å (bottom half each panel). Distances in the

structure indicated by a blue line correspond to residues in the ligand binding pockets and were not used in the NMR calculations. Each panel shows a violation analysis for one probe whose name is indicated on the upper half of the figure. Arrows indicate eight PRE-derived distance restraints that were systematically violated in ensemble by 0.5 to 2.7 Å (also partially shown in Figure 7A). (*b*) Fit of the experimental solution scattering of $IsdH^{N2N3}$ to the theoretical scattering curve (colored in green) of the NMR structure (χ = 0.96). The residual of the fit is shown at the top of the figure. The data was analyzed using the programs CalcSAXS [40] and CRYSOL [43]. (*c*) As in panel (*b*), but the coordinates of the crystal structure of the receptor in the $IsdH^{N2N3}$:Hb complex (PDB code: 4IJ2) were used to generate the theoretical scattering curve (χ = 0.92, colored green).

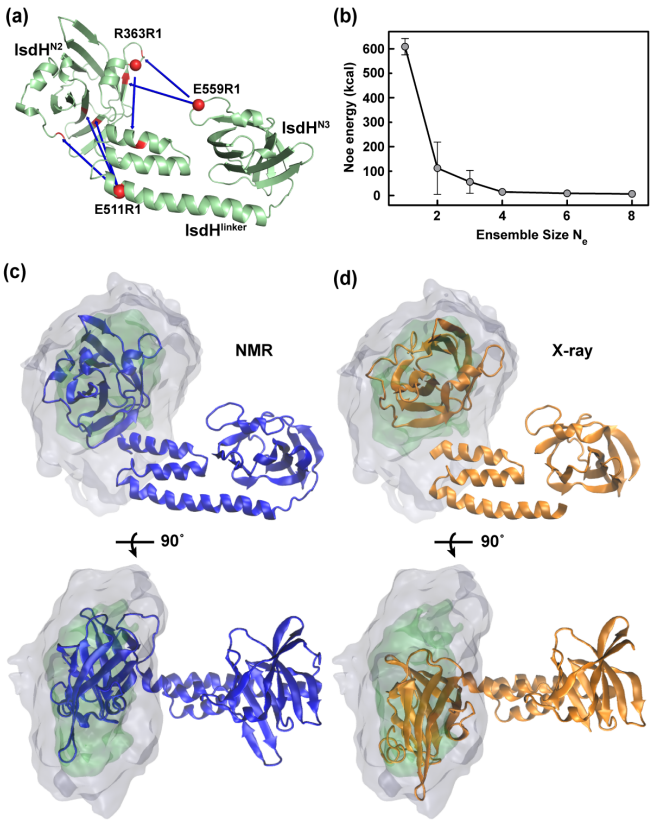

Figure 3.7 Estimation of the N2 domain motions in the Hb-free receptor

(a) Six of the 8 consistently violated PRE-derived distance restraints mapped onto the lowest energy structure calculated from the two-step procedure. The blue arrows point toward the location of each violated restraint (backbone atoms colored red) that originate from the E511R1, R363R1 and E559R1 probes (shown in red spheres). (b) The top 15 calculated NOE energies as a function of ensemble size with the standard deviation shown in bars, where ensemble sizes greater than 4 results in error bars are too small to be seen. (c and d) The estimated domain motions of the N2 domain are shown as a reweighted atomic probability density map plotted at 50% (green) and 10% (grey) of maximum. Two views are shown related by a 90° rotation. A cartoon representation of the single conformer Hb-free NMR model is shown in blue in panel (c), whereas a single receptor molecule from the crystal structure of the $IsdH^{N2N3}$:Hb tetrameric complex (PDB code: 4IJ2, chain G) is shown in orange in panel (d).

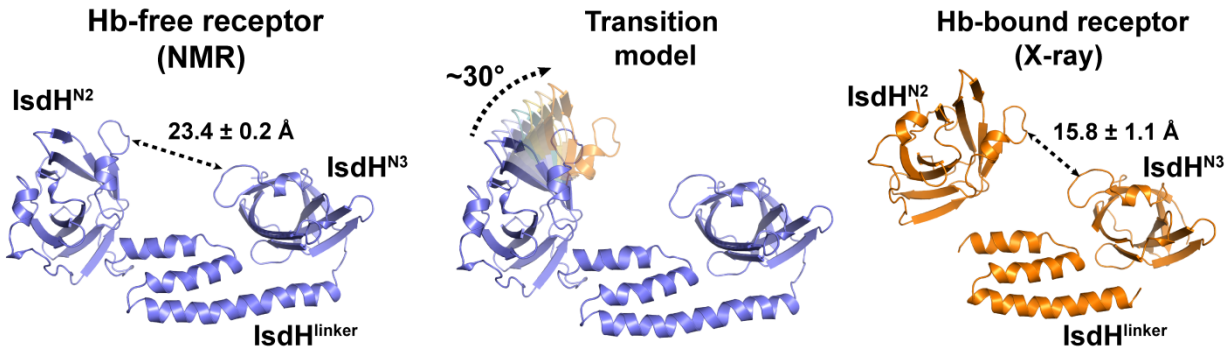

Figure 3.8 Structural differences between the Hb-free and -bound forms of IsdH^{N2N3}

The NMR apo-model of IsdH^{N2N3} is shown in blue (left) and a single receptor molecule from the crystal structure of the IsdH^{N2N3}:Hb tetrameric complex (PDB code: 4IJ2, chain G) is shown in orange (right). The distances shown are from the alpha carbon atoms of residues E362 and E559. The transition from the free form of the receptor into a more compact bound form is modeled in the figure by showing hypothetical structural intermediates of the Hb binding pocket in N2 (middle). Structural intermediates were calculated using the Rigimol plugin for PyMOL [89].

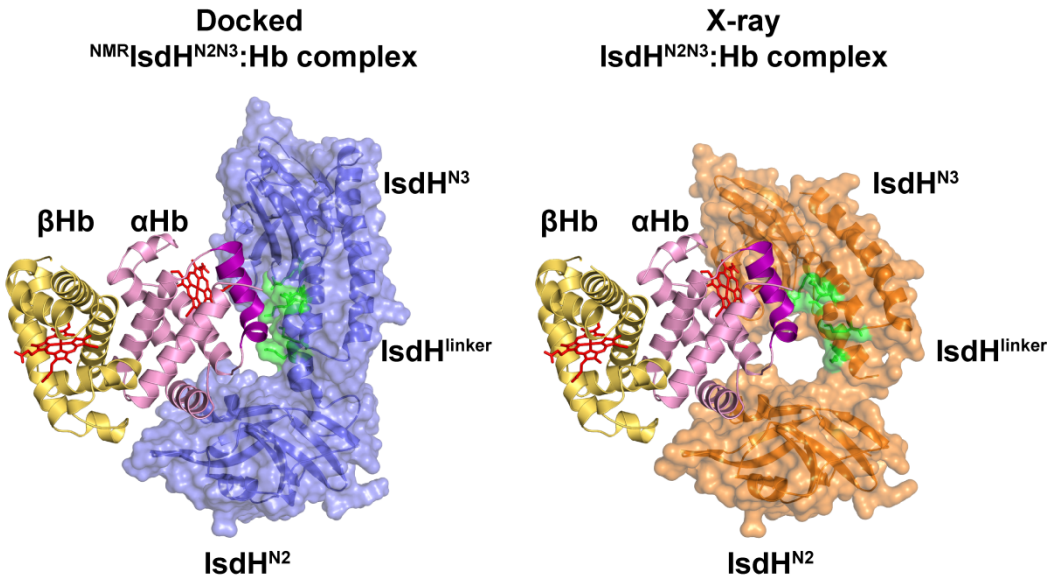

Figure 3.9 Model of hemin extraction by IsdH^{N2N3}

The panel on the left shows a hypothetical structure of the complex between the NMR model of IsdH^{N2N3} (blue) and dimeric Hb (αHb in pink with the F-helix colored in purple and βHb in yellow). The model was generated by superimposing the coordinates of the N2 domain in the NMR model and crystal structure of the IsdH^{N2N3}:Hb complex (PDB code: 4IJ2, chain G). The panel on the right shows the structure of the IsdH^{N2N3}:Hb complex for comparison (only one receptor is shown). The protein backbones of the receptors are shown in schematic and surface representation. The globin chains of Hb are shown in schematic and the hemin groups are colored red and shown in stick representation. Residues within the linker domain of IsdH^{N2N3} that are atomically overlapping with αHb are also shown in stick representation and colored green.

3.7 References

[1] R.M. Klevens, M.A. Morrison, J. Nadle, S. Petit, K. Gershman, S. Ray, L.H. Harrison, R.L. Eld, G. Dumyati, J.M. Townes, R. Lynfield, G. Dumyati, J.M. Townes, A.S. Craig, E.R. Zell, G.E. Fosheim, L.K. McDougal, R.B. Carey, S.K. Fridkin, Active Bacterial Core surveillance (ABCs) MRSA Investigators, Invasive methicillin-resistant Staphylococcus aureus infections in the United States., J. Am. Med. Assoc. 298 (2007) 1763–71. doi:10.1001/jama.298.15.1763.

[2] Centers for Disease Control and Prevention, Active Bacterial Core Surveillance Report, Emerging Infections Program Network, Methicillin- Resistant Staphylococcus aureus, (2011).

[3] U.E. Schaible, S.H.E. Kaufmann, Iron and microbial infection., Nat. Rev. Microbiol. 2 (2004) 946–53. doi:10.1038/nrmicro1046.

[4] S.T. Ong, J.Z.S. Ho, B. Ho, J.L. Ding, Iron-withholding strategy in innate immunity., Immunobiology. 211 (2006) 295–314. doi:10.1016/j.imbio.2006.02.004.

[5] A.J. Farrand, M.L. Reniere, H. Ingmer, D. Frees, E.P. Skaar, Regulation of Host Hemoglobin Binding by the Staphylococcus aureus Clp Proteolytic System, J. Bacteriol. 195 (2013) 5041–5050. doi:10.1128/JB.00505-13.

[6] M.L. Reniere, V.J. Torres, E.P. Skaar, Intracellular metalloporphyrin metabolism in Staphylococcus aureus., Biometals. 20 (2007) 333–45. doi:10.1007/s10534-006-9032-0.

[7] J.C. Grigg, G. Ukpabi, C.F.M. Gaudin, M.E.P. Murphy, Structural biology of heme binding in the Staphylococcus aureus Isd system., J. Inorg. Biochem. 104 (2010) 341–8. doi:10.1016/j.jinorgbio.2009.09.012.

[8] A.W. Maresso, O. Schneewind, Iron acquisition and transport in Staphylococcus aureus., Biometals. 19 (2006) 193–203. doi:10.1007/s10534-005-4863-7.

[9] S.K. Mazmanian, H. Ton-That, K. Su, O. Schneewind, An iron-regulated sortase anchors a class of surface protein during Staphylococcus aureus pathogenesis., Proc. Natl. Acad. Sci. U. S. A. 99 (2002) 2293–8. doi:10.1073/pnas.032523999.

[10] S.K. Mazmanian, E.P. Skaar, A.H. Gaspar, M. Humayun, P. Gornicki, J. Jelenska, A. Joachmiak, D.M. Missiakas, O. Schneewind, Passage of heme-iron across the envelope of Staphylococcus aureus., Science. 299 (2003) 906–9ma. doi:10.1126/science.1081147.

[11] H. Ton-That, L.A. Marraffini, O. Schneewind, Protein sorting to the cell wall envelope of Gram-positive bacteria., Biochim. Biophys. Acta. 1694 (2004) 269–78. doi:10.1016/j.bbamcr.2004.04.014.

[12] A. Dryla, D. Gelbmann, A. Von Gabain, E. Nagy, Identification of a novel iron regulated staphylococcal surface protein with haptoglobin-haemoglobin binding activity, Mol. Microbiol. 49 (2003) 37–53. doi:10.1046/j.1365-2958.2003.03542.x.

[13] N. Muryoi, M.T. Tiedemann, M. Pluym, J. Cheung, D.E. Heinrichs, M.J. Stillman, Demonstration of the Iron-regulated Surface Determinant (Isd) Heme Transfer Pathway in Staphylococcus aureus, J. Biol. Chem. 283 (2008) 28125–28136.

doi:10.1074/jbc.M802171200.
[14] H. Zhu, G. Xie, M. Liu, J.S. Olson, M. Fabian, D.M. Dooley, B. Lei, Pathway for heme uptake from human methemoglobin by the iron-regulated surface determinants system of Staphylococcus aureus., J. Biol. Chem. 283 (2008) 18450–60. doi:10.1074/jbc.M801466200.
[15] V.A. Villareal, T. Spirig, S.A. Robson, M. Liu, B. Lei, R.T. Clubb, Transient weak protein-protein complexes transfer heme across the cell wall of Staphylococcus aureus., J. Am. Chem. Soc. 133 (2011) 14176–9. doi:10.1021/ja203805b.
[16] R. Abe, J.M.M. Caaveiro, H. Kozuka-Hata, M. Oyama, K. Tsumoto, Mapping the ultra-weak protein-protein interactions between heme transporters of Staphylococcus aureus., J. Biol. Chem. 287 (2012) 16477–87. doi:10.1074/jbc.M112.346700.
[17] M.L. Reniere, G.N. Ukpabi, S.R. Harry, D.F. Stec, R. Krull, D.W. Wright, B.O. Bachmann, M.E. Murphy, E.P. Skaar, The IsdG-family of haem oxygenases degrades haem to a novel chromophore., Mol. Microbiol. 75 (2010) 1529–38. doi:10.1111/j.1365-2958.2010.07076.x.
[18] T. Matsui, S. Nambu, Y. Ono, C.W. Goulding, K. Tsumoto, M. Ikeda-Saito, Heme degradation by Staphylococcus aureus IsdG and IsdI liberates formaldehyde rather than carbon monoxide., Biochemistry. 52 (2013) 3025–7. doi:10.1021/bi400382p.
[19] M. Andrade, F. Ciccarelli, C. Perez-Iratxeta, P. Bork, NEAT: a domain duplicated in genes near the components of a putative Fe3+ siderophore transporter from Gram-positive pathogenic bacteria, Genome Biol. 3 (2002) research0047.1–research0047.5. doi:10.1186/gb-2002-3-9-research0047.
[20] R.M. Pilpa, S.A. Robson, V.A. Villareal, M.L. Wong, M. Phillips, R.T. Clubb, Functionally distinct NEAT (NEAr Transporter) domains within the Staphylococcus aureus IsdH/HarA protein extract heme from methemoglobin., J. Biol. Chem. 284 (2009) 1166–76. doi:10.1074/jbc.M806007200.
[21] A. Dryla, B. Hoffmann, D. Gelbmann, C. Giefing, M. Hanner, A. Meinke, A.S. Anderson, W. Koppensteiner, R. Konrat, A. von Gabain, E. Nagy, High-Affinity Binding of the Staphylococcal HarA Protein to Haptoglobin and Hemoglobin Involves a Domain with an Antiparallel Eight-Stranded -Barrel Fold, J. Bacteriol. 189 (2007) 254–264. doi:10.1128/JB.01366-06.
[22] K. Krishna Kumar, D.A. Jacques, G. Pishchany, T. Caradoc-Davies, T. Spirig, G.R. Malmirchegini, D.B. Langley, C.F. Dickson, J.P. Mackay, R.T. Clubb, E.P. Skaar, J.M. Guss, D.A. Gell, Structural basis for hemoglobin capture by Staphylococcus aureus cell-surface protein, IsdH., J. Biol. Chem. 286 (2011) 38439–47. doi:10.1074/jbc.M111.287300.
[23] S.R. Clarke, M.D. Wiltshire, S.J. Foster, IsdA of Staphylococcus aureus is a broad spectrum, iron-regulated adhesin., Mol. Microbiol. 51 (2004) 1509–19. doi:10.1111/j.1365-2958.2003.03938.x.
[24] C.L. Nobles, A.W. Maresso, The theft of host heme by Gram-positive pathogenic

bacteria., Metallomics. 3 (2011) 788–96. doi:10.1039/c1mt00047k.
[25] B. Lei, Benfang Lei's research on heme acquisition in Gram-positive pathogens and bacterial pathogenesis., World J. Biol. Chem. 1 (2010) 286–90. doi:10.4331/wjbc.v1.i9.286.
[26] T. Spirig, G.R. Malmirchegini, J. Zhang, S.A. Robson, M. Sjodt, M. Liu, K. Krishna Kumar, C.F. Dickson, D.A. Gell, B. Lei, J. a Loo, R.T. Clubb, Staphylococcus aureus uses a novel multidomain receptor to break apart human hemoglobin and steal its heme., J. Biol. Chem. 288 (2013) 1065–78. doi:10.1074/jbc.M112.419119.
[27] C.F.M. Gaudin, J.C. Grigg, A.L. Arrieta, M.E.P. Murphy, Unique heme-iron coordination by the hemoglobin receptor IsdB of Staphylococcus aureus., Biochemistry. 50 (2011) 5443–52. doi:10.1021/bi200369p.
[28] M.S. Hargrove, Quaternary Structure Regulates Hemin Dissociation from Human Hemoglobin, J. Biol. Chem. 272 (1997) 17385–17389. doi:10.1074/jbc.272.28.17385.
[29] C.F. Dickson, K. Krishna Kumar, D.A. Jacques, G.R. Malmirchegini, T. Spirig, J.P. Mackay, R.T. Clubb, J.M. Guss, D.A. Gell, Structure of the Hemoglobin-IsdH Complex Reveals the Molecular Basis of Iron Capture by Staphylococcus aureus., J. Biol. Chem. (2014). doi:10.1074/jbc.M113.545566.
[30] M.S. Hargrove, E.W. Singleton, M.L. Quillin, L.A. Ortiz, G.N. Phillips, J.S. Olson, A.J. Mathews, His64(E7)-->Tyr apomyoglobin as a reagent for measuring rates of hemin dissociation., J. Biol. Chem. 269 (1994) 4207–14.
[31] T. Spirig, R.T. Clubb, Backbone (1)H, (13)C and (15)N resonance assignments of the 39 kDa staphylococcal hemoglobin receptor IsdH., Biomol. NMR Assign. (2011). doi:10.1007/s12104-011-9348-8.
[32] G.M. Clore, J. Iwahara, Theory, practice, and applications of paramagnetic relaxation enhancement for the characterization of transient low-population states of biological macromolecules and their complexes., Chem. Rev. 109 (2009) 4108–39. doi:10.1021/cr900033p.
[33] B. Simon, T. Madl, C.D. Mackereth, M. Nilges, M. Sattler, An efficient protocol for NMR-spectroscopy-based structure determination of protein complexes in solution., Angew. Chem. Int. Ed. Engl. 49 (2010) 1967–70. doi:10.1002/anie.200906147.
[34] A.N. Volkov, J.A.R. Worrall, E. Holtzmann, M. Ubbink, Solution structure and dynamics of the complex between cytochrome c and cytochrome c peroxidase determined by paramagnetic NMR., Proc. Natl. Acad. Sci. U. S. A. 103 (2006) 18945–50. doi:10.1073/pnas.0603551103.
[35] R.C. Page, S. Lee, J.D. Moore, S.J. Opella, T.A. Cross, Backbone structure of a small helical integral membrane protein: A unique structural characterization., Protein Sci. 18 (2009) 134–46. doi:10.1002/pro.24.
[36] J. Iwahara, C.D. Schwieters, G.M. Clore, Ensemble approach for NMR structure refinement against (1)H paramagnetic relaxation enhancement data arising from a flexible paramagnetic group attached to a macromolecule., J. Am. Chem. Soc. 126 (2004) 5879–

5896. doi:10.1021/ja031580d.
[37] C.D. Mackereth, T. Madl, S. Bonnal, B. Simon, K. Zanier, A. Gasch, V. Rybin, J. Valcárcel, M. Sattler, Multi-domain conformational selection underlies pre-mRNA splicing regulation by U2AF., Nature. 475 (2011) 408–11. doi:10.1038/nature10171.
[38] G.A. Bermejo, M.-P. Strub, C. Ho, N. Tjandra, Determination of the solution-bound conformation of an amino acid binding protein by NMR paramagnetic relaxation enhancement: use of a single flexible paramagnetic probe with improved estimation of its sampling space., J. Am. Chem. Soc. 131 (2009) 9532–7. doi:10.1021/ja902436g.
[39] P. Dosset, J.-C.C. Hus, D. Marion, M. Blackledge, A novel interactive tool for rigid-body modeling of multi-domain macromolecules using residual dipolar couplings., J. Biomol. NMR. 20 (2001) 223–31. doi:10.1023/A:1011206132740.
[40] C.D. Schwieters, G.M. Clore, Using small angle solution scattering data in Xplor-NIH structure calculations., Prog. Nucl. Magn. Reson. Spectrosc. 80 (2014) 1–11. doi:10.1016/j.pnmrs.2014.03.001.
[41] G.M. Clore, C.A. Bewley, Using conjoined rigid body/torsion angle simulated annealing to determine the relative orientation of covalently linked protein domains from dipolar couplings., J. Magn. Reson. 154 (2002) 329–35. doi:10.1006/jmre.2001.2489.
[42] G.M. Clore, C.D. Schwieters, Theoretical and computational advances in biomolecular NMR spectroscopy, Curr. Opin. Struct. Biol. 12 (2002) 146–153. doi:10.1016/S0959-440X(02)00302-0.
[43] D. Svergun, C. Barberato, M.H. Koch, CRYSOL - A program to evaluate X-ray solution scattering of biological macromolecules from atomic coordinates, J. Appl. Crystallogr. 28 (1995) 768–773. doi:10.1107/S0021889895007047.
[44] C.D. Schwieters, G.M. Clore, Reweighted atomic densities to represent ensembles of NMR structures., J. Biomol. NMR. 23 (2002) 221–5.
[45] B.A. Fonner, B.P. Tripet, B. Eilers, J. Stanisich, R.K. Sullivan-Springhetti, R. Moore, M. Liu, B. Lei, V. Copie, Solution Structure and Molecular determinants of Hemoglobin Binding of the first NEAT Domain of IsdB in Staphylococcus aureus., Biochemistry. 53 (2014) 3922–3933. doi:10.1021/bi5005188.
[46] R.M. Pilpa, E.A. Fadeev, V.A. Villareal, M.L. Wong, M. Phillips, R.T. Clubb, Solution structure of the NEAT (NEAr Transporter) domain from IsdH/HarA: the human hemoglobin receptor in Staphylococcus aureus., J. Mol. Biol. 360 (2006) 435–47. doi:10.1016/j.jmb.2006.05.019.
[47] M. Watanabe, Y. Tanaka, A. Suenaga, M. Kuroda, M. Yao, N. Watanabe, F. Arisaka, T. Ohta, I. Tanaka, K. Tsumoto, Structural basis for multimeric heme complexation through a specific protein-heme interaction: the case of the third neat domain of IsdH from Staphylococcus aureus., J. Biol. Chem. 283 (2008) 28649–59. doi:10.1074/jbc.M803383200.
[48] H. Zhu, D. Li, M. Liu, V. Copié, B. Lei, Non-Heme-Binding Domains and Segments of the Staphylococcus aureus IsdB Protein Critically Contribute to the Kinetics and

Equilibrium of Heme Acquisition from Methemoglobin., PLoS One. 9 (2014) e100744. doi:10.1371/journal.pone.0100744.

[49] C.F. Bowden, M.M. Verstraete, L.D. Eltis, M.E.P. Murphy, Hemoglobin binding and catalytic heme extraction by IsdB NEAT domains., Biochemistry. (2014). doi:10.1021/bi500230f.

[50] R. Senturia, M. Faller, S. Yin, J.A. Loo, D. Cascio, M.R. Sawaya, D. Hwang, R.T. Clubb, F. Guo, Structure of the dimerization domain of DiGeorge critical region 8., Protein Sci. 19 (2010) 1354–65. doi:10.1002/pro.414.

[51] D. Reverter, C.D. Lima, A basis for SUMO protease specificity provided by analysis of human Senp2 and a Senp2-SUMO complex., Structure. 12 (2004) 1519–31. doi:10.1016/j.str.2004.05.023.

[52] F. Ascoli, M.R. Fanelli, E. Antonini, Preparation and properties of apohemoglobin and reconstituted hemoglobins., Methods Enzymol. 76 (1981) 72–87.

[53] P.I. Reisberg, J.S. Olson, Equilibrium binding of alkyl isocyanides to human hemoglobin., J. Biol. Chem. 255 (1980) 4144–30.

[54] Antonini E. & Brunori M., Hemoglobin and Myoglobin in their Reactions with Ligands, Amsterdam, Netherlands North-Holl. (1971).

[55] M. Fabian, E. Solomaha, J.S. Olson, A.W. Maresso, Heme transfer to the bacterial cell envelope occurs via a secreted hemophore in the Gram-positive pathogen Bacillus anthracis., J. Biol. Chem. 284 (2009) 32138–46. doi:10.1074/jbc.M109.040915.

[56] T.K. Nygaard, G.C. Blouin, M. Liu, M. Fukumura, J.S. Olson, M. Fabian, D.M. Dooley, B. Lei, The mechanism of direct heme transfer from the streptococcal cell surface protein Shp to HtsA of the HtsABC transporter., J. Biol. Chem. 281 (2006) 20761–71. doi:10.1074/jbc.M601832200.

[57] F. Delaglio, S. Grzesiek, G.W. Vuister, G. Zhu, J. Pfeifer, A. Bax, NMRPipe: a multidimensional spectral processing system based on UNIX pipes., J. Biomol. NMR. 6 (1995) 277–93.

[58] R. Keller, The Computer Aided Resonance Assignment Tutorial, (2004).

[59] T.D. Goddard, D.G. Kneller, Sparky NMR Analysis Software, (2001).

[60] J. Cavanagh, W.J. Fairbrother, A.G. Palmer, III, N.J. Skelton, Protein NMR Spectroscopy: Principles and Practice (Google eBook), Academic Press, 1995.

[61] M. Rückert, G. Otting, Alignment of Biological Macromolecules in Novel Nonionic Liquid Crystalline Media for NMR Experiments, J. Am. Chem. Soc. 122 (2000) 7793–7797. doi:10.1021/ja001068h.

[62] M.R. Hansen, L. Mueller, A. Pardi, Tunable alignment of macromolecules by filamentous phage yields dipolar coupling interactions., Nat. Struct. Biol. 5 (1998) 1065–74. doi:10.1038/4176.

[63] F. Cordier, A.J. Dingley, S. Grzesiek, A doublet-separated sensitivity-enhanced HSQC for the determination of scalar and dipolar one-bond J-couplings., J. Biomol. NMR. 13 (1999) 175–80.

[64] Y. Shen, F. Delaglio, G. Cornilescu, A. Bax, TALOS+: a hybrid method for predicting protein backbone torsion angles from NMR chemical shifts., J. Biomol. NMR. 44 (2009) 213–23. doi:10.1007/s10858-009-9333-z.

[65] P. V. Konarev, V. V. Volkov, A. V. Sokolova, M.H.J. Koch, D.I. Svergun, PRIMUS: A Windows PC-based system for small-angle scattering data analysis, J. Appl. Crystallogr. 36 (2003) 1277–1282. doi:10.1107/S0021889803012779.

[66] J.L. Battiste, G. Wagner, Utilization of site-directed spin labeling and high-resolution heteronuclear nuclear magnetic resonance for global fold determination of large proteins with limited nuclear overhauser effect data., Biochemistry. 39 (2000) 5355–65.

[67] L. Shi, N.J. Traaseth, R. Verardi, M. Gustavsson, J. Gao, G. Veglia, Paramagnetic-based NMR restraints lift residual dipolar coupling degeneracy in multidomain detergent-solubilized membrane proteins., J. Am. Chem. Soc. 133 (2011) 2232–41. doi:10.1021/ja109080t.

[68] H. Chen, F. Ji, V. Olman, C.K. Mobley, Y. Liu, Y. Zhou, J.H. Bushweller, J.H. Prestegard, Y. Xu, Optimal mutation sites for PRE data collection and membrane protein structure prediction., Structure. 19 (2011) 484–95. doi:10.1016/j.str.2011.02.002.

[69] S. Reckel, D. Gottstein, J. Stehle, F. Löhr, M.-K. Verhoefen, M. Takeda, R. Silvers, M. Kainosho, C. Glaubitz, J. Wachtveitl, F. Bernhard, H. Schwalbe, P. Güntert, V. Dötsch, Solution NMR structure of proteorhodopsin., Angew. Chem. Int. Ed. Engl. 50 (2011) 11942–6. doi:10.1002/anie.201105648.

[70] W. Zhang, S.S. Pochapsky, T.C. Pochapsky, N.U. Jain, Solution NMR structure of putidaredoxin-cytochrome P450cam complex via a combined residual dipolar coupling-spin labeling approach suggests a role for Trp106 of putidaredoxin in complex formation., J. Mol. Biol. 384 (2008) 349–63. doi:10.1016/j.jmb.2008.09.037.

[71] C. Göbl, T. Madl, B. Simon, M. Sattler, NMR approaches for structural analysis of multidomain proteins and complexes in solution., Prog. Nucl. Magn. Reson. Spectrosc. 80 (2014) 26–63. doi:10.1016/j.pnmrs.2014.05.003.

[72] I. Solomon, N. Bloembergen, Nuclear Magnetic Interactions in the HF Molecule, J. Chem. Phys. 25 (1956) 261. doi:10.1063/1.1742867.

[73] D. Gottstein, S. Reckel, V. Dötsch, P. Güntert, Requirements on paramagnetic relaxation enhancement data for membrane protein structure determination by NMR., Structure. 20 (2012) 1019–27. doi:10.1016/j.str.2012.03.010.

[74] B.M. Kroncke, P.S. Horanyi, L. Columbus, Structural origins of nitroxide side chain dynamics on membrane protein α-helical sites., Biochemistry. 49 (2010) 10045–60. doi:10.1021/bi101148w.

[75] E.M. Weiner, S. Robson, M. Marohn, R.T. Clubb, The Sortase A enzyme that attaches proteins to the cell wall of Bacillus anthracis contains an unusual active site architecture., J. Biol. Chem. 285 (2010) 23433–43. doi:10.1074/jbc.M110.135434.

[76] A.M. Mandel, M. Akke, A.G. Palmer, III, Backbone Dynamics ofEscherichia coliRibonuclease HI: Correlations with Structure and Function in an Active Enzyme, J.

Mol. Biol. 246 (1995) 144–163. doi:10.1006/jmbi.1994.0073.
[77] R. Brüschweiler, X. Liao, P.E. Wright, Long-range motional restrictions in a multidomain zinc-finger protein from anisotropic tumbling., Science. 268 (1995) 886–9.
[78] L.K. Lee, M. Rance, W.J. Chazin, A.G. Palmer, Rotational diffusion anisotropy of proteins from simultaneous analysis of 15N and 13C alpha nuclear spin relaxation., J. Biomol. NMR. 9 (1997) 287–98.
[79] C.D. Schwieters, J.J. Kuszewski, N. Tjandra, G.M. Clore, The Xplor-NIH NMR molecular structure determination package., J. Magn. Reson. 160 (2003) 65–73.
[80] P. Emsley, K. Cowtan, Coot: model-building tools for molecular graphics., Acta Crystallogr. D. Biol. Crystallogr. 60 (2004) 2126–32. doi:10.1107/S0907444904019158.
[81] G.M. Clore, C.D. Schwieters, How much backbone motion in ubiquitin is required to account for dipolar coupling data measured in multiple alignment media as assessed by independent cross-validation?, J. Am. Chem. Soc. 126 (2004) 2923–38. doi:10.1021/ja0386804.
[82] C.D. Schwieters, G.M. Clore, The VMD-XPLOR visualization package for NMR structure refinement., J. Magn. Reson. 149 (2001) 239–44. doi:10.1006/jmre.2001.2300.
[83] M. Nilges, A.M. Gronenborn, A.T. Brünger, G.M. Clore, Determination of three-dimensional structures of proteins by simulated annealing with interproton distance restraints. Application to crambin, potato carboxypeptidase inhibitor and barley serine proteinase inhibitor 2., Protein Eng. 2 (1988) 27–38.
[84] G.M. Clore, J. Kuszewski, Chi(1) rotamer populations and angles of mobile surface side chains are accurately predicted by a torsion angle database potential of mean force., J. Am. Chem. Soc. 124 (2002) 2866–7.
[85] C.D. Schwieters, J.-Y. Suh, A. Grishaev, R. Ghirlando, Y. Takayama, G.M. Clore, Solution structure of the 128 kDa enzyme I dimer from Escherichia coli and its 146 kDa complex with HPr using residual dipolar couplings and small- and wide-angle X-ray scattering., J. Am. Chem. Soc. 132 (2010) 13026–45. doi:10.1021/ja105485b.
[86] C.D. Schwieters, G.M. Clore, Internal coordinates for molecular dynamics and minimization in structure determination and refinement., J. Magn. Reson. 152 (2001) 288–302. doi:10.1006/jmre.2001.2413.
[87] L. Deshmukh, C.D. Schwieters, A. Grishaev, R. Ghirlando, J.L. Baber, G.M. Clore, Structure and dynamics of full-length HIV-1 capsid protein in solution., J. Am. Chem. Soc. 135 (2013) 16133–47. doi:10.1021/ja406246z.
[88] R. Koradi, M. Billeter, K. Wüthrich, MOLMOL: a program for display and analysis of macromolecular structures., J. Mol. Graph. 14 (1996) 51–5, 29–32.
[89] W.L. DeLano, The PyMOL Molecular Graphics System, Version 1.5.0.04, Schrödinger LLC. (2002).
[90] D. Fushman, R. Xu, D. Cowburn, Direct determination of changes of interdomain orientation on ligation: use of the orientational dependence of 15N NMR relaxation in Abl SH(32)., Biochemistry. 38 (1999) 10225–30. doi:10.1021/bi990897g.

[91] V.A. Daragan, K.H. Mayo, Motional model analyses of protein and peptide dynamics using 13C and 15N NMR relaxation, Prog. Nucl. Magn. Reson. Spectrosc. 31 (1997) 63–105.

[92] R.A. Laskowski, J.A. Rullmannn, M.W. MacArthur, R. Kaptein, J.M. Thornton, AQUA and PROCHECK-NMR: programs for checking the quality of protein structures solved by NMR., J. Biomol. NMR. 8 (1996) 477–486. doi:10.1007/BF00228148.

[93] V.B. Chen, W.B. Arendall, J.J. Headd, D.A. Keedy, R.M. Immormino, G.J. Kapral, L.W. Murray, J.S. Richardson, D.C. Richardson, MolProbity: all-atom structure validation for macromolecular crystallography., Acta Crystallogr. D. Biol. Crystallogr. 66 (2010) 12–21. doi:10.1107/S0907444909042073.

3.8 Supplementary Information

The PRE-Derived NMR Model of the 38.8 kDa Tri-Domain IsdH Protein from *Staphylococcus aureus* Suggests that it Adaptively Recognizes Human Hemoglobin

Figures 3.S1-3.S3

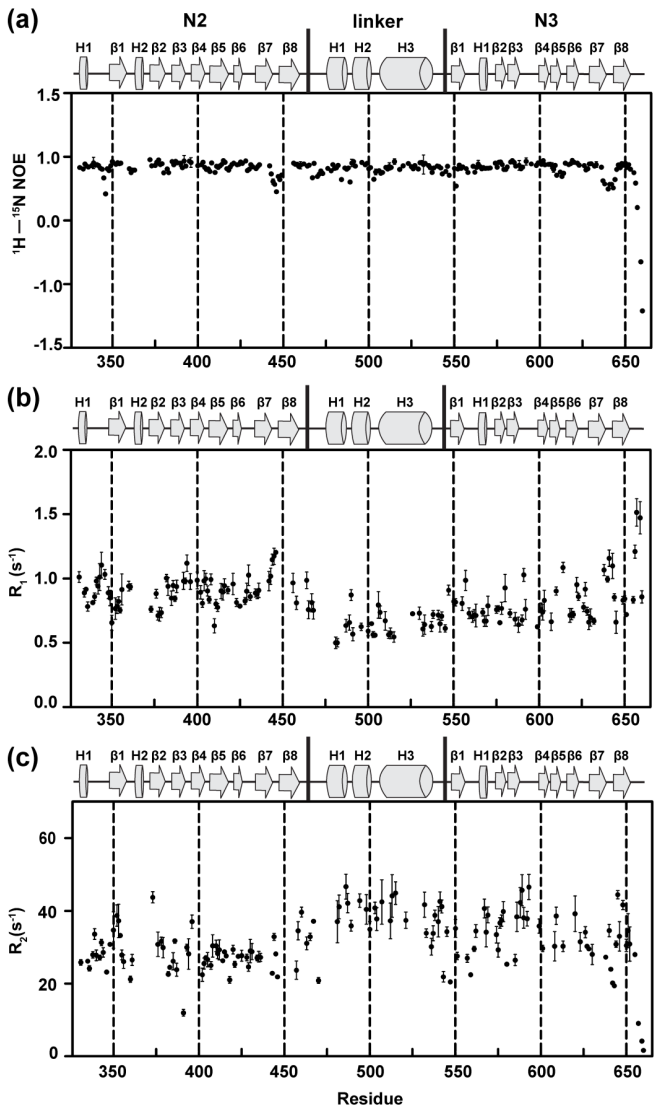

Figure 3.S1 ^{15}N relaxation analysis of IsdH^{N2N3}

(*a*) Backbone amide ^{1}H-^{15}N heteronuclear NOE for IsdH$^{N2N3(Y642A)}$. The peak intensity ratio between spectra with and without ^{1}H saturation as a function of the residue number is shown. The average heteronuclear NOE values and standard deviation values of two experiments are displayed. A total of 238 residues yielded HetNOE values. (*b*) Longitudinal, $R_{1,}$ and (*c*) transverse, $R_{2,}$ spin relaxation data for IsdH$^{N2N3(Y642A)}$. A total of 155 and 142 residues yielded R_1 and R_2 data, respectively. Secondary structure and domain boundaries are displayed at the top of each panel.

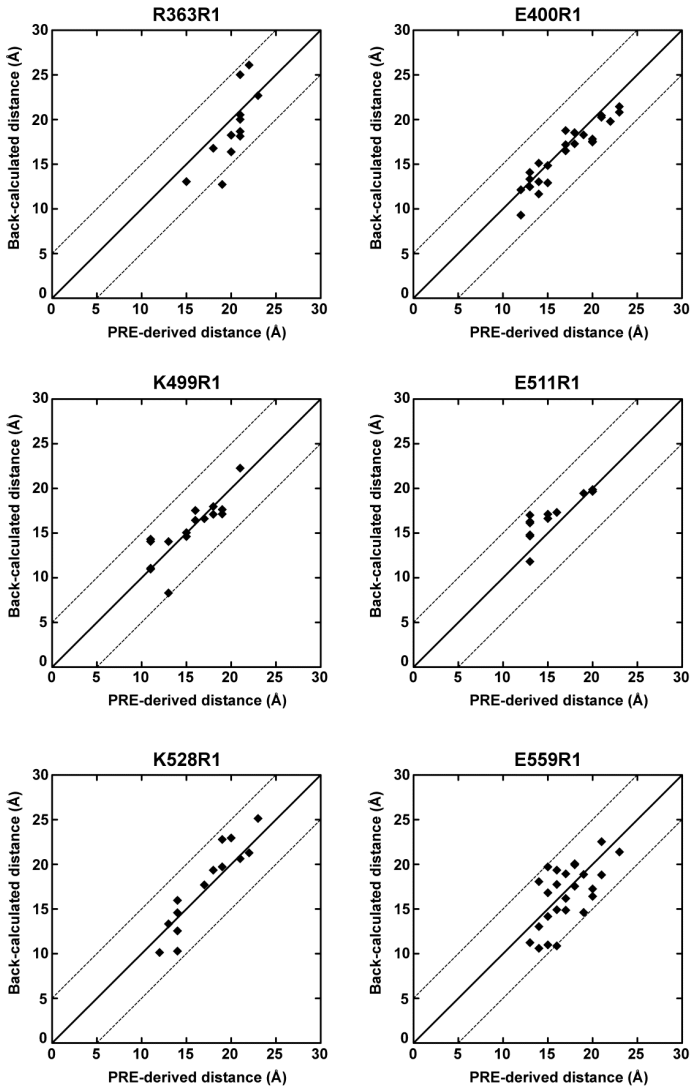

Figure 3.S2 Correlation between observed and back calculated intra-domain distances for each probe used the calculation of IsdH$^{N2N3(Y642A)}$

Each panel shows a correlation plot for all intra-domain attractive ($I_{ox}/I_{red} < 0.8$) restraints for a given probe in IsdH$^{N2N3(Y642A)}$. Dashed lines indicate ± 5 Å error bounds for the PRE-derived distance data. Intra-domain Q-factors for R363C (N2), E400C (N2), K499C (linker), E511C (linker), K528C (linker) and E559C (N3) are 0.24, 0.14, 0.28, 0.37, 0.10, 0.27, respectively.

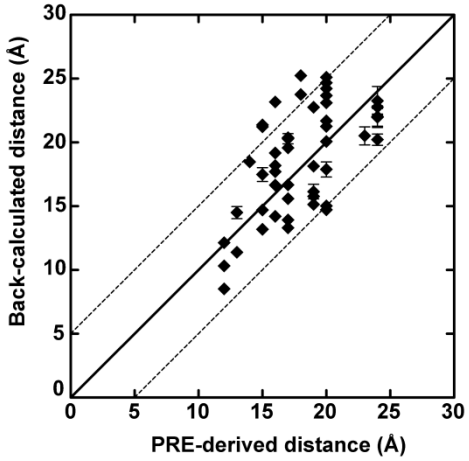

Figure 3.S3 Violation analysis of the NMR model of IsdH$^{N2N3(Y642A)}$ determined from the two-step calculation procedure

Correlation plot for all inter-domain attractive (I_{ox}/I_{red} < 0.8) PRE-derived distance restraints used to model the intact Hb-free receptor. Dashed lines indicate ± 5 Å error bounds for the PRE-derived distance data. The standard deviation of the back calculated distances of the top 20 lowest energy individual simulated annealing structures are shown in error bars. The 8 systematic violations originating to the N2 domain are shown as outliers and are from the following restraints: R363R1- F555, R363R1-E562, R363R1-V628, R363R1-R649, E511R1-H344, E511R1-T376, E559R1-M356, and E559R1-G362.

Chapter 4

The *S. aureus* IsdH Protein Accelerates Hemin Release from the α-Subunit of the Hemoglobin Tetramer by at least 10,000-fold

The work described in this chapter is a version of a manuscript to be submitted for publication.

Sjodt, M., Macdonald, R., Marshall, J.D., Phillips, M., Olson, J. S., & Clubb, R. T. 2016.

I was the primary author of this work. I designed the experiments, performed the biochemical assays, and analyzed data.

4.1 Overview

Staphylococcus aureus is a Gram-positive pathogen that during infections actively acquires iron from human hemoglobin (Hb) using two iron-regulated surface determinant (Isd) proteins, IsdH and IsdB. These receptors use a conserved tri-domain unit consisting of two NEAr iron Transporter (NEAT) domains connected by a helical linker domain to capture Hb and rapidly extract it hemin (oxidized form of heme). Previous studies have shown that IsdH's tri-domain unit ($IsdH^{N2N3}$, residues A326-D660) accelerates the rate of hemin release from Hb. However, these studies only described the overall hemin extraction process as Hb adopts various quaternary states that have different propensities to release hemin. We therefore developed a novel quantitative hemin transfer assay to probe the kinetic and thermodynamic determinants of hemin extraction. Utilization of a recombinant stabilized Hb tetramer (Hb0.1) and an α-globin specific $IsdH^{N2N3}$ receptor (α-IsdH) provided the selective measurement of hemin release from only the α-subunit of tetrameric Hb. Using a combination of analytical ultracentrifugation, stopped flow UV-Vis, and ITC methods, our studies reveal that α-IsdH accelerates the rate of hemin release from the α-subunit by least 10,000-fold, corresponding to an activation energy that is lowered by ~6 kcal/mol. Furthermore, direct hemin transfer from the β-subunit to wild-type $IsdH^{N2N3}$ was observed for the first time, illustrating the wild-type $IsdH^{N2N3}$ binds both α- and β-subunits and actively extracts their hemin. Additionally, Hb binding studies reveal that $IsdH^{N2N3}$ recognizes Hb via two energetically distinct interfaces. The first interface (N2-Hb) is an enthalpically favorable high affinity interface that presumably allows the receptor to maintain overall binding affinity so that the low affinity enthalpically unfavorable (LN3-Hb) interface can form. Moreover, the enthalpic penalty associated with the formation of the LN3-Hb interface is compatible with the receptor unwinding the iron-coordinating F-helix in Hb.

4.2 Introduction

Staphylococcus aureus is an opportunistic Gram-positive pathogen that causes a wide range of illnesses such as pneumonia, meningitis, endocarditis, toxic shock syndrome, bacteria, and septicemia [1]. Strains of *S. aureus* that are resistant to β-lactam antibiotics are not only a leading cause of life-threatening hospital-acquired infections, but have also become commonplace within communities [2,3]. Therefore, understanding the molecular mechanisms this microbe uses to survive and persist within the human host is a critical step in developing anti-infective treatments to counteract its virulence. Like most microorganisms, *S. aureus* requires micromolar (10^{-6} M) levels of iron in order to proliferate because this element functions as a key biocatalyst in microbial metabolism processes [4,5]. However, nutritional immunity mechanisms within its host limit microbial access to iron by sequestering it intracellularly through binding to proteins such as hemoglobin and ferritin, as well as extracellularly by being bound to proteins such as hemopexin and transferrin. Therefore, free iron is scarce in the human body and must be actively procured by *S. aureus* in order for it to successfully mount an infection [6,7]. Heme (protoporphyrin IX + iron) bound to hemoglobin (Hb) accounts for the ~75-80% of the total iron found in the human body and is preferentially used by *S. aureus* as an iron source [8,9]. Consequently, *S. aureus* and other microbial pathogens have evolved elaborate heme-acquisition systems to take advantage of this rich iron source.

S. aureus uses the iron-regulated surface determinant (Isd) system to extract the oxidized form of heme from Hb (hereafter called hemin). It is comprised of nine proteins that form a hemin relay system that captures Hb and rapidly extracts its hemin, transfers hemin across the cell wall, and then pumps the hemin into the cytoplasm where it is degraded to release free iron [10–12]. Four Isd proteins (IsdA, IsdB, IsdC, and IsdH/HarA) are covalently linked to the

bacterial cell wall via sortase transpeptidases [13,14]. The two surface receptor proteins, IsdH and IsdB, first bind Hb and extract its hemin [15–19]. Then the hemin is passed to IsdA, which is partially buried in the cell wall [20]. Holo-IsdA subsequently transfers hemin to the fully buried IsdC protein via an ultra-weak handclasp complex [21–24]. Lastly, holo-IsdC delivers the hemin to the bacterial ABC transporter complex, IsdDEF, which pumps hemin into the cytoplasm to be degraded by the hemin oxygenases, IsdG or IsdI, which liberate the iron for the microbe to use [25,26]. The Isd system is important for *S. aureus* virulence, as strains lacking genes within this system displayed attenuated infectivity in mice compared to wild-type strains and were also incapable of utilizing hemin or Hb as the sole source of iron [9,13,27–29]. Systems related to Isd are also used by other microbes to extract hemin.

Extraction of hemin from the oxidized form of Hb (called methemoglobin, MetHb) is mediated by the related IsdB and IsdH receptors [17,18,30–33]. They have similar primary sequences and contain NEAr iron Transporter (NEAT) domains, binding modules originally named because they were found in bacterial genes that are proximal to putative Fe^{3+} siderophore transporter genes [34]. Our studies of IsdH have shown that hemin extraction is mediated by a tri-domain unit that contains the second (N2) and third (N3) NEAT domains that are connected by a helical linker domain ($IsdH^{N2N3}$, residues A326-D660) (**Figure 4.1a**). Studies using native MetHb have shown that this unit captures hemin from MetHb ~500-fold faster than the rate at which hemin spontaneously dissociates from MetHb, suggesting that hemin release is triggered by an activated protein-protein complex. IsdB shares a functionally similar tri-domain unit that likely operates via a similar mechanism as less extensive studies have shown that is extracts hemin from MetHb at a comparable rate as $IsdH^{N2N3}$ [18,24,30,35].

Recent NMR and crystallography studies of the Hb-free and –bound states have provided insight into how IsdH promotes hemin release [31–33]. A low resolution (4.2Å) crystal structure of the complex revealed that the $IsdH^{N2N3}$ receptor can bind to each of the four globin chains within tetrameric MetHb. Each receptor adopts an extended dumbbell shape structure in which the N2 domain engages the A- and E-helices of MetHb, while the N3 domain is positioned within 12 Å of the hemin molecule of the same globin chain. This structure revealed the overall mode of binding, but left mechanistic details elusive. Subsequently, a higher resolution (2.6 Å) crystal structure of the MetHb-$IsdH^{N2N3}$ complex in which the IsdH protein was engineered to eliminate binding to the β-subunit revealed that the helical linker domain in the receptor distorted the F-helix in Hb that houses the iron-coordinating proximal histidine residue (HF8). The F-helix is partially unwound, suggesting that the receptor promotes hemin release by either weakening and/or exposing the HF8-iron bond to the solvent for hydrolysis. NMR studies of the apo-receptor uncovered the presence of inter-domain mobility between the N2 and linker domains, revealing that the receptor adaptively recognizes Hb through a combination of conformational selection and induced fit mechanisms.

We are lacking a quantitative understanding of the kinetics and thermodynamics that underlie hemin extraction. This is because several features of the transfer have thus far limited detailed biophysical characterization. First, MetHb can adopt distinct quaternary states that have different propensities to release hemin. This has prevented the accurate quantification of the transfer kinetics because MetHb adopts both tetrameric and dimeric states at concentrations typically used in stopped-flow UV-visible spectroscopy experiments [36,37]. Second, the α- and β-globin chains have distinct penchants for releasing hemin [38,39]. Thus, the measured rates of hemin transfer using native MetHb are an amalgamation of these distinct rates. Moreover, the

issue is further complicated by the fact that hemin release from one globin chain in the MetHb dimer or tetramer is known to increase the rate at which hemin is released from the remaining globin chains [40]. Finally, hemin release from the globin chains within the tetramer can cause MetHb to dissociate into its component globin chains, which can irreversibly aggregate [40,41]. As a result of these obstacles, all reported kinetics data only describe the overall process of hemin removal, and do not provide information about the rate at which hemin is removed from each globin chain when MetHb is in a defined oligomerization state. These have prevented a quantitative understanding of the energetics and kinetics underlying hemin extraction.

We have developed a novel quantitative assay that selectively monitors the kinetics of receptor-mediated hemin removal from only the α-globin chain of tetrameric MetHb. Using stopped-flow UV-vis spectroscopy, ultracentrifugation, and ITC experiments we demonstrate that IsdH accelerates the rate of hemin release from the α-subunit of tetrameric MetHb by at least 10,000-fold, significantly faster that previously reported measurements that were complicated by MetHb dissociation and hemin removal from the β-chain. Measurements of the activation energies of hemin transfer suggest that the enthalpic barrier required to hydrolyze the HF8-iron bond is the primary factor limiting hemin release from the α-subunit. Quantitative measurements of the Hb-receptor binding interactions, reveals that two molecular interfaces are needed to distort α-subunit to release its hemin. An interface between the N2 domain the A-helix of Hb is the primary contributor to overall binding affinity, and tethers the receptor to Hb enabling a very low affinity interaction between linker-N3 domains and the F-helix that contacts the hemin. Thermodynamic measurements of the binding energies indicate that interactions at the latter interface are enthalpically unfavorable, consistent with the notion that the receptor unwinds the F-helix to release hemin. Additionally, data is also presented that the shows the

receptor actively extracts hemin from the β-subunit. A model of the hemin extraction process is presented that incorporates the existing structural, kinetics and thermodynamic binding data.

4.3 Results

4.3.1 Development of a quantitative assay to probe hemin extraction

We developed an assay to quantitatively probe the kinetics of hemin transfer to the receptor from the α-globin chain within tetrameric MetHb. Two reagents are used in the assay. First, we constructed a mutant of $IsdH^{N2N3}$ that only binds to the α-subunit of Hb (α-IsdH, residues A326-D660, with ^{365}FYHYA^{369} → ^{365}YYHYF^{369} mutations). α-IsdH contains F365Y and A369F mutations in the 3_{10}-helix of the Hb binding N2 domain (**Figure 4.1b**). These mutations do not affect hemin binding or the structure of the receptor, but have previously been shown by the Gel group to selectively weaken the receptor's affinity for the β-subunit in Hb [33]. Second, we employed a recombinant form of Hb in which its two α-subunits are connected to one another to stabilize its tetrameric quaternary state. The subunits are connected by expressing them as a single polypeptide in which the C-terminus of one subunit is joined via a glycine residue to the N-terminus of the second subunit. This form of recombinant Hb (called Hb0.1) also contains a V1M mutation to facilitate expression in *E. coli*, but is otherwise structurally and functionally identical to native Hb and has a reduced propensity to dissociate into dimers [37,42].

We initially performed a series of control experiments to ensure that the Hb0.1 and α-IsdH protein reagents enable hemin extraction from only the α-subunit in tetrameric Hb to be selectively monitored. First, analytical ultracentrifugation (AUC) sedimentation equilibrium

experiments were performed to define the stoichiometry of the Hb0.1: α-IsdH complex at conditions that are to be used in stopped flow measurements of hemin transfer. To prevent complications caused by hemin transfer in the AUC experiments, Hb0.1 was maintained in its carbonmonoxy ligated state and a hemin binding deficient Y642A mutant of α-IsdH was employed that removes its iron coordinating tyrosine residue in the N3 domain. In the AUC experiments the concentration of hemoglobin is monitored by measuring the absorbance at 412 nm, the Soret band of the bound heme molecule. AUC using only Hb0.1 reveals as expected that it is a stable tetramer; Hb0.1 has a weighted average molecular mass of 64,212 ± 829 Da at 13,000 × *g* when its concentration is 5 μM (hemin units) (**Table 4.1**). Maintenance of its tetrameric state at 5 μM is desirable as native Hb at this concentration is a mixture of dimeric and tetrameric species. Interestingly, when the AUC experiments are repeated with α-IsdH^{Y642A} present at a 15-fold molar excess with respect to Hb0.1, a new complex forms that has an average molecular mass of 140,070 ± 2096 Da when the samples are centrifuged at 6,000 × *g* (a mass of 131,570 ± 894 Da is obtained when centrifuged at 13,000 × *g*). This data indicates that ~1.8 α-IsdH^{Y642A} receptors bind to each Hb0.1 tetramer, which is compatible with the receptor binding to only the α-subunits. Increasing the ratio of α-IsdH^{Y642A} to Hb0.1 to 30:1 did not increase this stoichiometry, indicating that Hb is saturated (**Figure 4.2a, red curve**). In contrast, an IsdH receptor that does not contain alterations in its Hb contacting 3_{10}-helix binds Hb0.1 at a ~3.2 stoichiometry, consistent with it being capable of binding to both the α- and β-subunits. This was demonstrated by monitoring receptor binding to Hb0.1 using IsdH^{Y642A}, which is identical to the wild-type IsdH protein, but contains a single amino acid change in its N3 domain that disrupts hemin binding. As shown in **Figure 4.2a**, AUC studies using a ratio of 1:30 Hb0.1: IsdH^{Y642A} reveal the proteins form a complex with molecular mass of 188,110 ± 1,518 Da at

6,000 × *g* or 175,120 ± 1045 Da at 13,000 × *g*, that is compatible with ~3.2 IsdH receptors bound one Hb0.1 tetramer. In principle, the ~1.8 finding stoichiometry observed for the α-IsdH^{Y642A}:Hb0.1 complex could result from α-IsdH^{Y642A} binding to the β-subunit of hemoglobin (Met-β). To test for this possibility, receptor binding to isolated β-globin chains was examined by AUC (**Figure 4.2b**). In isolation, hemin bound β-globin chains have been shown to primarily adopt a tetrameric structure; the tetramer-monomer equilibrium constant is 1.25×10^{-12} M^3 at pH 7 ($K_{4,1}$) [37,43]. Our AUC studies are consistent with these findings as the isolated β-globin chains have a molecular mass of 56,700 ± 724 Da at 6000 × *g* (56,300 ± 508 Da at 13,000 × *g*). Interestingly, when the AUC studies are repeated with excess IsdH^{Y642A} present, the receptor binds tetrameric β-subunit to form a complex in which ~2.0 IsdH^{Y642A} receptors are bound to each β-tetramer (molecular mass of 134,000 ± 1321 Da at 6000 × *g*). However, when similar experiments are performed using α-IsdH^{Y642A} no detectable binding is observed. Overall, these AUC results indicate that the α-IsdH^{Y642A} receptor only binds to the α-subunits within Hb0.1 and that both of these subunits are nearly saturated with the receptor when the proteins are present at a ratio of 15:1 α-IsdH^{Y642A}:Hb0.1. Data summarizing the results of the AUC experiments is presented in **Table 4.1.**

4.3.2 Stabilization of the Hb tetramer slows the rate of hemin capture from the α-subunit

It is well known that as hemin dissociates from the individual subunits within the hemoglobin tetramer, the rate of hemin release from the remaining subunits increases. The rate

acceleration is thought to be caused by two factors: irreversible tetramer dissociation into its component globin subunits that more rapidly release hemin, and the increased rate of hemin release from the semi-forms of tetrameric and dimeric Hb species. These effects greatly complicate kinetics measurements and are the reason why the quantitative assay was developed. To investigate the importance of tetramer dissociation on hemin transfer, stopped flow UV-Vis spectroscopy experiments were performed to measure the rate at which α-IsdH extracted hemin from either native MetHb or the stabilized MetHb0.1 tetramer. In these studies, the proteins were rapidly mixed with one another, and the amount of hemin transfer was determined by monitoring UV absorbance changes at 405 nm as previously described in detail. In the experiments, a 30-fold molar excess of receptor was employed (5 and 150 μM MetHb and receptor, respectively), to ensure that α-IsdH bound to both of the α-globin chains. Upon mixing MetHb0.1 with excess apo-α-IsdH, a rapid shift in the UV-spectrum occurs indicating hemin transfer from MetHb0.1 to the receptor (**Figure 4.3a**). Plotting the time-dependent spectral changes at 405 nm reveals (**Figure 4.3b**) that the transfer reaction exhibits biphasic kinetics, with half the magnitude of the total spectral change characterized by a rapid event defined by the k_{fast} rate constant and the remaining slower changes defined by a k_{slow} rate constant (**Figure 4.3b-d**). Importantly, hemin transfer is completed during the time course of the stopped flow experiment, as no significant spectral changes are observed when the proteins are incubated overnight. As the receptor is in excess and has higher affinity for hemin than hemoglobin (described below), we conclude that all of the hemin in hemoglobin has been captured by the receptor. The observed pseudo-first-order rate constants, k_{fast} and k_{slow} are 0.34 ± 0.01 s^{-1} and 0.026 ± 0.001 s^{-1}, respectively (**Table 4.2**). As α-IsdH only binds to the α-subunits of the stabilized Hb0.1 tetramer, we conclude that the rapid changes characterized by k_{fast} describe hemin removal from the α-subunit within

tetrameric Hb0.1, and that the slower changes result from hemin release from the β-subunit into the solvent, followed by subsequent binding to excess receptor present in solution. The kinetics of this slower phase are consistent with this hypothesis, as the β-subunit is known to spontaneously release hemin into solvent with a rate constant of ~0.013 s^{-1} after hemin has been removed from the α-subunit of the tetramer [37,40]. To investigate the effects of Hb tetramerization on the kinetics of extraction, we performed similar experiments using native MetHb, which is known to dissociate into its component globin chains after hemin is removed. Interestingly, native MetHb loses hemin to the receptor much faster, with k_{fast} and k_{slow} rate constants of 3.27 ± 0.07 s^{-1} and 0.041 ± 0.001 s^{-1}, respectively. We conclude that the increase in k_{fast} is caused by α-IsdH binding to monomeric α-globin chains produced as a result of tetramer dissociation; the monomers have weaker affinity for hemin. Interestingly, increases in k_{slow} are also observed and are presumably caused by rapid hemin release from the β-subunits that are produced as a result of tetramer dissociation, as the isolated β-subunits are known to release hemin more rapidly than β-subunits that are located in tetrameric hemoglobin [37].

Tetramer dissociation also increases the rate of hemin transfer to the native IsdH receptor that binds to both the α- and β-subunits of Hb. This was demonstrated by determining the ability of wild-type IsdH to remove hemin from either native MetHb or the stabilized MetHb0.1 tetramer. As with α-IsdH, significantly slower kinetics are observed for hemin removal from MetHb0.1 as compared to MetHb. This is consistent with the reduced propensity of MetHb0.1 to dissociate into dimeric and monomeric species that release hemin more rapidly. Interestingly, both the fast and slow phases of hemin transfer to IsdH from the stabilized MetHb0.1 tetramer occur more rapidly than transfer to α-IsdH (k_{fast} and k_{slow} values of 0.73 ± 0.03 s^{-1} and 0.038 ± 0.001 s^{-1}, respectively). As IsdH can also bind to β-subunits of the stabilized tetramer, it seems

possible that its larger k_{fast} and k_{slow} rate constants are caused by the increased rate of hemin transfer from the semi-forms of Hb that are produced as hemin is removed. This is because it is known that hemin removal from the α-subunit increases the rate of hemin loss from the β-subunit up to 3-fold, raising the possibility that IsdH bound to the β-subunit could more rapidly acquire its hemin once hemin has been lost from an adjacent α-subunit. Similar rate enhancements are observed for the α-subunit when hemin is first removed from the β-subunit. Combined, this data indicates that the propensity of Hb to dissociate during the extraction process increases the overall observed rate of transfer to the receptor by producing partially ligated states or dissociated forms of hemoglobin that have a greater predisposition to release their hemin molecules. Taken together, the results from the ultracentrifugation and stopped flow hemin transfer experiments clearly show that utilization of the stabilized Hb0.1 tetramer and alpha globin specific α–IsdH receptor enables the selective measurement of hemin removal from only the α-subunit of tetrameric Hb.

4.3.3 IsdH also accelerates the rate of hemin release from the β-subunit.

The ability of α-IsdH to rapidly remove hemin from Hb0.1 indicates that receptor can capture hemin from the α-subunit, but it has never been conclusively demonstrated that the receptor can also actively extract hemin from the β-subunit. In principle, it is possible that the receptor only actively extracts hemin from the α-subunit, whereas hemin loss from the β-subunit occurs subsequently from dissociated and semi-forms of hemoglobin. In order to investigate this issue, we determined the ability of the receptor to remove hemin from tetrameric Met-β, which only contains β-globin chains bound to hemin (**Table 4.1**). Initially, to probe the rate at which it

spontaneously releases hemin into the solvent, we initially mixed Metβ with recombinant H64Y/V68F apo-myoglobin (apo-Mb containing H64Y and V68F mutations) [40]. Apo-Mb does not physically interact with Metβ and undergoes unique absorbance changes that can be used to monitor hemin release by a hemoprotein. As shown in **Figure 4.4**, when 5 μM Metβ is mixed with excess apo-Mb only modest spectral changes are observed after 10 s. This indicates that apo-Mb does not actively remove hemin from Metβ and that Metβ does not rapidly release hemin into the solvent. In contrast, addition of IsdH to Metβ causes rapid changes in absorbance at 408 nm within the first 5 s of the experiment, indicating that hemin is being transferred from Metβ to IsdH. Furthermore, as expected, when α-IsdH is mixed with Metβ under similar conditions, little or no active transfer is observed as it is incapable of binding to the β-subunit based on the AUC data. It should be noted that in all of the experiments that monitored hemin removal from Metβ, absorbance changes are observed after ~20 s that are compatible with apo-β denaturation, which prevents the quantitative measurement of the extraction kinetics. These results clearly indicate that native IsdH can actively remove hemin from the Metβ, and suggest that it is capable of actively removing hemin from the β-globin chain within human hemoglobin. This ability further highlights the need for assays to selectively monitor hemin removal from specific globin chains. Data summarizing the results of the stopped flow experiments are presented in **Table 4.2.**

4.3.4 The IsdH receptor has a higher affinity for hemin than hemoglobin

Towards the goal of defining the micro rate constants that describe the hemin transfer process, we determined the relative hemin affinities of the IsdH receptor and MetHb. Hemin

binding competition studies were performed using the apo-Mb reagent, which has a known affinity for hemin and whose binding to this ligand can readily be measured at 600 nm. Mixing of either 5 μM MetHb or MetHb0.1 with a 10-fold molar excess of apo-Mb results in a measurable increase in absorbance at 600 nm indicating that hemin is transferred to apo-Mb (**Figure 4.5a**). Transfer from MetHb or MetHb0.1 occurs very slowly, compatible with hemin first being released into the solvent before it is bound by apo-Mb. This transfer data is compatible with the previously published hemin dissociation constants (K_{-H}) of MetHb and apo-Mb. In particular, the K_{-H} of apo-Mb is ~0.03 pM, which ~50-1,400x smaller than the K_{-H} of dimeric MetHb (1.7 and 42 pM for α and β chains, respectively), and it is ~25-140x smaller than K_{-H} of tetrameric MetHb (0.8 and 4.2 pM for α and β chains, respectively) [37]. Notably, the stabilized tetramer MetHb0.1 releases hemin more slowly than MetHb. This is consistent with previous studies that have shown that the tetrameric form of MetHb releases hemin more slowly than the dimeric form, and with the fact that MetHb0.1 is predominately tetrameric, whereas MetHb is a mixture of dimeric and tetrameric forms; at the 5 μM hemoglobin concentrations used in this study, ~65% of MetHb is tetrameric and ~35% is dimeric ($K_{4,2}$ of 1.5 μM) [37]. Interestingly, similar experiments using apo-Mb and hemin-saturated IsdH reveal that the receptor transfers little hemin to apo-Mb, indicating that, unlike Hb and Hb0.1, the receptor has higher affinity for hemin than apo-Mb. Moreover, α-IsdH also did not transfer its hemin to apo-Mb, indicating that mutations in the hemoglobin binding domain do not affect its hemin affinity (data not shown). Taken together, we conclude that IsdH and α-IsdH bind hemin with K_{-H} values < ~0.03 pM, such that they have substantially higher affinity for hemin than MetHb. Therefore, during the time-frame of the stopped flow experiments used to study the transfer reaction, transfer of hemin from hemoglobin to the receptor is effectively irreversible.

4.3.5 Kinetic Scheme Describing Hemin Transfer from Hb0.1 to α-IsdH

The ability to measure the kinetics of hemin removal from only the α-globin subunit in tetrameric Hb0.1 enables micro rate constants to be quantitatively measured for the first time. Based on the stopped flow and AUC results, it is possible to model the hemin transfer reaction as described in Scheme I. In the model, hemin-bound Hb0.1 forms a complex with apo-α-IsdH described by the association and dissociation rate constants, k_1 and k_{-1}. Within this complex hemin is then transferred from the α-subunit of tetrameric Hb0.1 to α-IsdH in a process described by the rate constant k_{trans}. This yields a semi-form of Hb0.1 in which one hemin molecule has been removed and the protein remains bound to holo-α-IsdH. At the conditions used in our stopped flow experiments, the measurable rate constant k_{fast} describes the kinetics of this entire process and accounts for the simultaneous removal of hemin from both α-subunits. This is consistent with the stopped flow data, as half of the overall spectral change is described by k_{fast}, which corresponds to hemin removal from the two globin chains within the tetramer.

$$\text{Hb[hemin]} + {}^{\alpha}\text{IsdH} \underset{k_{-1}}{\overset{k_1}{\rightleftharpoons}} \text{Hb[hemin]:}{}^{\alpha}\text{IsdH} \xrightarrow{k_{trans}} \text{Hb:}{}^{\alpha}\text{IsdH[hemin]}$$

Scheme I

To determine the micro rate constants, the kinetics of hemin transfer was measured for a series of reactions that contained 5 μM Hb0.1 and varying concentrations of apo-α-IsdH. At all receptor:Hb0.1 stoichiometries, k_{fast} accounted for ~50% of the total spectral change consistent with it monitoring team removal from the α-subunit only (**Figure 4.3b**), and k_{fast} increased

hyperbolically with increasing receptor concentrations (**Figure 4.5b, dark grey circles**). This is compatible with the rapid formation of a Hb:apo-α-IsdH complex followed by a rate-limiting transfer of the hemin to the receptor. In the hemin transfer experiments, apo-α-IsdH has a concentration more than ten times higher than the concentration of Hb0.1], such that the rate of hemin transfer is pseudo-first-order. The dependence of k_{fast} on the micro rate constants and receptor concentration can therefore be described by Equation 1 [44],

$$k_{fast} = \frac{k_1 k_{trans}[\alpha\text{−IsdH}]}{k_1[\alpha\text{−IsdH}] + k_{-1} + k_{trans}} \quad (1)$$

where k_1, k_{-1}, and k_{trans} are the micro rate constants of the individual reaction steps in Scheme I. As shown in **Figure 4.5b**, fitting of the kinetics data using Eq. 1, yields values of $2.81 \times 10^7 \pm 0.01$ $M^{-1}\cdot s^{-1}$, $2.41\times10^3 \pm 0.11$ s^{-1}, and 0.57 ± 0.02 s^{-1} for k_1, k_{-1}, and k_{trans}, respectively. The equilibrium dissociation constant (K_D) of the Hb0.1:apo-α-IsdH transfer complex calculated from the micro rate constants is 85.7 ± 3.8 μM, a value that is consistent with dissociation constants obtained using isothermal calorimetry (described below). Interestingly, measurement of k_{slow} reveals that it is independent of the receptor concentration under pseudo-first order conditions (**Figure 4.5b, light grey circles)**. This observation further supports the notion that k_{slow} describes the non-specific release of hemin from the β-globin chain into the solvent followed by hemin uptake by excess apo-α-IsdH.

4.3.6 An enthalpic barrier slows the rate of hemin transfer

To gain insight into the energetic barrier that the receptor must surmount in order to trigger hemin release from hemoglobin, we estimated the activation energy parameters using the Eyring equation. Stopped flow experiments were performed at temperatures ranging from 15 to 37°C using a molar ratio of 1:40 Hb0.1:apo-α-IsdH (**Figure 4.6a).** At this Hb:receptor ratio the contribution of k_1, k_{-1} to the measured k_{fast} rate constant becomes negligible, thus $k_{fast} \approx k_{trans}$ [44]. A plot of $\ln(k_{trans}/T)$ versus 1/T enables the activation parameters to be determined (**Figure 4.6b**) using the linearized form of the Eyring equation,

$$ln\frac{k}{T} = ln\left(\frac{k_B}{h}\right) + \frac{\Delta S^{\ddagger}}{R} - \frac{\Delta H^{\ddagger}}{RT} \quad (2)$$

where k_B, h, and R are the Boltzman, Planck, and ideal gas constants, respectively. The activation enthalpy ($\Delta H^{\ddagger}$) and entropy ($\Delta S^{\ddagger}$) are calculated from slope and intercept, respectively (**Figure 4.6b)**. The overall activation energy, $\Delta G^{\ddagger}$, is then calculated from $\Delta G^{\ddagger} = \Delta H^{\ddagger} - T\Delta S^{\ddagger}$. This analysis yielded $\Delta H^{\ddagger}$ and $S^{\ddagger}$ values of 19.45 ± 1.1 kcal/mol and 4.45 ± 0.31 cal/mol·K, respectively, and a $\Delta G^{\ddagger}$ value of 18.07 ± 1.1 kcal/mol at 37°C (**Table 4.3**). The measured activation free energy associated with hemin transfer from hemoglobin to the receptor is of similar magnitude to previously reported energetic barrier associated with the cleavage of the proximal histidine-heme (Nε-Fe) bond in hemoglobin (~17 kcal/mol) [45]. This suggests that a similar barrier may exist in the process of receptor-mediated hemin extraction from the α-subunit of hemoglobin. This is compatible with the finding that $\Delta H^{\ddagger}$ is the main contributor to the

activation energy describing hemin transfer, as there is presumably a large enthalpic penalty associated with breaking the bond to the metal.

Quantitative measurement of k_{trans} enables an estimate of how much the receptor reduces the activation energy associated with removing hemin from hemoglobin. Previous studies have shown that hemin dissociates from the α-globin chain of tetrameric Hb at a rate of 0.000083 s^{-1} [37]. Based on a modified version of the Arrhenius equation, the free energy of activation associated with spontaneous hemin release is described by,

$$\Delta G^{\ddagger} = -RTln\left(\frac{hk}{k_B T}\right) \quad (3)$$

where k_B, h, and R are the Boltzman, Planck and ideal gas constants, respectively, k is the rate constant and T is the temperature. This indicates that the $\Delta G^{\ddagger}$ of spontaneous hemin release is 23.96 kcal/mol at 37°C. Measurements of k_{trans} indicates that the receptor accelerates the rate of hemin release from the α-subunit at least 10,000-fold (k_{fast} = 0.88 s^{-1} vs. 0.000083 s^{-1} at 37°C). Thus, the receptor lowers the activation energy by 5.9 kcal/mol. How the receptor reduces the activation energy is not known, but could result from receptor-mediated distortions of hemoglobin that weaken the strength of the axial bond to iron.

4.3.7 Residues in the linker domain contribute to the accelerated rate of hemin release

In order to gain insight into the molecular mechanism of hemin extraction, the newly developed hemin transfer assay was used to measure the extraction kinetics of several receptor

mutants. Working with our collaborators, we have previously shown that residues in the helical linker domain of IsdH interact with the F-helix in Hb that coordinates the metal in heme [31,33] (**Figure 4.7b**). The interactions distort the F-helix which contains the iron-coordinating proximal histidine residue H87 (HF8). We therefore made several amino acid mutants of the receptor that altered residues at this interface and measured their ability to extract hemin from hemoglobin. These amino acid mutants included Y495A and K499A alterations that disrupted specific linker domain-F-helix interactions and a double Y495A/K499A mutant. In addition, a mutant receptor containing seven alterations in the linker domain was investigated. As shown in **Figure 4.7c and d**, the single amino acid Y495A and K499A are able to capture hemin nearly as well as the wild-type receptor, as they have k_{fast} values that are only ~3 and ~2 times slower than α-IsdH, respectively. The double alanine Y495A/K499A substitution exhibits a more pronounced ~5-fold reduction in k_{fast}. Interestingly, mutation of these residues does not abolish rapid hemin extraction, which might be expected if they were major contributors in the triggering of hemin release. We therefore tested a mutant receptor in which less conservative changes are made. Based on our modeling previous studies using the NMR structure of apo-IsdH, seven residues in the linker domain were postulated to interact with Hb's F-helix. We therefore constructed a mutant, termed 7-Ala, that changes these residues to alanine (7-Ala, is $IsdH^{N2N3}$ containing K479A, K486A, R492A, Y495A, E496A, K499A, and K503A mutations) [31]. Interestingly, the 7-Ala mutant captures hemin from Hb0.1 ~12-fold slower than α-IsdH. As 7-Ala is folded based on NMR studies (data not shown), this preliminary data suggests that several residues in the linker domain play an important role in promoting the release of hemin from hemoglobin. However, since the mutant can still rapidly capture hemin, receptor residues outside this contact

interface must also be important (discussed later). A more extensive analysis of the impact of these mutations on the activation energy of hemin transfer will be performed in the future.

4.3.8 Two energetically distinct receptor-hemoglobin interfaces promote hemin release

Using the crystal and NMR structural data as a guide, we measured the energetics associated with receptor binding to hemoglobin using ITC. The structure of the Hb-receptor complex and NMR dynamics data suggests that the receptor interacts with Hb via two distinct interfaces. The N2 domain binds to the A-helix of Hb, while the linker and N3 domains form a rigid unit that interacts with the F-helix of the same globin chain (**Figure 4.7a**). Previous studies have shown that the N2 domain can be studied in isolation. We therefore rigorously characterized the binding of the intact receptor and a polypeptide fragment containing only the N2 domain. Binding was measured by ITC to obtain estimates of the thermodynamic parameters. As with the AUC experiments, the carbonmonoxy form of Hb was used to prevent hemin transfer during the experiment. In addition, a Y642A mutation in α-IsdH^{Y642A} mutant of the receptor was employed that is incapable of binding hemin. In the ITC experiments, a syringe filled with 200 μM α-IsdH^{Y642A} was injected incrementally into a cell containing 30 μM of HbCO and the ensuing heat changes were recorded. A representative binding isotherm is shown in **Figure 4.8a**, which was fit using ORIGIN software. This analysis yields the dissociation constant and the stoichiometry of complex formation. Consistent with the AUC studies of the complex, α-IsdH^{Y642A} binds Hb at a ratio of ~2:1. The measured K_D value for the Hb:α-IsdH^{Y642A} complex is 4.6 ± 0.8 μM and has a similar order of magnitude as the value obtained from an analysis of the kinetics data (K_D = 85.7 ± 3.8 μM). At 25^{o}C, the enthalpy (ΔH^o) and

entropy (ΔS^o) of receptor binding are -5.6 ± 0.5 kcal/mol and 5.6 ± 2.0 cal/mol·deg, respectively (ΔG^o -7.3 ± 0.1 kcal/mol). Notably, the α-IsdH^{Y642A} receptor binds to tetrameric Hb0.1 with similar overall affinity K_D = 5.3 ± 1.4 μM (ΔG^o = -7.2 ± 0.2 kcal/mol), and similar enthalpic and entropic binding energies, ΔH^o = -8.4 ± 0.3 kcal/mol and ΔS^o = -3.9 ± 0.4 cal/mol·deg. This suggests that the receptor binds to the tetrameric and dimeric forms of hemoglobin in a similar manner. In order to selectively probe binding by the N2 domain to hemoglobin, a polypeptide containing only the N2 domain of α-IsdH with the appropriate amino acid mutations that confer binding selectivity for the α-globin chain was studied (α-IsdH^{N2}, residues A326-P466 of α-IsdH) (**Figure 4.8b**). ITC measurements indicate that α-IsdH^{N2} binds HbCO with high affinity that approaches the affinity of the larger α-IsdH protein that contains the linker and N3 domains, α-IsdH^{N2} binds to HbCO with a K_D of 7.7 ± 1.3 μM and similar ~2:1 stoichiometry. Interestingly, ΔH^o for α-IsdH^{N2} binding is similar to the intact protein (-9.6± 0.5 kcal/mol), whereas the entropy associated with binding is negative compared to the positive entropy of the intact protein (ΔS^o = -8.7 ± 2.7 kcal/mol·deg). The latter affects can presumably be attributed to changes in the 3_{10}-helix, since it has been shown to undergo a disordered to ordered change upon binding to Hb [31,46]. Similar ITC binding studies were performed using a polypeptide that contains only the linker and N3 domains of IsdH (IsdH^{LN3}, residues P466-D660, containing a Y642A mutation in the N3 domain to prevent hemin binding). IsdH^{LN3} binds to HbCO with very weak affinity, which could not be accurately quantified using ITC (**Figure 4.8c**). However, it is evident from this ITC data that IsdH^{LN3} binding is endothermic with unfavorable positive changes in ΔH^o occurring. The weak binding by this fragment of the receptor was further substantiated using NMR spectroscopy (data not shown). These results suggest that contacts at the N2-Hb interface are the primary contributor to the overall binding affinity, even though each interface buries a

similar amount of surface area (the N2-Hb and LN3-Hb interfaces bury 618 and 688 $Å^2$, respectively). Moreover, they reveal that unfavorable enthalpic changes are due to linker and N3 domain binding to the hemin pocket on the α-subunits, which is compatible with crystallographic data that has shown that the receptor distorts the F-helix. Data summarizing the results of the ITC experiments is presented in **Table 4.3.**

4.5 Discussion

To successfully establish an infection, *S. aureus* acquires iron from the human host using two surface receptors, IsdH and IsdB, which capture hemoglobin (Hb) and rapidly extract its hemin (oxidized form of heme). The receptors share a conserved tri-domain unit consisting of two NEAr iron Transporter domains (NEAT) connected by a helical linker domain (**Figure 4.1a**). The tri-domain unit in IsdH consists of the second (N2) and third (N3) domains that bind distinct ligands ($IsdH^{N2N3}$); the N2 domain binds Hb and the N3 domain binds with hemin. Previously we've shown that the domains within $IsdH^{N2N3}$ work synergistically to extract hemin from Hb at an accelerated rate compared to the spontaneous rate Hb releases hemin into the solvent. However, these results only describe the overall process of hemin removal as Hb is known to adopt various quaternary states that have different propensities to release hemin. We therefore developed a novel quantitative hemin transfer assay to selectively monitor hemin extraction from only the α-subunit of tetrameric Hb. Two reagents were employed in this assay. The first is a stabilized tetramer of Hb (Hb0.1) where both α-globin chains are expressed as a single polypeptide with a glycine residue connecting the C-terminus of one subunit and the N-terminus of the other [42]. The second reagent is a version of $IsdH^{N2N3}$ that only binds the α-

subunit of Hb (α-IsdH) where two interfacial residues in the N2 domain were mutated to selectively remove binding to the β-globin chain [33]. Analytical ultracentrifugation (AUC) experiments confirmed that at the conditions used for quantitative hemin transfer measurements, α-IsdH binds only the α-subunits of tetrameric Hb0.1 (**Figure 4.2 and Table 4.1**). Stopped flow UV-Vis kinetic experiments reveal that α-IsdH captures hemin from MetHb0.1 in a biphasic manner in which the fast phase, k_{fast}, accounts for half the magnitude of the total spectral change and describes the active removal of hemin from the α-subunit. Conversely, the slow phase, k_{slow}, depicts the non-specific release of hemin from the β–subunit followed by subsequent uptake of hemin by excess apo-receptor present in solution (**Figure 4.3**). These experiments also illustrated that stabilization of the Hb tetramer reduces the rate of hemin release, as similar studies with α-IsdH and native MetHb display hemin transfer rates that are ~10-fold faster than MetHb0.1 (**Table 4.2**). This is presumably due to accelerated release of hemin from α-subunits that are in either in the monomeric or dimeric state as a result of Hb tetramer dissociation, as it is well known that quaternary structure affects the rate of hemin release from Hb's globin chains [37]. This is further substantiated by previous ESI-MS studies, showing that the presence of the IsdH receptor promotes Hb tetramer dissociation [17]. Similar results were obtained for the wild-type IsdH receptor, but its rates were faster than α-IsdH. This is likely due to the fact that wild-type IsdH can bind both α- and β-subunits as shown by AUC (**Figure 4.2**). To that end, we showed for the first time that wild-type IsdH can directly extract hemin from Metβ-globin chains; it was previously unclear if hemin release from the β-subunit was an active process or the accelerated release from dissociated and semi-forms of Hb (**Figure 4.4**).

Establishment of a selective assay for hemin removal from the α-subunit of tetrameric Hb enables for the first time the quantitative measurement of the micro rate constants of the hemin

extraction process. A model of this reaction is presented in Scheme I, in which the apo-α-IsdH receptor associates with Hb to form a Hb:$^{\alpha}$IsdH complex. Within this complex, hemin is transferred unidirectionally to the receptor by a process described by the fast phase of the kinetics (**Figure 4.5b**). The micro rate constants for this process were thereby obtained by fitting the observed k_{fast} values to Eq. 1, which yielded values that are consistent with a rapid association of the receptor:Hb complex, followed by a rate-limiting transfer of hemin prior to complex dissociation. Interestingly, these experiments revealed that k_{slow} values are independent of α-IsdH concentration, further supporting the notion that this rate describes the non-specific hemin release from Metβ-subunits and subsequent uptake of hemin by excess α-IsdH present in solution. Additionally, k_{slow} values are faster but on the same order as the rate of spontaneous hemin release from monomeric β-subunits (0.025 s^{-1} at 25°C vs. 0.011 s^{-1} at 37°C). This is consistent with the widely known elevated rates of spontaneous hemin release from dissociated or semi-globin forms. Interestingly, semi-globins have reduced helical content suggesting the increased rate of spontaneous hemin release is facilitated by localized unfolding of the hemin pocket [40,47].

The energetic barrier that the IsdH receptor overcomes to trigger hemin release from Hb was estimated using our quantitative assay and revealed that an enthalpic component was the largest contributor to the overall activation energy (**Figure 4.6**). Our measurement of $\Delta G^{\ddagger}$ at 37°C is 18.07 ± 1.1 kcal/mol and is similar in magnitude to the published $\Delta G^{\ddagger}$ for the cleavage of the proximal histidine-heme (Nε-Fe) bond in hemoglobin (~17 kcal/mol) [45]. This suggests that the large enthalpic penalty measured in our studies is associated with the breakage of this bond. According to Eq. 3, the activation energy of spontaneous hemin release for the α-subunit of tetrameric Hb is ~24 kcal/mol. Therefore α-IsdH-mediated hemin transfer effectively lowers the

$\Delta G^{\ddagger}$ by ~6 kcal/mol, which is consistent with the 10,000-fold rate enhancement observed in our hemin transfer experiments (k_{fast} = 0.88 s^{-1} vs 0.000083 s^{-1} at 37°C). How the receptor lowers the activation energy is still unclear. However, it is possible that receptor-induced perturbation of Hb's F-helix could weaken the HF8-iron bond. Interestingly, various studies have reported helical fluctuations in globin chains, which govern overall hemin affinity [41,47–51]. Therefore, it is possible that the receptor exploits these fluctuations to stabilize a partially unwound state of the F-helix of Hb. This phenomena is also seen in the mechanism of α-hemoglobin stabilizing protein (AHSP), which promotes autooxidation of α-globin chains by binding to a distal site on the α-chain that causes localized distortions in its F-helix [52–54]. Distortion of the helix could presumably weaken the HF8-iron bond, however our $\Delta G^{\ddagger}$ measurements contain a similar energy barrier as the energy required to cleave the Fe-N_{ε} bond, suggesting additional factors help promote hemin release. It is therefore possible that the receptor triggers hemin release by permitting water ingress into the normally apolar hemin pocket, facilitating hydrolytic cleavage of the bond as water is known to compete with HF8 as a ligand for the Fe(III) hemin moiety [55]. The hemin would then only need to travel ~12 Å to be coordinated by the receptor's N3 domain, whose interface with Hb forms a hydrophobic pathway for the hemin to partition [33]. In support of this notion, hemin transfer kinetics are attenuated in IsdH mutants that lack important interfacial residues in the linker domain that were shown to interact with Hb residues that normally make up a hydrophobic "cage" (**Figure 4.7**). These mutations presumably prevent the linker domain from imparting a perturbed state in the F-helix, therefore causing an increase in the energetic barrier that must be overcome for hemin egress. However, future work is necessary to test this hypothesis.

Isothermal calorimetry studies of Hb binding revealed that IsdH employs two energetically distinct interfaces to promote hemin transfer. These interfaces were visualized by NMR and x-ray crystallography, where the first interface is comprised of the N2 domain that binds the A- and E-helices of Hb (N2-Hb), and the second interface is defined by the linker and N3 domains that interact with F-helix, EF- and FG-corners of Hb (LN3-Hb) (**Figure 4.7a and b**). Interestingly, ITC experiments uncovered that the N2-Hb interface binds Hb with similar affinity as the intact receptor, suggesting that this domain maintains the overall binding affinity of the complex (**Figure 4.8 and Table 4.3**). Conversely, the LN3-Hb interface is a much lower affinity complex and is enthalpically unfavorable, which is likely associated with perturbation of the F-helix. A model of the hemin extraction mechanism based on existing structural, kinetics and thermodynamic binding data is presented in **Figure 4.9**. The relative free energies associated with each step of the reaction define the Y-axis while the reaction coordinate depicting the progress of the transfer reaction is plotted along the X-axis. First, the N2 domain employs inter-domain motions to adaptively recognize Hb. Second, the N2-Hb interface is formed by a high affinity and ethalpically favorable interaction (ΔG^o -7.1 ± 0.1 kcal/mol). IsdH likely maintains its overall binding to Hb via this high affinity N2-Hb interface as the overall free energy of the intact receptor is similar to the energy of the N2-Hb interface alone (ΔG^o -7.3 ± 0.1 kcal/mol). This would allow the linker and N3 domains to form a lower affinity interface with Hb, as ITC results show that the intact receptor displays a ΔH^o value that is increased relative to α-IsdH^{N2} and is likely due to unfavorable enthalpic changes associated with distorting the F-helix (-5.6 ± 0.5 kcal/mol and -9.6 ± 0.1 kcal/mol for the intact receptor and α-IsdH^{N2}, respectively). In principle these two interfaces can form simultaneously, but are presented in a two-step process for simplicity. The rate limiting step is depicted in step 3 and is presumed to be the hydrolytic

cleavage of the proximal histidine-hemin bond (Nε-Fe) as kinetic experiments show that the activation energy of hemin transfer is of similar magnitude as the energy required to cleave this bond. Once hemin is transferred, the hemin-bound receptor dissociates from Hb, which is shown in a two-step process for simplicity but could also happen simultaneously.

Our quantitative hemin transfer assay has provided the first ever insight in the kinetics and thermodynamics of hemin extraction of Hb in a defined quaternary state. Future studies using this assay will further probe the energetics associated with this process. As mutations in the interfacial residues of the linker domain did not prevent the receptor from rapidly acquiring hemin from Hb, it is likely that residues outside of this interface are important in the hemin extraction mechanism. Furthermore, the LN3-Hb interface is also composed of residues in the N3 domain that make contacts with Hb residues and the hemin molecule itself. In particular, E562, V564, and S563 all interact with Q54 (HE3) and Y646 makes contacts with H89 (HFG1), H45(HCE3), and the propionate oxygens of hemin. These residues could therefore help facilitate hemin coordination after the iron-histidine bond is broken.

Lastly, the role of inter-domain dynamics between the N2 and linker-N3 domains likely plays a role in the hemin extraction mechanism. However, it is unclear how this dynamic interface facilitates accelerated hemin release. One possibility is that the receptor uses the plasticity of the N2-LN3 interface to recognize both α- and β-subunits of Hb, which are structurally similar but undergo various transitions in their quaternary state that the receptor would need to recognize. Another prospect is that the high affinity N2-Hb interface tethers the linker and N3 domains with just enough flexibility to increase their effective molarity (M_{eff}) relative to Hb. This would then increase the likelihood of the enthalpically unfavorable LN3-Hb interface to form [56]. The N2-mediated increases in M_{eff} would not only depend on domain-

domain interactions in the receptor but also the length and flexibility of the polypeptide segment that connects the N2 and linker-N3 domains. An interface that is either too long or too short would prevent transient inter-domain interactions from occurring, resulting in a decrease of M_{eff} thus precluding the LN3-Hb interface from forming [57,58]. However, a more rigorous study on the effect of inter-domain mobility on receptor-mediated hemin release will have to be performed to test this theory.

4.5 Materials and Methods

4.5.1 Cloning, Protein Expression, and Purification, and Preparation

The IsdH constructs used in this study were produced from pET-28b-based expression plasmids and initially contained a removable N-terminal hexahistidine-small-ubiquitin-like modifier (SUMO) tag under an inducible promoter to facilitate purification (pHis-SUMO) [59,60]. Plasmids pRM208 encoding for amino acids A326-D660 in IsdH ($IsdH^{N2N3}$), pRM216 encoding for amino acids A326-D660 in IsdH ($IsdH^{N2N3}$) with an alanine substitution of Y642 ($IsdH^{N2N3}$-Y642A), and pMMS322 encoding for amino acids A326-D660 with substitution of FYHYA (365-369) → YYHYF (365-369) (α-$IsdH^{N2N3}$) have been described previously [17,33,61]. The expression plasmids pMMS323 (α-$IsdH^{N2N3}$-Y642A), pMMS327 (α-$IsdH^{N2N3}$-Y495A), pMMS329 (α-$IsdH^{N2N3}$-K499A), pMMS333 (α-$IsdH^{N2N3}$-K479A/K486A/R492A/Y495A/E496A/K499A/K503A), pMMS334 (α-$IsdH^{N2N3}$-Y495A/K499A), and pMMS336 were generated using site directed mutagenesis (QuickChange site-directed mutagenesis kit, Stratagene, La Jolla, CA) and are a modified version of pMMS322. An expression plasmid containing recombinant sperm whale myoglobin H64Y/V68F was also

generated by restriction enzyme cloning between the BamHI and XhoI sites of the pHis-SUMO vector.

The proteins were expressed by transforming the aforementioned plasmids into *Escherichia coli* BL21-DE3 cells (New England Biolabs, Beverly, MA). Protein expression and purification has been described previously [17]. Briefly, expression proceeded overnight at 25°C by adding 1 mM isopropyl-*β*-D-thiogalactoside to cell cultures. The bacterial cells were then harvested by centrifugation, lysed by sonication, and the proteins were purified using a Co^{2+}-chelating column (Thermo Scientific, Waltham, MA). The amino terminal 6x-His-SUMO tags were then cleaved using ULP1 protease and reapplied to the Co^{2+}-chelating column to remove the protease and cleaved SUMO tags. The apo-forms of the proteins were generated by hemin extraction with methyl ethyl ketone [62] followed by buffer exchange into 20 mM NaH_2PO_4, 150 mM NaCl, pH 7.5. To create hemin saturated proteins, a 1.5 molar excess of hemin was added to purified protein solutions followed by removal of excess hemin using a Sephadex G-25 column (GE Healthcare) that was equilibrated with 20 mM Tris-HCl, pH 8.0. The hemin saturation level was checked by recording UV-visible spectra and calculating the A_{Soret}/A_{280}.

4.5.2 Preparation of Human Hemoglobin

Human hemoglobin was purified from the blood of a healthy donor provided by the CFAR Virology Core Lab at the UCLA AIDS Institute and has been described previously [63]. Briefly, red blood cells were washed in 0.9% NaCl solution and then lysed under hypotonic conditions. Hb was purified from the hemolysate by two ion-exchange chromatography steps: the first being cation-exchange (SP Sepharose, GE Healthcare Life Sciences) and the second being anion-exchange chromatography (Q Sepharose, GE Healthcare Life Sciences). During Hb

purification, the globin chains were maintained in the carbon monoxide-ligated state to inhibit autooxidation and subsequent denaturation.

Recombinant genetically stabilized human hemoglobin containing V1M mutations in both α- and β-globin chains and a glycine linker between the C-terminus of one α-subunit and the N-terminus of another α-subunit (Hb0.1) [42,64] was transformed into *Escherichia coli* BL21-DE3 cells (New England Biolabs, Beverly, MA). The cells were grown in M9 minimal media supplemented with 3 g/L glucose and 1 g/L NH_4Cl. Prior to induction, exogenous hemin was added to the cell cultures at a final concentration of 8 μM. Expression was performed at 16°C overnight by adding 1 mM isopropyl-*β*-D-thiogalactoside to cell cultures. After the cells were harvested by centrifugation, the cells were washed twice with lysis buffer (50 mM Tris-HCl, 17 mM NaCl, pH 8.5) to remove excess hemin. Then the cell suspension was purged with a steady stream of CO for 15min in an ice-water bath. All buffers used during the purification were kept at pH 8.5 and were purged with CO to prevent oxidation. The cells were then lysed by sonication and purified in a single step over a Co^{2+}-chelating column (Thermo Scientific, Waltham, MA) via interactions with the naturally occurring His residues on the surface of Hb. The column was washed with three buffers prior to elution: 5 column volumes (CV) of lysis buffer (*vida supra*), 5 CVs wash 1 buffer (20 mM Tris-HCl, 500 mM NaCl, pH 8.5), and 5 CVs wash 2 buffer (20 mM Tris-HCl, pH 8.5). Column-bound Hb was then eluted with 5 CVs of elution buffer (20 mM Tris-HCl, 100 mM imidazole, pH 8.5).

Both Hb purified from human blood and Hb0.1 were converted to the ferric states by the same procedure. HbCO was converted to HbO_2 by delivering a pure stream of oxygen over a cold protein solution held in an ice-water batch and illuminated with a high-intensity (100 W) light source. Removal of CO and conversion to HbO_2 was considered complete when the ratio of

A_{577}:A_{560} was ~1.8 [65]. Oxidation of HbO_2 (Fe^{2+}) to generate MetHb (Fe^{3+}) was carried out by incubating Hb with a five-fold molar excess of potassium ferricyanide for 30 min and then the mixture was loaded onto a Sephadex G-25 column (GE Healthcare) to remove the excess ferricyanide. MetHb was then buffer exchanged into 20 mM NaH_2PO_4, 150 mM NaCl, pH 7.5. The concentration of hemin within metHb was determined using the extinction coefficient of 179 mM^{-1} cm^{-1} at a wavelength of 405 nm [66].

4.5.3 Hemin Transfer Experiments

Hemin transfer reactions from MetHb (hemin donor) to the apo-IsdH receptors (hemin acceptors) were monitored using an Applied Photophysics SX18.MV stopped-flow spectrophotometer (Applied Photopysics, Surrey, UK). The samples were buffer matched using stopped flow buffer (20 mM NaH_2PO_4, 150 mM NaCl, pH 7.5 supplemented with 0.45 M sucrose to prevent absorbance changes due to apoprotein aggregation) [40]. Unless stated elsewhere, holo-protein (Hb) in one syringe was mixed with apo-acceptor at ≥ 10 molar excess (in hemin units) in another syringe to maintain pseudo-first-order conditions. The absorbance changes at 373 and 405 nm were monitored individually for 1000 s (deadtime of 3 ms). The observed time courses and fitted rate constants for each wavelength were in agreement with previously reported values [31], therefore only the change in absorbance at 405 nm was monitored thereafter. Each representative time course reflects a minimum of three consecutive traces for each condition and were analyzed by fitting the observed time courses to a double-phase exponential expression to obtain the apparent pseudo-first-order rate constants using GraphPad Prism version 5.01 for Windows (GraphPad Software, La Jolla, CA). The rate of

hemin transfer was obtained by fitting the dependence of the observed fast phase kinetic rate constant to the concentration of apo-receptor according to scheme I and Equation 1 using Mathematica software (Wolfram Research, Inc., Mathematica, Version 9.0, Champaign, IL, 2012). The rates of hemin transfer from MetHb, MetHb0.1, and holo-IsdH^{N2N3} to 10-fold molar excess apo-Mb$^{H64Y/V68F}$ [40] were measured using a conventional UV–Vis spectrophotometer (Cary50; Varian, Inc., Palo Alto, CA) at Rice University. The entire spectrum was recorded over 17 h and the absorbance changes at 600 nm were plotted using GraphPad Prism Software.

4.5.4 Analytical Ultracentrifugation

Sedimentation equilibrium runs were performed at 25 °C in a Beckman Optima XL-A analytical ultracentrifuge using absorption optics at 412 nm so that only the heme was detected. Samples were tested using the exact same conditions as the stopped-flow hemin transfer experiments (20 mM sodium phosphate, 150 mM NaCl, 0.45 M sucrose, pH 7.5) with the exception of an alanine substitution at Y642 for the apo-receptors and the carbon monoxide-ligated state of Hb0.1 to prevent heme transfer over the course of the multi-day run. Three mm pathlength double sector cells were used for all samples and were purged with CO before sealing the cells to prevent oxidation. Sedimentation equilibrium profiles were measured at speeds of 9,000 (~6,000 × *g*) and 13,000 rpm (~13,000 × *g*). Samples contained Hb0.1 or the isolated β-globin chains at a concentration of 5 μM and were mixed with either 0, 75 μM, and 150 μM α-IsdH^{Y642A}. Experiments using wild-type IsdH^{Y642A} made use of a 150 μM sample. Weight-average molecular masses were determined by fitting with a non-linear least-squares exponential fit for a single ideal species using the Beckman Origin- based software (Version 3.01). Partial specific volumes were calculated from the amino acid compositions and corrected to 25 °C

[67,68]. They were 0.749 for the αβ Hb heterodimer and β-globin chains, 0.735 for apo-receptor, and 0.739 for the complex. At higher concentrations of receptor, the fitted molecular weights were slightly lower than lower concentrations which is compatible with the increased non-ideality of the solution.

4.5.5 Isothermal Titration Calorimetry

Isothermal titration calorimetry (ITC) measurements were performed using a MicroCal iTC200 calorimeter (GE Healthcare) at 25^0C. To prevent heat changes due to heme transfer the Hb was maintained in the carbonmonoxy ligated state and heme binding deficient receptor proteins containing an alanine substitution for Y642. The HbCO and apo-receptor proteins were buffer matched in ITC buffer (50 mM NaH_2PO_4, 150 mM NaCl, 0.45M sucrose, pH 7.5). The cell was filled with 30 μM HbCO and the syringe was filled with 200, 300, and 850 μM α-$IsdH^{Y642A}$, α-$IsdH^{N2}$, $IsdH^{LN3(Y642A)}$, respectively. Sixteen injections were performed using 2.5 μL aliquots at 180 s intervals and were performed in triplicate. The data were analyzed using MicroCal iTC200 analysis software (GE Healthcare).

4.6 Figures and Tables

Table 4.1 Stoichiometry of Hb:receptor complexes

	Weighted average molecular masses (Da)[a,b]	Receptor/globin
Hb0.1[c]		
13,000 × g	64,212 ± 829	
Hb0.1 + α-IsdH^{Y642A}[c,d]		
6,000 × g	140,070 ± 2096	2.0
13,000 × g	131,570 ± 894	1.7
Hb0.1 + α-IsdH^{Y642A}[c,e]		
6,000 × g	134,660 ± 1,872	1.8
13,000 × g	128,490 ± 1115	1.7
Hb0.1 + IsdH^{Y642A}[c,e]		
6,000 × g	188,110 ± 1,518	3.2
13,000 × g	175,120 ± 1045	2.9
β-globin [c]		
6,000 × g	56,700 ± 724	
13,000 × g	56,300 ± 508	
β-globin + α-IsdH^{Y642A}[c,e]		
6,000 × g	54,500 ± 97	0.0
13,000 × g	54,500 ± 65	0.0
β-globin + IsdH^{Y642A}[c,e]		
6,000 × g	134,000 ± 1321	2.0
13,000 × g	116,500 ± 617	1.6

[a] Samples were centrifuged at 25°C in buffer containing 20 mM sodium phosphate, 150 mM NaCl, 450 mM sucrose, pH 7.5

[b] Molecular masses were obtained by non-linear least squares exponential fitting of data using Beckman Origin-based software (Version 3.01)

[c] Globin chains were held at a concentration of 5 μM (hemin units)

[d] Receptor concentrations were in a 15-fold molar excess (75 μM)

[e] Receptor concentrations were in a 30-fold molar excess (150 μM)

Table 4.2 Apparent rate constants of hemin transfer

Hemin donor	Hemin acceptor	k_{fast} (s^{-1})[a]	k_{slow} (s^{-1})[a]
MetHb	α-IsdH[b]	3.27 ± 0.07	0.038 ± 0.001
	IsdH[b]	3.12 ± 0.08	0.039 ± 0.001
	apo-Mb[d,e]	0.004[f] (0.01)[g]	0.0002[f] (0.003)[g]
MetHb0.1	α-IsdH[b]	0.34 ± 0.01	0.026 ± 0.001
	IsdH[b]	0.73 ± 0.03	0.041 ± 0.001
	α-IsdH^{Y495A}[c]	0.12 ± 0.01	0.007 ± 0.001
	α-IsdH^{K499A}[c]	0.22 ± 0.01	0.014 ± 0.002
	α-IsdH$^{Y495A/K499A}$[c]	0.08 ± 0.01	0.004 ± 0.002
	α-IsdH$^{7\text{-}Ala}$[c]	0.03 ± 0.01	0.002 ± 0.001
	apo-Mb[d,e]	0.0004[h]	0.00008[h]

[a] k_{fast} and k_{slow} values were obtained by fitting to a double exponential expression.
[b] Rates were determined at a 30-fold excess [Receptor] pH 7.5, 25°C.
[c] Rates were determined at a 40-fold excess [Receptor] pH 7.5, 25°C.
[d] Rates were determined at pH 7.0, 37°C.
[e] The data are from Ref. [37].
[f] k_{fast} and k_{slow} are from the β- and α-globin chains in dimeric Hb, respectively.
[g] k_{fast} and k_{slow} are from the β- and α-globin chains in monomeric Hb, respectively.
[h] k_{fast} and k_{slow} are from the β- and α-globin chains in tetrameric Hb, respectively. These values are also the same for tetrameric native Hb.

Table 4.3 Thermodynamic parameters and affinity data for Hb binding

	K_D	ΔH°	ΔS°	ΔG°[a]	n[b]
	μM	*kcal/mol*	*cal/mol·K*	*kcal/cmol*	
Hb + αIsdH^{Y642A}	4.6 ± 0.8	-5.6 ± 0.5	5.6 ± 2.0	-7.3 ± 0.1	0.64 ± 0.04
Hb + αIsdH^{N2}	7.7 ± 1.3	-9.6 ± 0.1	-8.7 ± 2.7	-7.0 ± 0.1	0.61 ± 0.05
Hb + αIsdH$^{LN3(Y642A)}$	≥ mM	endothermic	positive	ND[c]	ND
Hb0.1 + αIsdH^{Y642A}	5.3 ± 1.4	-8.4 ± 0.3	-3.9 ± 0.4	-7.2 ± 0.2	1.00 ± 0.06

[a] Samples were in buffer containing 20 mM sodium phosphate, 150 mM NaCl, 450 mM sucrose, pH 7.5, 298K
[b] n refers to the molar ratio protein:Hb.
[c] ND refers to "not determined".

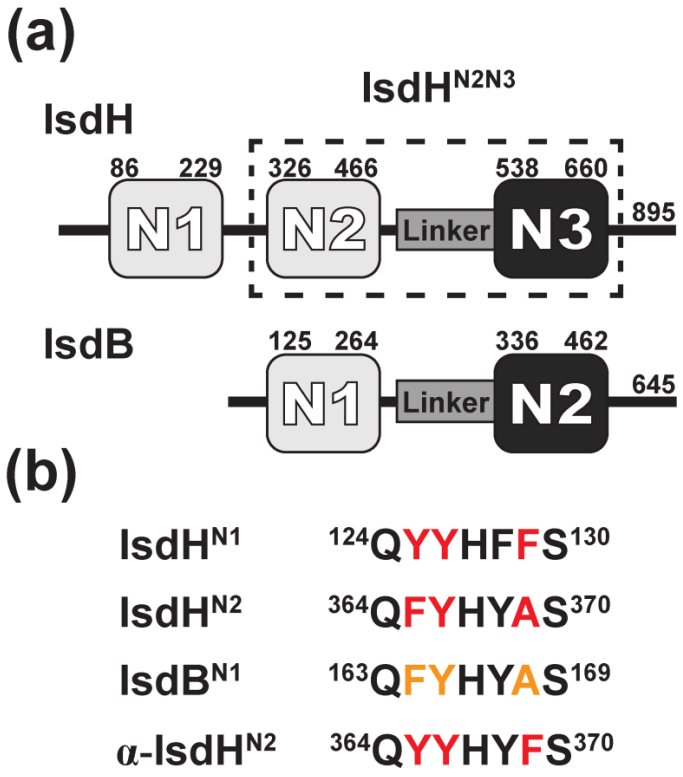

Figure 4.1 ***S. aureus*** **uses conserved tri-domain receptors to capture Hb via an aromatic-rich motif.**

(a) Schematic of the conserved NEAT domains of *S. aureus* Hb receptors, IsdH and IsdB. NEAT domains that bind Hb and hemin (oxidized form of heme) are shown in gray and black, respectively. Residue numbers of the functionally homologous NEAT domains and the linker connecting them are indicated. (b) Sequence alignment of the aromatic 3_{10}-helix Hb-binding motif. Interfacial residues shown to interact with the A- and E-helices of Hb are colored in red, whereas interfacial residues proposed to bind Hb are colored in orange.

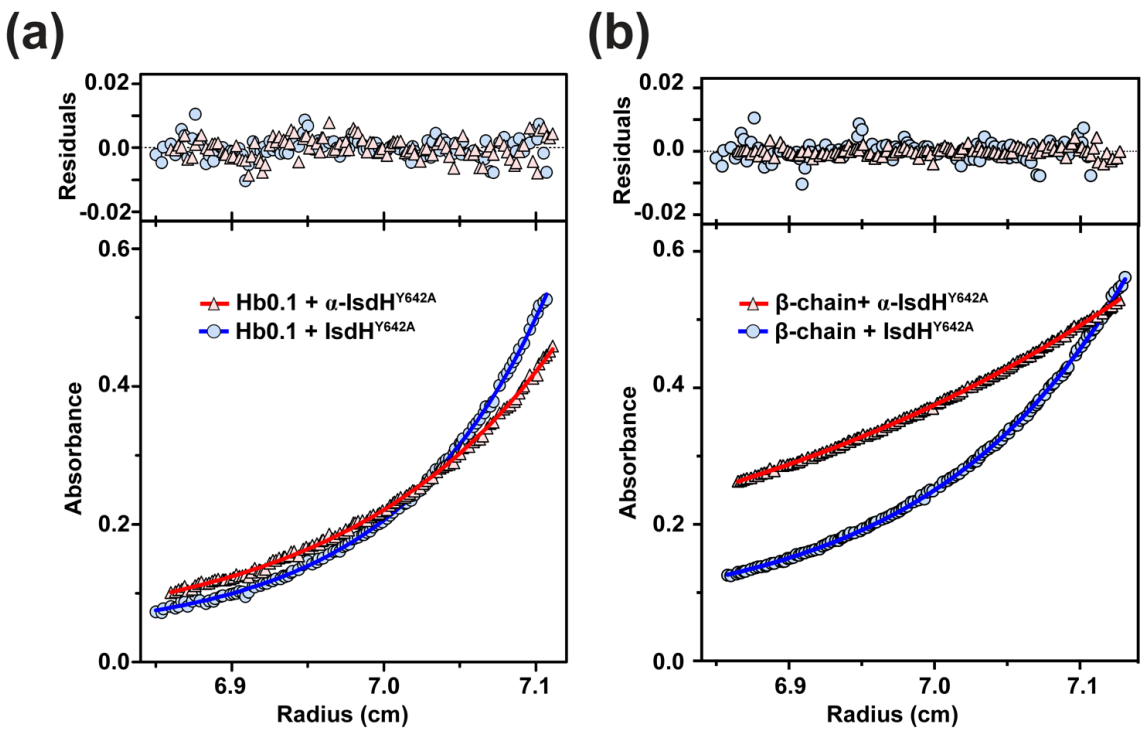

Figure 4.2 Stoichiometry of Hb:receptor complexes determined by Analytical Ultracentrifugation

(a) Representative absorbance scans at 412 nm at equilibrium are plotted versus the distance from the axis of rotation for a mixture of Hb0.1 + IsdH (blue circles) and Hb0.1 + α-IsdH (red triangles). Hb0.1 was maintained in the carbonmonoxy ligated state, and both receptors contained a Y642A mutation to prevent heme transfer. Protein samples were mixed at a ratio of 5 μM Hb0.1 and 150 μM receptor and were centrifuged at 25 °C for at least 48 h at 13,000 rpm. The solid lines represent the global nonlinear least squares best-fit of all the data to a single molecular species with a baseline fit. Residuals of the fit are shown above. (b) Representative scans identical to the conditions described in (a) with the exception of 5 μM isolated β-chains and a speed of 9,000 rpm.

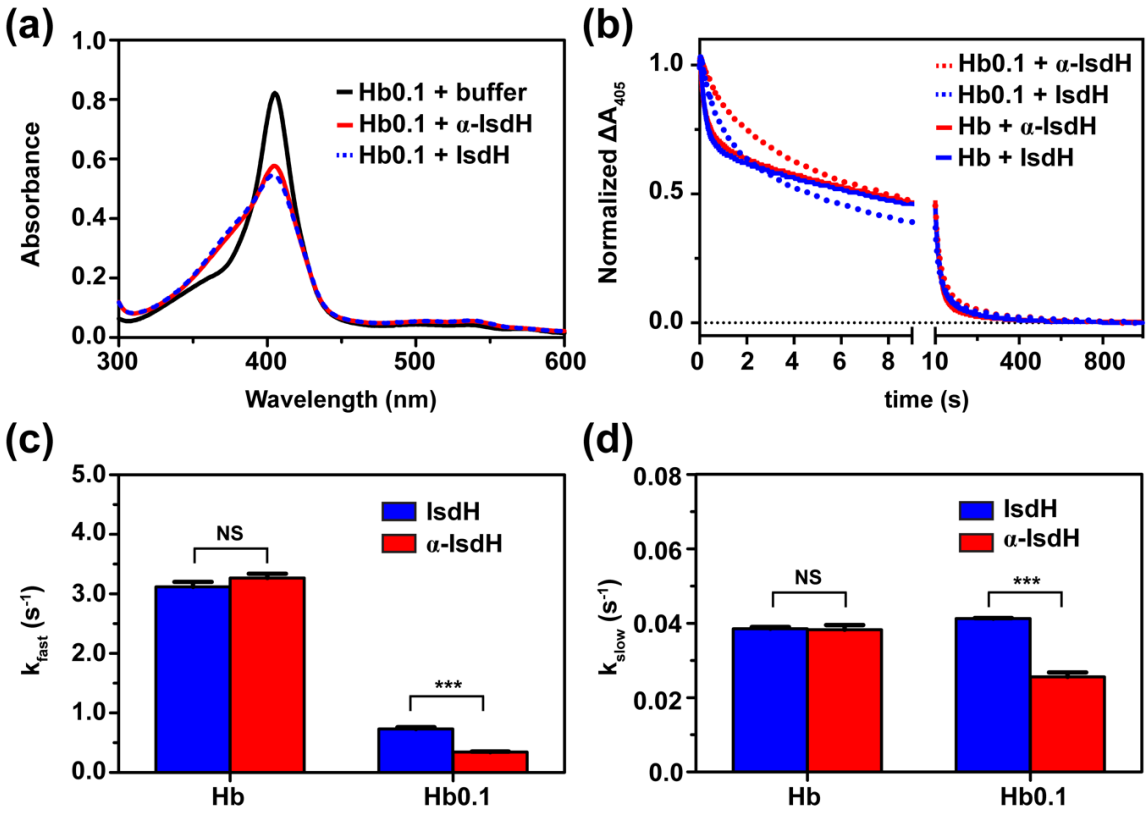

Figure 4.3 Hemin transfer by various Hb and receptors species

(a) Spectral changes in the UV–Vis spectrum of the reaction of 5 μM MetHb0.1 with buffer (solid black line), 150 μM IsdH (dotted blue line), and 150 μM α-IsdH (solid red line). Spectral traces were recorded at 1000 s post mixing. (b) Representative stopped flow time courses of the absorbance change at 405 nm after mixing 5 μM Hb with 150 μM apo-receptor. The data were fit to a double-exponential equation and yielded hemin transfer rate constants shown in (c) and (d). Spectral traces were normalized for comparison using the following equation: $y = (y_t - y_0) / (y_t + y_0)$. (c) and (d) The observed pseudo-first-order k_{fast} and k_{slow} rate constants, respectively. Values were derived from the time courses in (b). A two-way ANOVA was used to access the significance in the difference of rates. NS and *** corresponds to p-values > 0.05 and < 0.001, respectively.

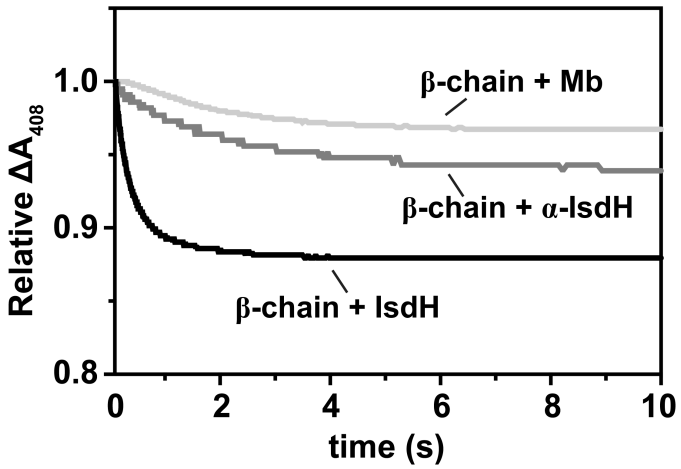

Figure 4.4 Hemin transfer from isolated β-globin chains

Representative stopped flow time courses of the absorbance change at 408 nm after mixing 5 μM isolated Metβ-globin chains with 150 μM apo-receptor or 50 μM apo-Mb. Relative spectral traces are shown for comparison in which all starting absorbance values were adjusted to one by addition or subtraction of a constant from the observed data. Only the first 10 s are shown as absorbance artifacts due to apo-globin denaturation appeared afterwards.

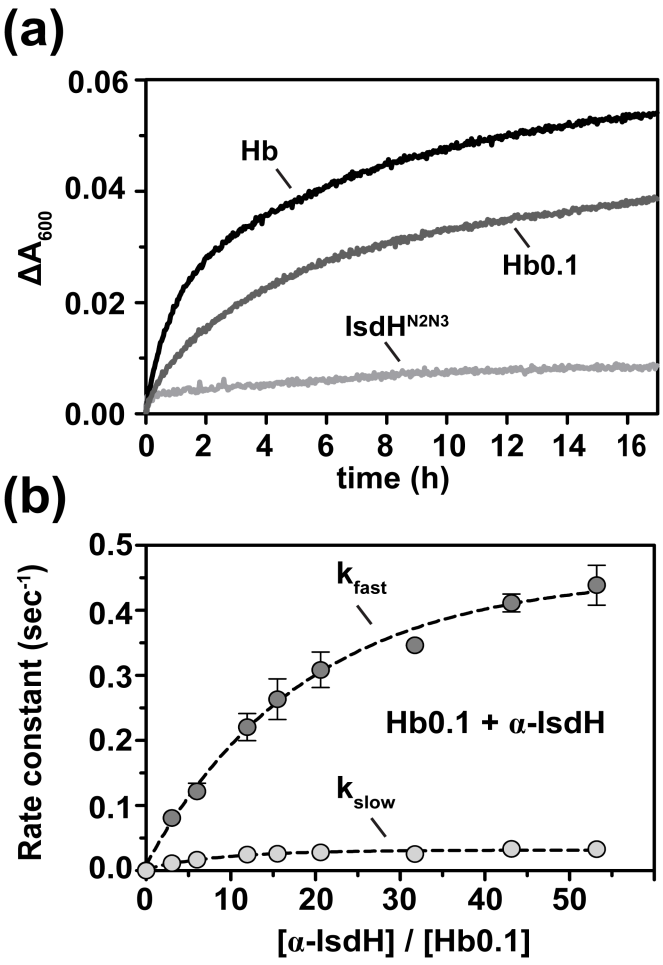

Figure 4.5 Kinetic parameters of hemin extraction mechanism

(a) Time courses of the absorbance change at 600 nm of a mixture of H64Y/V68F apomyoglobin with Hb (black line), Hb0.1 (dark grey line), and IsdH (light grey line) at a final concentration of 50 μM apo-Mb to 5 μM holo-protein. (b) Plots of the observed rate constants, k_{fast} (dark gray circles) and k_{slow} (light gray circles) versus the initial ratio of [apo-α-IsdH] to [Hb0.1]. The concentration of Hb0.1 was held constant at 5 μM. The observed values were obtained in experiments similar to those described in the legend in figure 4.3. The curves are theoretical curves obtained by fitting the data to Equation 1.

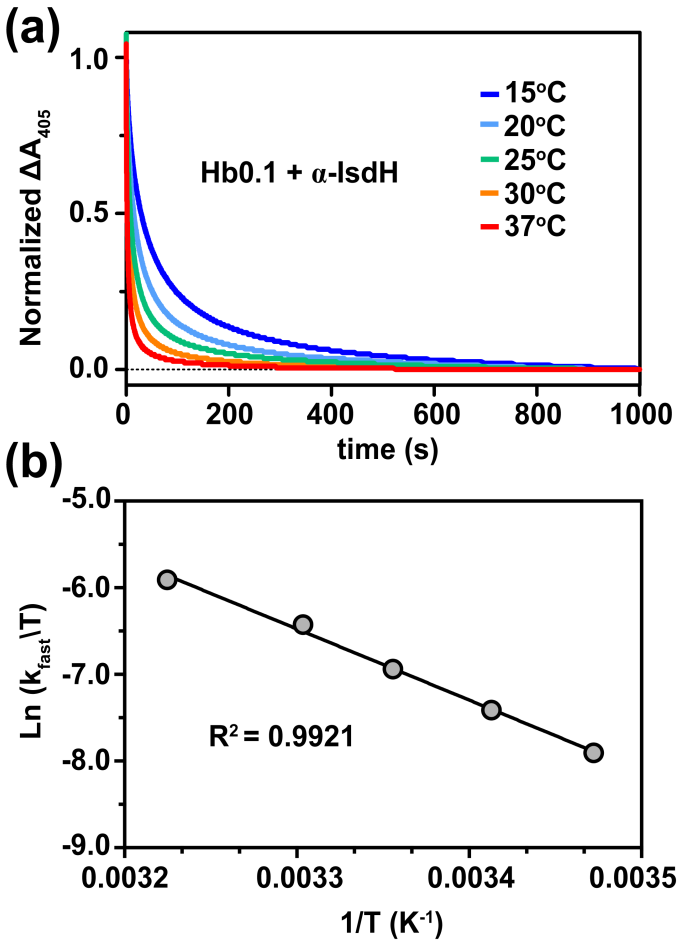

Figure 4.6 Effect of temperature on the observed rate constant

(a) Representative normalized stopped flow time courses of the absorbance change at 405 nm upon mixing 5 μM Hb0.1 with 200 μM α-IsdH. Spectral traces were normalized using the following equation: $y = (y_t - y_0) / (y_t + y_0)$. (b) Plots of $\ln(k_{fast}/T)$ versus 1/T. The observed k_{fast} values obtained in experiments similar to those described in the legend in figure. 4.3. The correlation factor, R^2, is indicated on the plot.

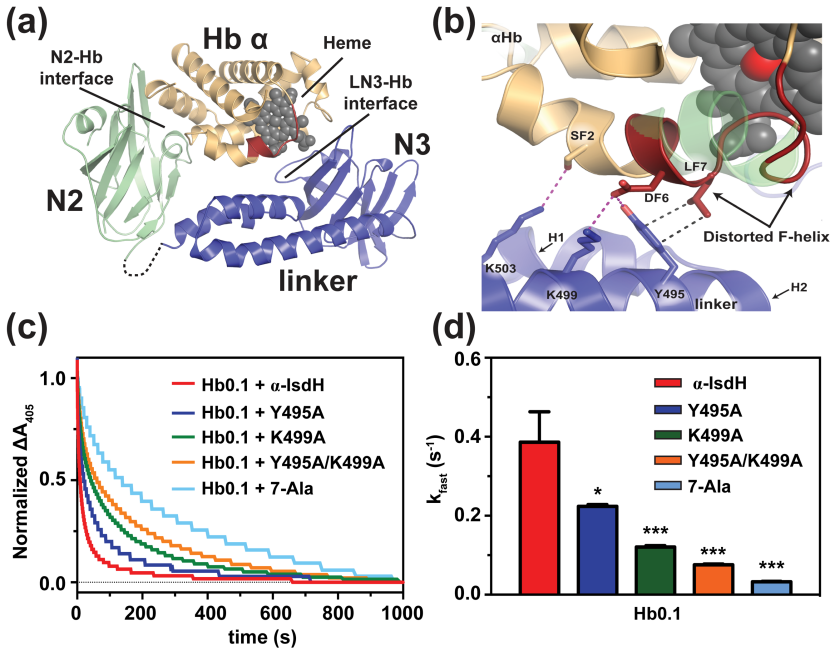

Figure 4.7 Linker domain residues play a role in the hemin transfer mechanism

(a) Crystal structure of the Hb:α-IsdH^{N2N3} complex (pdb 4XS0). Only receptor contacts to the α-subunit are shown. Proteins are shown as ribbon format, while the hemin group is represented by a space filling model. Residues in the segment connecting the N2 and linker domains that were not modeled into the electron density are indicated by a dashed line. (b) Close up view of the linker-Hb interface. α-IsdH and αHb are shown in blue and yellow, respectively, with the αHb's perturbed F-helix colored in red and an overlay of the native F-helix structure is shown in green (PDB code: 2DN2). The hemin molecule is shown in grey surface representation with the iron atom shown as a red sphere. (c) Representative stopped flow time courses of the absorbance change at 405 nm after mixing 5 μM Hb0.1 with 200 μM apo-receptor. (d) The observed k_{fast} rate constants were obtained in experiments similar to those described in the legend in figure 4.3. A one-way ANOVA was used to access the significance in the difference of rates. * and *** corresponds to p-values < 0.05 and < 0.001, respectively.

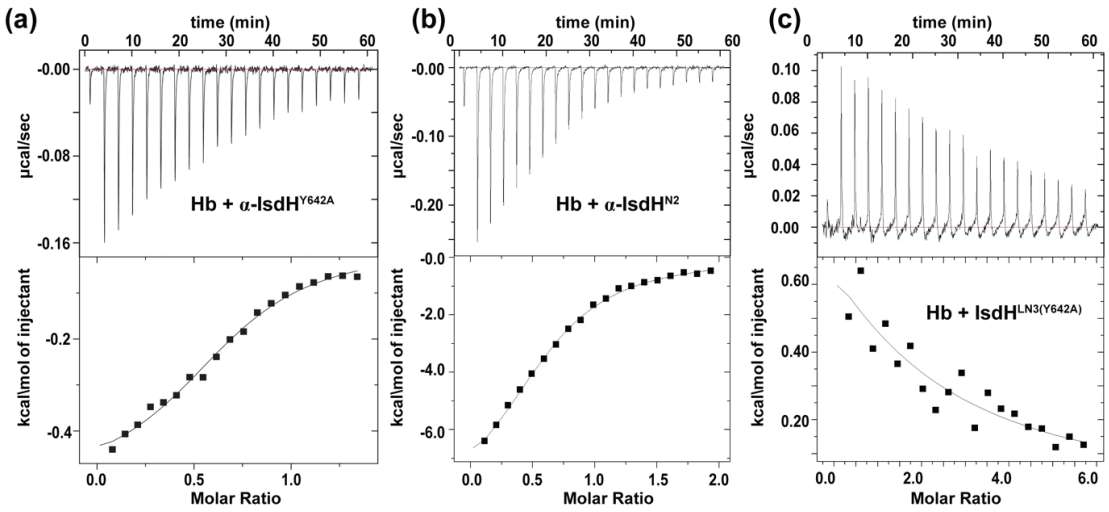

Figure 4.8 IsdH used two distinct interfaces to promote hemin transfer

(a) Representative ITC data for the titration of 200 µM α-IsdH^{Y642A} into 30 µM HbCO. Injections were made at 180 s intervals at 25°C. (b) Representative ITC data for the titration of 300 µM α-IsdH^{N2} into 30 µM HbCO. (c) Representative ITC data for the titration of 850 µM α-IsdH$^{LN3(Y642A)}$ into 30 µM HbCO. The top panels show the time course of the titration (black) and baseline (red). The bottom panels show the integrated isotherms. The program ORIGIN was used to fit the data using non-linear regression to a one-site binding model to derive thermodynamic parameters.

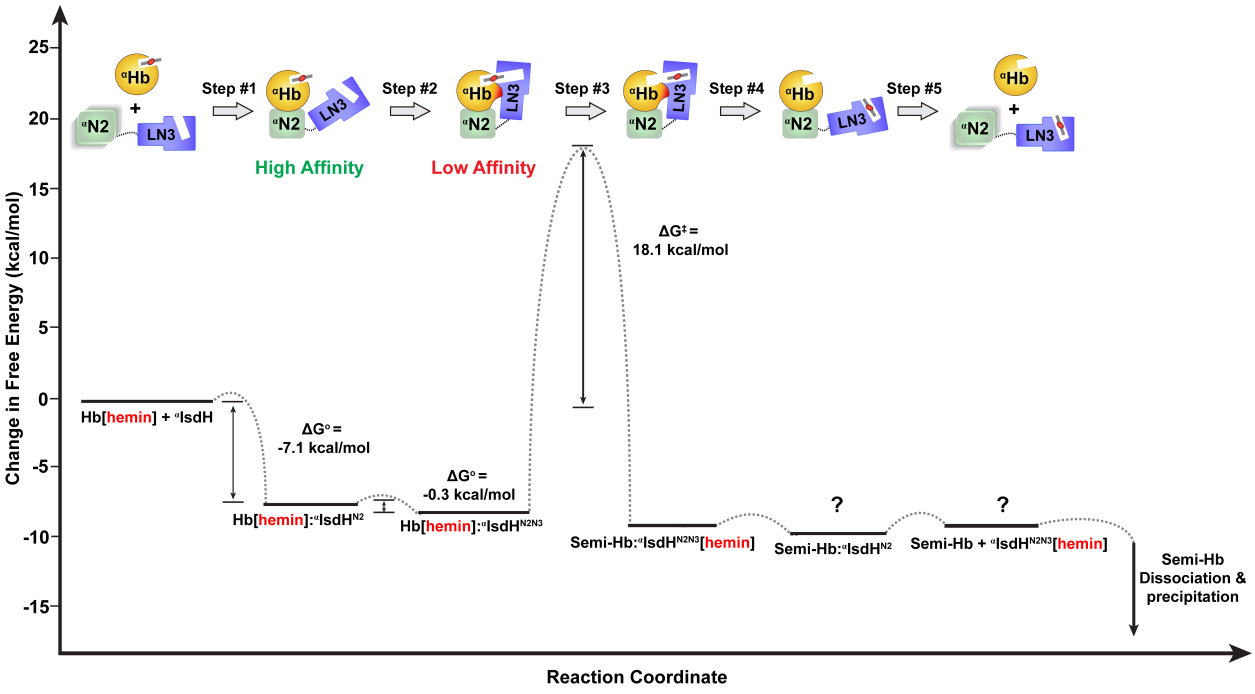

Figure 4.9 Model of the hemin extraction mechanism

Proposed hemin transfer reaction coordinate. The IsdH receptor recognizes Hb via two energetically distinct interfaces. See "discussion" for more details. Top, schematic showing the steps in hemin transfer. Bottom, relative free energies of the intermediates. Free energies calculated from this study are labeled along reaction coordinate. Steps without known energies are labeled with a "?". Breakage of the axial Fe-Nε bond is presumably rate limiting (step #3).

4.7 References

[1] R.M. Klevens, M.A. Morrison, J. Nadle, S. Petit, K. Gershman, S. Ray, L.H. Harrison, R. Lynfield, G. Dumyati, J.M. Townes, A.S. Craig, E.R. Zell, G.E. Fosheim, L.K. McDougal, R.B. Carey, S.K. Fridkin, Active Bacterial Core surveillance (ABCs) MRSA Investigators, Invasive methicillin-resistant Staphylococcus aureus infections in the United States., J. Am. Med. Assoc. 298 (2007) 1763–71. doi:10.1001/jama.298.15.1763.

[2] Centers for Disease Control and Prevention, Active Bacterial Core Surveillance (ABCs) Report Emerging Infections Program Network Methicillin-Resistant Staphylococcus aureus, 2013, (2013).

[3] V.M. Dukic, D.S. Lauderdale, J. Wilder, R.S. Daum, M.Z. David, Epidemics of community-associated methicillin-resistant Staphylococcus aureus in the United States: a meta-analysis., PLoS One. 8 (2013) e52722. doi:10.1371/journal.pone.0052722.

[4] U.E. Schaible, S.H.E. Kaufmann, Iron and microbial infection., Nat. Rev. Microbiol. 2 (2004) 946–53. doi:10.1038/nrmicro1046.

[5] P. Cornelis, S.C. Andrews, eds., Iron Uptake and Homeostasis in Microorganisms, Caister Academic Press, (2013) Norfolk, UK.

[6] S.T. Ong, J.Z.S. Ho, B. Ho, J.L. Ding, Iron-withholding strategy in innate immunity., Immunobiology. 211 (2006) 295–314. doi:10.1016/j.imbio.2006.02.004.

[7] K.P. Haley, E.P. Skaar, A battle for iron: host sequestration and Staphylococcus aureus acquisition., Microbes Infect. 14 (2012) 217–27. doi:10.1016/j.micinf.2011.11.001.

[8] A.J. Farrand, M.L. Reniere, H. Ingmer, D. Frees, E.P. Skaar, Regulation of Host Hemoglobin Binding by the Staphylococcus aureus Clp Proteolytic System, J. Bacteriol. 195 (2013) 5041–5050. doi:10.1128/JB.00505-13.

[9] E.P. Skaar, M. Humayun, T. Bae, K.L. DeBord, O. Schneewind, Iron-source preference of Staphylococcus aureus infections., Science. 305 (2004) 1626–8. doi:10.1126/science.1099930.

[10] S.K. Mazmanian, E.P. Skaar, A.H. Gaspar, M. Humayun, P. Gornicki, J. Jelenska, A. Joachmiak, D.M. Missiakas, O. Schneewind, Passage of heme-iron across the envelope of Staphylococcus aureus., Science. 299 (2003) 906–9ma. doi:10.1126/science.1081147.

[11] A.W. Maresso, O. Schneewind, Iron acquisition and transport in Staphylococcus aureus., Biometals. 19 (2006) 193–203. doi:10.1007/s10534-005-4863-7.

[12] M.L. Reniere, V.J. Torres, E.P. Skaar, Intracellular metalloporphyrin metabolism in Staphylococcus aureus., Biometals. 20 (2007) 333–45. doi:10.1007/s10534-006-9032-0.

[13] S.K. Mazmanian, H. Ton-That, K. Su, O. Schneewind, An iron-regulated sortase anchors a class of surface protein during Staphylococcus aureus pathogenesis., Proc. Natl. Acad. Sci. U. S. A. 99 (2002) 2293–8. doi:10.1073/pnas.032523999.

[14] H. Ton-That, L.A. Marraffini, O. Schneewind, Protein sorting to the cell wall envelope of Gram-positive bacteria., Biochim. Biophys. Acta. 1694 (2004) 269–78. doi:10.1016/j.bbamcr.2004.04.014.

[15] R.M. Pilpa, S.A. Robson, V.A. Villareal, M.L. Wong, M. Phillips, R.T. Clubb, Functionally distinct NEAT (NEAr Transporter) domains within the Staphylococcus aureus IsdH/HarA protein extract heme from methemoglobin., J. Biol. Chem. 284 (2009) 1166–76. doi:10.1074/jbc.M806007200.

[16] G. Pishchany, J.R. Sheldon, C.F. Dickson, M.T. Alam, T.D. Read, D.A. Gell, D.E. Heinrichs, E.P. Skaar, IsdB-dependent Hemoglobin Binding Is Required for Acquisition of Heme by Staphylococcus aureus., J. Infect. Dis. (2014). doi:10.1093/infdis/jit817.

[17] T. Spirig, G.R. Malmirchegini, J. Zhang, S.A. Robson, M. Sjodt, M. Liu, K. Krishna Kumar, C.F. Dickson, D.A. Gell, B. Lei, J. a Loo, R.T. Clubb, Staphylococcus aureus uses a novel multidomain receptor to break apart human hemoglobin and steal its heme., J. Biol. Chem. 288 (2013) 1065–78. doi:10.1074/jbc.M112.419119.

[18] H. Zhu, D. Li, M. Liu, V. Copié, B. Lei, Non-Heme-Binding Domains and Segments of the Staphylococcus aureus IsdB Protein Critically Contribute to the Kinetics and Equilibrium of Heme Acquisition from Methemoglobin., PLoS One. 9 (2014) e100744. doi:10.1371/journal.pone.0100744.

[19] A. Dryla, D. Gelbmann, A. Von Gabain, E. Nagy, Identification of a novel iron regulated staphylococcal surface protein with haptoglobin-haemoglobin binding activity, Mol. Microbiol. 49 (2003) 37–53. doi:10.1046/j.1365-2958.2003.03542.x.

[20] G. Pishchany, S.E. Dickey, E.P. Skaar, Subcellular localization of the Staphylococcus aureus heme iron transport components IsdA and IsdB., Infect. Immun. 77 (2009) 2624–34. doi:10.1128/IAI.01531-08.

[21] V. a Villareal, T. Spirig, S.A. Robson, M. Liu, B. Lei, R.T. Clubb, Transient weak protein-protein complexes transfer heme across the cell wall of Staphylococcus aureus., J. Am. Chem. Soc. 133 (2011) 14176–9. doi:10.1021/ja203805b.

[22] R. Abe, J.M.M. Caaveiro, H. Kozuka-Hata, M. Oyama, K. Tsumoto, Mapping the ultra-weak protein-protein interactions between heme transporters of Staphylococcus aureus., J. Biol. Chem. 287 (2012) 16477–87. doi:10.1074/jbc.M112.346700.

[23] N. Muryoi, M.T. Tiedemann, M. Pluym, J. Cheung, D.E. Heinrichs, M.J. Stillman, Demonstration of the Iron-regulated Surface Determinant (Isd) Heme Transfer Pathway in Staphylococcus aureus, J. Biol. Chem. 283 (2008) 28125–28136. doi:10.1074/jbc.M802171200.

[24] H. Zhu, G. Xie, M. Liu, J.S. Olson, M. Fabian, D.M. Dooley, B. Lei, Pathway for heme uptake from human methemoglobin by the iron-regulated surface determinants system of Staphylococcus aureus., J. Biol. Chem. 283 (2008) 18450–60. doi:10.1074/jbc.M801466200.

[25] T. Matsui, S. Nambu, Y. Ono, C.W. Goulding, K. Tsumoto, M. Ikeda-Saito, Heme degradation by Staphylococcus aureus IsdG and IsdI liberates formaldehyde rather than carbon monoxide., Biochemistry. 52 (2013) 3025–7. doi:10.1021/bi400382p.

[26] M.L. Reniere, G.N. Ukpabi, S.R. Harry, D.F. Stec, R. Krull, D.W. Wright, B.O. Bachmann, M.E. Murphy, E.P. Skaar, The IsdG-family of haem oxygenases degrades

haem to a novel chromophore., Mol. Microbiol. 75 (2010) 1529–38. doi:10.1111/j.1365-2958.2010.07076.x.

[27] V.J. Torres, G. Pishchany, M. Humayun, O. Schneewind, E.P. Skaar, Staphylococcus aureus IsdB is a hemoglobin receptor required for heme iron utilization., J. Bacteriol. 188 (2006) 8421–9. doi:10.1128/JB.01335-06.

[28] G. Pishchany, A.L. McCoy, V.J. Torres, J.C. Krause, J.E. Crowe, M.E. Fabry, E.P. Skaar, Specificity for human hemoglobin enhances Staphylococcus aureus infection., Cell Host Microbe. 8 (2010) 544–50. doi:10.1016/j.chom.2010.11.002.

[29] H.K. Kim, A. DeDent, A.G. Cheng, M. McAdow, F. Bagnoli, D.M. Missiakas, O. Schneewind, IsdA and IsdB antibodies protect mice against Staphylococcus aureus abscess formation and lethal challenge., Vaccine. 28 (2010) 6382–92. doi:10.1016/j.vaccine.2010.02.097.

[30] B.A. Fonner, B.P. Tripet, B. Eilers, J. Stanisich, R.K. Sullivan-Springhetti, R. Moore, M. Liu, B. Lei, V. Copie, Solution Structure and Molecular determinants of Hemoglobin Binding of the first NEAT Domain of IsdB in Staphylococcus aureus., Biochemistry. 53 (2014) 3922–3933. doi:10.1021/bi5005188.

[31] M. Sjodt, R. Macdonald, T. Spirig, A.H. Chan, C.F. Dickson, M. Fabian, J.S. Olson, D.A. Gell, R.T. Clubb, The PRE-Derived NMR Model of the 38.8kDa Tri-Domain IsdH Protein from Staphylococcus aureus Suggests that it Adaptively Recognizes Human Hemoglobin., J. Mol. Biol. (2015). doi:10.1016/j.jmb.2015.02.008.

[32] C.F. Dickson, K. Krishna Kumar, D.A. Jacques, G.R. Malmirchegini, T. Spirig, J.P. Mackay, R.T. Clubb, J.M. Guss, D.A. Gell, Structure of the Hemoglobin-IsdH Complex Reveals the Molecular Basis of Iron Capture by Staphylococcus aureus., J. Biol. Chem. (2014). doi:10.1074/jbc.M113.545566.

[33] C.F. Dickson, D.A. Jacques, R.T. Clubb, J.M. Guss, D.A. Gell, The structure of haemoglobin bound to the haemoglobin receptor IsdH from Staphylococcus aureus shows disruption of the native α-globin haem pocket, Acta Crystallogr. Sect. D Biol. Crystallogr. 71 (2015). doi:10.1107/S1399004715005817.

[34] M. Andrade, F. Ciccarelli, C. Perez-Iratxeta, P. Bork, NEAT: a domain duplicated in genes near the components of a putative Fe3+ siderophore transporter from Gram-positive pathogenic bacteria, Genome Biol. 3 (2002) research0047.1–research0047.5. doi:10.1186/gb-2002-3-9-research0047.

[35] C.F. Bowden, M.M. Verstraete, L.D. Eltis, M.E.P. Murphy, Hemoglobin binding and catalytic heme extraction by IsdB NEAT domains., Biochemistry. (2014). doi:10.1021/bi500230f.

[36] R.E. Benesch, S. Kwong, Coupled reactions in hemoglobin. Heme-globin and dimer-dimer association., J. Biol. Chem. 270 (1995) 13785–6.

[37] M.S. Hargrove, T. Whitaker, J.S. Olson, R.J. Vali, A.J. Mathews, Quaternary Structure Regulates Hemin Dissociation from Human Hemoglobin, J. Biol. Chem. 272 (1997) 17385–17389. doi:10.1074/jbc.272.28.17385.

[38] H.F. Bunn, J.H. Jandl, Exchange of heme among hemoglobins and between hemoglobin and albumin., J. Biol. Chem. 243 (1968) 465–75.
[39] M. Gattoni, A. Boffi, P. Sarti, E. Chiancone, Stability of the heme-globin linkage in alphabeta dimers and isolated chains of human hemoglobin. A study of the heme transfer reaction from the immobilized proteins to albumin., J. Biol. Chem. 271 (1996) 10130–6.
[40] M.S. Hargrove, E.W. Singleton, M.L. Quillin, L.A. Ortiz, G.N. Phillips, J.S. Olson, A.J. Mathews, His64(E7)-->Tyr apomyoglobin as a reagent for measuring rates of hemin dissociation., J. Biol. Chem. 269 (1994) 4207–14.
[41] Y. Leutzinger, S. Beychok, Kinetics and mechanism of heme-induced refolding of human alpha-globin., Proc. Natl. Acad. Sci. U. S. A. 78 (1981) 780–4.
[42] D. Looker, D. Abbott-Brown, P. Cozart, S. Durfee, S. Hoffman, A.J. Mathews, J. Miller-Roehrich, S. Shoemaker, S. Trimble, G. Fermi, A human recombinant haemoglobin designed for use as a blood substitute., Nature. 356 (1992) 258–60. doi:10.1038/356258a0.
[43] P. McGovern, P. Reisberg, J.S. Olson, Aggregation of deoxyhemoglobin subunits., J. Biol. Chem. 251 (1976) 7871–9.
[44] J.H. Espenson, Chemical Kinetics and Reaction Mechanisms, McGraw-Hill, 1995.
[45] M.F. Perutz, Regulation of oxygen affinity of hemoglobin: influence of structure of the globin on the heme iron., Annu. Rev. Biochem. 48 (1979) 327–86. doi:10.1146/annurev.bi.48.070179.001551.
[46] R.M. Pilpa, E.A. Fadeev, V.A. Villareal, M.L. Wong, M. Phillips, R.T. Clubb, Solution structure of the NEAT (NEAr Transporter) domain from IsdH/HarA: the human hemoglobin receptor in Staphylococcus aureus., J. Mol. Biol. 360 (2006) 435–47. doi:10.1016/j.jmb.2006.05.019.
[47] Y. Kawamura-Konishi, K. Chiba, H. Kihara, H. Suzuki, Kinetics of the reconstitution of hemoglobin from semihemoglobins alpha and beta with heme., Eur. Biophys. J. 21 (1992) 85–92.
[48] M.S. Hargrove, D. Barrick, J.S. Olson, The association rate constant for heme binding to globin is independent of protein structure., Biochemistry. 35 (1996) 11293–9. doi:10.1021/bi9603711.
[49] M.Y. Rose, J.S. Olson, The kinetic mechanism of heme binding to human apohemoglobin., J. Biol. Chem. 258 (1983) 4298–303.
[50] L. Makowski, J. Bardhan, D. Gore, J. Lal, S. Mandava, S. Park, D.J. Rodi, N.T. Ho, C. Ho, R.F. Fischetti, WAXS Studies of the Structural Diversity of Hemoglobin in Solution, J. Mol. Biol. 408 (2011) 909–921. doi:10.1016/j.jmb.2011.02.062.
[51] L. V Abaturov, N.G. Nosova, S. V Shliapnikov, D.A. Faĭzullin, The conformational dynamic of the tetramer hemoglobin molecule as revealed by hydrogen exchange. I. Influence pH, temperature and ligand binding., Mol. Biol. (Mosk). 40 (n.d.) 326–40.
[52] C.F. Dickson, A.M. Rich, W.M.H. D'Avigdor, D.A.T. Collins, J.A. Lowry, T.L. Mollan, E. Khandros, J.S. Olson, M.J. Weiss, J.P. Mackay, P.A. Lay, D.A. Gell, α-Hemoglobin-

stabilizing protein (AHSP) perturbs the proximal heme pocket of oxy-α-hemoglobin and weakens the iron-oxygen bond., J. Biol. Chem. 288 (2013) 19986–20001. doi:10.1074/jbc.M112.437509.

[53] K. Krishna Kumar, C.F. Dickson, M.J. Weiss, J.P. Mackay, D. a Gell, AHSP (α-haemoglobin-stabilizing protein) stabilizes apo-α-haemoglobin in a partially folded state., Biochem. J. 432 (2010) 275–82. doi:10.1042/BJ20100642.

[54] S. Zhou, J.S. Olson, M. Fabian, M.J. Weiss, A.J. Gow, Biochemical fates of alpha hemoglobin bound to alpha hemoglobin-stabilizing protein AHSP., J. Biol. Chem. 281 (2006) 32611–8. doi:10.1074/jbc.M607311200.

[55] E.C. Liong, Y. Dou, E.E. Scott, J.S. Olson, G.N. Phillips, Waterproofing the heme pocket. Role of proximal amino acid side chains in preventing hemin loss from myoglobin., J. Biol. Chem. 276 (2001) 9093–100. doi:10.1074/jbc.M008593200.

[56] V.M. Krishnamurthy, V. Semetey, P.J. Bracher, N. Shen, G.M. Whitesides, Dependence of effective molarity on linker length for an intramolecular protein-ligand system., J. Am. Chem. Soc. 129 (2007) 1312–20. doi:10.1021/ja066780e.

[57] D.M. Jacobs, K. Saxena, M. Vogtherr, P. Bernado, M. Pons, K.M. Fiebig, Peptide Binding Induces Large Scale Changes in Inter-domain Mobility in Human Pin1, J. Biol. Chem. 278 (2003) 26174–26182. doi:10.1074/jbc.M300796200.

[58] N.J. Anthis, G.M. Clore, The Length of the Calmodulin Linker Determines the Extent of Transient Interdomain Association and Target Affinity, J. Am. Chem. Soc. 135 (2013) 9648–9651. doi:10.1021/ja4051422.

[59] R. Senturia, M. Faller, S. Yin, J.A. Loo, D. Cascio, M.R. Sawaya, D. Hwang, R.T. Clubb, F. Guo, Structure of the dimerization domain of DiGeorge critical region 8., Protein Sci. 19 (2010) 1354–65. doi:10.1002/pro.414.

[60] D. Reverter, C.D. Lima, A basis for SUMO protease specificity provided by analysis of human Senp2 and a Senp2-SUMO complex., Structure. 12 (2004) 1519–31. doi:10.1016/j.str.2004.05.023.

[61] T. Spirig, R.T. Clubb, Backbone (1)H, (13)C and (15)N resonance assignments of the 39 kDa staphylococcal hemoglobin receptor IsdH., Biomol. NMR Assign. (2011). doi:10.1007/s12104-011-9348-8.

[62] F. Ascoli, M.R. Fanelli, E. Antonini, Preparation and properties of apohemoglobin and reconstituted hemoglobins., Methods Enzymol. 76 (1981) 72–87.

[63] D. Gell, Y. Kong, S. a Eaton, M.J. Weiss, J.P. Mackay, Biophysical characterization of the alpha-globin binding protein alpha-hemoglobin stabilizing protein., J. Biol. Chem. 277 (2002) 40602–9. doi:10.1074/jbc.M206084200.

[64] D. Looker, A.J. Mathews, J.O. Neway, G.L. Stetler, Expression of recombinant human hemoglobin in Escherichia coli., Methods Enzymol. 231 (1994) 364–74.

[65] J.M. Manning, [14] Preparation of hemoglobin carbamylated at specific NH2-terminal residues, Methods Enzymol. 76 (1981) 159–167. doi:10.1016/0076-6879(81)76124-X.

[66] Antonini E. & Brunori M., Hemoglobin and Myoglobin in their Reactions with Ligands,

Amsterdam, Netherlands North-Holl. (1971).
[67] J.T. Cohn, E. J. & Edsall, Proteins, Amino Acids and Peptides as Ions and Dipolar Ions (Cohn, Edwin J.; Edsall, John T.), Reinhold Publishing Corporation, New York, 1943.
[68] T. Laue, B. Shah, T. Ridgeway, S. Pelletier, Computer-aided interpretation of analytical sedimentation data for proteins, in: H.J. Harding SE, Rowe AJ (Ed.), Anal. Ultracentrifugation Biochem. Polym. Sci., Cambridge: The Royal Society of Chemistry, 1992: pp. 90–125.

Chapter 5

Nitroxide Labeling and Derivation of Paramagnetic NMR Distance Restraints for Protein Structure Determination

The work described in this chapter is a version of a manuscript to be submitted for publication

Sjodt, M and Clubb, R.T. 2015

I was the primary author of this work. I designed experiments, prepared the samples, performed the NMR experiments, and analyzed data.

5.1 Introduction

This protocol describes the use of nitroxide spin labels to derive paramagnetic relaxation enhancement (PRE) distance restraints for nuclear magnetic resonance (NMR) protein structure determination. Site-specific labeling of proteins using paramagnetic spin labels enhances the transverse relaxation rates of nearby nuclei leading to line-broadening effects that can be used to derive distant restraints for protein structure determination [1-3]. This approach has been used in a wide variety of studies including, but not limited to, membrane proteins [4], multi-domain proteins displaying inter-domain dynamics [5], protein-DNA complexes [1], transient protein-protein [6,7] interactions, and intrinsically disordered proteins [8]. There are generally two approaches to obtain PRE-derived distances. The first is a quantitative measurement of transverse relaxation rates described in detail by Iwahara and Clore [1,2] and the other is the simplified measurement of peak intensity ratios described by Battiste and Wagner [3], with the latter method depicted in this protocol. The two most common types of spin labels used are EDTA-based chelators that bind paramagnetic metal ions and organic compounds with nitroxide radicals. The ease of sample preparation and long history of use in electron paramagnetic resonance (EPR) studies have made disulfide-linked nitroxide spin-labels such as the methanesulfonothioate compound, MTSL, the most frequently used approach for PRE studies. The aim of this protocol is to describe the considerations taken when designing probe locations, labeling of proteins with nitroxide spin labels, NMR data acquisition and analysis, and finally the Battiste and Wagner approach to the derivation of PRE-based distance restraints to define protein structure.

5.2 Materials and Reagents

1. MTSL (*S*-(1-oxyl-2,2,5,5-tetramethyl-2,5-dihydro-1H-pyrrol-3-yl)methyl methanesulfonothioate, Toronto Research Chemicals, catalog number: O87500)
2. Sodium Ascorbate (Sigma-Aldrich, catalog number: A7631)
3. Acetonitrile (Fisher Scientific, catalog number: A996)
4. Tris-HCl (Tris(hydroxymethyl)aminomethane Hydrochloride, Fisher Scientific, catalog number: BP153)
5. Sodium Phosphate Monobasic (Fisher Scientific, catalog number: S369)
6. Sodium Chloride (Fisher Scientifiic, catalog number: S271)
7. DTT (Dithiothreitol, Goldbio, catalog number: DTT50)
8. Sodium Azide (Fisher Scientific, catalog number: BP9221)
9. Deuterium oxide (Sigma Aldrich, catalog number: 617385)
10. Zeba Spin Desalting Column, 7k MWCO, 2 mL (Thermo Fisher, catalog number: 89889)
11. Amicon Ultra-15 centrifugal filter (Millipore, catalog number: UFC900308)
12. Standard 5 mm NMR tube (Wilmad, catalog number: 535-PP-7)

5.3 Equipment

1. Centrifuge (Beckman coulter, model Allegra X-14R)
2. SX4750A swinging bucket rotor (Beckman Coulter)
3. MALDI-TOF Mass Spectrometer (Applied Biosystems, model Voyager-DE-STR)

4. NMR experiments used in this protocol are part of the Bruker standard pulse sequence library and were performed on Bruker Avance spectrometers equipped with triple-resonance cryogenic probes (Bruker Corporation)

5.4 Procedure

5.4.1 Preparation of Cysteine Mutants of Protein of Interest

1. Check the protein's primary sequence for any native cysteines that could be labeled by MTSL. If necessary, mutate these residues to alanine (for buried cysteines) or serine (for solvent exposed cysteines) to prevent non-specfic labeling. Check that these mutations do not effect protein fold and function.
2. Choose the desired location of the spin-label probe. This location needs to be at a residue that is solvent exposed and known to be either in a structured loop or lie within defined secondary stucture. Increased flexibility of the probe leads to averageing affects that reduce the quantitative strength of the technique.
3. Perform site-directed mutagenesis to incorporate a cysteine residue at the desired location to be labeled my MTSL.
4. Purfiy ^{15}N-labeled protein with the cysteine mutation. Use buffers that are supplemented with 2.5 mM DTT to prevent formation of inter-molecular disufide bonds that can lead to aggregation (see note 1).
5. Prior to labeling the purified protein with MTSL, verify that the cysteine mutation does not affect the native stuctutural fold by comparing its ^{1}H-^{15}N-HSQC spectrum to a spectrum of the wild-type protein. The cross-peaks should overlay well between the two spectra.

5.4.2 Site-Specific Nitroxide-Labeling for NMR Experiments

1. Make a 200 mM stock of MTSL by adding acetonitrile directly to the amber vial. Store the MTSL stock at -20°C (see notes 2 and 3).
2. Buffer exchange the ^{15}N-labeled protein with the cysteine mutation into MTSL labeling buffer that is supplemented with fresh 2.5 mM DTT. If not immediately labeling with MTSL, store the protein at -80°C.
3. Immediately prior to labeling with MTSL, dilute the protein to a concentation of 250-300 μM (total volume 1 mL) using MTSL labeling buffer without DTT. From this step forward do not use DTT in any of the buffers.
4. Equilibrate a Zeba Spin Desalting Column with MTSL labeling buffer per manufacture's protocol.
5. In a clean 15 mL conical tube, pipette 2.5 mL of MTSL labeling buffer. Add a 10x molar amount of MTSL (relative to protein concentration). Make sure to keep MTSL away from light by covering the tube with foil first.
6. Place the equilibrated desalting column into the conical tube from step 5. Slowly pipette the protein onto the center of the column's resin bed.
7. Spin as per manufacture's protocol, check to make sure there is ~3.5 mL of sample in the bottom of the collection tube. Discard the column.
8. Cover the collection tube with foil and put on a rotisserie for 15 min at room temperature.
9. After 15 min, dilute the sample to a total volume of 6 mL with MTSL labeling buffer. Add another 10x molar excess of MTSL (20x molar excess in total).

10. Place tube back onto the rotisserie and let the protein:MTSL mixture incubate overnight at room temperature (~16hrs).
11. Buffer exchange the MTSL-labeled protein sample into NMR buffer using a fresh Amicon Ultra-15 centrifugal filter to remove any excess (unligated) MTSL (see notes 4 and 5).
12. Check the efficiency of MTSL labeling by MALDI-TOF. Look for ~186 Da increase in size compared to unligated protein.
13. Dilute the MTSL-labeled protein sample in NMR buffer supplemented with 8-10% D_2O to a final concentration of 300 μM (see note 6). Place the sample in a standard NMR tube. Shield the NMR tube from light.

5.4.3 NMR Experimental Set up

1. Begin the NMR data acquitistion in the paramagnetic state using standard ^{1}H-^{15}N-HSQC pulse sequences. The ^{1}H and ^{15}N dimensions are usually collected with 2048 and 256 complex points, respectively.
2. After paramagnetic experiments conclude, add a 5x molar excess of sodium ascorbate (relative to MTSL concentration) to the NMR tube by carefully pipetting up and down with a long pipette. This will reduce MTSL's unpaired electron and form the diamagnetic state. Let the sample reduce for a minimum of 3 hours.
3. Collect the diamagnetic ^{1}H-^{15}N-HSQC data using identical conditions as the paramagnetic experiments in step 1.

5.5 Data Analysis

5.5.1 Analysis of NMR ^{15}N-HSQC Paramagetic and Diamagnetic Spectra

1. Process both the paramagnetic and diamagnetic ^{1}H-^{15}N-HSQC data identically using standard NMRPipe [9] or Bruker TopSpin™ software. Generally, both of the ^{1}H and ^{15}N dimensions are processed to a digital resolution of ~0.25 ppm.
2. Import the processed spectra into Sparky software [10]. Copy backbone resonance assignments from the assigned ^{1}H-^{15}N-HSQC spectrum of the native protein. Begin with diamagetic spectrum as it should overlay well with the native spectrum.
3. Make sure to center the copied peak assignments on the resonances in the diamagnetic spectrum. Only use cross-peaks that are isolated from from other peaks (see note 7).
4. Copy all the formatted diamagetic peak assigments to the paramagnetic spectrum. Repeat step 3.
5. Once both the diamagetic and paramagnetic spectra have been assigned and throroughly inspected, export the assignments, peak height intensities, and linewidths to a .txt file.
6. Import the assignments into data analysis software (e.g. Microsoft Excel). Calculate the ratio of the paramagetic peak height intentsities (I_{ox}) to the diamagnetic peak hight intensities (I_{red}).

5.5.2 Derivation of Paramagtic Distance Restraints

1. Use a series of distances, r, to back calculate the spin contibution to the enhanced relaxation rate, R_2^{sp}, using a modified version of the Solomon-Bloembergen in equation 1 [3,11],

$$r = \left[\frac{K}{R_2^{sp}}\left(4\tau_C + \frac{3\tau_C}{1+\omega_h^2\tau_C^2}\right)\right]^{1/6} \quad (1)$$

where K is a constant (1.23 x 10^{-32} cm^6 s^{-2}) that describes the spin properties of the MTSL spin label [3], ω_h is the Larmor frequency of the proton spin, and τ_C is the apparent PRE correlation time [12].

2. From the back calculated R_2^{sp} values, back calculate I_{ox}/I_{red} ratios using the equation 2 [3],

$$\frac{I_{ox}}{I_{red}} = \frac{R_2\, e^{-R_2^{sp}t}}{R_2+R_2^{sp}} \quad (2)$$

where R_2 is the intrinsic amide proton transverse relaxation rate (calculated from the cross-peak linewidths), and t is the total INEPT evolution time recorded during the NMR experiments (e.g. 11 ms).

3. Assign distances for each experimental I_{ox}/I_{red} ratio based on the back calculated I_{ox}/I_{red} ratios using equations 1 and 2. See Sjodt *et al.* (2015) for more information [5].
4. When generating a restraint table for NMR structure calculations, the restraint should be between the nitrogen atom of the MTSL ring and the affected amide proton. Use two types of distance restraints:
    a. If I_{ox}/I_{red} is < 0.80, the restraint is called "attractive" and is given the assigned distance from step 3 and assuming an error of ± 5 Å.
    b. If I_{ox}/I_{red} ≥ 0.80, the restraint is called "repulsive" and is given a lower bound distance of 20 Å and no upper bound distance [3,13,14].
5. Perform NMR structure calculations using standard XPLOR-NIH software using PRE-dervied distance restraints from step 4 as NOE parameters [15].

6. Assess the quality of the calculated structures by a quality factor, *Q*, using equation 3,

$$Q = \sqrt{\frac{\Sigma(V_{backcalc} - V_{exp})^2}{\Sigma(V_{exp})^2}} \quad (3)$$

where $V_{backcalc}$ *and* V_{exp} are the back calculated and experimental I_{ox}/I_{red} ratios for a given spin label. This equation is described in [12,16] and is a modified version of the PRE *Q*-factor used in other studies and employs peak intensity ratios in place of enhanced relaxation rates [1,3]. See Sjodt *et al.* (2015) for more information [5].

5.6 Notes

1. Make fresh DTT before each use.
2. MTSL will precipitate at high concentrations of acetonitrile, so keep the conentration below 200 mM.
3. MTSL is light and air sensitive.
4. Make sure to extensively wash the protein in step 11. Excess MTSL will give rise to artifacts in the NMR experiments.
5. The NMR buffer should be optomized for the protein of interest. For a review on buffers suitible for NMR see Kelly *et al.* (2002) [17].
6. The protein concentration should be kept low to prevent inter-molecular PRE effects.
7. It has been reported that the tail of a cross-peak that is completely broadened by PRE effects can reduce the height of a neighboring peak by up to 15%, giving rise to false positive broadening effects [3].

5.7 Recipes

A. MTSL labeling buffer

50 mM	Tris-HCl (pH 7.8)
50 mM	NaCl

B. NMR buffer

20 mM	Sodium Phosphate Monobasic (pH 6.0)
50mM	NaCl
0.01%	NaN_3

5.8 Acknowledgements

This protocol was adapted from Sjodt *et al.* (2015) [5]. This work was supported by National Institutes of Health Grants AI52217 (to R.T.C.) and the National Institutes of Health Award F31GM101931 (to M.S.).

5.9 References

[1] G.M. Clore, J. Iwahara, Theory, practice, and applications of paramagnetic relaxation enhancement for the characterization of transient low-population states of biological macromolecules and their complexes., Chem. Rev. 109 (2009) 4108–39. doi:10.1021/cr900033p.

[2] J. Iwahara, C.D. Schwieters, G.M. Clore, Ensemble approach for NMR structure refinement against (1)H paramagnetic relaxation enhancement data arising from a flexible paramagnetic group attached to a macromolecule., J. Am. Chem. Soc. 126 (2004) 5879–5896. doi:10.1021/ja031580d.

[3] J.L. Battiste, G. Wagner, Utilization of site-directed spin labeling and high-resolution heteronuclear nuclear magnetic resonance for global fold determination of large proteins with limited nuclear overhauser effect data., Biochemistry. 39 (2000) 5355–65.

[4] T.P. Roosild, J. Greenwald, M. Vega, S. Castronovo, R. Riek, S. Choe, NMR structure of Mistic, a membrane-integrating protein for membrane protein expression., Science. 307 (2005) 1317–21. doi:10.1126/science.1106392.

[5] M. Sjodt, R. Macdonald, T. Spirig, A.H. Chan, C.F. Dickson, M. Fabian, J.S. Olson, D.A. Gell, R.T. Clubb, The PRE-Derived NMR Model of the 38.8kDa Tri-Domain IsdH Protein from Staphylococcus aureus Suggests that it Adaptively Recognizes Human Hemoglobin., J. Mol. Biol. (2015). doi:10.1016/j.jmb.2015.02.008.

[6] V. a Villareal, T. Spirig, S.A. Robson, M. Liu, B. Lei, R.T. Clubb, Transient weak protein-protein complexes transfer heme across the cell wall of Staphylococcus aureus., J. Am. Chem. Soc. 133 (2011) 14176–9. doi:10.1021/ja203805b.

[7] C. Tang, C.D. Schwieters, G.M. Clore, Open-to-closed transition in apo maltose-binding protein observed by paramagnetic NMR., Nature. 449 (2007) 1078–82. doi:10.1038/nature06232.

[8] C.W. Bertoncini, Y.-S. Jung, C.O. Fernandez, W. Hoyer, C. Griesinger, T.M. Jovin, M. Zweckstetter, Release of long-range tertiary interactions potentiates aggregation of natively unstructured alpha-synuclein., Proc. Natl. Acad. Sci. U. S. A. 102 (2005) 1430–5. doi:10.1073/pnas.0407146102.

[9] F. Delaglio, S. Grzesiek, G.W. Vuister, G. Zhu, J. Pfeifer, A. Bax, NMRPipe: a multidimensional spectral processing system based on UNIX pipes., J. Biomol. NMR. 6 (1995) 277–93.

[10] T.D. Goddard, D.G. Kneller, Sparky NMR Analysis Software, (2001).

[11] I. Solomon, N. Bloembergen, Nuclear Magnetic Interactions in the HF Molecule, J. Chem. Phys. 25 (1956) 261. doi:10.1063/1.1742867.

[12] B. Simon, T. Madl, C.D. Mackereth, M. Nilges, M. Sattler, An efficient protocol for NMR-spectroscopy-based structure determination of protein complexes in solution., Angew. Chem. Int. Ed. Engl. 49 (2010) 1967–70. doi:10.1002/anie.200906147.

[13] D. Gottstein, S. Reckel, V. Dötsch, P. Güntert, Requirements on paramagnetic relaxation

enhancement data for membrane protein structure determination by NMR., Structure. 20 (2012) 1019–27. doi:10.1016/j.str.2012.03.010.

[14] S. Reckel, D. Gottstein, J. Stehle, F. Löhr, M.-K. Verhoefen, M. Takeda, R. Silvers, M. Kainosho, C. Glaubitz, J. Wachtveitl, F. Bernhard, H. Schwalbe, P. Güntert, V. Dötsch, Solution NMR structure of proteorhodopsin., Angew. Chem. Int. Ed. Engl. 50 (2011) 11942–6. doi:10.1002/anie.201105648.

[15] C.D. Schwieters, J.J. Kuszewski, N. Tjandra, G.M. Clore, The Xplor-NIH NMR molecular structure determination package., J. Magn. Reson. 160 (2003) 65–73.

[16] C.D. Mackereth, T. Madl, S. Bonnal, B. Simon, K. Zanier, A. Gasch, V. Rybin, J. Valcárcel, M. Sattler, Multi-domain conformational selection underlies pre-mRNA splicing regulation by U2AF., Nature. 475 (2011) 408–11. doi:10.1038/nature10171.

[17] Alexander E. Kelly, H.D. Ou, A. Richard Withers, V. Dötsch, Low-Conductivity Buffers for High-Sensitivity NMR Measurements, (2002).